CARBON MOLECULAR SIEVE HOLLOW FIBER MEMBRANES FOR OLEFIN/PARAFFIN SEPARATIONS

A Dissertation
Presented to
The Academic Faculty

By

Liren Xu

In Partial Fulfillment
Of the Requirements for the Degree
Doctor of Philosophy in the
School of Chemical & Biomolecular Engineering

Georgia Institute of Technology

December 2012

CARBON MOLECULAR SIEVE HOLLOW FIBER MEMBRANES FOR OLEFIN/PARAFFIN SEPARATIONS

Approved by:

Dr. William Koros, Advisor
School of Chemical & Biomolecular Engineering
Georgia Institute of Technology

Dr. Tom Fuller
School of Chemical & Biomolecular Engineering
Georgia Institute of Technology

Mr. Mark Brayden
Hydrocarbons R&D
The Dow Chemical company

Dr. Dennis Hess
School of Chemical & Biomolecular Engineering
Georgia Institute of Technology

Dr. David Bucknall
School of Materials Science and Engineering
Georgia Institute of Technology

Date Approved: September 17, 2012

ACKNOWLEDGEMENTS

My stay at Georgia Tech has been truly a life changing experience. During the past four years, many people helped me, in many ways, and deserve my sincere gratitude.

First and foremost, I have to thank my advisor Dr. Koros. The experience with Dr. Koros has been absolutely amazing. I received the best education from Dr. Koros, both on a professional and personal level. I have been so lucky to have so many enjoyable interactions with him. His enthusiasm, relentless dedication and wisdom will continuously inspire me. His influence has been built into my attitude to work, life and the world. One of the reasons making me work hard is to make him proud of me in the future. I cannot have a better advisor.

Mark Brayden and Marcos Martinez have given me endless support, technically and non-technically. I would really regard both of them as my "co-advisors". I would like to express my earnest gratitude to Mark and Marcos.

I would like to thank my committee members, Dr. David Bucknall, Dr. Tom Fuller and Dr. Dennis Hess for their time and valuable insights.

I have been very fortunate to work in Koros group. All members deserve thanks. I have to give special credit to my collaborator Meha Rungta for all her support. I must also thank Kuang Zhang for introducing me into Koros group when I arrived at Georgia Tech and also for helping me start my life in Atlanta. I would like to thank senior members Dr. Chien-Chiang Chen, Dr. Wulin Qiu, Dr. Cheng Chen, Dr. Dhaval Bhandari, Dr. Naoki Bessho, Dr. Junqiang Liu, Dr. Ryan Lively, Dr. Jong Suk Lee, Dr. Omoyemen Esekhile, Dr. JR Johnson, and Dr. Oguz Karvan for helping me develop my skills and all

the helpful discussions. Justin Vaughn, Canghai Ma, Vinod Babu, Nitesh Bhuwania, Chen Zhang, Xue Ning, John Hessler, and Dr. Ying Dai were all good colleagues to work with.

I have always been fortunate to have good friends who have been present during my good and tough times. So many friends have made the grocery shopping, Friday dinner and Friday night fun. The list is so long that I have to give a group acknowledgement. I have to express my special thanks to my classmate and friend Wei-Ming Yeh for his patience and endless support.

I must thank my family for their unconditional love and support from China. Nothing is possible without their support.

The funding support from Dow is also greatly appreciated.

TABLE OF CONTENTS

LIST OF TABLES

LIST OF FIGURES

SUMMARY

Olefin/paraffin separation is a large potential market for membrane applications. Carbon molecular sieve membranes (CMS) are promising for this application due to the intrinsically high separation performance and the viability for practical scale-up.

Intrinsically high separation performance of CMS membranes for olefin/paraffin separations was demonstrated. The translation of intrinsic CMS transport properties into the hollow fiber configuration is considered in detail. Substructure collapse of asymmetric hollow fibers was found during Matrimid® CMS hollow fiber formation. To overcome the permeance loss due to the increased separation layer thickness, 6FDA-DAM and 6FDA/BPDA-DAM polyimides with higher rigidity were employed as alternative precursors, and significant improvement has been achieved. Besides the macroscopic morphology control of asymmetric hollow fibers, the micro-structure was tuned by optimizing pyrolysis temperature protocol and pyrolysis atmosphere. In addition, unexpected physical aging was observed in CMS membranes, which is analogous to the aging phenomenon in glassy polymers. For performance evaluation, multiple "proof-of-concept" tests validated the viability of CMS membranes under realistic conditions.

The scope of this work was expanded from binary ethylene/ethane and propylene/propane separations for the debottlenecking purpose to mixed carbon number hydrocarbon processing. CMS membranes were found to be olefins-selective over corresponding paraffins; moreover, CMS membranes are able to effectively fractionate the complex cracked gas stream in a preferable way. Reconfiguration of the hydrocarbon processing in ethylene plants is possible based on the unique CMS membranes.

CHAPTER 1

INTRODUCTION

1.1 Olefin/paraffin separations

Olefins, such as ethylene and propylene, are among the most important building blocks in chemistry [1]. Currently, the worldwide commercial production of ethylene and propylene is mainly based on thermal cracking of a wide range of hydrocarbon feedstocks (ethane, propane, butane, naphtha, etc.). The feedstocks are cracked into smaller molecules in cracking furnaces. The resulting product mixtures, which can vary widely, are then separated into the desired products by using a complex sequence of separation and chemical-treatment steps [2, 3]. Figure 1.1 shows the schematic of a typical simplified ethylene plant [4]. In an ethylene plant, separation units have a large footprint and separation processes consume significant energy.

Besides seeking economical alternative feedstocks and improving cracking processes, improving the recovery processes is also of great interest. Traditionally, the separation of olefins from paraffins is dominated by distillation processes. For example, C2-splitters are used to separate ethylene from ethane, and C3-splitters are used to separate propylene from propane. Besides the last two columns for binary separations, deethanizers separate C2 hydrocarbons (ethylene and ethane) from C3 hydrocarbons (propylene and propane); demethanizers separate hydrogen and methane from C2 and C3 hydrocarbons (ethylene, ethane, propylene and propane). Since the physicochemical properties (such as volatility and boiling point) of the compounds are very similar, large towers and high reflux ratios are required to achieve effective separations. Therefore, the

current purification process is very capital and energy intensive. For example, due to the very low and close boiling points of ethylene (169.4 K) and ethane (184.5 K), a typical C2-splitter contains over 100 trays and is performed at around -25 ^{o}C and 320 psig [2-4].

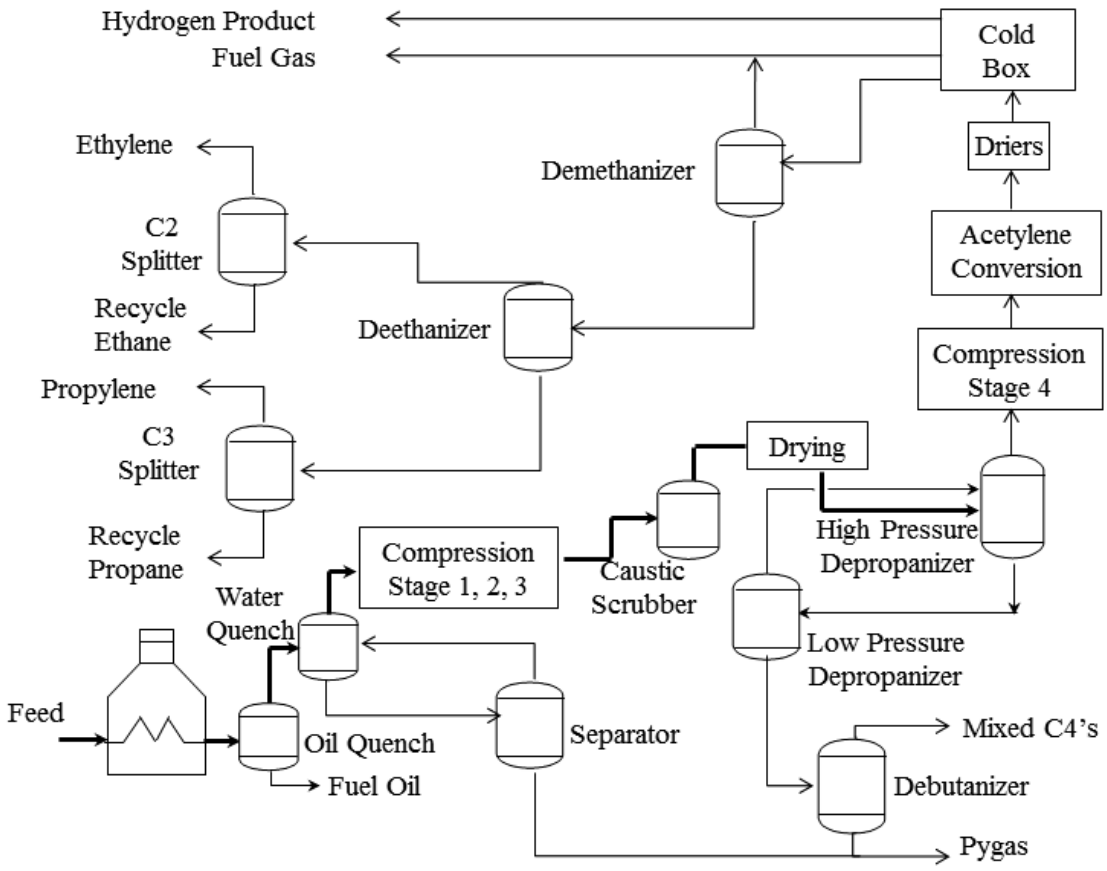

Figure 1.1 Schematic of a simplified ethylene plant [4]

To reduce the large cost in separation processes, various technologies have been proposed in recent years. Membranes have emerged as a promising energy efficient alternative. Currently, replacing distillation columns with membrane modules is still not quite feasible due to the relatively low separation efficiency and stability of available

membrane materials. Nevertheless, a hybrid membrane-distillation system has been proposed by several researchers [2-7]. The hybrid system, which consists of a distillation column and a parallel membrane unit, provides a practical way for retrofitting current distillation units. Substantial savings in energy and capital costs can be obtained based on simulation results. Multiple configurations of membrane units and distillation columns have been studied [2, 3, 5-7]. Rather than to optimize the integration of membrane and distillation processes, this research will primarily focus on the development of membrane materials to provide tools for such optimization approaches.

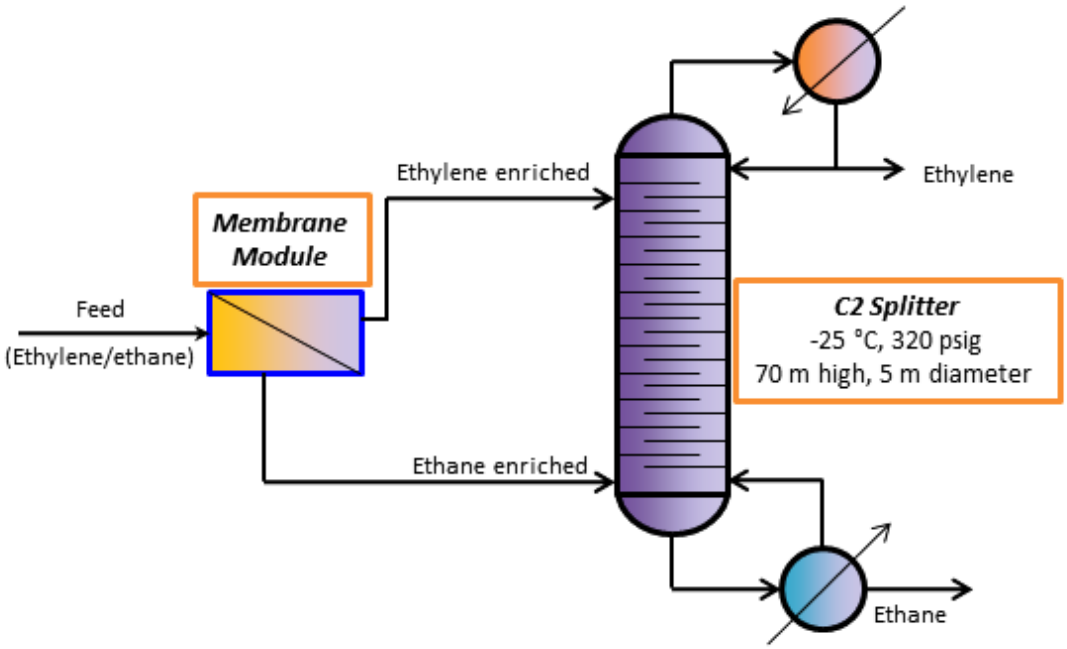

Figure 1.2 Schematic of a hybrid membrane-distillation system

1.2 Membrane technology

Membrane technology has emerged as a very attractive separation alternative, as compared to the traditional thermally-driven processes [8, 9]. The primary advantage is the low energy requirement of membrane processes due to the economical driving force—pressure difference across membranes. Besides the energy efficiency, membrane technology also offers small footprint, low capital, low operational cost, as well as adaptability and flexibility. Membranes are also environmentally friendly and contribute to long-term sustainability for our planet.

Membranes for liquid separations have been successfully used in a number of applications. Reverse osmosis purification of water was the first large scale commercially viable micromolecularly selective membrane application for fractioning liquid mixtures [8]. Due to the huge impact of applications, in the past decades, the interest and endeavor in gas separation membranes have increased significantly, with potential/existing large markets including natural gas purification, air separation, hydrogen separation, and petrochemical application [8, 9]. Tremendous efforts have been devoted to gas separation membrane development, and some commercial membrane modules are now available for carbon dioxide removal from natural gas, air separation and hydrogen separation [9]. Large and growing opportunities of membranes for gas separations exist in olefin/paraffin separations, with the potential membrane market for olefin/paraffin separations predicted to rise from 0 dollars in 2000 to about 125 million dollars in 2020. The 125 million figure represents 16.4% of the predicted entire membrane market of 2020 [9]; however, currently, no commercial membranes are available for olefin/paraffin separations.

In order to implement membranes for large scale applications, four essential elements must be enabled: (1) development of high-efficiency modules with large amounts of area per volume; (2) creation of advanced materials with tunable capabilities to separate molecularly similar components; (3) control of morphology of a membrane cross-section; (4) the development of high-speed manufacturing methods to rapidly link the earlier three elements into economical devices with minimal defects [8]. To meet these key requirements, asymmetric hollow fiber membranes are the preferred membrane configuration for most industrial gas separations. Hollow fiber configuration provides the highest surface area to volume ratio, compared to other membrane configurations, such as plate and frame, spiral wound. Ultra-thin selective skin layers, formed via morphology control, minimize the transport resistance and contribute to high productivity. The compact module, together with the ultra-thin separation layer, provides the required high productivity with small footprint for large scale applications. Currently, the asymmetric hollow fiber spinning technology and the fiber module formation technology have been commercialized. Therefore, for future endeavors, asymmetric hollow fiber membranes will most likely be the preferable membrane format for pursuing.

1.3 Gas separation membranes

Membranes differentiate gas molecules based on their differences in size, shape or physical/chemical nature. Depending on the membrane materials and separation mechanism, gas separation membranes are classified into several categories. Polymeric membranes, zeolite membranes, metal organic framework (MOF) membranes, mixed matrix membranes, facilitated transport membranes and carbon molecular sieve (CMS)

membranes are the mostly studied gas separation membranes.

Currently, most installed gas separation membranes are made from polymer materials. Polymeric membranes separate gases by the solution-diffusion mechanism. Polymers are inexpensive, have good mechanical properties and can be relatively easily processed into membrane modules. The major challenge for expanding the applications of polymer materials is mostly easily seen from the so-called trade-off upper bound between permeability and selectivity [10, 11]. The upper bound curves for multiple gas pairs have been well established and accepted by the membrane community. For olefin/paraffin separations, polymer upper bound for propylene/propane separation has been defined previously [12]; polymer upper bound for ethylene/ethane separation will be discussed in this work. Another critical drawback of polymer materials is lack of stability under aggressive feed conditions. Exposure to a high pressure stream of carbon dioxide, or heavy hydrocarbons may plasticize polymeric membranes and result in severe selectivity loss and thus ineffective separations [13, 14].

Microporous molecular sieve materials such as inorganic zeolites [15] and recently discovered metal organic frameworks (MOFs) [16] enable more effective separation with the well-defined porous structure, as compared to polymer materials. With the rigid porous structure, these membranes are able to overcome the polymer upper bound. These materials are more chemically inert and thermally stable compared to organic polymers; however, these membranes are quite expensive and difficult to handle and process, so applications of these membranes are limited to small scale.

Hybrid membranes, also called mixed matrix membranes, are of great interest in past years [17]. Mixed matrix membranes combine the polymer processability and high

separation performance of molecular sieving fillers. Such membranes are also able to exceed the polymer upper bound and can be processed into modules. However, the compatibility of sieve fillers and polymer remains a very challenging problem. To successfully fabricate good mixed matrix membranes, several hurdles must be overcome: matrix rigidification, sieve-in-a-cage morphology and "clogged" sieves [18]. Of course, to create membranes in asymmetric hollow fiber form requires work, since to date, no defect-free commercial asymmetric mixed matrix hollow fiber membranes exist.

Facilitated transport membranes have shown high performance for olefin/paraffin separations; however, the intrinsic instability of these membranes makes them questionable for practical applications [2, 19].

To address the current challenges in membranes for gas separations, carbon molecular sieve membranes have emerged as a promising option for next generation membrane material [20-27]. Like other microporous molecular sieve materials, due to the rigid porous structure, carbon molecular sieve membranes are also able to outperform polymer materials. Unlike zeolites and MOFs, carbon molecular sieves are derived from polymer precursors, and this has the potential for greatly reduced costs. While polymer membranes are the state of commercial art membrane technology, CMS membranes can also be relatively easily fabricated into practical hollow fiber modules. The only additional step beyond the current technology platform is the scale-up of pyrolysis, which makes CMS not only capable of delivering high separation performance from the material aspect, but also viable for large scale application. The stability of CMS membranes under aggressive feed conditions is another exciting feature that enables practical application of CMS membranes under aggressive feed conditions [23].

Therefore, CMS membranes are potentially viable for large scale gas separation applications.

1.4 Research objectives

This research aims to develop high performance carbon molecular sieve hollow fiber membranes for olefin/paraffin separations. The challenging ethylene/ethane separation is the primary target to address in this work. Extension to other applications (e.g., propylene/propane separation and multi-component separation) in olefins production processes is also considered. For the purpose of large scale applications, the asymmetric hollow fiber configuration is investigated intensively to gain a realistic view of this new class of membrane materials. Based on different precursor polymers, the control of macroscopic asymmetric morphology and tailoring of microscopic molecular sieving structure based on different precursor polymers are integrated to achieve the goal of this research. The objectives of this research are as follows:

Objective 1: Characterize and control the morphology of CMS hollow fibers and illustrate the formation mechanism.

The first objective relates to the macroscopic morphology of CMS hollow fiber membranes. Effective membrane separation layer thickness must be controlled to meet the productivity requirement of a practical membrane. Previously, few studies considered the morphology of CMS hollow fiber membranes [28-30]. Several key items are described below: first, identify the difference of morphology between precursor and CMS

fibers; second, propose and justify the mechanism for CMS fiber morphology formation; third, effectively control the CMS fiber morphology based on previous studies.

Objective 2: Develop pyrolysis protocols for high performance CMS hollow fiber membranes.

The second objective aims to optimize the micro-structure of CMS membranes for specific gas separation applications while the macroscopic morphology control is also under consideration. The ultramicroporous structure of CMS materials must be tuned to achieve high separation performance for specific olefin/paraffin applications. Considering the morphological difference between dense film and hollow fiber, pyrolysis protocols also require special aspects for hollow fiber pyrolysis. Several detailed items are listed as below: develop optimum pyrolysis temperature protocols for CMS hollow fiber membranes; investigate the effect of pyrolysis atmosphere on CMS hollow fiber membrane performance; consider some pre-treatments on precursors and post-treatments on CMS fibers.

Objective 3: Investigate effect of precursor properties on CMS fiber membrane performance and formation of desired precursor fibers.

The precursor properties include properties of precursor polymers and properties attributed to the precursor asymmetric hollow fiber configuration. Obviously, the starting polymers have significant impacts on both macroscopic morphology and microscopic molecular sieving structure of CMS hollow fiber membranes. The insight of underlying correlation between polymer and carbon properties will guide the future precursor material selection. The specific properties related to the asymmetric hollow fiber morphology, such as the defect-free property, which may also play a role in the final

CMS fiber performance, require careful examination. Formation of desired precursor fibers via a dry-jet/wet-quench spinning process is another target in this objective.

Objective 4: Evaluate CMS fiber performance under realistic permeation conditions.

Mixed gas tests under realistic feed conditions will be used to evaluate CMS fiber performance. The realistic testing conditions include feed compositions, feed pressure, and testing temperature similar to the conditions in an ethylene plant. The stability of CMS membranes will also be examined.

1.5 Dissertation organization

This dissertation is divided into 9 chapters including the current chapter and is organized in the following manner. Chapter 2 describes gas transport mechanisms through membranes and other essential background materials relevant to this research. Chapter 3 provides the materials, experimental methods and equipment used throughout this research. Chapter 4 identifies the experimental conditions for making proper asymmetric precursor hollow fibers. Chapter 5 discusses the formation and properties of Matrimid® derived carbon membranes. This chapter describes a model system for studying detailed morphology evolution of CMS hollow fiber membrane formation. Chapter 6 extends the precursor material from Matrimid® to 6FDA-polymers for CMS membrane fabrication. Chapter 7 describes the newly discovered history dependence of membrane transport properties (or so-called aging) in carbon membranes. Chapter 8 extends the previously proposed work of binary olefin/paraffin separations to mixed carbon number olefin-paraffin separations. Based on the olefins-selective feature of carbon membranes, an advantageous new hybrid membrane-distillation concept is

described in details. Chapter 9 summarizes the findings of this research and includes some recommendations for future work to further advance the project.

1.6 References

[1] W.R. True, Global ethylene producers add record capacity in 2010, Oil Gas J. 109 (2011) special report; Pg. 100.

[2] A. Motelica, O.S.L. Bruinsma, R. Kreiter, M. den Exter, J.F. Vente, Membrane retrofit option for paraffin/olefin separation—a technoeconomic evaluation, Ind. Eng. Chem. Res. 51 (2012) 6977-6986.

[3] J.A. Caballero, I.E. Grossmann, M. Keyvani, E.S. Lenz, Design of hybrid distillation-vapor membrane separation systems, Ind. Eng. Chem. Res. 48 (2009) 9151-9162.

[4] M.K. Brayden, G.A. Barbay, The Dow Chemical Company's membrane test unit, in: 2011 North American Membrane Society Annual Meeting, Las Vegas, NV, 2011.

[5] M. Benali, B. Aydin, Ethane/ethylene and propane/propylene separation in hybrid membrane distillation systems: Optimization and economic analysis, Sep. Purif. Technol. 73 (2010) 377-390.

[6] E. Ayotte-Sauve, M. Sorin, F. Rheault, Energy requirement of a distillation/membrane parallel hybrid: a thermodynamic approach, Ind. Eng. Chem. Res. 49 (2010) 2295-2305.

[7] W. Stephan, R.D. Noble, C.A. Koval, Design methodology for a membrane distillation column hybrid process, Journal of Membrane Science 99 (1995) 259-272.

[8] W.J. Koros, Evolving beyond the thermal age of separation processes: Membranes can lead the way, AlChE J. 50 (2004) 2326-2334.

[9] R.W. Baker, Future directions of membrane gas separation technology, Ind. Eng. Chem. Res. 41 (2002) 1393-1411.

[10] L.M. Robeson, The upper bound revisited, J. Membr. Sci. 320 (2008) 390-400.

[11] L.M. Robeson, Correlation of separation factor versus permeability for polymeric membranes, J. Membr. Sci. 62 (1991) 165-185.

[12] R.L. Burns, W.J. Koros, Defining the challenges for C_3H_6/C_3H_8 separation using polymeric membranes, J. Membr. Sci. 211 (2003) 299-309.

[13] W. Qiu, C.-C. Chen, L. Xu, L. Cui, D.R. Paul, W.J. Koros, Sub-T_g cross-linking of a polyimide membrane for enhanced CO_2 plasticization resistance for natural gas separation, Macromolecules 44 (2011) 6046-6056.

[14] C.-C. Chen, W. Qiu, S.J. Miller, W.J. Koros, Plasticization-resistant hollow fiber membranes for CO_2/CH_4 separation based on a thermally crosslinkable polyimide, J. Membr. Sci. 382 (2011) 212-221.

[15] M. Yu, R.D. Noble, J.L. Falconer, Zeolite membranes: microstructure

characterization and permeation mechanisms, Acc. Chem. Res. 44 (2011) 1196-1206.

[16] M. Shah, M.C. McCarthy, S. Sachdeva, A.K. Lee, H.-K. Jeong, Current status of metal–organic framework membranes for gas separations: promises and challenges, Ind. Eng. Chem. Res. 51 (2011) 2179-2199.

[17] W.J. Koros, R. Mahajan, Mixed matrix gas separation membranes., Abstracts of Papers of the American Chemical Society 219 (2000) U751-U751.

[18] T.T. Moore, W.J. Koros, Non-ideal effects in organic–inorganic materials for gas separation membranes, Journal of Molecular Structure 739 (2005) 87-98.

[19] R.J.B. Tim Charles Merkel, Process for regenerating facilitated-transport membranes, in: U.S. Patent (Ed.) United States Patent, Membrane Technology and Research Inc., Menlo Park, CS, United States, 2006.

[20] K.M. Steel, W.J. Koros, An investigation of the effects of pyrolysis parameters on gas separation properties of carbon materials, Carbon 43 (2005) 1843-1856.

[21] S.M. Saufi, A.F. Ismail, Fabrication of carbon membranes for gas separation - a review, Carbon 42 (2004) 241-259.

[22] K.M. Steel, W.J. Koros, Investigation of porosity of carbon materials and related effects on gas separation properties, Carbon 41 (2003) 253-266.

[23] D.Q. Vu, W.J. Koros, S.J. Miller, High pressure CO_2/CH_4 separation using carbon molecular sieve hollow fiber membranes, Ind. Eng. Chem. Res. 41 (2002) 367-380.

[24] A.F. Ismail, L.I.B. David, A review on the latest development of carbon membranes for gas separation, J. Membr. Sci. 193 (2001) 1-18.

[25] J.E. Koresh, A. Soffer, The carbon molecular-sieve membranes-general properties and the permeability of CH4/H2 mixture, Sep. Sci. Technol. 22 (1987) 973-982.

[26] J.E. Koresh, A. Soffer, Mechanism of permeation through molecular-sieve carbon membrane. 1. The effect of adsorption and the dependence on pressure, J. Chem. Soc., Faraday Trans. 82 (1986) 2057-2063.

[27] J.E. Koresh, A. Sofer, Molecular-sieve carbon permselective membrane. Part 1. Presentation of a new device for gas-mixture separation, Sep. Sci. Technol. 18 (1983) 723-734.

[28] M. Kiyono, Carbon molecular sieve membranes for natural gas separations, in: Chemical Engineering, Georgia Institute of Technology, 2010.

[29] A. Singh, Membrane materials with enhanced selectivity: an entropic interpretation, in: Chemical Engineering, The University of Texas at Austin, 1997.

[30] K.M. Steel, Carbon membranes for challenging gas separations, in: Chemical Engineering, The University of Texas at Austin, 2000.

CHAPTER 2

BACKGROUND AND THEORY

This chapter provides essential background and theory. The first part of this chapter relates to gas transport through membranes. The second part pertains to structure and properties of CMS membranes. The third part explains the formation and structure of asymmetric hollow fiber membrane.

2.1 Membrane transport theory

The membrane materials relevant to this research are polymers and carbon molecular sieves. Gas transport through these two types of membrane materials is described in the following sections.

2.1.1 Permeation

Gas transport in nonporous polymer membranes and CMS membranes follows the sorption-diffusion mechanism [1, 2]. Specifically, gas molecules first sorb on the high pressure upstream side of a membrane, then diffuse through the membrane along with the concentration gradient and finally desorb on the low pressure downstream side. Figure 2.1 shows a schematic of gas permeation through a membrane to illustrate this process.

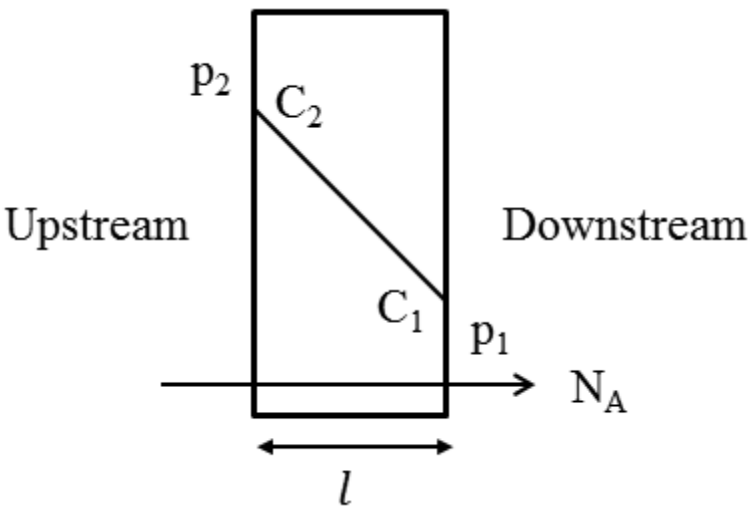

Figure 2.1 Schematic of gas permeation through a nonporous polymer membrane or a CMS membrane

Permeability and selectivity are commonly used to characterize productivity and separation efficiency of membrane materials. The permeability of penetrant "A" in a membrane is defined as the steady state gas flux (N_A), normalized by the trans-membrane partial pressure difference (Δp_A) and effective membrane separation layer thickness (l):

$$P_A = \frac{N_A \bullet l}{\Delta p_A} \tag{2.1}$$

The common unit for permeability is "Barrer", defined as:

$$1\ Barrer = 1\times 10^{-10}\ \frac{cm^3(STP)\cdot cm}{cm^2 \cdot s \cdot cmHg} \tag{2.2}$$

For asymmetric membranes, the actual membrane separation layer thickness is not readily known, so productivity of these membranes is described by permeance, which is simply defined by the trans-membrane pressure difference normalized flux:

$$(\frac{P}{l})_A = \frac{N_A}{\Delta p_A} \tag{2.3}$$

"Gas Permeation Unit" (GPU) is usually used as the unit for permeance, which is defined as:

$$1\ GPU = 1\times10^{-6}\ \frac{cm^3(STP)}{cm^2 \cdot s \cdot cmHg} \tag{2.4}$$

Membrane selectivity is defined as the ratio of gas permeabilities or permeances:

$$\alpha_{A/B} = \frac{P_A}{P_B} = \frac{(P/l)_A}{(P/l)_B} \tag{2.5}$$

For sorption-diffusion permeation, permeability can also be described as the product of diffusion coefficient and sorption coefficient:

$$P_A = D_A \bullet S_A \tag{2.6}$$

In this manner, selectivity can be partitioned into a diffusion selectivity (D_A/D_B) multiplied by a sorption selectivity (S_A/S_B):

$$\alpha_{A/B} = \frac{D_A}{D_B} \bullet \frac{S_A}{S_B} \tag{2.7}$$

2.1.2 Sorption and diffusion

Both sorption and diffusion coefficients depend on the physical and chemical nature of gas molecules and their interactions with membrane materials.

Sorption in glassy polymers follows the dual mode model [3-5]. Two idealized types of sorption are accounted in this model. Penetrant gas molecules may sorb in the normally densely packed region of polymers (dissolved mode) and non-equilibrium "microvoid" domains in the polymer matrix (hole-filling mode). These two modes can be described by Henry's Law and Langmuir isotherms, respectively, so sorption in glassy polymers is generally expressed as the following additive two-state model:

$$C_A = C_{DA} + C_{HA} \tag{2.8}$$

where C_A is the total concentration of penetrant A in the polymer, C_{DA} is the penetrant A concentration in the dissolved mode, and C_{HA} is the penetrant concentration in the Langmuir mode.

The pressure dependence of sorption for a single component is given by:

$$C_A = k_{DA} p_A + \frac{C'_{HA} b_A p_A}{1 + b_A p_A} \tag{2.9}$$

where k_{DA} is the Henry's law constant, C'_{HA} is the Langmuir capacity constant, b_A is the Langmuir affinity constant and p_A is the penetrant pressure.

Sorption coefficient is defined as the secant slope of sorption isotherm:

$$S_A = \frac{C_A}{p_A} = k_{DA} + \frac{C'_{HA} b_A}{1 + b_A p_A} \tag{2.10}$$

In the case of carbon molecular sieve membranes, only Langmuir sorption is considered to be significant, since sorption is believed to occur only in the micropores of CMS materials.

The sorption coefficient is, therefore, given by:

$$S_A = \frac{C_A}{p_A} = \frac{C'_{HA} b_A}{1 + b_A p_A} \tag{2.11}$$

Sorption coefficients of gases in a membrane are strongly influenced by the condensability of the gas molecule and the interaction with the sorption medium. Critical temperature is a good measure of the condensability of a gas penetrant. Generally, gases with higher critical temperatures tend to be more condensable and more sorptive in membranes.

Gas molecules diffuse through a dense non-porous polymer membrane via random jumps through thermally activated penetrant-scale transient gaps in the polymer matrix [1], as demonstrated in Figure 2.2. The diffusivity of a penetrant in a given polymer membrane is determined by the size of the penetrant molecules, indicated by the kinetic diameter.

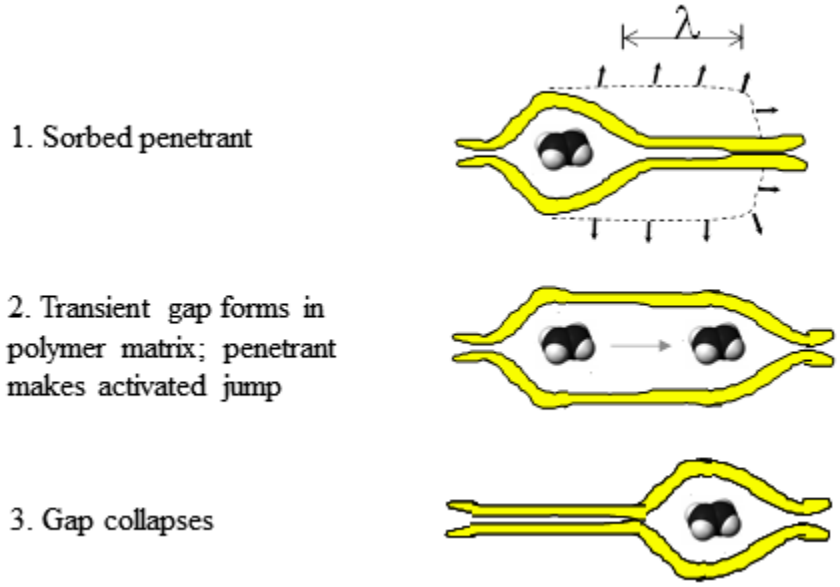

Figure 2.2 Schematic of gas diffusion through a nonporous dense polymer membrane via transient gap formation, where λ is the average length of random diffusion jumps

Gas transport through porous membranes can be categorized by four different mechanisms: (1) Knudsen diffusion, (2) partial condensation/diffusion, (3) selective adsorption with surface diffusion, and (4) molecular sieving [6-8]. Knudsen diffusion occurs when the mean free path of a gas is large enough relative to the pore size that the gas transport becomes dominated by gas-wall collision. The selectivity of Knudsen diffusion separation is dominated by the gas molecular weight [9]. Partial (or selective)

condensation occurs when one or more components in the feed stream condense in the pores of the membranes [10]. This mechanism is difficult to control and is rarely used in carbon membranes. Selective adsorption/surface diffusion mechanism relies on the adsorption of gases in porous membranes. This type of membranes is mainly used to separate non-adsorbable or weakly adsorbable gases (O_2, N_2, etc.) from adsorbable gases (NH_3, H_2S, etc.) [6, 10, 11]. In the case of molecular sieving carbon materials, the diffusion selectivity via molecular sieving dominates the overall separation, while sorption may also play a role in some particular examples. This latter, molecular sieving, mechanism is the focus of work in this thesis.

Gas molecules diffuse through carbon molecular sieve membranes via activated jumps from one sorptive micropore to another by passing the restrictive ultramicropores [7], as shown in Figure 2.3. Since in most cases, the free volume (pore volume) in carbon membranes is higher than in polymers due to decomposition of polymers and removal of small components, carbon membranes are more much permeable than polymer membranes. Generally, CMS materials can be regarded as more "open" materials, compared to polymers. Unlike in polymer membranes, in carbon molecular sieve membranes, due to the very rigid porous structure, both gas size and shape are very important for the activated diffusion. This means CMS membranes provide additional discrimination of gas molecules via the shape of gases. The additional feature is also called "entropic selectivity", which enables CMS membranes to be more selective than polymers [12-14]. Therefore, in general, CMS membranes are able to outperform polymer materials in terms of both permeability and selectivity.

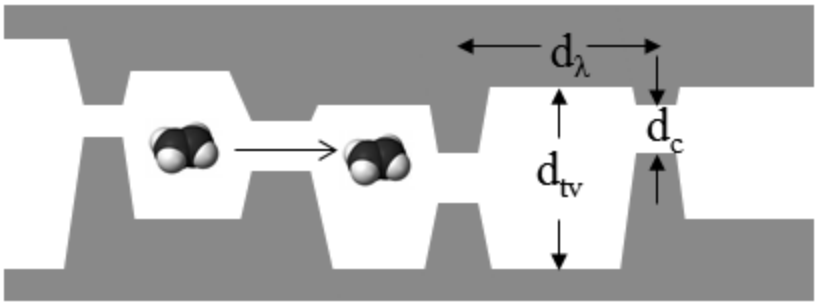

Figure 2.3 Schematic of the slit-like structure of CMS membranes and gas diffusion in a CMS membrane by a diffusive jump, where d_c is the ultramicropore dimension, d_{tv} is the adsorptive micropore dimension and d_λ is the jump length

2. 2 CMS membranes

2.2.1 Structure of CMS membranes

Carbon molecular sieve membranes are formed via high temperature pyrolysis of polymer precursors under controlled conditions. When a polymer is pyrolyzed, it can either form coke or char. Coke can be further heated to form graphite while char remains in an amorphous form [15]. At early stages of decomposition, both cokes and chars have very little long-range order and are composed of aggregates of small crystallites. Therefore, polymers that form both coke and char can be used to fabricate CMS membranes in the early stages of decomposition, although polymers that form char are more often used as practical starting precursors.

Carbon membranes used for gas separation usually have a "turbostratic" structure with very little long-range order and are considered essentially isotropic [15, 16], as shown in Figure 2.4 (a). Pores are formed from packing imperfections between microcrystalline regions in the material, or so-called "graphene-like" sheets, as shown in Figure 2.4 (b). The porous structure of molecular sieve carbons is not as well defined as

other crystalline molecular sieve materials, such as zeolites. The structure of carbon molecular sieve membranes can be idealized as a slit-like structure [17, 18], which is shown in Figure 2.3. The pore size distribution, which is largely dependent upon precursor materials and preparation protocols, can be represented by the bimodal pore size distribution [17, 18], as shown in Figure 2.5. The unique combination of ultramicropores (< 5 Å, responsible for molecular sieving) and micropores (5 Å-20 Å, responsible for sorption) enables CMS membranes to be ideal for gas separations.

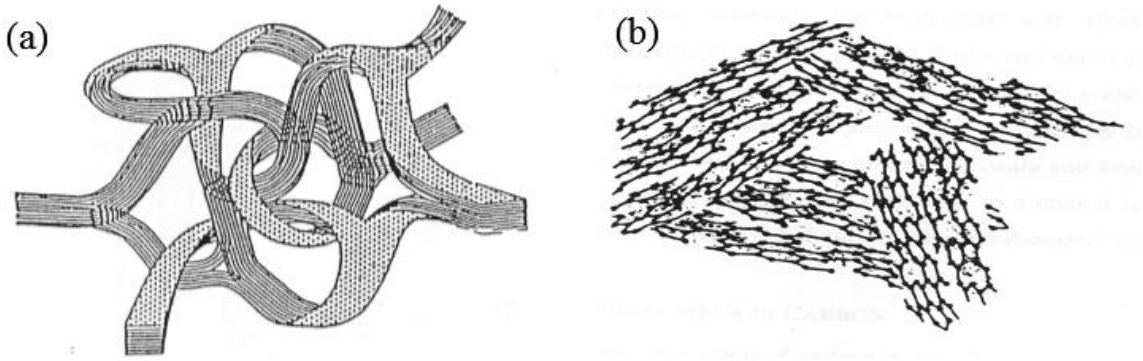

Figure 2.4 (a) Structure of turbostratic carbon [16]; (b) Slit-like pores formed from imperfect packing of microcrystallite regions in turbostratic carbon [15]

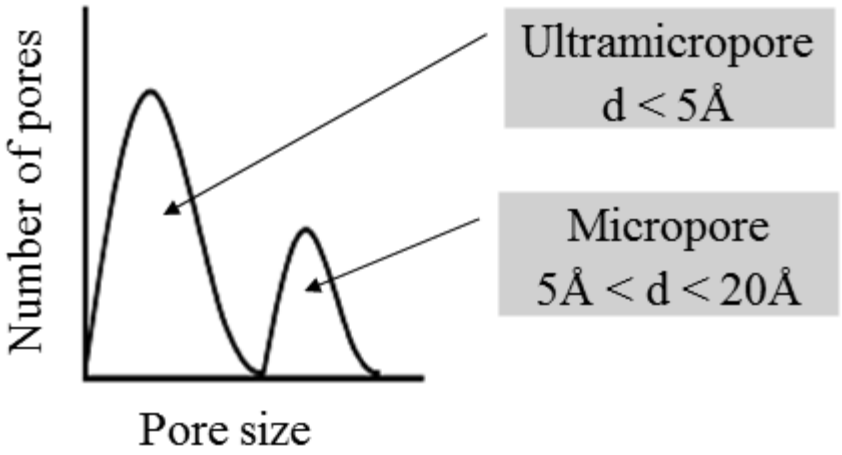

Figure 2.5 Bimodal pore size distribution for carbon molecular sieve materials [17, 18]

2.2.2 Formation of CMS membranes

CMS membranes are produced from controlled pyrolysis of precursor polymer membranes. The formation procedure includes the formation of precursor materials and subsequent pyrolysis steps for carbonization and structural rearrangement. The starting materials and each processing step of the membrane fabrication affect resultant CMS membrane performance. CMS membranes can be prepared in various formats, but mostly flat sheets and hollow fibers are preferred. Starting precursor materials have a significant impact on CMS membrane fabrication. The impact affects all aspects of resultant carbon membranes. The pyrolysis step transforms polymer materials into carbon materials, which creates the microporous structure of carbon membranes for gas separations. During pyrolysis, several parameters that affect the pore size distribution have been identified: (1) pyrolysis temperature; (2) thermal ramp rate; (3) thermal soak time; (4) pyrolysis atmosphere. Sometimes, before and after pyrolysis, pre-treatment and post-treatment methods are also important. These primary parameters are discussed in details below.

2.2.2.1 CMS membrane configuration

Like polymers, carbon membranes can be processed into different configurations [6]. They can be generalized into two groups, supported and unsupported. Supported carbon membranes are usually produced from polymer membrane cast on flat-sheet or tubular porous inorganic materials. Unsupported or so-called free-standing membranes can be mainly categorized into two forms: flat sheet film (dense homogeneous or asymmetric) and hollow fiber. The supported membranes are usually used for lab-scale research. The porous inorganic supports (i.e., aluminum support, ceramic support) are

quite expensive for large scale membrane fabrication. Moreover, considering the membrane area to volume ratio, supported carbon membranes are not favorable compared to hollow fiber membranes. Due to structural simplicity, free-standing homogeneous dense film carbon membranes are the best for studying fundamentals of the material fabrication and characterization. Considering scale-up potential and industrial viability, unsupported hollow fiber carbon membranes are of particular interest of this research.

2.2.2.2 Polymer precursor

A wide variety of polymers have been used as CMS precursors. Several polymer types that have been investigated extensively includes polyimides [17-21], polyacrylonitrile (PAN) [22], phenolic resin [23, 24], polyfurfuryl alcohol (PFA) [25, 26], poly(vinylidene) based polymers [27], and cellulose derivatives [28]. Because of their high glass transition temperature, ease of processability, high separation performance and good mechanical properties, polyimides have been chosen as precursor materials by many researchers. In addition, carbon fibers from several polyimides have been successfully fabricated, which offers valuable guiding information in terms of both precursor fiber spinning and pyrolysis [19, 29, 30].

The correlation of the structure of precursor polymers and final CMS microstructure and properties is a very interesting and important topic in carbon membrane research. Several studies have been recently performed to illustrate the guiding relationship [8, 31]. In most studies, a series of polymers were processed and pyrolyzed under the same conditions to compare the resultant CMS membrane properties.

One aspect of such correlations is that the precursor free volume can impact the

pore volume of CMS structure, so the intrinsic transport properties of CMS membranes can be correlated to the precursor polymer transport properties. Polyimides can be synthesized from various diamines and dianhydrides and copolymers can also be used to further tune the intrinsic transport properties of polyimides. When coupled with the tenability offered by pyrolysis conditions, an almost unlimited array of properties is achievable. To study the impact of starting materials, commercially available polyimide Matrimid® and non-commercial 6FDA/BPDA-DAM have been used as precursors for both CMS dense film and hollow fiber. The gas pairs investigated were CO_2/CH_4 (natural gas separation), O_2/N_2 (air separation) and also C_3H_6/C_3H_8 (olefin/paraffin separation) [12, 17-19, 30]. Comparative study in dense film and fiber showed that under the same pyrolysis conditions Matrimid® derived CMS membranes were more selective and less permeable than 6FDA/BPDA-DAM derived CMS membranes [17, 18]. The trend in transport behavior was supported by pore size distribution analysis from CO_2 sorption isotherms. The cumulative pore volume for pores in the range of 4 Å - 11 Å was approximately 39% and 30% larger for the 6FDA/BPDA-DAM derived material as compared to the corresponding Matrimid® derived materials at 550 ℃ and 800 ℃, respectively. This trend suggests that the intrinsically more packing-disrupted 6FDA/BPDA-DAM precursor leads to a more permeable CMS material than the more densely packed Matrimid®.

In the current study, besides the precursor intrinsic transport properties, more parameters are introduced and evaluated for CMS hollow fiber membrane formation.

2.2.2.3 Pyrolysis temperature protocol

Pyrolysis is the key step for carbon materials formation. The carbonization reaction requires a certain high temperature. The temperature protocol includes several parameters: pyrolysis temperature (the highest temperature during a pyrolysis), ramp rate (the heating rate reaching the highest temperature) and thermal soak time (the time at which the membrane is held at the highest pyrolysis temperature).

Pyrolysis temperature is usually selected at a temperature above its decomposition temperature but well below graphitization temperature. The temperature should be high enough to decompose polymers and transform them into a carbon form; however, to maintain the porous structure, a densely packed graphitic structure is not desirable. For most studies, pyrolysis temperatures are between 500 ^{o}C and 800 ^{o}C. Pyrolysis temperature has a strong impact on the CMS membrane properties in terms of permeability and selectivity. The optimum temperature depends on the precursor used and the specific application as well. Generally, an increase in pyrolysis temperature results in a decrease in permeability and an increase in selectivity [12, 17, 30, 32]. The optimum pyrolysis temperature depends upon various purposes of applications. For example, pyrolysis temperature suitable for producing small pores suitable for hydrogen separation membranes probably is not appropriate for propylene/propane separation, which requires larger pores. The effect of pyrolysis temperature on CMS structure can be illustrated by Figure 2.6. The ultramicropores are tightened at high temperature; meanwhile, the adsorptive micropore size may also decrease. This trend may result in reduction in both diffusion coefficient and sorption coefficient.

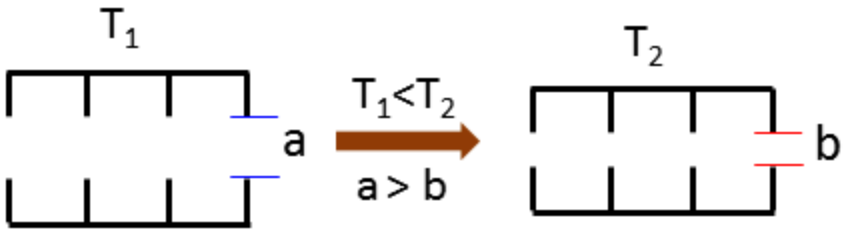

Figure 2.6 Effect of pyrolysis temperature on CMS membrane microstructure

Increasing ramp rate tends to increase the permeability and to lower the selectivity [33, 34]. This dependence may be explained by two reasons: (1) the rate of evolution of by-products and (2) the pyrolysis time that allows pore sintering to occur. Besides the impact on microstructure of CMS membranes, attention must be paid to the ramp rate near the final pyrolysis temperature. A slow "buffering" or stabilization step is usually used to avoid overheating of membranes above the desired pyrolysis temperature, based on the furnace control capacity.

Most decomposition reactions occur during the ramp steps. During the thermal soak stage, mostly, the microstructure of the carbon membrane is finely tuned to achieve desired transport properties. The effect is probably caused by sintering of the pores and narrowing the pore size distribution by pore sintering. Further decomposition may be another secondary factor and the thermal soak time and the pyrolysis temperature are often coupled to achieve a desired result. At a certain pyrolysis temperature, increasing the thermal soak time increases the selectivity and decreases the permeability of the CMS membranes. Usually, the impact is more obvious on the permeability while the selectivity is affected less [17, 18, 30].

2.2.2.4 Pyrolysis atmosphere

The systematic study about the impact of pyrolysis atmosphere can be traced to the middle 1990s by Geiszler and Koros [35]. Before the study mentioned above, both inert purge and vacuum pyrolysis techniques have been used in separate studies but never compared [35]. Recent developments regarding pyrolysis atmospheres are important for the production of CMS membranes in a controlled manner [8, 36]. Besides the repeatability issue, pyrolysis atmosphere can now be effectively used as a tool to tailor the microstructure of CMS membranes. The major parameters concerning pyrolysis atmosphere are: vacuum versus inert gas purge and oxygen content in a purge gas. Recently, vacuum pyrolysis has been realized to lack reproducibility, due to the poor control of subtle vacuum levels. The vacuum level in a pyrolysis tube is strongly correlated to the oxygen exposure of carbon membranes during pyrolysis since the leaks are due to air. Vacuum levels can be affected by the sealing of pyrolysis systems and the power of vacuum pumps used. Therefore, a slight modification of pyrolysis setup may lead to significant changes of pyrolysis atmosphere. Controlled inert gas purge has been demonstrated to be advantageous over vacuum pyrolysis, especially for practical scale-up. The positive pressure in pyrolysis tubes helps avoid the invasion of oxygen from atmosphere. Oxygen can selectively chemisorb on the edges of ultramicropores [37, 38], and thus significantly affect the molecular sieving properties of carbon membranes. Oxygen doping method has been developed by Kiyono, Williams and Koros as a tool to tune carbon membrane transport properties [38-40]. CO_2/CH_4 separation is a very successful example that benefits from the new tool: an optimum “ppm-scale” oxygen level was shown to exist for the natural gas separation. The mechanism of oxygen doping

can be illustrated by Figure 2.7. At the same pyrolysis temperature, oxygen chemisorbs to the "tips" of pores in carbon membranes. By using oxygen doping, the "collapse" of micropores is avoided when high pyrolysis temperature is applied to achieve high selectivity. Therefore, from this perspective, the sorption capacity is maintained when oxygen doping is applied. Based on the reactive nature of oxygen with carbon materials, alternative dopants may be pursued for future research. Of course, besides the oxygen level, the pyrolysis temperature at which oxygen doping is applied must be optimized as well. The application of oxygen doping should be coordinated with pyrolysis temperature, precursor polymers and target gas pairs.

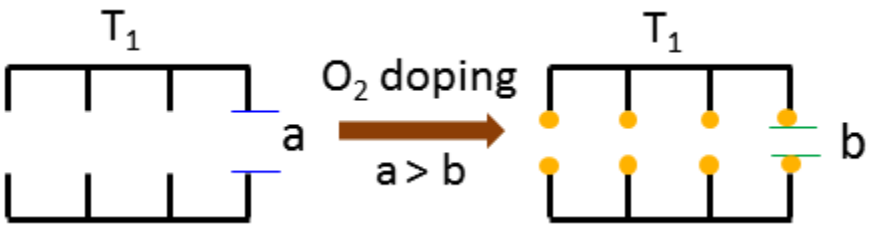

Figure 2.7 Effect of oxygen doping on CMS membrane microstructure

2.2.2.5 Pre-treatment and post-treatment

Several pretreatments have been used to stabilize precursors. The main method is oxidation. Oxidative stabilization can cause oxidation and cyclization in PAN fibers [22]. Previous researchers also reported that the oxidative treatment produces more thermally stable structure of 6FDA/BPDA-DDBT derived carbon hollow fiber membranes [41, 42]. However, it seems that no systematic research on oxidative pre-treatment has been performed, especially about the effect on membrane separation performance. In fact, by

pre-treatment, essentially, the starting materials for pyrolysis are changed. In another words, pre-treatment creates new precursor materials for pyrolysis.

Several thermochemical post-treatments have been performed to finely adjust the pore dimensions and distributions. Post-oxidation is the favorite method. Chemical vapor deposition (CVD), post-pyrolysis and coating are also used [43]. Post-oxidation in air is usually used to increase the pore volume, so the permeability can be increased [44]. The challenge is to maintain a high selectivity simultaneously. By combining these methods, structure and separation performance can be tuned to a large extent. For example, post-oxidation and chemical vapor deposition have been investigated extensively by Soffer et al., and various protocols have been developed on cellulose derived CMS fibers for specific gas pairs [45].

2.3 Asymmetric hollow fiber membranes

2.3.1 Formation of asymmetric hollow fiber membranes

The final membrane format of this research is asymmetric carbon hollow fiber. To form asymmetric carbon hollow fiber membranes, the first step is to produce asymmetric polymeric hollow fiber membranes. The second step is the pyrolysis of polymer fibers while maintaining asymmetric hollow fiber morphology.

Asymmetric polymeric hollow fiber membranes are produced via a dry-jet/wet-quench spinning process [46-50], illustrated in Figure 2.8. The key spinning parameters are listed in Table 2.1. During a spinning process, dope (polymer solution) and bore fluid are coextruded from a spinneret into an air gap ("dry-jet") and then immersed into an aqueous quench bath ("wet-quench"). The "dry-jet" step produces the dense skin layer

while the "wet-quench" step forms the porous support structure.

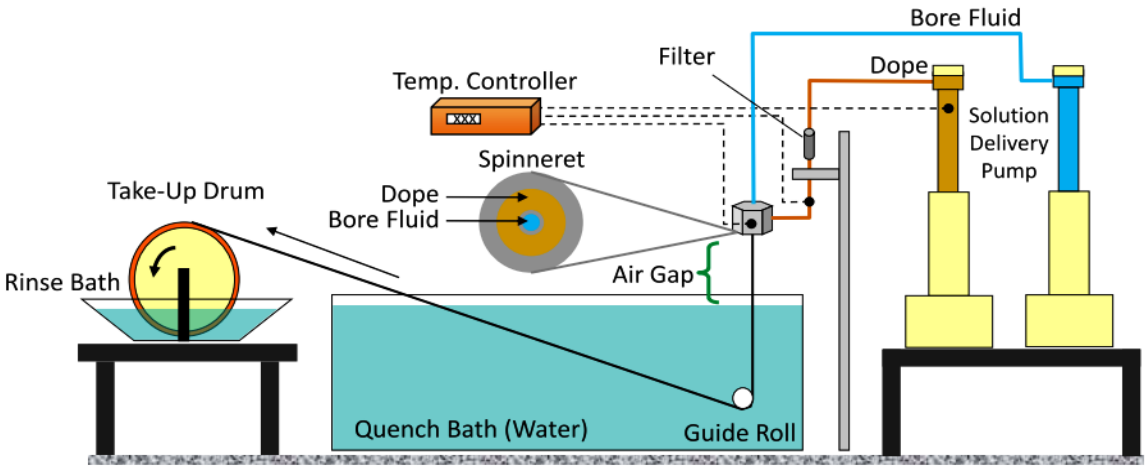

Figure 2.8 Schematic of the dry-jet/wet-quench spinning process for asymmetric hollow fiber membrane fabrication.

Table 2.1 Key parameters in a dry-jet/wet-quench hollow fiber spinning process

Dope composition	Air gap height	Quench bath temperature
Bore fluid composition	Take-up rate	Quench bath composition
Dope/bore fluid flow rate	Spinning temperature	Humidity

The qualitative dope composition trajectories during a spinning process are shown in Figure 2.9. Before spinning, the phase boundary (binodal line) is established. The dope composition should sit in the one phase region and close to the binodal line for rapid phase separation in the quench bath. In the air gap, due to the evaporation of volatile components in the dope, the composition is driven to the vitrified region and the dense skin layer is formed on the outer of fibers. In the water quench bath, non-solvent water diffuses into the polymer solution and induces phase separation. The polymer solution precipitates in the water quench and gain mechanical strength. The porous support

structure is formed during the phase separation step. In this way, a desirable asymmetric morphology, a dense layer on top of a porous substructure, is formed.

The hollow fiber configuration is formed by the extrusion of a bore fluid along with the dope. The bore fluid is a neutral fluid which occupies space and can be further removed during solvent exchange and drying steps.

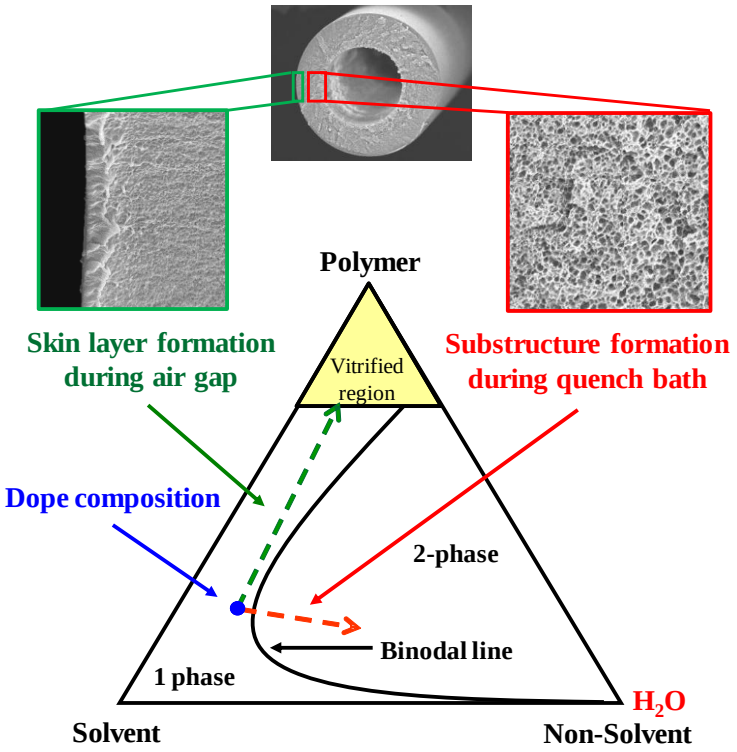

Figure 2.9 Ternary phase diagram demonstrating asymmetric hollow fiber membrane formation during a dry-jet/wet-quench spinning process

During the pyrolysis step, besides material transition from polymer into carbon, it is also critical to maintain the asymmetric morphology. Unlike asymmetric polymeric hollow fiber membranes, the morphology of CMS hollow fiber membranes has not been well studied. Especially, considering the complexity of asymmetric hollow fiber

membranes, maintaining the asymmetric morphology can be very challenging. The evolution of asymmetric hollow fiber morphology during pyrolysis is investigated intensively in this research.

2.3.2 Considerations regarding asymmetric hollow fiber properties

For asymmetric hollow fiber membranes, several properties are quite important for realistic applications. The key factors are skin integrity, skin layer thickness, substructure transport resistance and macroscopic properties.

Skin integrity is the most important property of asymmetric membranes. In asymmetric membranes, only the thin separation layer is ideally responsible for separations, while the majority of membrane structure only serves as non-selective support function. Therefore, it is critical that the skin layer is defect-free. In terms of polymeric membranes, defect-free typically means that the selectivity of asymmetric membrane is at least of 90% of the intrinsic dense film value [49]. Defective fibers result in ineffective separations. Considering the thickness of desired skin layer thickness (~100 nm), it is very challenging to develop integral asymmetric hollow fiber membranes. In the case of CMS hollow fiber membranes, few studies consider the defect-free properties. There is also almost no study correlating the precursor defect-free properties and resultant carbon fiber performance. In terms of skin integrity, in this research, it was found to be important to form defect-free precursor polymer fibers, then maintain the integral skin during intense heat-treatment. In addition, establishing relationships between precursor defect-free properties and resultant carbon fiber performance is important to guide the precursor fiber fabrication.

Separation layer thickness is very important for the productivity of a membrane. The main purpose of developing asymmetric membranes is to take advantages of the thin separation layer thickness. The actual productivity of a membrane is represented by the permeance, which is the permeability divided by effective membrane separation layer thickness. As far as the skin layer is integral and defect-free, for the same material, a thinner separation layer is always desirable. Currently, commercial membrane producers can form nearly defect-free membranes with relatively thin skins (i.e., less than 100 nm) [51]. The main challenge related to this research is to keep the thin separation layer thickness after intense heat-treatment. This issue is discussed intensively in this research.

Substructure resistance is another property that should be considered in asymmetric membranes [48, 51]. To illustrate the asymmetric membrane morphology in detail, the membrane cross-section is usually divided into three separate regions: the skin layer, the transition layer and the porous underlying substructure. Ideally, permeation should be dominated by the thin skin, with little or no contribution from the membrane substructure. If substructure resistance cannot be neglected, it may reduce both gas permselectivities and gas permeances, especially when performing separations involving fast gases such as H_2, He and CO_2. In most cases of carbon membranes for olefin/paraffin separations, substructure resistance could be considered as a secondary factor, but attention should still be paid to ensure that this factor does not affect the performance.

The macroscopic properties of asymmetric hollow fiber membranes should also be considered. The outer diameter (OD) of hollow fibers relates to the packing density of a hollow fiber module. Smaller diameter fibers are favored since they contribute more surface area per module and withstand higher pressure [2, 52]. Comparing to polymer

fibers, carbon fibers have higher pressure resistance due to the intrinsically higher mechanical strength. Previous work in carbon hollow fibers demonstrated that pressure resistance of carbon fiber up to 1000 psi [30]. Generally, ~200 micron outer diameter is desired. Usually, the inner diameter is designed to be half of the outer diameter [52]. Some undesirable macroscopic morphologies can jeopardize the mechanical strength of hollow fibers. These phenomena include non-concentric bore, oval shape, and macrovoids. Non-concentric bore is usually caused by the misalignment of the spinneret; oval shape is caused by the insufficient phase separation in quench bath; the formation of macrovoids is more complicated and is mainly related to the phase separation kinetics of the nascent membrane and can be avoided by higher draw ratio or higher polymer concentration [48, 53]. In this research, these macroscopic properties are also considered in the carbon fiber form. The resultant carbon fibers are tested under realistic conditions similar to operations in an ethylene plant.

2.4 References

[1] W.J. Koros, G.K. Fleming, Membrane-based gas separation, J. Membr. Sci. 83 (1993) 1-80.

[2] R.W. Baker, Membrane technology and applications, 2 ed., John Wiley & Sons Ltd, West Sussex, England, 2004.

[3] W.R. Vieth, J.M. Howell, J.H. Hsieh, Dual sorption theory, J. Membr. Sci. 1 (1976) 177-220.

[4] R.M. Barrer, J.A. Barrie, J. Slater, Sorption and diffusion in ethyl cellulose. Part III. Comparison between ethyl cellulose and rubber, J. Polym. Sci. 27 (1958) 177-197.

[5] W.J. Koros, Sorption and transport in glassy polymers, in: Chemical Engineering, The University of Texas at Austin, 1977.

[6] A.F. Ismail, L.I.B. David, A review on the latest development of carbon membranes for gas separation, J. Membr. Sci. 193 (2001) 1-18.

[7] P.J. Williams, W.J. Koros, Gas separation by carbon membranes, in: N.N. Li, A.G. Fane, W.W.S. Ho, T. Matsuura (Eds.) Advanced membrane technology and applications, John Wiley & Sons, Inc., 2008.

[8] P.J. Williams, Analysis of factors influenceing the performance of CMS membranes for gas separation, in: Chemical Engineering, Georgia Insitute of Technology, 2006.

[9] A.L. Hines, R.N. Maddox, Mass transfer fundamentals and applications, Prentice-Hall, Englewood Cliffs, New Jersey, 1985.

[10] M.B. Rao, S. Sircar, Nanoporous carbon membranes for separation of gas mixtures by selective surface flow, J. Membr. Sci. 85 (1993) 253-264.

[11] M.B. Rao, S. Sircar, Nanoporous carbon membrane for gas separation, Gas Sep. Purif. 7 (1993) 279-284.

[12] A. Singh-Ghosal, W.J. Koros, Air separation properties of flat sheet homogeneous pyrolytic carbon membranes, J. Membr. Sci. 174 (2000) 177-188.

[13] A. Singh-Ghosal, W.J. Koros, Energetic and entropic contributions to mobility selectivity in glassy polymers for gas separation membranes, Ind. Eng. Chem. Res. 38 (1999) 3647-3654.

[14] A. Singh, W.J. Koros, Significance of entropic selectivity for advanced gas separation membranes, Ind. Eng. Chem. Res. 35 (1996) 1231-1234.

[15] H.O. Pierson, Handbook of carbon, graphite, diamond, and fullerenes, Noyes Publication, Park Ridge, NJ, 1993.

[16] G.M. Jenkins, Polymeric carbons - carbon fiber, glass and char, Cambridge

University Press, 1976.

[17] K.M. Steel, W.J. Koros, An investigation of the effects of pyrolysis parameters on gas separation properties of carbon materials, Carbon 43 (2005) 1843-1856.

[18] K.M. Steel, W.J. Koros, Investigation of porosity of carbon materials and related effects on gas separation properties, Carbon 41 (2003) 253-266.

[19] C.W. Jones, W.J. Koros, Carbon molecular sieve gas separation membranes-I. Preparation and characterization based on polyimide precursors, Carbon 32 (1994) 1419-1425.

[20] H. Hatori, Y. Yamada, M. Shiraishi, H. Nakata, S. Yoshitomi, Carbon molecular sieve films from polyimide, Carbon 30 (1992) 719-720.

[21] A.B. Fuertes, D.M. Nevskaia, T.A. Centeno, Carbon composite membranes from Matrimid® and Kapton® polyimides for gas separation, Micropor. Mesopor. Mat. 33 (1999) 115-125.

[22] L.I.B. David, A.F. Ismail, Influence of the thermastabilization process and soak time during pyrolysis process on the polyacrylonitrile carbon membranes for O_2/N_2 separation, J. Membr. Sci. 213 (2003) 285-291.

[23] T.A. Centeno, A.B. Fuertes, Supported carbon molecular sieve membranes based on a phenolic resin, J. Membr. Sci. 160 (1999) 201-211.

[24] S.S. Wang, M.Y. Zeng, Z.H. Wang, Asymmetric molecular sieve carbon membranes, J. Membr. Sci. 109 (1996) 267-270.

[25] M.B. Shiflett, H.C. Foley, Ultrasonic deposition of high-selectivity nanoporous carbon membranes, Science 285 (1999) 1902-1905.

[26] M. Acharya, H.C. Foley, Spray-coating of nanoporous carbon membranes for air separation, J. Membr. Sci. 161 (1999) 1-5.

[27] T.A. Centeno, A.B. Fuertes, Carbon molecular sieve gas separation membranes based on poly(vinylidene chloride-co-vinyl chloride), Carbon 38 (2000) 1067-1073.

[28] J.E. Koresh, A. Sofer, Molecular-sieve carbon permselective membrane. Part 1. Presentation of a new device for gas-mixture separation, Sep. Sci. Technol. 18 (1983) 723-734.

[29] C.W. Jones, W.J. Koros, Carbon molecular-sieve gas separation membranes-II. Regeneration following organic exposure, Carbon 32 (1994) 1427-1432.

[30] D.Q. Vu, W.J. Koros, S.J. Miller, High pressure CO_2/CH_4 separation using carbon molecular sieve hollow fiber membranes, Ind. Eng. Chem. Res. 41 (2002) 367-380.

[31] K.M. Steel, Carbon membranes for challenging gas separations, in: Chemical Engineering, The University of Texas at Austin, 2000.

[32] D.S. Lafyatis, J. Tung, H.C. Foley, Poly (furfuryl alcohol)-derived carbon molecular sieves: dependence of adsorptive properties on carbonization temperature, time, and poly (ethylene glycol) additives, Ind. Eng. Chem. Res. 30 (1991) 865-873.

[33] H. Suda, K. Haraya, Gas permeation through micropores of carbon molecular sieve membranes derived from Kapton polyimide, J. Phys. Chem. B 101 (1997) 3988-3994.

[34] H. Hatori, Y. Yamada, M. Shiraishi, M. Yoshihara, T. Kimura, The mechanism of polyimide pyrolysis in the early stage, Carbon 34 (1996) 201-208.

[35] V.C. Geiszler, W.J. Koros, Effects of polyimide pyrolysis conditions on carbon molecular sieve membrane properties, Ind. Eng. Chem. Res. 35 (1996) 2999-3003.

[36] M. Kiyono, Carbon molecular sieve membranes for natural gas separations, in: Chemical Engineering, Georgia Institute of Technology, 2010.

[37] R.O. Grisdale, The properties of carbon contacts, J. Appl. Phys. 24 (1953) 1288-1296.

[38] M. Kiyono, P.J. Williams, W.J. Koros, Effect of pyrolysis atmosphere on separation performance of carbon molecular sieve membranes, J. Membr. Sci. 359 (2010) 2-10.

[39] M. Kiyono, P.J. Williams, W.J. Koros, Generalization of effect of oxygen exposure on formation and performance of carbon molecular sieve membranes, Carbon 48 (2010) 4442-4449.

[40] M. Kiyono, P.J. Williams, W.J. Koros, Effect of polymer precursors on carbon molecular sieve structure and separation performance properties, Carbon 48 (2010) 4432-4441.

[41] N. Tanihara, H. Shimazaki, Y. Hirayama, S. Nakanishi, T. Yoshinaga, Y. Kusuki, Gas permeation properties of asymmetric carbon hollow fiber membranes prepared from asymmetric polyimide hollow fiber, J. Membr. Sci. 160 (1999) 179-186.

[42] Y. Kusuki, H. Shimazaki, N. Tanihara, S. Nakanishi, T. Yoshinaga, Gas permeation properties and characterization of asymmetric carbon membranes prepared by pyrolyzing asymmetric polyimide hollow fiber membrane, J. Membr. Sci. 134 (1997) 245-253.

[43] S.M. Saufi, A.F. Ismail, Fabrication of carbon membranes for gas separation - a review, Carbon 42 (2004) 241-259.

[44] A.B. Fuertes, Effect of air oxidation on gas separation properties of adsorption-selective carbon membranes, Carbon 39 (2001) 697-706.

[45] A. Soffer, Azariah A., AmarA., Cohem H., Golub D., Saguee S., Method of improving the selectivity of carbon membranes by chemical vapor deposition, in: United States Patent, United States, 1997.

[46] C.-C. Chen, W. Qiu, S.J. Miller, W.J. Koros, Plasticization-resistant hollow fiber membranes for CO_2/CH_4 separation based on a thermally crosslinkable polyimide, J.

Membr. Sci. 382 (2011) 212-221.

[47] I.C. Omole, S.J. Miller, W.J. Koros, Increased molecular weight of a cross-linkable polyimide for spinning plasticization resistant hollow fiber membranes, Macromolecules 41 (2008) 6367-6375.

[48] M.R. Kosuri, W.J. Koros, Defect-free asymmetric hollow fiber membranes from Torlon®, a polyamide-imide polymer, for high-pressure CO_2 separations, J. Membr. Sci. 320 (2008) 65-72.

[49] S.B. Carruthers, G.L. Ramos, W.J. Koros, Morphology of integral-skin layers in hollow-fiber gas-separation membranes, J. Appl. Polym. Sci. 90 (2003) 399-411.

[50] D.T. Clausi, W.J. Koros, Formation of defect-free polyimide hollow fiber membranes for gas separations, J. Membr. Sci. 167 (2000) 79-89.

[51] D.T. Clausi, S.A. McKelvey, W.J. Koros, Characterization of substructure resistance in asymmetric gas separation membranes, J. Membr. Sci. 160 (1999) 51-64.

[52] S.A. McKelvey, D.T. Clausi, W.J. Koros, A guide to establishing hollow fiber macroscopic properties for membrane applications, J. Membr. Sci. 124 (1997) 223-232.

[53] S. Husain, W.J. Koros, Macrovoids in hybrid organic/inorganic hollow fiber membranes, Ind. Eng. Chem. Res. 48 (2009) 2372-2379.

CHAPTER 3

MATERIALS AND EXPERIMENTAL METHODS

This chapter describes the materials and experimental methods. First, the polymers and gases used in this research are described; second, the membrane fabrication procedures for both polymer and carbon membranes are discussed in detail; third, gas permeation methods and other characterization techniques are presented.

3.1 Materials

3.1.1 Polymers

Polyimides are the primary precursor polymer materials for this research. Three polyimides were studied extensively for both polymer and carbon membrane fabrication and characterization. Matrimid® is a commercially available polyimide purchased from Huntsman International LLC. 6FDA-DAM and 6FDA/BPDA-DAM were in-house synthesized or custom synthesized by Akron Polymer Systems, Inc. The structures of the three polyimides are shown in Figure 3.1. 6FDA/BPDA-DAM was synthesized via condensation of dianhydrides 6FDA and BPDA with diamine DAM, while in the 6FDA-DAM synthesis, no BPDA dianhydride was added. The synthesis was a two-step reaction in which the first step produced a high molecular weight polyamic acid at low temperature (~5 ^{o}C), and the second or chemical imidization step followed by a post-chemical drying step at 210 ^{o}C under vacuum yielded the polyimides. All polymers were dried under vacuum at 110 ^{o}C overnight before use.

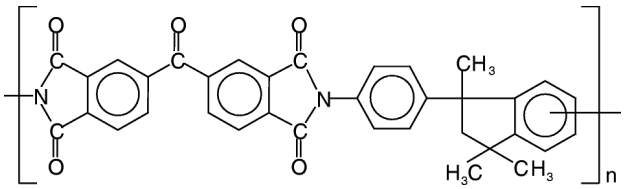

(a) Matrimid®

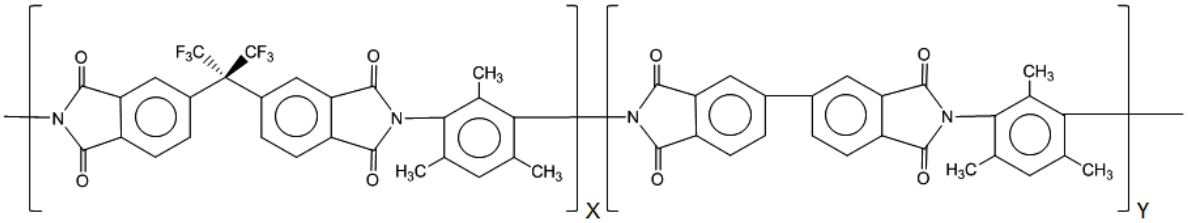

(b) 6FDA/BPDA-DAM (in this work, X:Y=1:1)

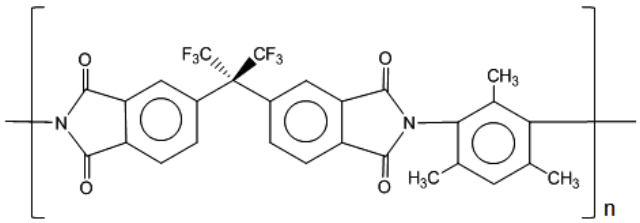

(c) 6FDA-DAM

Figure 3.1 Chemical structures of three primary precursor polyimides: (a) Matrimid®; (b) 6FDA/BPDA-DAM; (c) 6FDA-DAM

Besides the three primary polyimides, 6FDA-DAM/DABA (3:2) polyimide was also considered as a cross-linkable precursor. The structure of 6FDA-DAM/DABA (3:2) is shown in Figure 3.2. Defect-free 6FDA-DAM/DABA (3:2) asymmetric hollow fiber membranes were kindly provided by Chien-Chiang Chen [1].

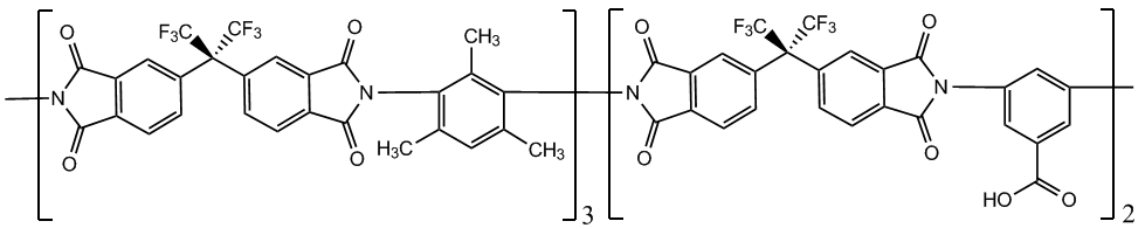

Figure 3.2 Chemical structure of 6FDA-DAM/DABA (3:2) polyimide

3.1.2 Gases

Gases were mainly used for permeation tests. Some gases were used as purge gas for pyrolysis. All pure gases (He, O_2, N_2, CH_4, CO_2, Argon, C_2H_4, C_2H_6, C_3H_6, C_3H_8) were purchased from Airgas. Argon gas with "ppm" level oxygen was purchased from Praxair. C_2H_4/C_2H_6 and C_3H_6/C_3H_8 gas mixtures were purchased from Praxair.

3.2 Membrane formation

Membrane formation in this research includes the formation of polymer membranes and subsequent pyrolysis step for producing carbon membranes.

3.2.1 Formation of asymmetric polymeric hollow fiber membranes

The membrane formats relevant to this research are flat sheet dense film and asymmetric hollow fiber. Research on flat sheet dense film membranes was used to explore the fundamentals of CMS membranes and this work was performed by my collaborator Meha Rungta [2]. Homogeneous polymeric dense films were formed using a solution casting method. The preparation procedure of film casting was described in

previous work [3-6]. The primary membrane format in this research is the more applicable hollow fiber membrane and is described in details.

Asymmetric hollow fiber spinning is a very complex process. One spinning trial usually takes weeks and many variables in the process may affect the membrane properties. The spinning process is divided into the sections below for further discussion: (1) dope formulation; (2) asymmetric hollow fiber spinning.

3.2.1.1 Dope formulation

Dope composition is usually regarded as the most important variable for the solution spinning process [1, 7-10]. The dope typically consists of the polymer, solvents and non-solvents. The purpose for adding non-solvents in the dope is to achieve fast phase separation in the water quench bath. One guideline for choosing solvents and non-solvents is the water miscibility, since water is the preferred quench bath medium. NMP (N-methylpyrrolidone) was chosen as the non-volatile solvent due to its strong interaction with the polymer, miscibility with water, and it is relatively benign from a health standpoint. THF (tetrahydrofuran) was chosen as the volatile solvent to assist skin layer formation. Ethanol was chosen as a non-solvent. Compared to the strong non-solvent water, ethanol is regarded as a weak non-solvent that allows a big window for tuning dope formulation. In addition, the high volatility of ethanol also assists the skin layer formation in the air gap. $LiNO_3$ (lithium nitrate) was sometimes added as an additive to assist phase separation and also build up viscosity.

Considerations of a good dope include “spinnability” and the potential for defect-free skin formation. Sufficient viscosity is the first factor required for a successful

spinning. Polymer molecular weight and polymer concentration are the dominant parameters for sufficient viscosity that allows polymer extrusion and taking-up as fibers. Ternary phase diagrams are constructed via the cloud point technique [1, 8]. At a fixed polymer concentration, a series of dope samples with increasing non-solvent amounts (and accordingly decreasing solvents amount) were made. With increasing non-solvent amount, the dope changes from one-phase into two-phase. The compositions on the phase boundary are called "cloud points", and these points together form the binodal line. The dope composition should sit in the one-phase region and be close to the binodal line. The formulation together with spinning conditions should drive the dope composition to the vitrified region, rapidly without crossing the two-phase region (entering the two-phase region may introduce defects in the skin layer). To achieve the optimum composition, the dope formulation step may be iterated based on the performance of resultant fibers.

3.2.1.2 Asymmetric hollow fiber spinning

Asymmetric hollow fiber membranes were formed via a dry-jet/wet-quench spinning process. Schematic of the spinning setup is described in Figure 2.8. Polymer powder was first dried in a vacuum oven at 110 ℃ overnight to remove moisture and residual organics. A spinning dope was then made in a Qorpak® glass bottle sealed with a Teflon® cap and dissolved by placing on a roller at room temperature. Sometimes, heat was applied to assist the dope mixing in some extremely viscous dopes. Once the dope was homogeneous based on visual inspection (usually several days), it was loaded into a 500-mL syringe pump (ISCO Inc., Lincoln, NE) and allowed to degasing overnight. Sometimes, a moderate temperature (i.e. 50 ^{o}C) was applied to facilitate the degas

process. Bore fluid was loaded into a separate 100-mL syringe pump. The dope and bore fluid were then co-extruded through a spinneret. Both the dope and the bore fluid were filtered in-line between the delivery pumps and the spinneret. Temperature control was applied for the spinning process. Thermocouples were placed on the spinneret, the dope filter and the dope pump. After passing through an air gap, the nascent membrane was immersed into a water quench bath. The phase-separated fiber line was collected on a 0.32 m diameter rotating polyethylene cylinder after passing over Teflon® guides. The rotating speed of the take-up drum is adjustable and can be used to control the draw ratio and fiber size. Once cut from the take-up drum, the fibers were rinsed in at least four separate water baths over a course of 48 hrs. The fibers were then solvent exchanged in glass containers with three separate 20 min methanol baths followed by 3 separate 20 min hexane baths and dried under vacuum at ~75 ℃ for ~3 hrs.

3.2.2 Pyrolysis

3.2.2.1 Pyrolysis setup

The pyrolysis setup was similar to previously reported systems [3, 6, 11, 12]; however, some modifications were made to achieve a better control of pyrolysis parameters. The schematic of the pyrolysis setup is shown in Figure 3.3. A 3-zone furnace (Thermcraft, Inc., model XST-3-0-24-3C, Winston-Salem, NC) was well controlled by a multi-channel temperature controller (Omega Engineering, Inc., model CN1504TC, Stamford, CT). With 3 thermocouples independently connected to 3 channels of the controller, the temperature distribution inside the quartz tube (National Scientific Company, GE Type 214 quartz tubing, Quakertown, PA) was quite uniform.

Sealing of the quartz tube was insured by an assembly of a metal flange with silicon O-rings (MTI Corporation, Richmond, CA), which was applied to both ends of the quartz tube. The furnace can be operated under vacuum or inert gas purge mode. For vacuum pyrolysis, a vacuum pump (RV3 Vacuum Pump, Edwards Ltd.) was equipped to evacuate the system and the vacuum level was monitored by a 0-1000 mtorr range pressure transducer (MKS, model 628 Absolute Capacitance Manometer, Andover, MA). For inert gas purge pyrolysis, an oxygen sensor (Rapidox 2100, Cambridge Sensotec Ltd, UK) was used to monitor the oxygen level in the tube throughout the pyrolysis process.

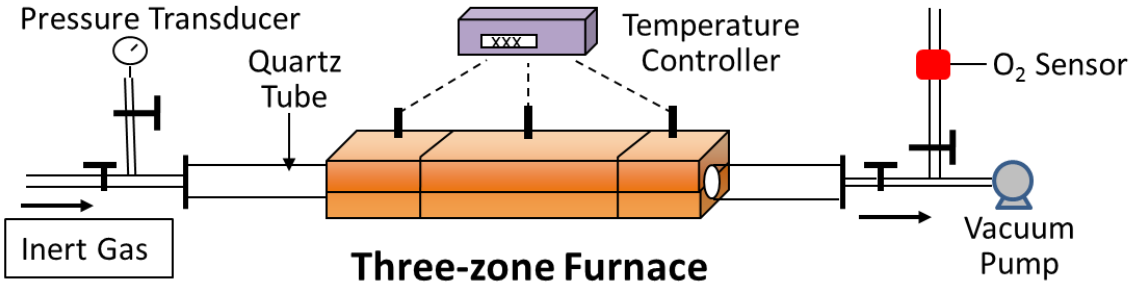

Figure 3.3 Schematic of the pyrolysis setup

3.2.2.2 Pyrolysis protocol

The pyrolysis processes for dense film and hollow fiber were quite similar, except that a quartz plate with 2 mm deep and 2 mm wide ribs (United Silica Products, Franklin, NJ) was used as the support for films and a stainless steel wire mesh plat (McMaster Carr, Robbinsville, NJ) was used as the support for hollow fibers. The hollow fibers on the mesh plate were bound separately with thin wires.

The pyrolysis atmosphere was either under vacuum or inert gas purge (sometimes

containing trace amount of oxygen). Under vacuum operations, the system was evacuated until the vacuum level in the quartz tube reached steady state. Usually, the vacuum level monitored was between 5 mtorr – 15 mtorr. In the case of inert gas (or inert gas with trace amount of oxygen) purge operations, the purge gas was controlled at a 200 sccm purge rate for most pyrolysis. The oxygen level in the pyrolysis tube was ensured to be stable and close to the cylinder value before launching the heating protocol. The initial purge mostly took more than 6 hours. In the case of low oxygen level, i.e., UHP argon purge pyrolysis, it took more purge time to reach the steady state. Oxygen level inside the tube was monitored throughout the pyrolysis process.

After the vacuum level or the oxygen level in the tube was stable, the heating protocol was launched. The pyrolysis temperature was between 500 ^{o}C and 800 ^{o}C. Most heating protocols were modified based on a typical 550 ^{o}C protocol used previously in Koros Research Group and found to be desirable. Temperature protocols A1 and A2 in Tables 3.1 and 3.2 were the mostly used ones. For Matrimid® pyrolysis, in the investigation of the effect of pyrolysis temperature, protocol A1 was used for 500 ^{o}C and 550 ^{o}C pyrolysis and protocol A2 was used for pyrolysis temperatures above 550 ^{o}C. These protocols feature slow ramp towards the final pyrolysis temperature.

Table 3.1 Pyrolysis temperature protocol A1

	Start temperature (℃)	End temperature (℃)	Ramp rate (℃/min)
Step 1	50	250	13.3
Step 2	250	T_{max}-15	3.85
Step 3	T_{max}-15	T_{max}	0.25
Step 4	T_{max}	T_{max}	Soak for 2 hrs

Table 3.2 Pyrolysis temperature protocol A2

	Start temperature (℃)	End temperature (℃)	Ramp rate (℃/min)
Step 1	50	250	13.3
Step 2	250	535	3.85
Step 3	535	550	0.25
Step 4	550	T_{max}-15	3.85
Step 5	T_{max}-15	T_{max}	0.25
Step 6	T_{max}	T_{max}	Soak for 2 hrs

For Matrimid® hollow fiber pyrolysis, another 675 ℃ temperature protocol (also referred as 675 ^{o}C, 10 min protocol) with short soak time was developed. The shorter ramp time and thermal soak time was used to increase the permeance of Matrimid® CMS hollow fiber.

Table 3.3 Pyrolysis temperature protocol B: a 675 ℃ temperature protocol with short soak time for the pyrolysis of hollow fibers

	Start temperature (℃)	End temperature (℃)	Ramp rate (℃/min)
Step 1	50	600	10
Step 2	600	675	2
Step 3	675	675	Soak for 10 min

Since the temperature protocol A2 in Table 3.2 contains the complete typical 550 ℃ temperature protocol, the ramp step of the protocol is relatively long. For pyrolysis temperature above 550 ^{o}C, protocol A1 (listed in Table 3.1) ignoring the 550 ^{o}C point was frequently used in later experiments.

After the heating cycle was complete, the furnace was allowed to cool down naturally to below 50 ℃ before venting and unloading samples. After each pyrolysis, the

quartz tube and wire mesh plate were rinsed and brushed with acetone and then baked in air at 800 ℃ for 2 hrs in order to remove deposited materials.

3.2.3 Hollow fiber module formation

Hollow fibers were potted into lab-scale membrane module for permeation tests. A typical module is shown in Figure 3.4. The detailed protocol for module making was documented previously [8, 12]. The number of fibers required for a membrane module was determined by the membrane transport properties and testing protocol. For fibers with slow permeation rates, multiple fibers were required to build up the flux for testing. Mostly, due to the difficulty of carbon fiber formation, single-fiber modules for carbon fiber were mostly used. Multiple-fiber modules (up to 25 fibers) were also constructed.

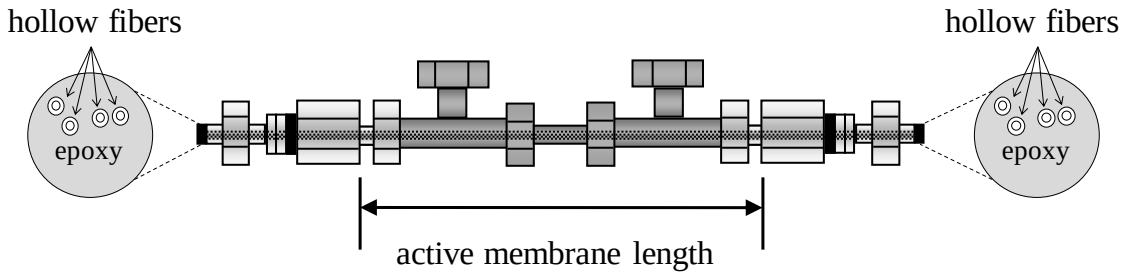

Figure 3.4 Schematic of a lab-scale hollow fiber membrane module

3.3 Membrane characterization

3.3.1 Pure gas permeation

Permeation tests for precursor fibers were mostly performed with a constant pressure system, which was described in previous work [9, 10]. The measurements were

taken at 35 ℃ using a feed on the bore side of the fiber at nominally 100 psig with permeate at atmospheric pressure. Bubble flowmeters were used to measure gas permeation rate. The 100 psig feed pressure was only applied for gases without plasticization effect, i.e., O_2, N_2, He. In the case of feed gases that may plasticize asymmetric polymer membranes, i.e., CO_2, C_2H_4, C_2H_6, C_3H_6, C_3H_8, the feed gas pressure was controlled at a relatively low level (1~2 atmospheric pressure) to avoid any changes that may occur to the membrane material. For some fibers with low permeation flux, a constant volume permeation system was used to measure the gas permeation. Some fibers were measured in both systems and the results were very consistent (<5% deviation).

For CMS hollow fiber, a constant pressure permeation system was used as well if the permeation rate was high. In most cases, a constant volume permeation system was used, which was similar to the concept of most dense film tests and similar procedures were also applied [13, 14]. After evacuation of both upstream and downstream, leak test was performed to make sure the leak rate was less than 1% of the permeation rate. After the leak rate was ensured at a low level, the shell side of module was exposed to feed gas at desired feed pressure (mostly 100 psi in this research), while the bore side pressure rise was monitored by a pressure transducer (MKS, Model 127AA, Andover, MA) and recorded by Labview (National Instruments, Austin, TX). The rate of pressure rise was used to calculate permeance of fibers.

3.3.2 Mixed gas permeation test

Mixed gas permeation test were used to evaluate membrane performance under

realistic conditions. In this research, ethylene/ethane mixed gas permeation test was the most investigated one. Constant volume permeation systems were used. Mixed gas permeation was performed with 63.2 mol% ethylene/ 36.8 mol% ethane mixture, which was close to the industrial feed composition. Similar to the pure gas tests, feed was introduced at shell side of the hollow fiber module and permeate was collected at bore side. The stage cut (ratio of permeate flow rate to feed flow rate) was maintained less than 1% to avoid concentration polarization. The selectivity was calculated from the GC (gas chromatography) analysis of permeate composition, while permeance was obtained from the pressure rise in the downstream. Steady state was insured by multiple analyses of permeate composition with GC as well as time lag check. Based on the pressure rise rate on the permeate side, an overall permeation rate was obtained. The downstream mixture composition analyzed by GC was used to split the permeation rate into individual components. The driving force for each component was calculated by the partial pressure difference between upstream and downstream.

Multi-component olefin/paraffin mixed gas permeation was performed in a Dow laboratory by Mark Brayden and Gregory Barbay. Multiple feed pressure and testing temperatures were used. In one case, for some specific membrane module, due to flow requirement of downstream side mass flowmeter, 30 psig argon was used as permeate sweep and again gas chromatography was used to analyze the permeate composition. In another particular case, the membrane test was performed at cryogenic conditions (0 ^{o}F) to simulate the realistic industrial conditions. Details about testing conditions are described in each test.

3.3.3 Other characterization techniques

3.3.3.1 Scanning electron microscopy

Scanning electron microscopy (SEM) was used to characterize the morphology of precursor and CMS hollow fiber membranes. The LEO 1530 and LEO 1550 SEM were equipped with a thermally assisted field emission gun, and the operation voltage was 10 kV. For polymeric fibers, the fibers were soaked in hexane and then shear fractured in liquid nitrogen using tweezers to preserve the morphology of hollow fiber cross-sections. For carbon fibers, the hexane and liquid nitrogen soaking steps were not performed. All fibers were coated with gold before SEM examinations.

3.3.3.2 Differential scanning calorimetry

Differential scanning calorimetry (DSC) was used to analyze the glass-rubber transition of polymer samples. The measurement was performed on a TA Q200 instrument. A heat-cool-heat protocol with 10 ^{o}C/min heating and cooling rate was used. Transition in the second heat step was used to analyze the glass-rubber transition temperature.

3.3.3.3 Dynamic mechanical analysis

Dynamic mechanical analysis (DMA) was used to analyze the rigidity of polymers. Thin dense films, prepared by solution casting, were used for analysis. The films were cut into rectangular geometry for experiments. The analysis was performed using a TA Q800 DMA instrument. Storage modulus and loss modulus were measured in

temperature sweep mode (1 Hz; 3 ^{o}C/min).

3.3.3.4 Gel permeation chromatography

Molecular weight (M_w) and polydispersity (PDI) of polymer samples were analyzed by using gel permeation chromatography (GPC) by American Polymer Standards Corporation (Mentor, OH). The samples were dissolved in THF at 1 mg/mL concentration. Polystyrene standards were used for calibration. Some GPC results were also provided by Akron Polymer Systems, Inc.

3.3.3.5 Thermogravimetric analysis

Thermogravimetric analysis (TGA) was conducted on a thermogravimetric analyzer (Q5000, TA Instruments) at a heating rate of 10 ^{o}C/min under nitrogen purge.

3.3.3.6 X-ray photoelectron spectroscopy

X-ray photoelectron spectroscopy (XPS) was performed on a Thermo K-Alpha XPS system. The analysis provided elemental information of samples.

3.3.3.7 Raman spectroscopy

Raman spectroscopy for carbon samples was performed on a Thermo Scientific* Nicolet Almega XR Micro and Macro Raman Analysis System. It was used to analyze carbon structures.

3.4 References

[1] C.-C. Chen, W. Qiu, S.J. Miller, W.J. Koros, Plasticization-resistant hollow fiber membranes for CO_2/CH_4 separation based on a thermally crosslinkable polyimide, J. Membr. Sci. 382 (2011) 212-221.

[2] M. Rungta, Carbon molecular sieve dense film membranes for ethylene/ethane separations, in: Chemical Engineering, Georgia Institute of Technology, 2012.

[3] M. Kiyono, P.J. Williams, W.J. Koros, Effect of pyrolysis atmosphere on separation performance of carbon molecular sieve membranes, J. Membr. Sci. 359 (2010) 2-10.

[4] K.M. Steel, W.J. Koros, An investigation of the effects of pyrolysis parameters on gas separation properties of carbon materials, Carbon 43 (2005) 1843-1856.

[5] K.M. Steel, W.J. Koros, Investigation of porosity of carbon materials and related effects on gas separation properties, Carbon 41 (2003) 253-266.

[6] M. Rungta, L. Xu, W.J. Koros, Carbon molecular sieve dense film membranes derived from Matrimid® for ethylene/ethane separation, Carbon 50 (2012) 1488-1502.

[7] I.C. Omole, S.J. Miller, W.J. Koros, Increased molecular weight of a cross-linkable polyimide for spinning plasticization resistant hollow fiber membranes, Macromolecules 41 (2008) 6367-6375.

[8] M.R. Kosuri, W.J. Koros, Defect-free asymmetric hollow fiber membranes from Torlon®, a polyamide-imide polymer, for high-pressure CO_2 separations, J. Membr. Sci. 320 (2008) 65-72.

[9] D.T. Clausi, W.J. Koros, Formation of defect-free polyimide hollow fiber membranes for gas separations, J. Membr. Sci. 167 (2000) 79-89.

[10] S.B. Carruthers, G.L. Ramos, W.J. Koros, Morphology of integral-skin layers in hollow-fiber gas-separation membranes, J. Appl. Polym. Sci. 90 (2003) 399-411.

[11] L. Xu, M. Rungta, W.J. Koros, Matrimid® derived carbon molecular sieve hollow fiber membranes for ethylene/ethane separation, J. Membr. Sci. 380 (2011) 138-147.

[12] D.Q. Vu, W.J. Koros, S.J. Miller, High pressure CO_2/CH_4 separation using carbon molecular sieve hollow fiber membranes, Ind. Eng. Chem. Res. 41 (2002) 367-380.

[13] D.G. Pye, H.H. Hoehn, M. Panar, Measurement of gas permeability of polymers. II. Apparatus for determination of permeabilities of mixed gases and vapors, J. Appl. Polym. Sci. 20 (1976) 287-301.

[14] D.G. Pye, H.H. Hoehn, M. Panar, Measurement of gas permeability of polymers. I. Permeabilities in constant volume/variable pressure apparatus, J. Appl. Polym. Sci. 20 (1976) 1921-1931.

CHAPTER 4

FORMATION OF ASYMMETRIC POLYMERIC PRECURSOR HOLLOW FIBER MEMBRANES

Chapter 1 describes the need for robust high performance carbon molecular sieve hollow fiber membranes for olefin/paraffin separations. Chapter 2 and 3 follow up with theory and background of gas transport in membranes, experimental protocols of membrane fabrication and characterization. To form CMS hollow fiber membranes, the first step is to spin asymmetric precursor hollow fiber membranes. A key challenge is to produce defect-free asymmetric hollow fiber membranes. In this chapter, the details of developing such asymmetric hollow fiber membranes are described. The analyses of asymmetric hollow fiber structure and transport properties are also discussed in detail. The precursor fibers developed in this chapter are used for subsequent pyrolysis studies in following chapters.

4.1 Overview of defect-free asymmetric fiber spinning

In the background, it was noted that asymmetric hollow fiber membrane is the desired membrane format for large scale gas separations. In order to achieve effective separations of gas molecules with sub-Angstrom size difference, the defect-free skin layer is regarded as a critical feature of asymmetric hollow fiber membranes. In the current industrial scale membrane fabrication, nearly defect-free membranes can be formed. Usually, a caulking step (or so-called silicon rubber post-treatment) is applied to caulk pinhole defects in the skin layer and has been proved to be effective. However, the

caulked membranes may not be stable under aggressive feed conditions. In general, we found it to be desirable to form defect-free asymmetric hollow fiber membranes with thin skin layer thickness. Before this study, the impact of precursor defect-free properties on CMS membrane performance was not clear. Defects in the skin layer introduce an undesirable additional variable for the carbon membrane fabrication, so, to simplify the complexity of carbon membrane formation, it is wise to work with defect-free polymeric fibers for pyrolysis. After bench marking with defect-free precursor fibers, the effect of defect-free properties on CMS membrane performance can be investigated by incorporating partially defective precursor fibers.

Defect-free asymmetric fiber spinning is very challenging, and it is truly amazing that such a thin defect-free layer can be formed on top of the porous support structure during the high-speed dry-jet/wet-quench spinning. Pores of ~ 5 Å wide in the skin layer exceeding area fractions of one in one million will render the entire membrane ineffective [1], thereby making the requirement for skin integrity of asymmetric membranes challenging, indeed. Lack of a comprehensive theoretical framework for this complex process introduces the need for systematic art development to achieve the most desirable precursor morphology. Usually, it takes several iterations for developing desired defect-free asymmetric hollow fiber membranes, and so far, only a few polymers have currently been spun into defect-free asymmetric hollow fiber membranes.

Three polyimides (Matrimid®, 6FDA-DAM and 6FDA/BPDA-DAM) are the primary precursor polyimides in this research. Matrimid® is a commercially available polyimide and has been investigated extensively. Defect-free asymmetric Matrimid® hollow fiber spinning has been reported by Clausi and Koros. So far, no defect-free

6FDA-DAM and 6FDA/BPDA-DAM asymmetric hollow fiber membranes have been reported. In the following sections, defect-free fiber spinning of each polymer is described in detail.

4.2 Asymmetric Matrimid® hollow fiber membrane spinning

4.2.1 Review of Matrimid® spinning

Since defect-free asymmetric Matrimid® hollow fiber membrane has been reported previously, the current research is based on the previous dope composition and spinning conditions. While the chemical structure of Matrimid® remains the same, molecular weight (M_w) and polydispersity index (PDI) of the polymer still vary from batch to batch and bring extra challenges into hollow fiber spinning. This fact means that the Matrimid® fiber spinning presented here is a typical example that can provide a starting point to tune, based on specific differences in batch to batch samples.

Clausi and Koros reported the defect-free Matrimid® fiber spinning for the first time [2], and Carruthers and Koros investigated the details of integral skin layer formation of Matrimid® hollow fiber membranes [1]. The first study proposed an excellent dope formulation, and the second study verified the viability the proposed conditions. The reported Matrimid® hollow fiber had the same selectivity as the dense film, while the thinnest defect-free skin layer was only ~100 nm thick. The dope composition and spinning conditions are listed in Tables 4.1 and 4.2, respectively.

Table 4.1 Dope composition of defect-free asymmetric Matrimid® hollow fiber spinning [2]

Component	wt%
Matrimid®	26.2
NMP	53
THF	5.9
Ethanol	14.9

Table 4.2 Spinning conditions for defect-free asymmetric Matrimid® hollow fiber membranes [2]

Spinning parameter	Value
Dope flow rate	180 mL/hr
Bore fluid flow rate	60 mL/hr
Bore fluid composition	96 wt%/4 wt% NMP/H_2O
Take-up rate	50 m/min
Quench bath temperature	25 ^oC
Spinneret temperature	50 ^oC
Air gap height	2.5-18.5 cm

To verify the defect-free properties, O_2/N_2 selectivity is commonly used due to its low degree of interaction with polymer materials. For defect-free fibers, He/N_2 selectivity is commonly used to evaluate the substructure resistance. Therefore, these two gas pairs are important for examining precursor hollow fiber membrane properties. The intrinsic gas transport properties for most common gases in Matrimid® are listed in Table 4.3.

Table 4.3 Gas transport properties in Matrimid® membranes at 35 °C

Material	Permeability (Barrer)					Selectivity				
	O_2	C_2H_4	CO_2	C_3H_6	He	$\frac{O_2}{N_2}$	$\frac{C_2H_4}{C_2H_6}$	$\frac{CO_2}{CH_4}$	$\frac{C_3H_6}{C_3H_8}$	$\frac{He}{N_2}$
Matrimid®	2.0	0.45	9.9	0.1	23	6.7	4.5	36	10	122

Pure gas feed, <100 psi, C_3H_6 and C_3H_8 data were cited from previous work [3]

4.2.2 Fiber spinning – initial trials

The conditions mentioned above had been used over past years in Koros Research Group, and were found to be quite desirable. At the beginning of this research, the previous batch of Matrimid® polyimide was consumed, and a new batch of polymer was purchased from Huntsman International LLC. In order to spin defect-free fiber from this new polymer batch, a ternary phase diagram was constructed to confirm the phase behavior of this new polymer batch. The previously reported phase diagram used pure NMP or 50 wt%/50 wt% NMP/THF as solvent(s); however, the actual optimized dope composition reported used 90 wt%/10 wt% NMP/THF as solvents [2]. In order to better identify the phase behavior, in this research, 90 wt%/10 wt% NMP/THF was used to construct the ternary phase diagram, as shown in Figure 4.1. Based on the new phase diagram, the spinning dope composition (listed in Table 4.1) sits in the one-phase region and was very close to the binodal line (only 2-3 wt% difference). This verifies that the dope formulation is also suitable for this new batch.

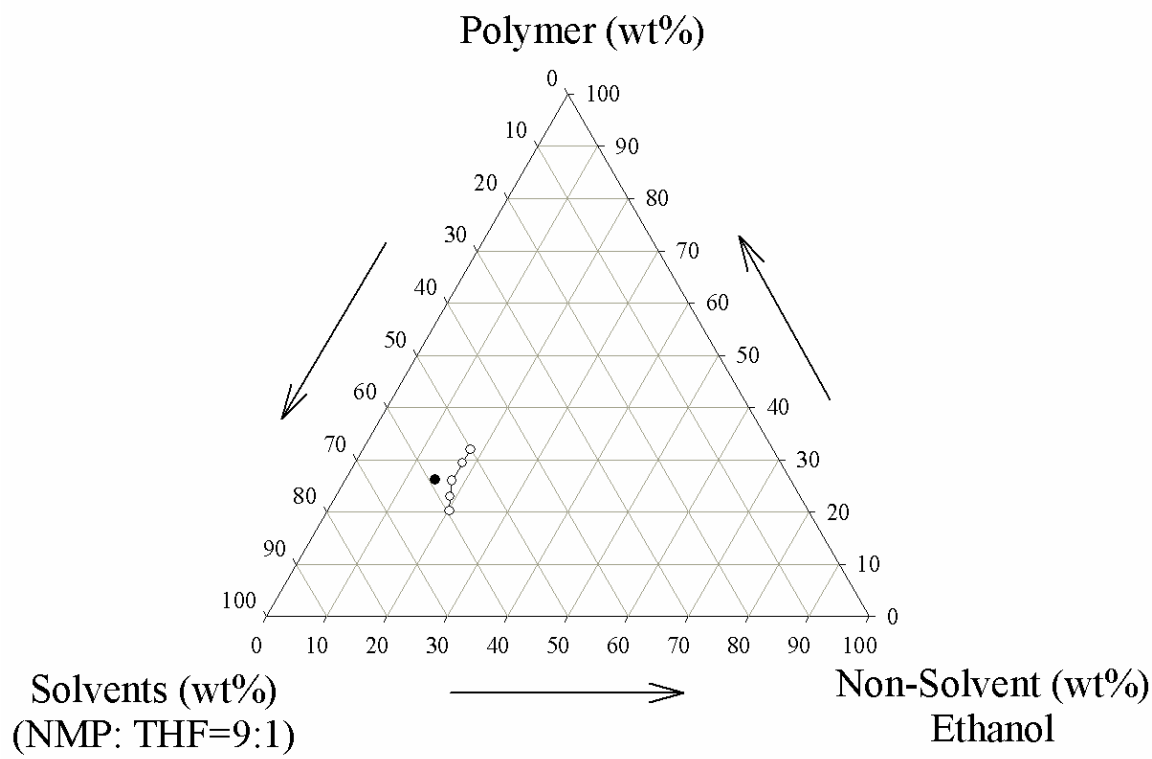

Figure 4.1 Ternary phase diagram of Matrimid®. Open circle: compositions on the phase boundary; solid circle: spinning dope composition

The first several spinning trials aimed to repeat the spinning conditions listed in Table 4.2. All the spinning conditions were repeated exactly. However, with the new polymer batch, the resultant fibers were defective based on permeation results. The ideal O_2/N_2 selectivity was around 6.7, while these fibers showed selectivity well below the idea value. SEM was used to investigate the overall morphology and skin layer of Matrimid® hollow fiber. During the spinning and post-spinning processing, by visual observation, it was found that some of the fibers had an oval shape rather than an desired round shape. The fiber shape was confirmed by SEM, as shown in Figure 4.2. The skin layer of the asymmetric hollow fiber membrane was illustrated in Figure 4.3. It was very clear that a dense layer sat on the top of the fiber. It was hypothesized that the overall

skin layer formation was not totally bad, but some small pinhole defects in the skin layer compromised the overall selectivity. The overall shape indicated that the phase separation in the water quench bath was too slow. When the nascent fiber contacts the guiding roll in the water quench bath, insufficient mechanical strength caused the collapse of the overall shape, and the "shape collapse" may also cause small defects in the skin layer.

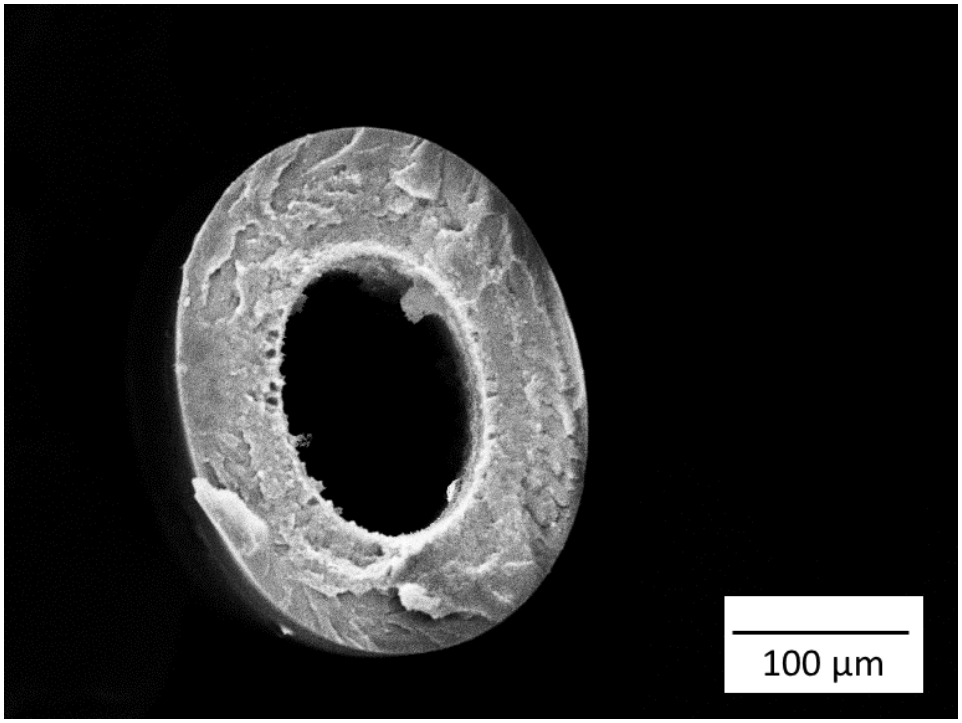

Figure 4.2 SEM picture of the cross-section of a Matrimid® fiber from the first spinning trials

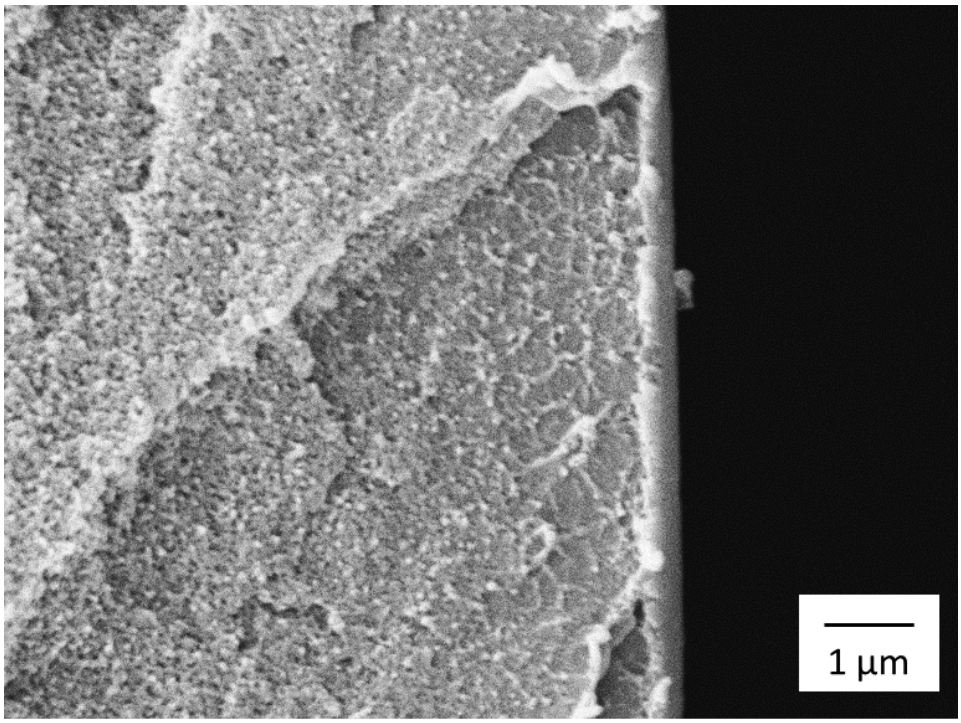

Figure 4.3 SEM picture of the skin layer of a Matrimid® fiber from the first spinning trials

While the defects in the skin layer cannot be "visually" observed by any existing technology, the observation of the macroscopic properties during spinning process becomes very important, since, sometimes, these properties may indicate issues related to the microscopic skin integrity.

Besides polymer properties, the phase separation rate also relies on the diffusion of non-solvent water into the spinning dope and the counter diffusion of solvents from the dope to the quench bath. The viscosity of a dope plays an important role in the phase separation. The mass transfer coefficient is also strongly correlated to the viscosity of the polymer solution [4, 5], so high dope viscosity may cause a slow phase separation rate. Viscosity measurement was carried out for the old and new polymer batches and the results are shown in Figure 4.4. The composition of the polymer solution was the same as

the prior spinning dope, and it was found that the new polymer had much higher viscosity. This discovery indicated that the mass transfer rate was reduced by the increased viscosity. While the chemical structure of Matrimid® polyimide remains the same, properties such as molecular weight and molecular weight distribution can play a role. Gel permeation chromatography (GPC) was used to determine the molecular weight and PDI. The results are shown in Table 4.4. The new polymer has a higher molecular weight, thereby explaining the higher viscosity of the dope formulated from the new polymer.

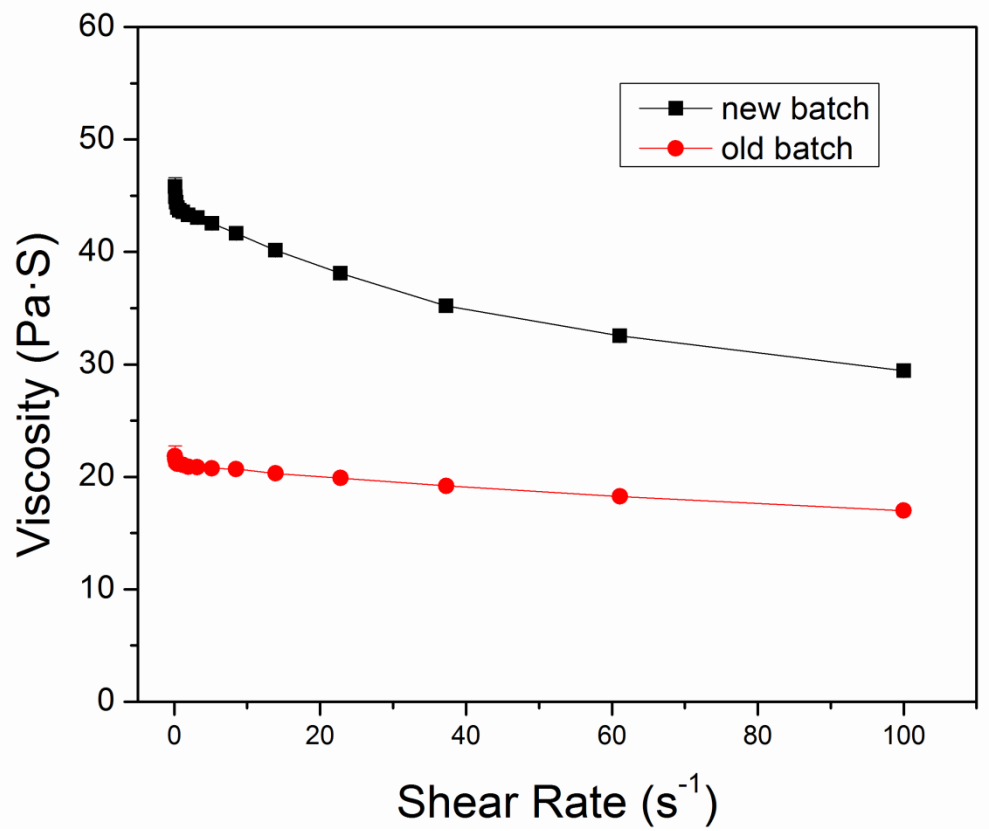

Figure 4.4 Comparison of viscosity of spinning dopes made from old and new Matrimid® batches (50 °C)

Table 4.4 GPC results of the old and new Matrimid® batches

Batch	M_w (Da)	PDI (M_w/M_n)
Old	63600	3.79
New	72500	4.12

Results provided by American Polymer Standards Corporation

4.2.3 Defect-free fiber spinning

The strategy for moving toward defect-free fiber spinning with the new polymer batch was to accelerate the phase separation rate with the same dope composition. Therefore, the dope formulation was kept the same, and some external variables were adjusted to meet the challenge of phase separations. The three key adjustments were: (1) the spinneret temperature was increased from ~50 ^oC to ~60 ^oC, in order to further increase the solvents/non-solvent evaporation in the air gap and facilitate the skin formation; (2) the water quench bath temperature was increased from ~25 ^oC to ~50 ^oC, in order to increase the mass transfer rate in water bath and increase the phase separation rate; (3) the take-up rate was decreased from 50 m/min to 10-30 m/min, in order to increase the residential time of spinning line in the water quench and also decrease the stress when the line was guided by the guiding roll.

After the above improvement, defect-free asymmetric Matrimid® hollow fiber membranes were successfully spun. Precursor fiber O_2/N_2 selectivity was raised to 6.0-6.7, which was above 90% of the intrinsic value (6.7) of Matrimid®. The best spinning state showed exactly 6.7 O_2/N_2 selectivity with skin layer thickness less than 200 nm. The SEM pictures of the cross-section and skin layer of a defect-free hollow fiber are shown in Figures 4.5 and 4.6.

Previously, the importance of skin layer formation in the air gap was clearly demonstrated [1], while the impact of quench condition on defect-free properties was not well documented. This study illustrated that improper phase separation conditions may also introduce defects into the skin layer. Therefore, during the dry-jet/wet-quench spinning, attention must be paid to both steps.

Several new dope formulations were also tried in this research. This includes the adjustment of polymer concentration, the ratio of volatile/non-volatile solvents and the incorporation of other additives such as lithium nitrate. However, none of these endeavors appeared to be advantageous over the old dope formulation proposed by Clausi and Koros. The formulation of spinning dope, at this point, is as noted earlier, still largely an “art”.

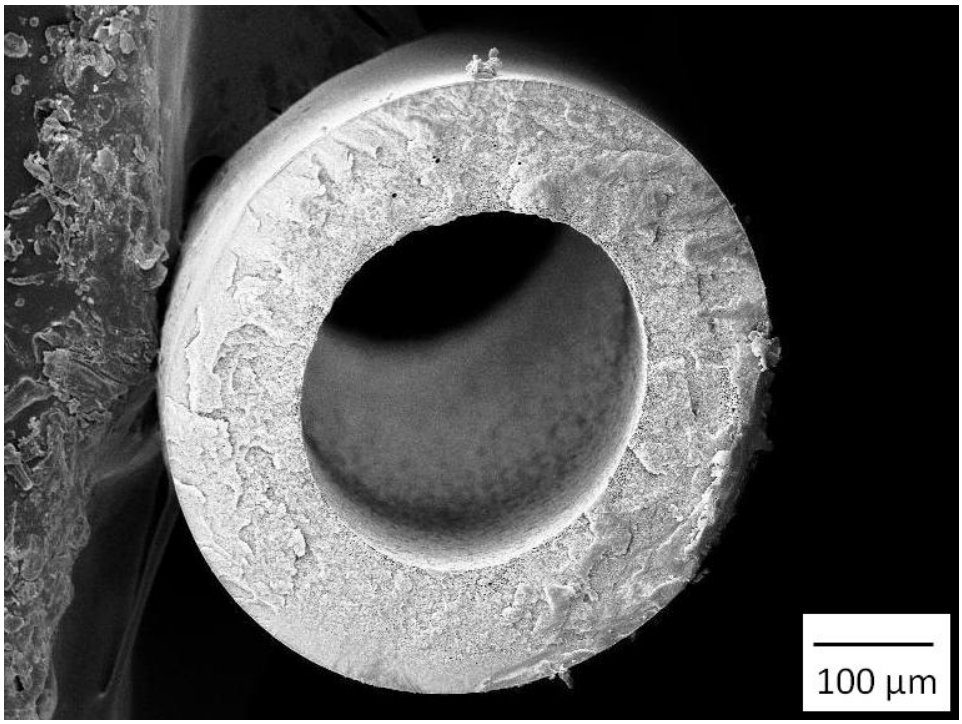

Figure 4.5 SEM picture of the cross-section of a defect-free Matrimid® hollow fiber

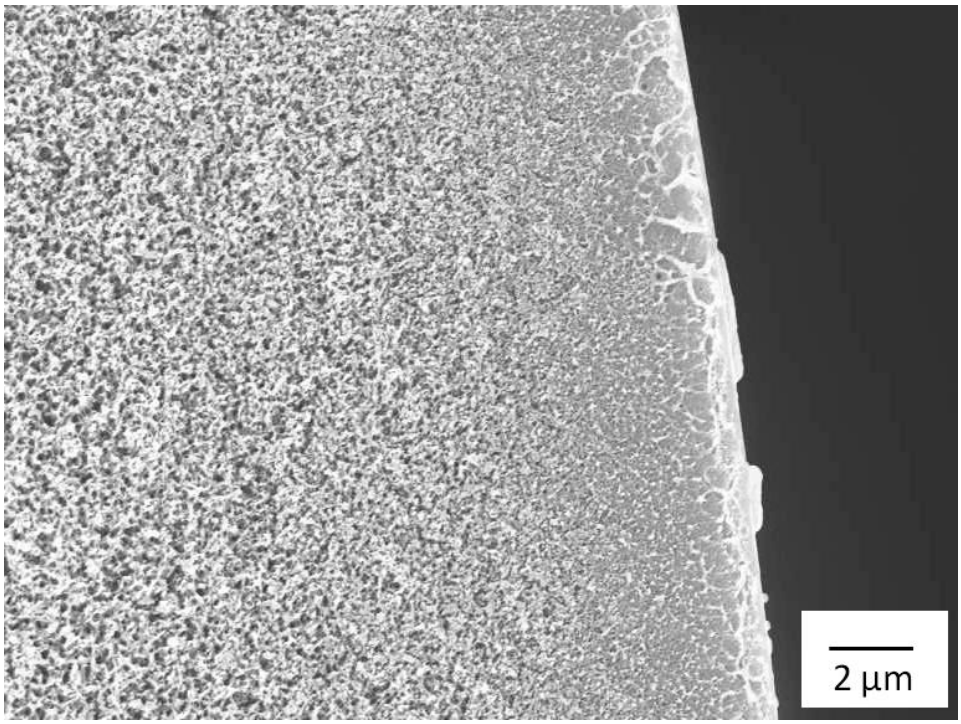

Figure 4.6 SEM picture of the skin layer of a defect-free Matrimid® hollow fiber

4.3 Asymmetric hollow fiber membrane spinning from 6FDA-DAM and 6FDA/BPDA-DAM polyimides

4.3.1 Properties of 6FDA-polymers

Due to the high rigidity and versatility of monomer choices, 6FDA-based polyimides are of great interest in membrane materials research. Unlike the commercially available Matrimid®, 6FDA-polymers are currently primarily in-house synthesized. The batch size of synthesis, control of polymer molecular weight and molecular weight distribution remain as issues for consistent lab-scale hollow fiber spinning. So far, no polymeric membranes based on 6FDA-polymers have been commercialized.

Several attempts in defect-free fiber spinning have been performed by previous

researchers on 6FDA-polymers. Wallace started the exploration of asymmetric hollow fiber membrane formation based on 6FDA-DAM/DABA (4:1) polyimide [6]. Omole formed defect-free PDMC (1,3-propanediol monoesterified cross-linkable) (3:2) polyimide asymmetric hollow fiber membranes [7]. Chen successfully spun defect-free asymmetric 6FDA-DAM/DABA (3:2) polyimide hollow fiber membranes [8]. Liu explored dual-layer fiber spinning of 6FDA-DAM polyimide on a cellulose acetate support; however, the attempt was not quite successful in terms of defect-free skin formation [9]. 6FDA/BPDA-DAM fiber spinning has been studied by Weinberg [10]; however, no defect-free asymmetric fiber formation was reported. In addition, dimethyl sulfoxide (DMSO) was used as one of the solvents, and the skin permeability of DMSO to human health made the previous process very unfavorable. Therefore, 6FDA-DAM and 6FDA/BPDA-DAM were two quite new polyimides for defect-free asymmetric hollow fiber membrane formation.

A key property of 6FDA-polymers is that they appear to be more "hydrophilic" than Matrimid® polyimide. The "hydrophiliicity" term here does not mean a small water droplet contact angle on polymer films. Instead, in terms of phase diagrams, "hydrophilic" polymer means the binodal line is closer to the non-solvents angle, which means more non-solvents are required for phase separation on the same level of polymer concentration. This has been demonstrated by Wallace by comparing 6FDA-DAM/DABA (4:1) polyimide and Matrimid®. Therefore, attention must be paid for the slow phase separation problem. In order to achieve sufficient phase separation in the water quench bath, dope formulation is the primary variable and spinning conditions are secondary factors to consider.

In past research, the low molecular weight of synthesized polymer appeared to be a problem for fiber spinning [11], and higher molecular weight were needed to provide sufficient viscosity for a spinnable dope. In this research, for both 6FDA-DAM and 6FDA/BPDA-DAM, the quality of polymer was excellent for hollow fiber spinning. The GPC results of polymers used in this research are shown in Table 4.5.

Table 4.5 GPC results of 6FDA-DAM and 6FDA/BPDA-DAM polymers

Polymer	Batch	M_w (kDa)	PDI (M_w/M_n)
6FDA-DAM	1	526	2.29
	2	165	1.92
6FDA/BPDA-DAM	1	160	1.85
	2	117	2.51

Results provided by Akron Polymer Systems, Inc.

Gas transport properties in 6FDA-DAM and 6FDA/BPDA-DAM dense film membranes were first determined, as shown in Table 4.6.

Table 4.6 Gas transport properties in 6FDA-DAM and 6FDA/BPDA-DAM membranes at 35 ^{o}C

Material	Permeability (Barrer)				Selectivity			
	O_2	C_2H_4	CO_2	C_3H_6	$\frac{O_2}{N_2}$	$\frac{C_2H_4}{C_2H_6}$	$\frac{CO_2}{CH_4}$	$\frac{C_3H_6}{C_3H_8}$
6FDA-DAM	135	64	817	15.7	3.5	3.0	17.6	12.4
6FDA/BPDA-DAM	64	46	309	11.8	4.1	3.3	22	13

Pure gas feed, <100 psi; 6FDA/BPDA-DAM CO_2, CH_4, C_3H_6 and C_3H_8 data were cited from Steel's work [3], 6FDA-DAM C_3H_6 and C_3H_8 data were cited from Chen's work [12]

4.3.2 6FDA-DAM fiber spinning

4.3.2.1 6FDA-DAM fiber spinning - 1st attempt

For the 1st 6FDA-DAM fiber spinning, a similar solvent system to that used for Matrimid® spinning was used. NMP was used as the non-volatile solvent, THF was used as the volatile solvent, and ethanol was used as the volatile non-solvent. The polymer used was Batch 1 6FDA-DAM listed in Table 4.5.

This work aims to develop an efficient approach to spin asymmetric hollow fiber membranes. The first step is to determine the polymer concentration based on the viscosity of dope. The guideline is to achieve sufficient viscosity for spinnability. In this system, viscosity is mostly determined by the polymer concentration. A high concentration is preferred for the skin layer formation. However, at high polymer concentration, it may take very long time for dope mixing or sometimes the polymer can even not be dissolved. Therefore, the strategy is to find a high polymer concentration that can also be handled efficiently. Experimentally, this objective was achieved by using a series of dopes with polymer dissolved in NMP only. The optimum polymer concentration was empirically decided by observing the homogeneity and viscosity of polymer dopes. A 22 wt% 6FDA-DAM dope was found to be a reasonable polymer concentration.

The second step required determination of optimum levels of solvents and non-solvent. This requires a ternary phase diagram. To simply the phase diagram construction, the volatile solvent THF was first fixed at 10 wt% and was found to be desirable based on previous work [13]. Altering the ratio of solvent NMP-to-ethanol finalized the phase boundary. The resultant ternary phase diagram is shown in Figure 4.7.

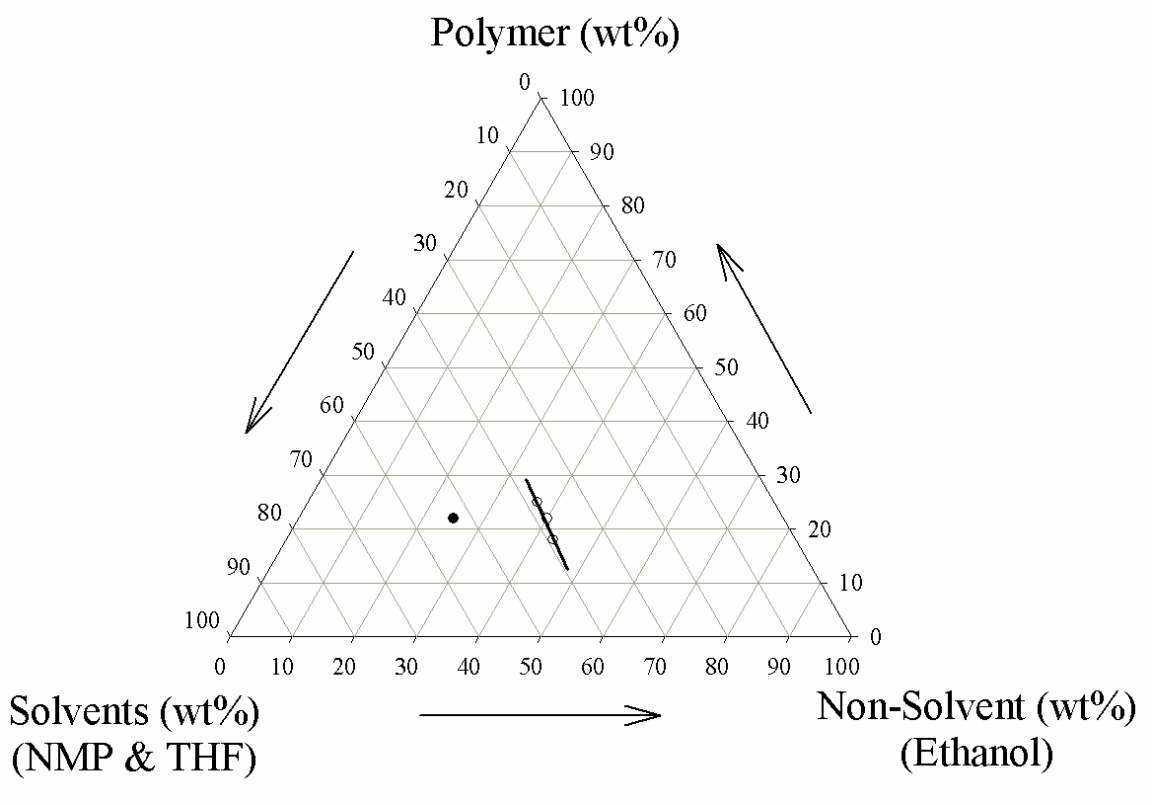

Figure 4.7 Ternary phase diagram of 6FDA-DAM (without $LiNO_3$). Open circle: compositions on the phase boundary; solid circle: spinning dope composition

Based on the above assessment of spinnability and phase behavior, the dope composition for the 1st 6FDA-DAM spinning was determined, as shown in Table 4.7 and the dope composition relative to the phase boundary is shown in Figure 4.7.

The spinning conditions are listed in Table 4.8. In order to keep the neutral nature of the bore fluid, the bore fluid composition was adjusted to 80 wt% NMP/20 wt% H_2O, as compared to 96 wt% NMP/4 wt% H_2O for Matrimid®. A high spinneret temperature (70 ^oC) was used to accelerate the evaporations of volatiles. In most states, 50 ^oC water quench temperature was used to accelerate phase separation. During spinning, it was observed that a fast take-up rate (> 10 m/min) caused the fiber wall collapse at the first Teflon guide. This was caused by the insufficient phase separation. The mechanical

strength of the fiber was insufficient to maintain the shape of fibers. To reduce the stress, a slow take-up rate (5 m/min) was used for spinning. Also, the ratio of dope flow rate to bore fluid flow rate was adjusted to 1:1, in order to create a large bore and thin fiber wall. Even at very low dope flow rate (50 mL/hr), the spinning line was still quite stable and uniform fiber size was obtained. The solvent exchange and drying protocols were the same as Matrimid® spinning.

Table 4.7 Dope composition of 6FDA-DAM hollow fiber spinning (1st attempt)

Component	wt%
6FDA-DAM	22
NMP	43
THF	10
Ethanol	25

Table 4.8 Spinning conditions for 6FDA-DAM hollow fiber membranes (1st attempt)

Spinning parameter	Value
Dope and bore fluid flow rate	50/50, 75/75,150/150 mL/hr
Bore fluid composition	80 wt%/20 wt% NMP/H_2O
Take-up rate	5 m/min
Quench bath temperature	20, 50 ^oC
Spinneret temperature	70 ^oC
Air gap height	5-30 cm

SEM pictures of one spinning state are shown in Figure 4.8. Figure 4.8 (a) shows the overall cross-section of a hollow fiber; Figure 4.8 (b) shows the morphology of the fiber wall; Figure 4.8 (c) shows the skin layer of the fiber. Overall, the macroscopic properties were reasonable. In this particular state, the skin layer thickness was more than

2 μm from the SEM observation, and this was further verified by the gas permeation measurement.

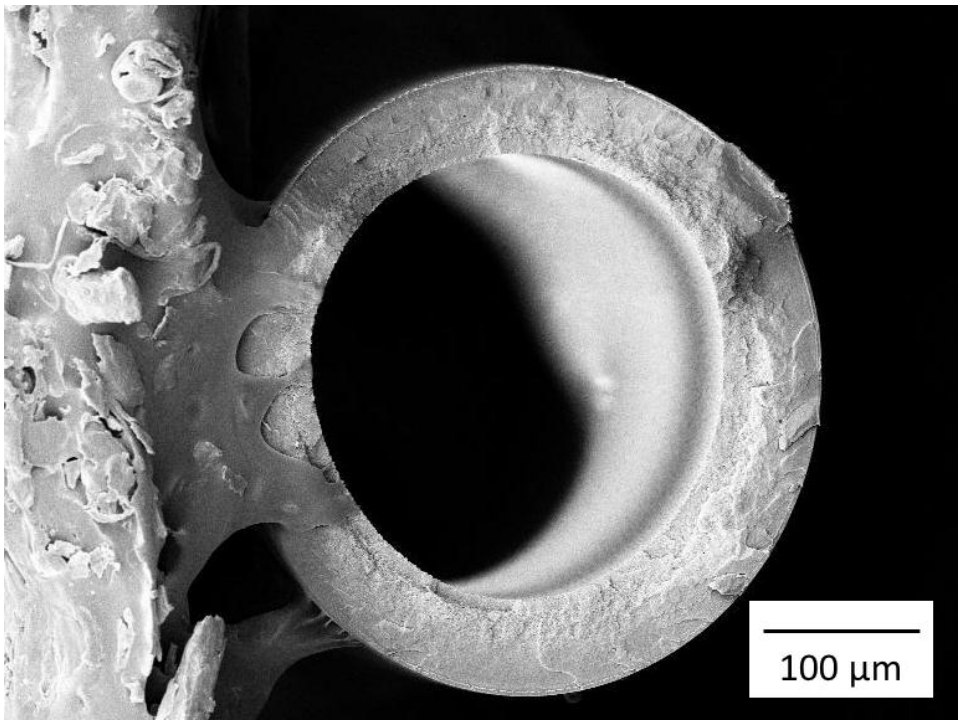

(a) Cross-section

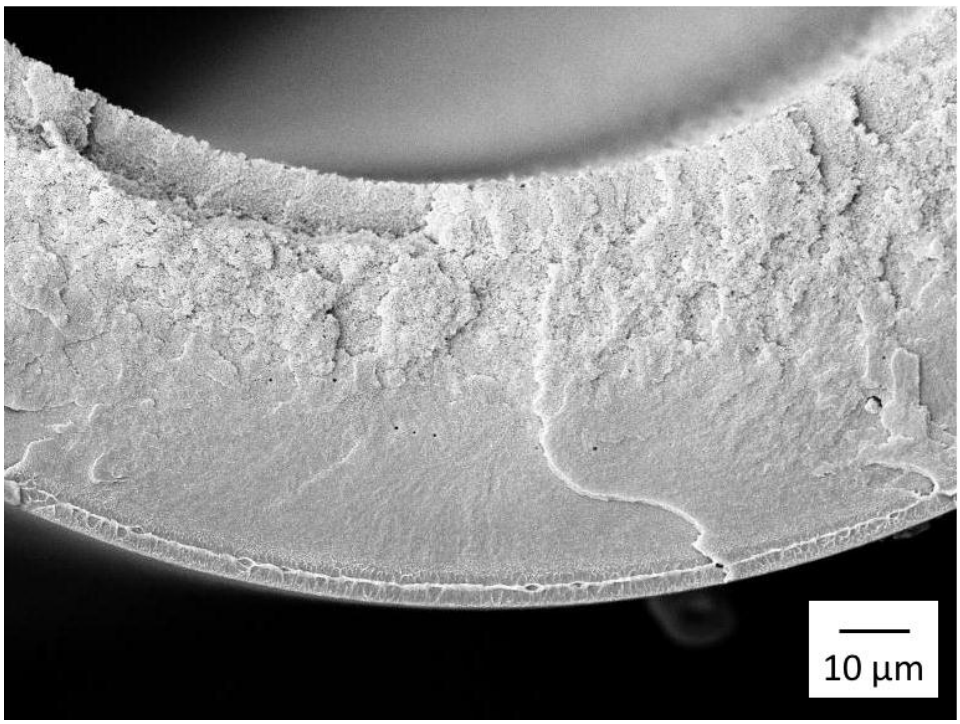

(b) Fiber wall

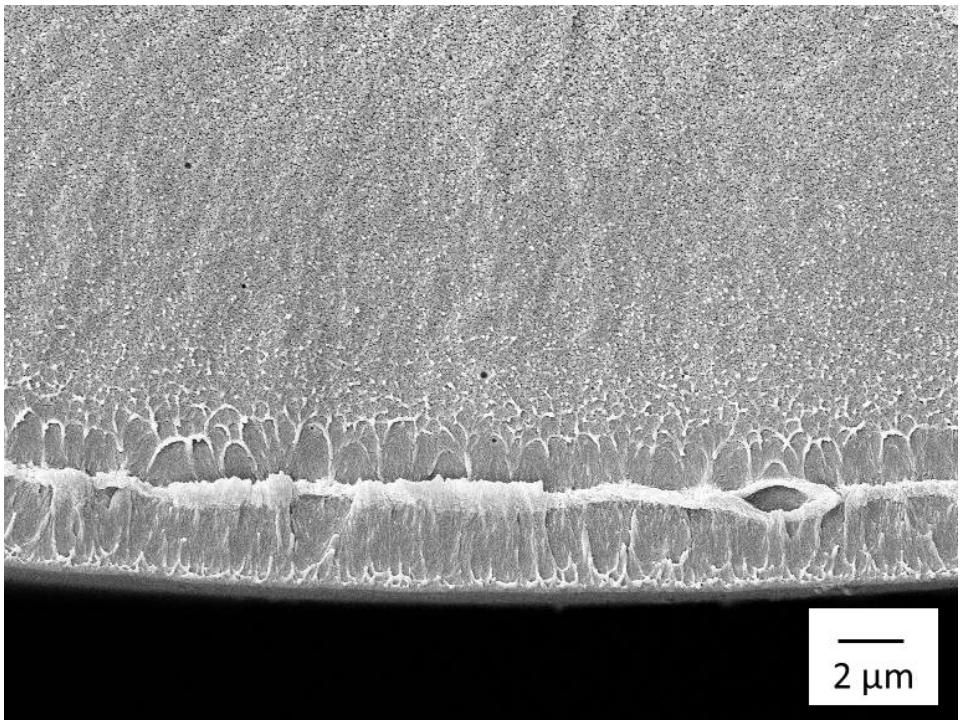

(c) Skin layer

Figure 4.8 SEM picture of the skin layer of a 6FDA-DAM hollow fiber (1st spinning, without $LiNO_3$)

Gas permeation experiments were used to evaluate the defect-free properties of the resultant hollow fiber membranes. All 6 spinning states were defect-free, based on O_2/N_2 permeation results. While the intrinsic 6FDA-DAM O_2/N_2 selectivity is 3.5, all fibers showed the O_2/N_2 selectivity of 3.4-3.6. The skin layer thickness ranged from 0.85 μm to 3.3 μm, based on nitrogen permeation results. Table 4.9 shows the permeation results of a typical spinning state. Selectivity of all the gas pairs tested (O_2/N_2, C_2H_4/C_2H_6, CO_2/CH_4, He/N_2, n-butane/iso-butane) matched the intrinsic dense film values very well. 6FDA-DAM polyimide was reported to be ideal for butane isomers separation [14, 15], and this is the first report of defect-free asymmetric 6FDA-DAM fibers which are able to separate the very challenging n-butane and iso-butane mixture. This extends the gas separation application of polymer membranes from small gas molecules to the relatively large molecules such as butane isomers.

Table 4.9 Comparison of 6FDA-DAM polymer fiber performance with intrinsic dense film transport properties

	$\alpha_{O2/N2}$	$\alpha_{C2H4/C2H6}$	$\alpha_{CO2/CH4}$	$\alpha_{He/N2}$	$\alpha_{nC4/iC4}$
Film	3.5	3	17.6	9.7	21
Fiber	3.5	3	17.1	10	20

Pure gas permeation test; 15 psi feed, 35 ^{o}C testing temperature except 100 ^{o}C for C4s;

Air gap height is very important for skin layer development. The evaporation of volatiles in the air gap drives the dope composition to the vitrified region and thus forms the skin layer. The longer the residence time in the air gap, the thicker the resultant skin layer. The effect of air gap height on 6FDA-DAM skin layer thickness is shown in Figure 4.9. The spinning conditions for the three spinning states only differ in the air gap height.

For all three spinning states, the dope and bore fluid flow rates were 75 mL/hr, and a linear relationship is obvious in the plot.

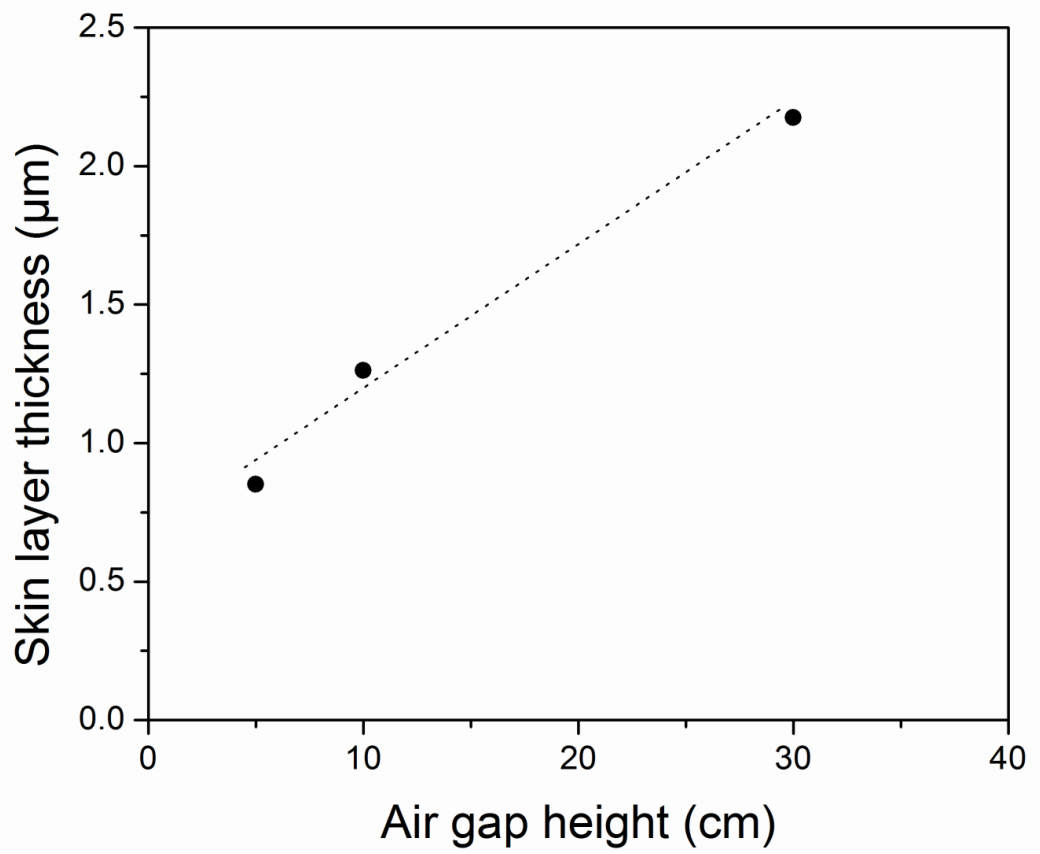

Figure 4.9 Effect of air gap height on 6FDA-DAM fiber skin thickness

The effect of water quench temperature was also evaluated in this study. The comparison was between 20 ^{o}C and 50 ^{o}C while all other conditions were kept the same. In the case of low temperature water quench, the estimated skin layer thickness was 37% thicker, possibly due to further skin layer development caused by the slower phase separation in the water quench.

The 1st attempt of 6FDA-DAM fiber spinning was very successful in terms of

defect-free membrane formation. There were also some issues that could be improved. The major issue was the slow take-up rate. As a result, the fiber size was relatively large compared to industrial gas separation hollow fibers. Additionally, the skin layer could be further minimized in order to increase the productivity of the membranes.

4.3.2.2 6FDA-DAM fiber spinning - 2nd attempt

The second attempt aimed to evaluate the effect of polydispersity on defect-free asymmetric hollow fiber membrane formation. Even with the same chemical structure, polymers may have significant difference due to their molecular weight and molecular weight distribution. Empirically, narrow molecular weight distribution or low PDI value is desired for asymmetric hollow fiber membrane spinning, which presents some challenges for polymer synthesis. This study attempted to spin 6FDA-DAM with high PDI.

Batch 1 and 2 were blended into 50 wt%/50 wt%. GPC results showed the blended polymer had M_w of 332 kDa and PDI of 7.25. The PDI value was quite high as compared to most reported values in previous studies. The dope composition and spinning conditions in the 1st attempt were used, in order to keep the polymer as the only variable during this investigation.

Permeation results showed that the polymer fibers formed from this study were also defect-free. The O_2/N_2 selectivity was consistent with the dense film value. This study revealed that at some point, if the average molecular weight of a polymer was sufficiently high, even with a PDI at about 7, it was still possible to form defect-free asymmetric hollow fiber membranes. Of course, a low PDI is still desired if the

molecular weight distribution can be controlled during polymer synthesis.

4.3.2.3 6FDA-DAM fiber spinning - 3rd attempt

This spinning aimed to solve the issues found in the 1st 6FDA-DAM spinning: (1) increase the phase separation rate and thus speed up the take-up rate and reduce the fiber size; (2) decrease the skin layer thickness.

In the dope formulation, lithium nitrate was introduced as an additive for assisting phase separation. Lithium nitrate complexes solvent NMP molecules in the dope. When water quench occurs, the complex dissociates and phased separation is accelerated. Lithium nitrate in the dope has other roles as well: (1) it acts as a non-solvent, so the ethanol content may be reduced in order to keep the dope in one-phase region; (2) it also increases the dope viscosity significantly, so the polymer concentration may be reduced in order to achieve easy processability. 6.5 wt% lithium nitrate has been used by several researchers in the past [7, 13], therefore, this concentration was also chosen in this study. The phase diagram (with $LiNO_3$) is shown in Figure 4.10. While constructing the phase diagram, $LiNO_3$ and THF amounts were fixed at 6.5 wt% and 10 wt%, respectively.

The detailed dope composition is shown in Table 4.10. The spinning conditions are listed Table 4.11. The modified dope composition improved the spinnability greatly. The take-up rate was significantly increased, and even 50 m/min take-up rate (desired industrial value) was workable with this spinning dope. Another important adjustment was the bore fluid composition: 90 wt%/10 wt% NMP/H_2O was used instead of 80 wt%/20 wt% NMP/H_2O in the previous spinning. Due to change in phase behavior, 20 wt% H_2O in the bore fluid induced early phase separation from bore side and caused instability

of the spinning line.

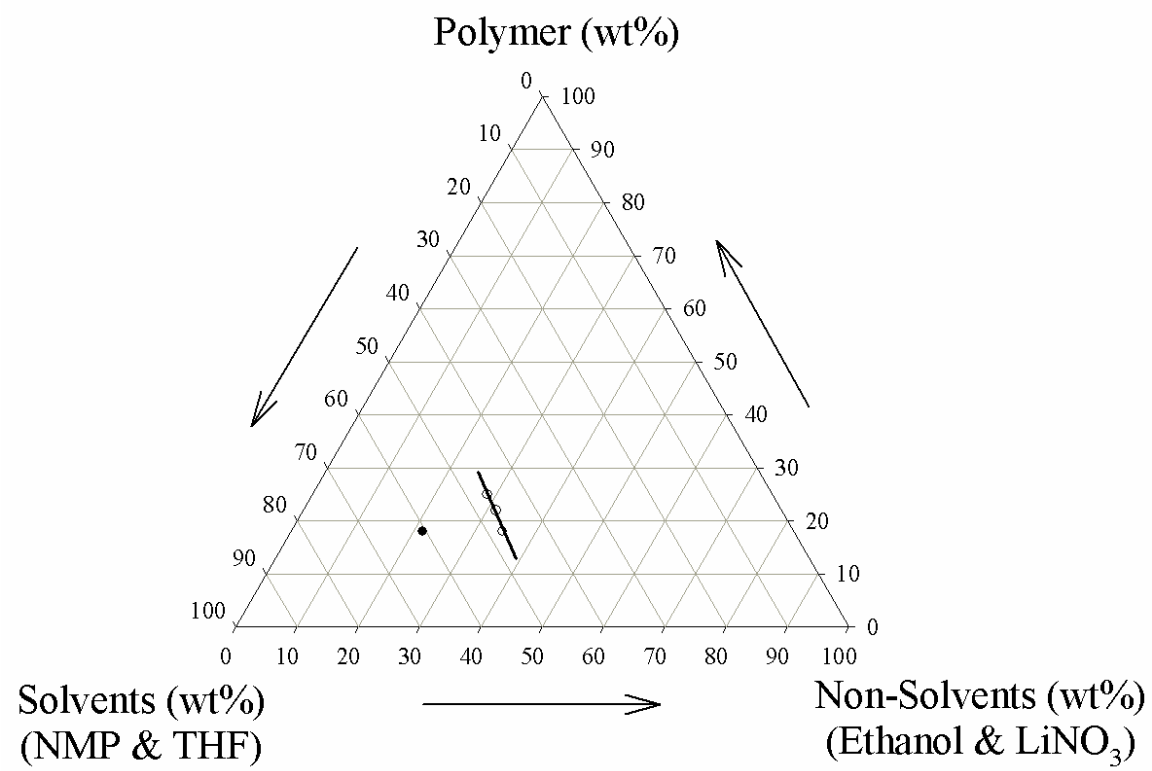

Figure 4.10 Ternary phase diagram of 6FDA-DAM (with $LiNO_3$). Open circle: compositions on the phase boundary; solid circle: spinning dope composition

Table 4.10 Dope composition of 6FDA -DAM hollow fiber spinning (3rd attempt)

Component	wt%
6FDA-DAM	18
NMP	50.5
THF	10
Ethanol	15
$LiNO_3$	6.5

Table 4.11 Spinning conditions for 6FDA -DAM hollow fiber membranes (3rd attempt)

Spinning parameter	Value
Dope and bore fluid flow rate	180/60 mL/hr
Bore fluid composition	90 wt%/10 wt% NMP/H_2O
Take-up rate	20-50 m/min
Quench bath temperature	25, 50 ^oC
Spinneret temperature	70 ^oC
Air gap height	5-30 cm

SEM was used to examine the macroscopic properties of resultant 6FDA-DAM hollow fibers. Due to the fast take-up rate, the size of fibers was significantly reduced from previous spinning. The minimum outer diameter was 237 μm, which was produced via a 50 m/min take-up rate. SEM pictures of a typical state (20 m/min take-up rate) are shown in Figure 4.11. In Figure 4.11 (a), the bore of the fiber looks “irregular”, this was caused by the suboptimal nature of the bore fluid, and to improve the bore morphology, water content in the bore side can be increased slightly. The skin layer shown in Figure 4.11 (c) is less than 1 μm, which is consistent with further permeation tests.

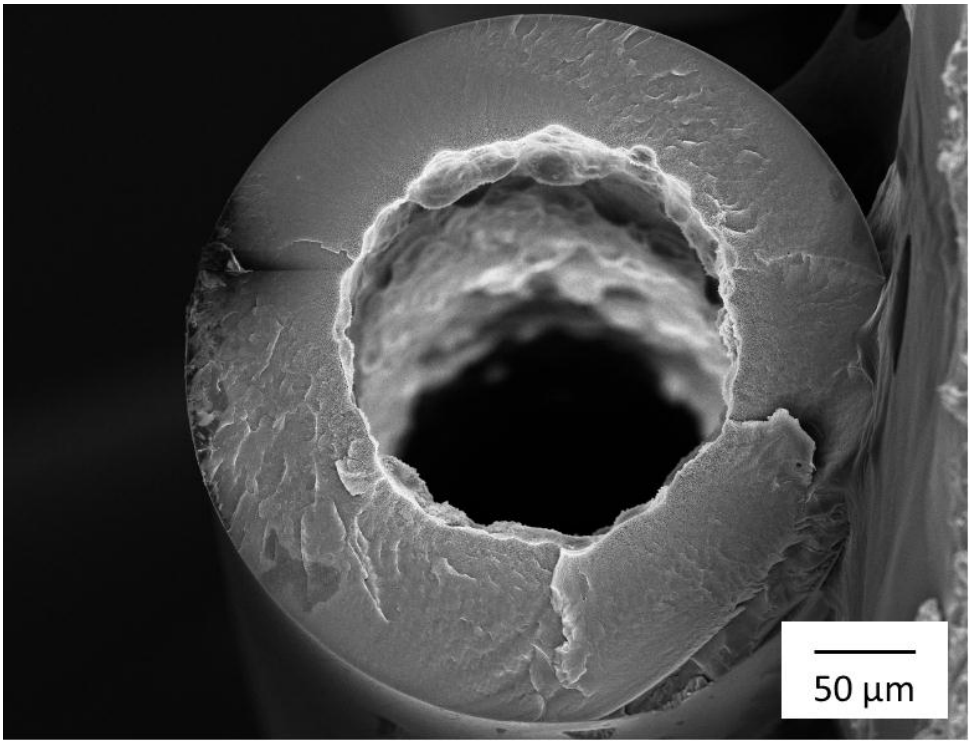

(a) Cross-section

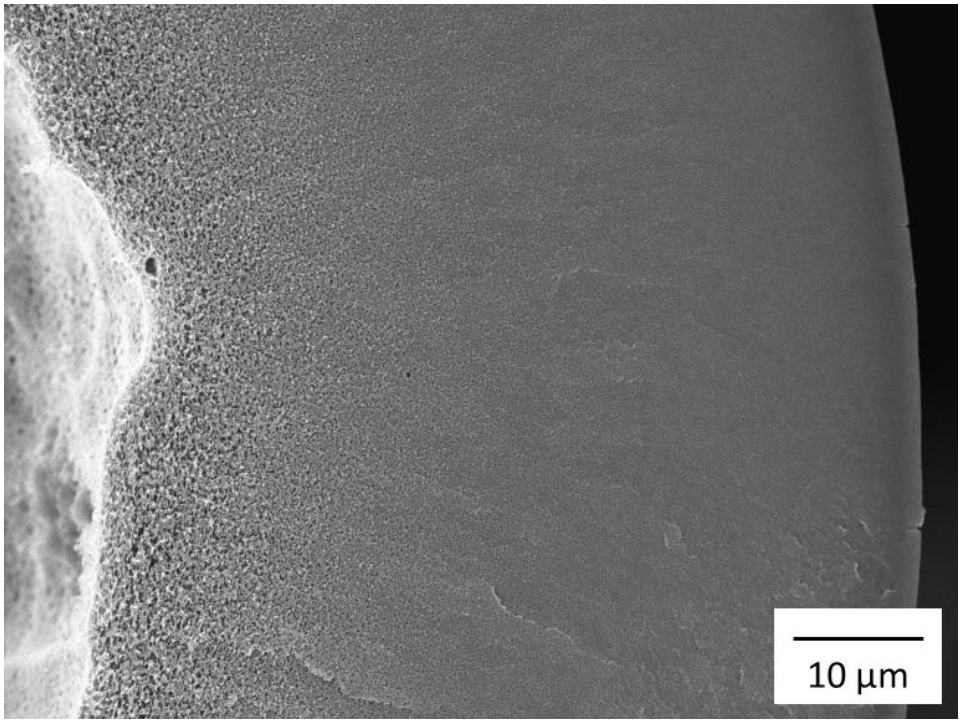

(b) Fiber wall

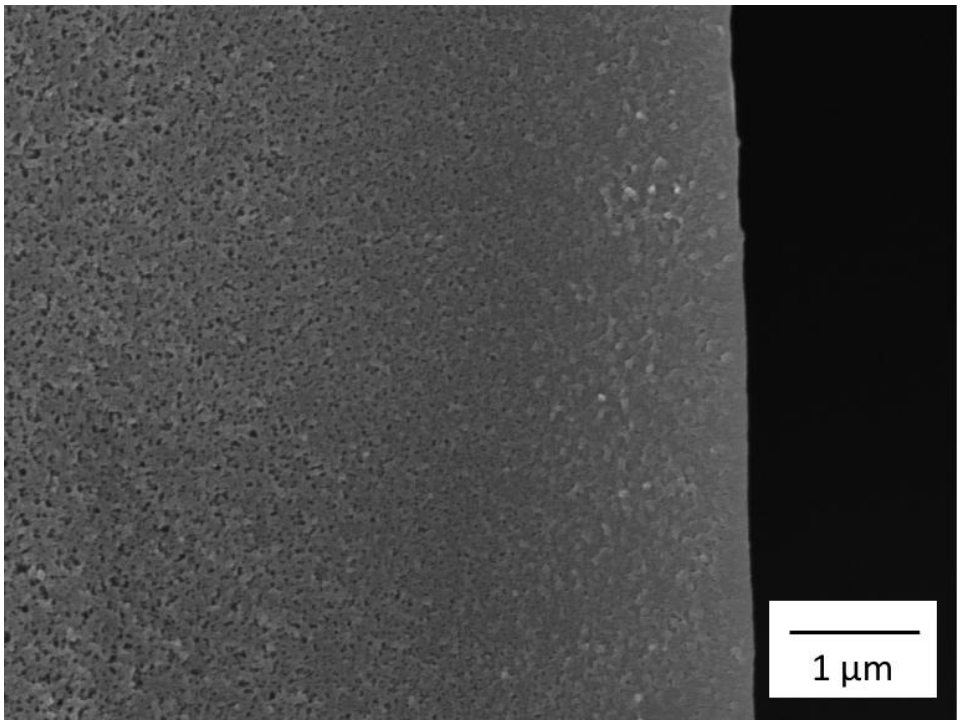

(c) Skin layer

Figure 4.11 SEM picture of a 6FDA-DAM hollow fiber (3rd spinning, with $LiNO_3$)

Gas permeation was used to examine the polymeric hollow fiber performance. Most of the spinning states (6 out of 8) in this spinning were defect-free, as indicated by the O_2/N_2 selectivity. The defect-free fibers showed O_2/N_2 selectivity of 3.3-3.9. The skin layer thickness was also reduced significantly, compared to the previous spinning without $LiNO_3$. The skin layer thickness calculated from nitrogen permeation was 0.26-1.54 µm. The minimum skin layer thickness was quite thin for defect-free asymmetric hollow fiber membranes.

There were also two defective states, showing that a good dope alone is not sufficient for defect-free fiber formation. Attention must also be paid to the spinning conditions, which must also be optimized based on the dope formulation. For example,

the slow take-up rate (5 m/min), which was used in the 1st and 2nd attempts, led to defective fibers in this spinning. Slow take-up increased the residence time in the air gap, and this may cause more water absorbance in the skin layer during the air gap. Small defects may also be caused by excessively fast phase separation. For future practice, it is wise to try different spinning conditions even for the same dope composition, in order to locate the optimum spinning conditions. The key adjustable parameters which may have significant impact during a spinning process are: spinneret temperature, take-up rate, air gap height and water quench bath temperature.

With the incorporation of lithium nitrate in the spinning dope, this spinning was quite successful. Defect-free fibers with thin skin thickness and small fiber size were formed. The take-up rate was also improved to a desirable rate.

4.3.3 6FDA/BPDA-DAM spinning

4.3.3.1 6FDA/BPDA-DAM spinning without $LiNO_3$

The properties of copolymer 6FDA/BPDA-DAM are quite similar to 6FDA-DAM polyimide. The spinning dope formulation and composition can be adjusted from the 6FDA-DAM spinning.

6FDA-DAM spinning without $LiNO_3$ showed reasonable skin formation. Therefore, for the 1st attempt, a similar dope composition was used. The dope formulation and phase boundary are shown in Figure 4.12. The dope formulation and spinning conditions are shown in Tables 4.12 and 4.13, respectively. Most spinning conditions were the same as conditions used in the 6FDA-DAM spinning. Based on the thick skin layer of 6FDA-DAM fiber, the air gap height in one spinning state was

decreased to 2 cm in order to decrease the skin layer thickness.

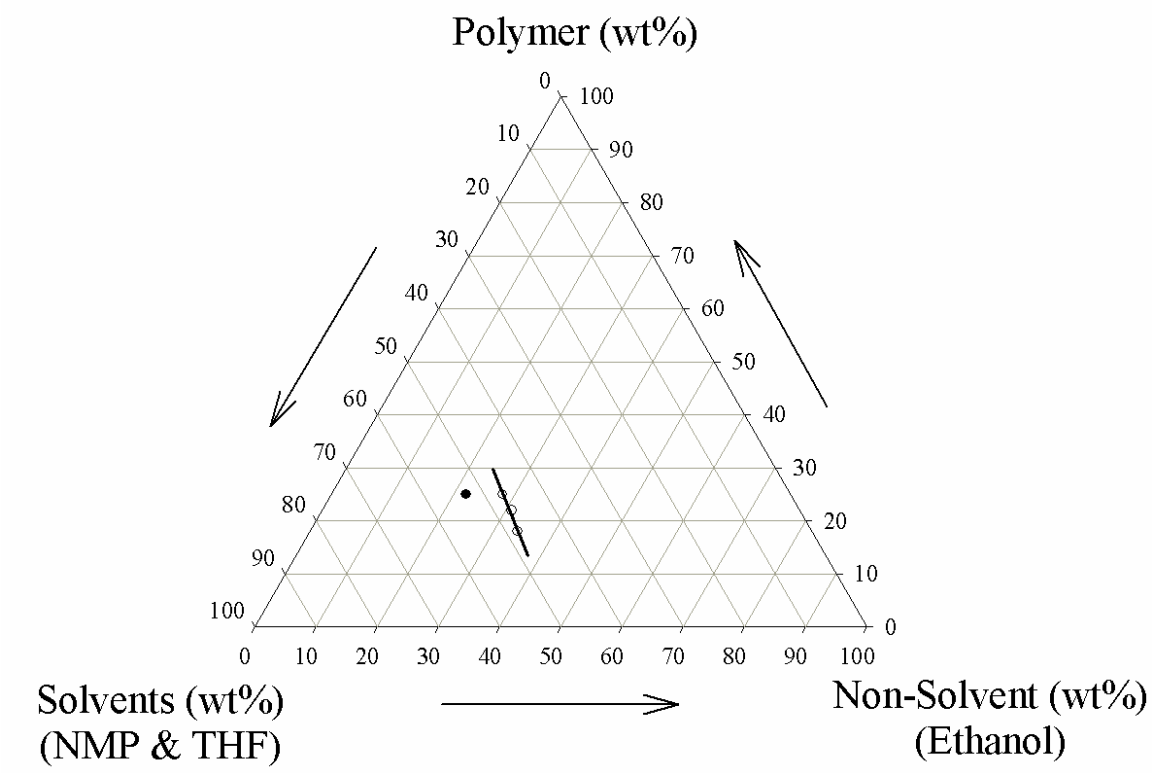

Figure 4.12 Ternary phase diagram of 6FDA/BPDA-DAM (without $LiNO_3$). Open circle: compositions on the phase boundary; solid circle: spinning dope composition

Table 4.12 Dope composition of 6FDA/BPDA-DAM hollow fiber spinning (1st attempt)

Component	wt%
6FDA/BPDA-DAM	25
NMP	43
THF	10
Ethanol	22

Table 4.13 Spinning conditions for 6FDA/BPDA-DAM hollow fiber membranes (1st attempt)

Spinning parameter	Value
Dope and bore fluid flow rate	75/100, 100/100 mL/hr
Bore fluid composition	80%/20% NMP/H_2O
Take-up rate	5 m/min
Quench bath temperature	50 ^oC
Spinneret temperature	70 ^oC
Air gap height	2-30 cm

SEM was used to check the macroscopic properties and the skin layer of resultant asymmetric 6FDA/BPDA-DAM hollow fiber membranes. The cross-section, fiber wall and skin layer of a 6FDA/BPDA-DAM hollow fiber are shown in Figures 4.13. The hollow fiber has good macroscopic properties. A distinct skin layer clearly sits on top of the porous support structure.

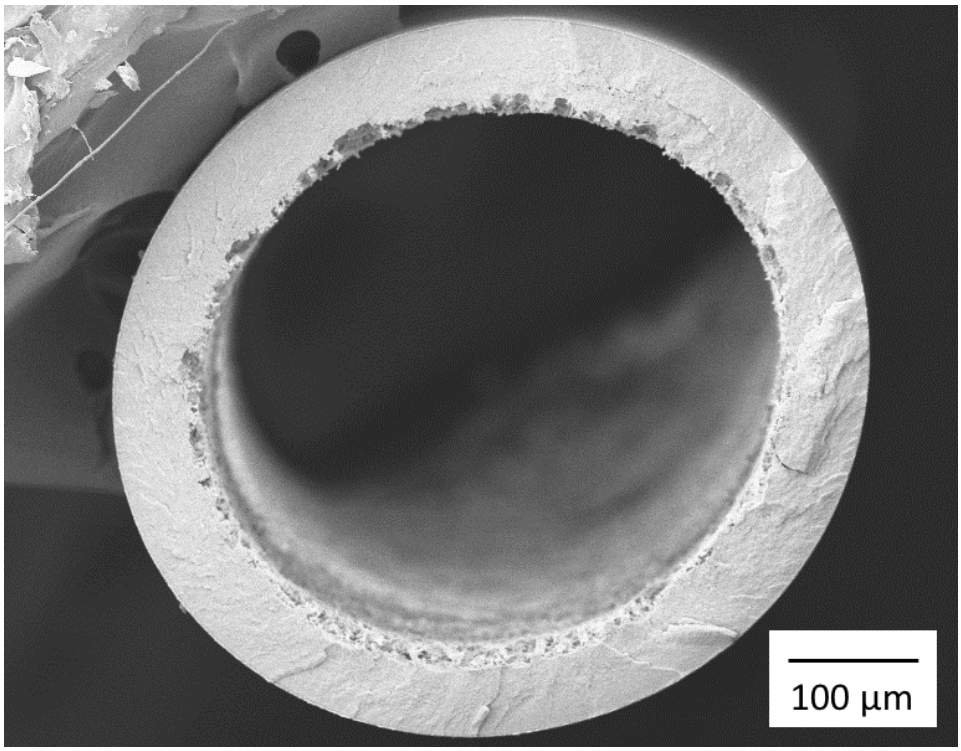

(a) Cross-section

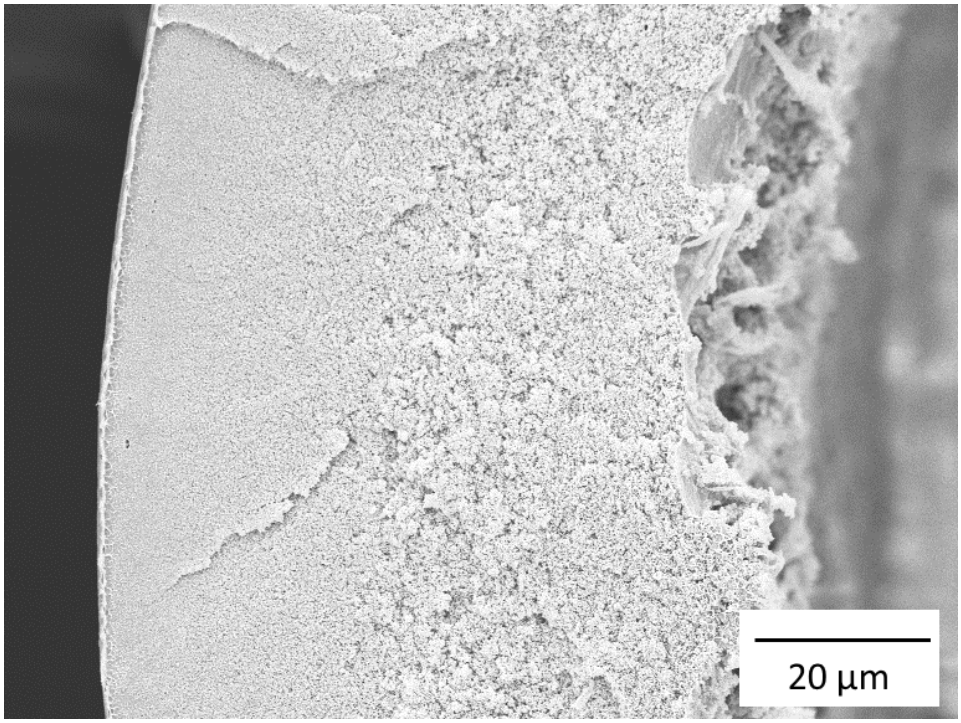

(b) Fiber wall

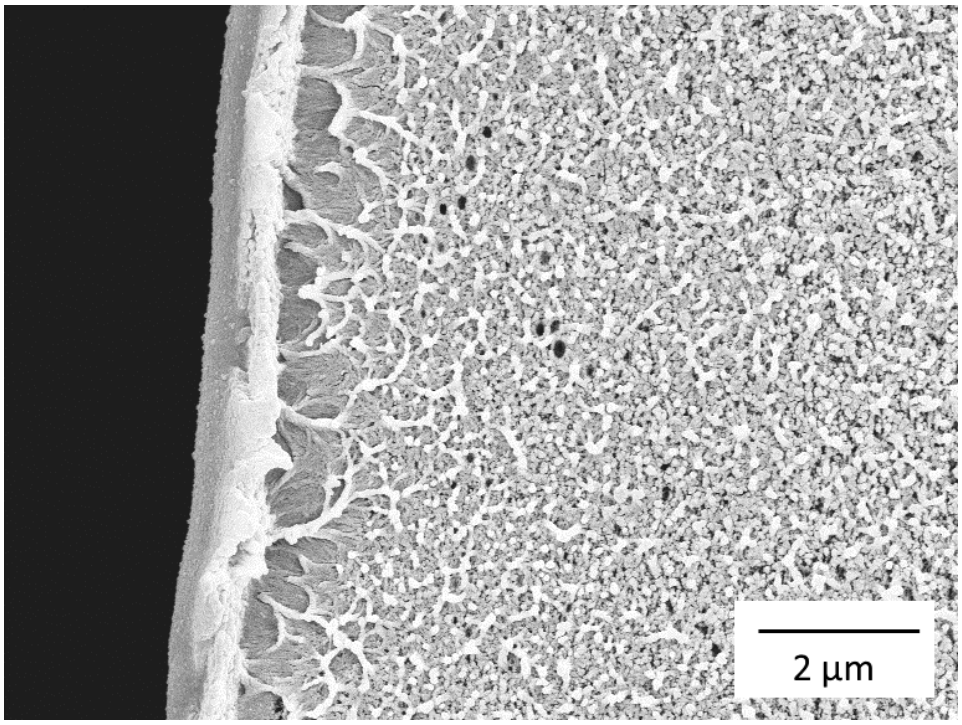

(c) Skin layer

Figure 4.13 SEM picture of a 6FDA/BPDA-DAM hollow fiber (1st spinning, without $LiNO_3$)

Pure gas permeation tests were used to determine the defect-free properties of the hollow fiber membranes. Most fibers formed in this spinning had O_2/N_2 selectivity higher than 90% of the intrinsic value (4.1), which demonstrated the defect-free skin layer formation. For two spinning states, the O_2/N_2 selectivity were 4.8 and 5.0, respectively. These two values were about 20% higher than the intrinsic value of 4.1. This phenomenon was observed previously in other 6FDA-polymers. The possible cause of the high selectivity of polymeric hollow fiber membranes was that the polymer chains may align due to the shear stress during fiber spinning. This induced oriented packing of polymer chains in the dense skin layer and may increase the selectivity. The gas permeation results of one such spinning state is shown in Table 4.14. For O_2/N_2,

C_2H_4/C_2H_6 and CO_2/CH_4, all the selectivities are higher than the intrinsic values. The 2 cm air gap height was enough for defect-free skin layer formation. Based on nitrogen permeation results, about 1.4 μm defect-free skin layer was formed. The thickest skin layer in this spinning was about 3.1 μm, which was formed in a 30 cm high air gap.

The outcome of this spinning was quite similar to 6FDA-DAM spinning. Defect-free fibers were successfully obtained. The issues remaining were the slow phase separation and slow take-up rate, which resulted in big fiber size and also the thick separation layer thickness.

Table 4.14 Comparison of 6FDA/BPDA-DAM polymer fiber performance with intrinsic dense film transport properties

	$\alpha_{O2/N2}$	$\alpha_{C2H4/C2H6}$	$\alpha_{CO2/CH4}$
Film	4.1	3.3	22
Fiber	5.0	4.1	27

Pure gas permeation test; 15 psi feed, 35 ^{o}C testing temperature

4.3.3.2 6FDA/BPDA-DAM spinning with $LiNO_3$

As for 6FDA-DAM spinning, lithium nitrate was added in the dope for the purpose of accelerating phase separation. The phase diagram and dope formulation are shown in Figure 4.14. The dope composition and spinning conditions are listed in Table 4.15 and Table 4.16, respectively.

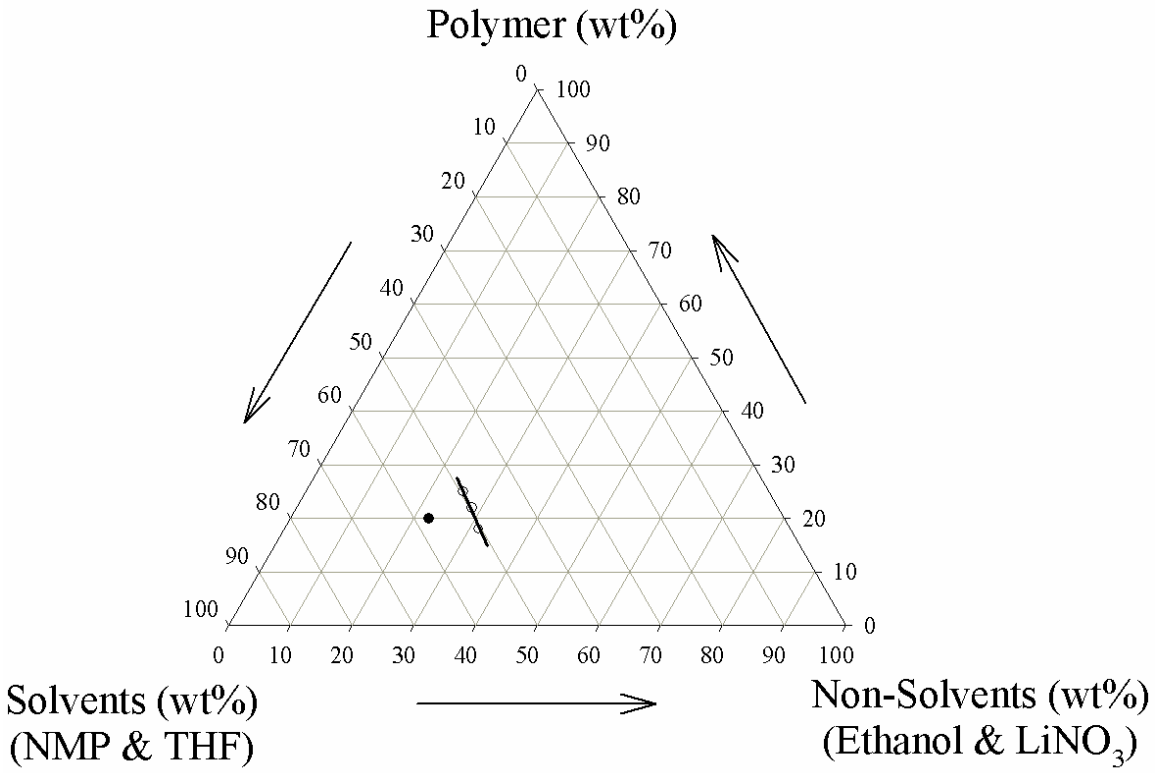

Figure 4.14 Ternary phase diagram of 6FDA/BPDA-DAM (with $LiNO_3$). Open circle: compositions on the phase boundary; solid circle: spinning dope composition

Table 4.15 Dope composition of 6FDA/BPDA-DAM hollow fiber spinning (with $LiNO_3$)

Component	wt%
6FDA/BPDA-DAM	20
NMP	47.5
THF	10
Ethanol	16
$LiNO_3$	6.5

Table 4.16 Spinning conditions for 6FDA/BPDA-DAM hollow fiber membranes (with $LiNO_3$)

Spinning parameter	Value
Dope and bore fluid flow rate	180/60 mL/hr
Bore fluid composition	80%/20% NMP/H_2O
Take-up rate	15 m/min
Quench bath temperature	50 ^oC
Spinneret temperature	70 ^oC
Air gap height	2-10 cm

SEM pictures of resultant hollow fiber membranes are shown in Figures 4.15. The fiber showed decent macroscopic properties. The skin layer thickness was quite thin, less than 1 μm. Gas transport properties were also obtained via pure gas permeation tests. Multiple fibers were tested for this spinning. Defect-free fibers were obtained based on O_2/N_2 permeation results, with calculated skin thickness of 0.54-1.36 μm. Some defective fibers were also observed, and this may be caused by contaminations of the dope filter from the last spinning. The dope composition and spinning conditions have been demonstrated to be excellent for potential defect-free fiber formation. Of course, due to the molecular weight variation of different polymer batches, the polymer concentration may be adjusted to a proper level for processing. To achieve the optimum dope formulation and spinning conditions, several iterations of spinning and permeation tests may be required.

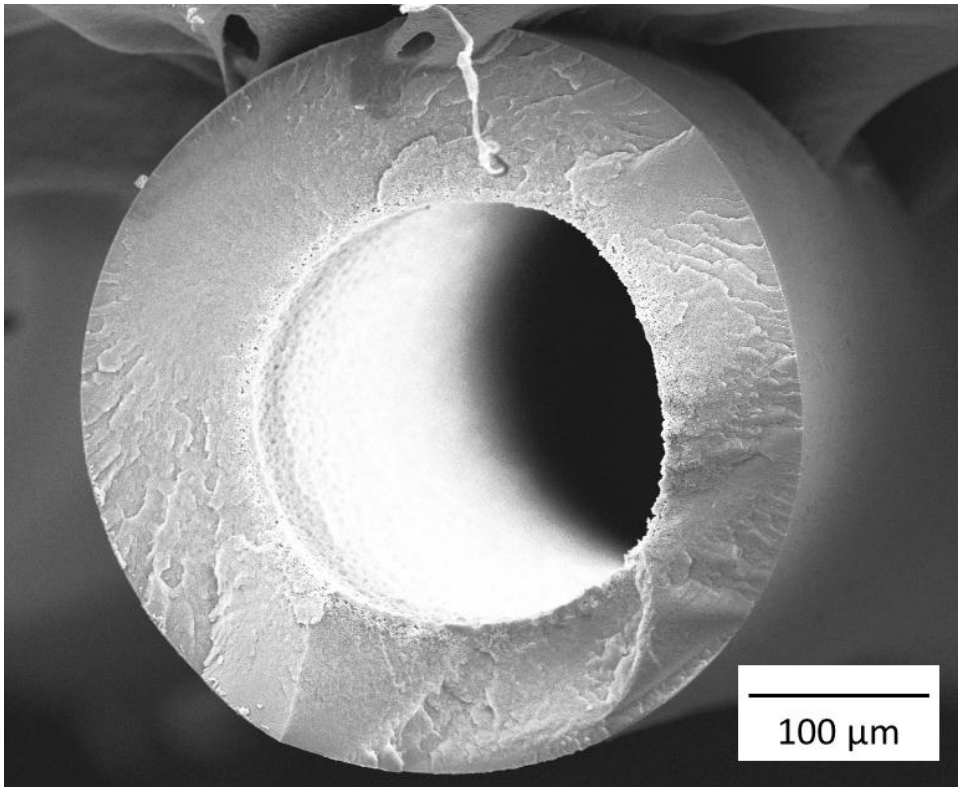

(a) Cross-section

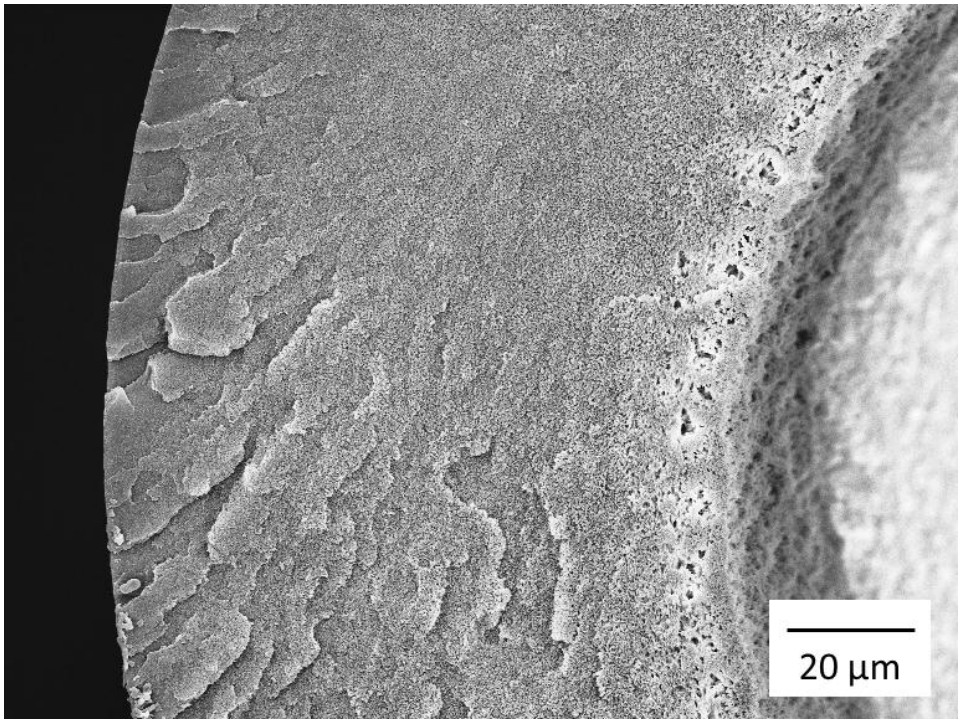

(b) Fiber wall

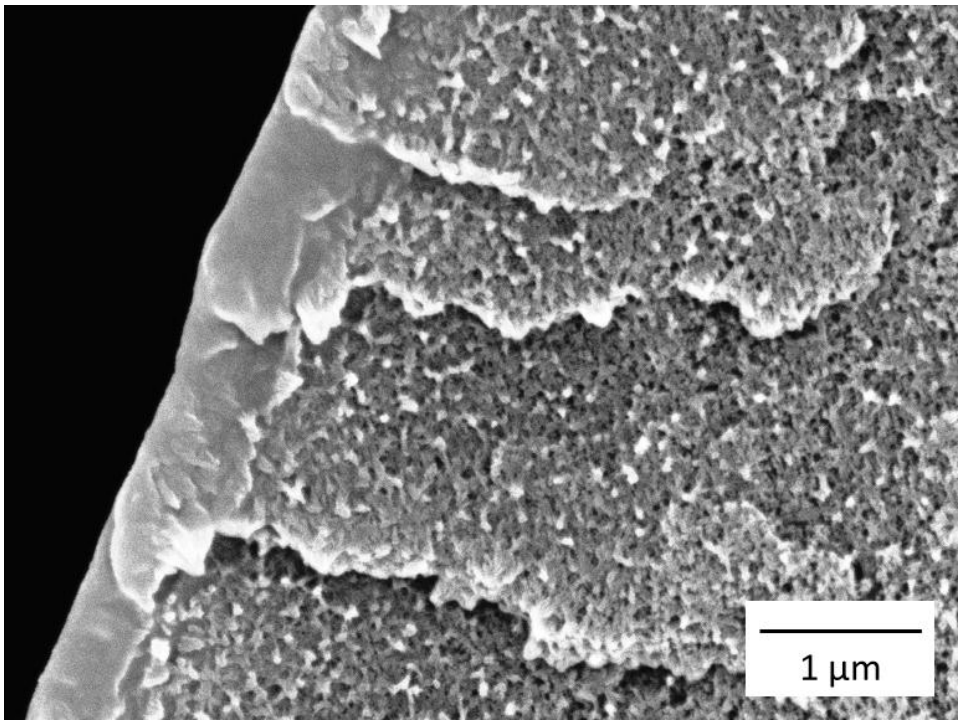

(c) Skin layer

Figure 4.15 SEM picture of a 6FDA/BPDA-DAM hollow fiber (with $LiNO_3$)

4.4 Plasticization in asymmetric polymeric hollow fiber membranes

This section mainly addresses the gas transport in polymeric asymmetric hollow fiber membranes, specifically, the permeation tests related to plasticization issues.

Plasticization occurs when a strongly sorbing penetrant reaches a certain concentration in the polymer membrane and dilates the polymer matrix. In the dilated polymer matrix, diffusion coefficients of all gases are increased. On the chain segmental scale, plasticization reflects an increase in chain mobility and gas permeability but a reduction in selectivity. The sorption of gases in polymer membranes can be represented by the condensability, which is determined primarily by the critical temperature. Strongly sorbing hydrocarbons and CO_2 are typical gases causing plasticization. In polymeric

membranes for olefin/paraffin separations, plasticization caused by propylene/propane was investigated previously [16-20], while ethylene/ethane induced plasticization was rarely studied. Plasticization pressure refers to the pressure at which gas permeability starts to increase with increasing pressure. Since plasticization reduces the gas separation selectivity, this phenomenon is not desirable in polymeric membranes for gas separations. Crosslinking is the most common and effective method to stabilize the polymer matrix and maintain high separation performance of polymer membranes. Of course, the focus of this work, carbon membranes, prevents the plasticization problem and is intrinsically more stable than polymer materials.

For the same polymer, it was illustrated previously that the plasticization pressure was significantly affected by the membrane thickness. Membranes with thin thickness are more prone to be plasticized. Therefore, due to the thin membrane thickness, plasticization effect is more obvious in asymmetric hollow fiber membranes. The effect was demonstrated by CO_2 permeation isotherms of Matrimid® dense film and asymmetric hollow fiber [8, 21, 22]. Plasticization occurs at lower CO_2 plasticization pressure in the asymmetric hollow fiber form and shows more pronounced effect than the dense film form.

Ethylene/ethane separation using polymeric membranes was not well studied in previous research, and the plasticization effect was not explored in ethylene/ethane separations. Plasticization by C2 hydrocarbons was first observed in pure gas permeation test in 6FDA-DAM asymmetric hollow fiber membranes. In order to determine the defect-free properties of asymmetric polymeric hollow fiber membranes, initially, several common gases were tested in the following order: $N_2 \rightarrow O_2 \rightarrow He \rightarrow C_2H_4 \rightarrow C_2H_6 \rightarrow N_2 \rightarrow$

O_2→ He. A constant pressure system was used and pure gas was fed at 100 psi. One typical example is shown in Table 4.17. In the first set of experiments, O_2/N_2 and He/N_2 matched the ideal selectivity of 6FDA-DAM dense film very well. Then, the membrane was exposed to 100 psi C_2H_4 and then C_2H_6. Surprisingly, the C_2H_4/C_2H_6 selectivity was only 1.6, which was well below its intrinsic value of 3.0. N_2, O_2 and He were tested again in order to verify the transport properties. However, both O_2/N_2 and He/N_2 selectivity were lower than the values in the first set of tests. N_2, O_2 and He permeance were increased by 69%, 46% and 8%, respectively. The experiments demonstrated that the membrane material was "changed" during tests. This phenomenon was confirmed by testing several spinning states. It was hypothesized that the membranes were plasticized during the tests of C_2H_4 and C_2H_6.

Table 4.17 Example of gas permeation in defect-free asymmetric 6FDA-DAM hollow fiber membranes

	Test order (from left to right)							
	Set 1			Set 2		Set 3		
	N_2	O_2	He	C_2H_4	C_2H_6	N_2	O_2	He
Permeance (GPU)	45	158	468	143	89	76	230	507
Selectivity	$\alpha_{O2/N2}$=3.5 $\alpha_{He/N2}$=10.3			$\alpha_{C2H4/C2H6}$=1.6		$\alpha_{O2/N2}$=3.0 $\alpha_{He/N2}$=6.7		

100 psi pure gas feed, 35 ^oC

To verify the plasticization effect caused by ethylene and ethane, pure gas permeation isotherms were obtained. Defect-free 6FDA-DAM asymmetric fiber was tested in constant volume system. The feed gas pressure was increased from 15 psi to 200 psi gradually, and then the membrane was depressurized from 200 psi to 15 psi with the

same pressure gaps as pressurization. Pure gas permeance was calculated for each test. The ethylene and ethane permeation isotherms are plotted in Figures 4.16 and 4.17, respectively. As demonstrated by the plots, for both gases, the permeance decreased first with increasing feed gas pressure, which followed the pressure dependence of permeability based on Langmuir type of sorption; after a certain pressure, the permeance showed an upswing with increasing feed gas pressure. In the depressurization process, it was clear that all the permeance values at various pressures were higher than the values during pressurization process. When the feed gases were depressurized back to the starting pressure of 15 psi, the permeance of ethylene and ethane were increased by 53% and 85%, respectively. Therefore, ethylene and ethane induced plasticization in 6FDA-DAM asymmetric hollow fiber membranes, which decreased the selectivity of gas pairs after the hydrocarbons exposure. The plasticization pressures of both ethylene and ethane were quite low, only about 100 psi and 75 psi, respectively.

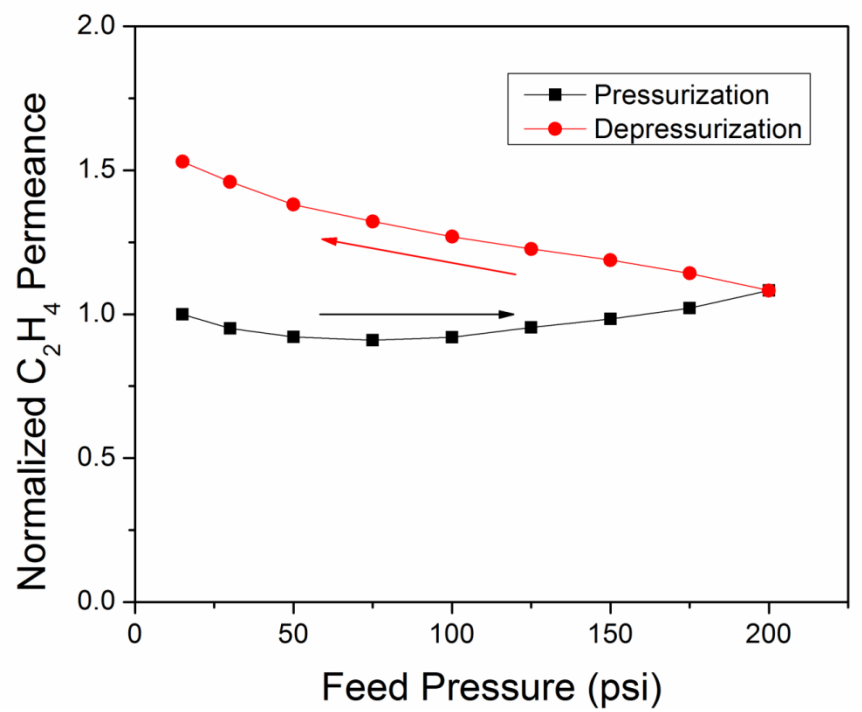

Figure 4.16 Normalized pure ethylene permeation isotherm in defect-free 6FDA-DAM asymmetric hollow fiber membranes (35 ^{o}C)

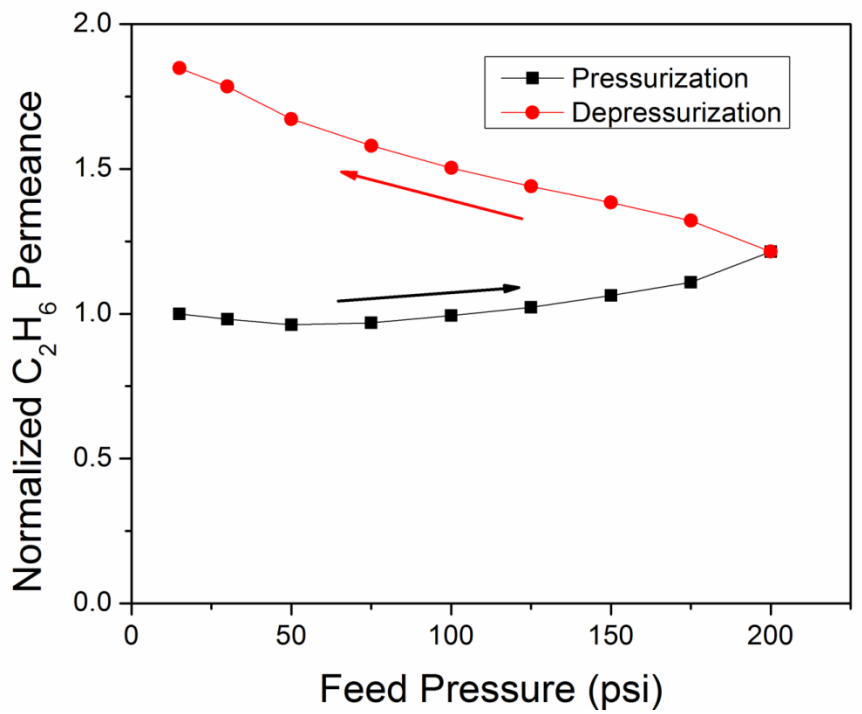

Figure 4.17 Normalized pure ethane permeation isotherm in defect-free 6FDA-DAM asymmetric hollow fiber membranes (35 ^{o}C)

After the asymmetric hollow fiber tests, ethylene and ethane permeation isotherms in dense film membranes were then plotted. Plasticization was also observed in 6FDA-DAM dense film membranes. The permeation isotherms of pressurization processes were plotted in Figure 4.18. The trend was less obvious due to the thick membrane thickness (~ 70 μm). At 700 psi, the ethylene permeability exceeded the value at 25 psi; at 600 psi, the ethane permeability exceeded the permeability at 15 psi. The plasticization pressure was 300 psi for ethane and 400 psi for ethylene, which were much higher than the asymmetric hollow fiber membrane values. At 25 psi, the C_2H_4/C_2H_6 selectivity was 3.0, while at 600 psi, the C_2H_4/C_2H_6 selectivity decreased to 2.5.

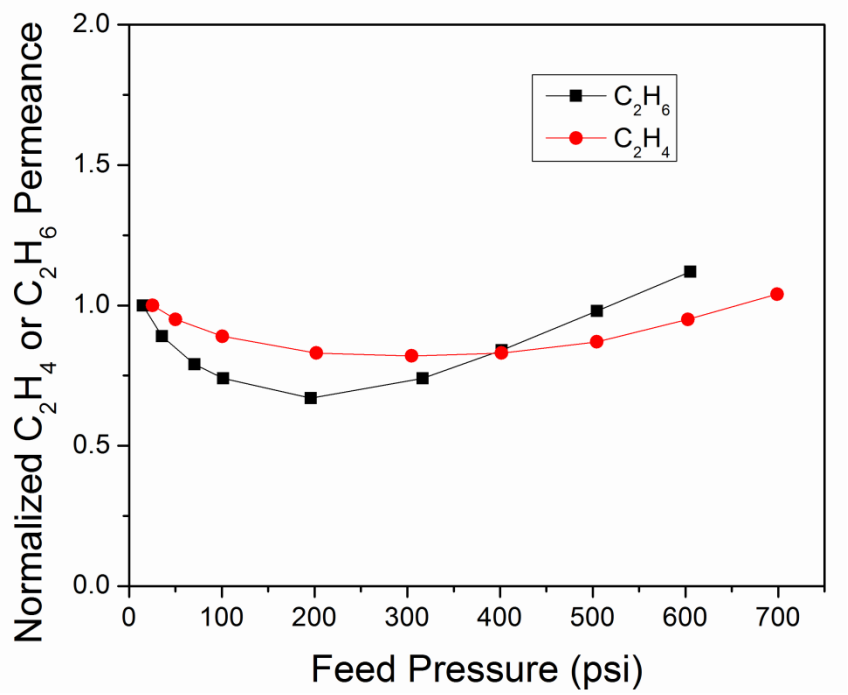

Figure 4.18 Normalized ethylene and ethane pure gas permeation isotherms in 6FDA-DAM dense film membranes (35 ^{o}C)

Due to the plasticization effect, in order to obtain the intrinsic transport properties,

the testing protocols must be designed to avoid any complications that may induce structural changes in membranes, such as plasticization. Therefore, in the asymmetric membrane tests, testing pressures for gases such as CO_2, C_2H_4 and C_2H_6 must be kept at a low level. In the previous tests, clearly 100 psi feed of C_2H_4 and C_2H_6 were too high and caused plasticization. To gain systematic transport properties, verification of defect-free properties was then carried out at low pressures such as about 15 psi.

Ethylene and ethane induced plasticization was first systematically studied in 6FDA-DAM asymmetric hollow fiber and dense film membranes. These results revealed the challenges of ethylene/ethane separation using polymeric membranes. While the upper bound trade-off limits the separation performance of polymeric membranes, the stability issue caused by plasticization appears to be another serious problem that must be handled properly. Although methods such as crosslinking and annealing can be used to stabilize polymer membranes, CMS membranes obviously are more advantageous due to the intrinsically high stability and capability of overcoming the polymer performance upper bound. These advantages are demonstrated in the later chapters.

4.5 Summary and conclusions

Defect-free asymmetric hollow fiber membranes were successfully spun from Matrimid®, 6FDA-DAM and 6FDA/BPDA-DAM. The fiber spinning conditions for each polyimide were pursued in a case-by-case manner. Intrinsic polymer properties and molecular weight have significant impacts on asymmetric fiber spinning. Without $LiNO_3$, the phase separation rate of 6FDA-DAM and 6FDA/BPDA-DAM polyimides in water quench bath was very slow, while the integral thick skin layer could be formed. $LiNO_3$

was then incorporated into the dope formulation, and decent spinning speed as well as fiber size were obtained. Plasticization induced by ethylene and ethane was observed and investigated in both dense film and asymmetric hollow fiber polyimide membranes.

4.6 References

[1] S.B. Carruthers, G.L. Ramos, W.J. Koros, Morphology of integral-skin layers in hollow-fiber gas-separation membranes, J. Appl. Polym. Sci. 90 (2003) 399-411.

[2] D.T. Clausi, W.J. Koros, Formation of defect-free polyimide hollow fiber membranes for gas separations, J. Membr. Sci. 167 (2000) 79-89.

[3] K.M. Steel, W.J. Koros, An investigation of the effects of pyrolysis parameters on gas separation properties of carbon materials, Carbon 43 (2005) 1843-1856.

[4] A.L. Hines, R.N. Maddox, Mass transfer fundamentals and applications, Prentice-Hall, Englewood Cliffs, New Jersey, 1985.

[5] S.U. Li, J.L. Gainer, Diffusion in polymer solutions, Ind. Eng. Chem. Fundam. 7 (1968) 433-440.

[6] D.W. Wallace, Crosslinked hollow fiber membranes for natural gas purification and their manuscript form novel polymers, in: Chemical Engineering, The University of Texas at Austin, 2004.

[7] I.C. Omole, Crosslinked polyimide hollow fiber membranes for aggressive natural gas feed streams in: Chemical Engineering, Georgia Institute of Technology, 2008.

[8] C.-C. Chen, Thermally crosslinked polyimide hollow fiber membranes for natural gas purification, in: Chemical Engineering, Georgia Institute of Technology, 2011.

[9] J. Liu, Development of next generation mixed matrix hollow fiber membranes for butane isomers separation, in: Chemical Engineering, Georgia Institute of Technology, 2010.

[10] M.G. Weinberg, Polyimide gas separation membranes for carbon dioxide enrichment, in: U.S. Patent (Ed.) United States Patent, E. I. du Pont de Nemours and Company, L'Air Liquide S.A., United States, 1993.

[11] I.C. Omole, S.J. Miller, W.J. Koros, Increased molecular weight of a cross-linkable polyimide for spinning plasticization resistant hollow fiber membranes, Macromolecules 41 (2008) 6367-6375.

[12] C. Zhang, Y. Dai, J.R. Johnson, O. Karvan, W.J. Koros, High performance ZIF-8/6FDA-DAM mixed matrix membrane for propylene/propane separations, J. Membr. Sci. 389 (2012) 34-42.

[13] C.-C. Chen, W. Qiu, S.J. Miller, W.J. Koros, Plasticization-resistant hollow fiber membranes for CO_2/CH_4 separation based on a thermally crosslinkable polyimide, J. Membr. Sci. 382 (2011) 212-221.

[14] O. Esekhile, W. Qiu, W.J. Koros, Permeation of butane isomers through 6FDA-DAM dense films, J. Polym. Sci., Part B: Polym. Phys. 49 (2011) 1605-1620.

[15] J. Liu, T.-H. Bae, W. Qiu, S. Husain, S. Nair, C.W. Jones, R.R. Chance, W.J. Koros, Butane isomer transport properties of 6FDA–DAM and MFI–6FDA–DAM mixed matrix membranes, J. Membr. Sci. 343 (2009) 157-163.

[16] C. Staudt-Bickel, W.J. Koros, Olefin/paraffin gas separations with 6FDA-based polyimide membranes, J. Membr. Sci. 170 (2000) 205-214.

[17] S.S. Chan, T.-S. Chung, Y. Liu, R. Wang, Gas and hydrocarbon (C2 and C3) transport properties of co-polyimides synthesized from 6FDA and 1,5-NDA (naphthalene)/Durene diamines, J. Membr. Sci. 218 (2003) 235-245.

[18] S.S. Chan, R. Wang, T.-S. Chung, Y. Liu, C2 and C3 hydrocarbon separations in poly(1,5-naphthalene-2,2'-bis(3,4-phthalic) hexafluoropropane) diimide (6FDA-1,5-NDA) dense membranes, J. Membr. Sci. 210 (2002) 55-64.

[19] M. Das, W.J. Koros, Performance of 6FDA–6FpDA polyimide for propylene/propane separations, J. Membr. Sci. 365 (2010) 399-408.

[20] T. Visser, A. Wessling, Auto and mutual plasticization in single and mixed gas C-3 transport through Matrimid-based hollow fiber membranes, J. Membr. Sci. 312 (2008) 84-96.

[21] G.C. Kapantaidakis, G.H. Koops, M. Wessling, S.P. Kaldis, G.P. Sakellaropoulos, CO_2 plasticization of polyethersulfone/polyimide gas-separation membranes, AIChE J. 49 (2003) 1702-1711.

[22] A. Bos, I.G.M. Punt, M. Wessling, H. Strathmann, Plasticization-resistant glassy polyimide membranes for CO_2/CH_4 separations, Sep. Purif. Technol. 14 (1998) 27-39.

CHAPTER 5

MATRIMID® DERIVED CMS HOLLOW FIBER MEMBRANES

In Chapter 4, defect-free asymmetric polymeric precursor fibers were spun from three precursor polyimides: Matrimid®, 6FDA-DAM and 6FDA/BPDA-DAM. Since Matrimid® is commercially available and has been studied extensively as a membrane material, in this Chapter, Matrimid® was chosen as a model precursor for CMS membrane fabrication. The first part of this chapter discusses the ethylene/ethane separation performance of Matrimid® CMS dense film and hollow fiber membranes. The comparative study of dense film and hollow fiber membranes revealed a significant morphology difference between the two configurations. The second part of this chapter describes the so-called "substructure collapse" in CMS hollow fiber formation. The impact of precursor defect-free properties on CMS hollow fiber membrane performance is also assessed. The third part of this chapter discusses the effort for overcoming substructure collapse with Matrimid® polyimide. The last part of this chapter discusses the evaluation of membrane performance under realistic testing conditions.

5.1 Transport properties of Matrimid® derived CMS dense film membranes

It is widely accepted that there is an upper bound for separating gases using spinnable polymer materials. Robeson has identified the upper limit for O_2/N_2, CO_2/CH_4, CO_2/N_2, N_2/CH_4, etc. [1, 2]. Burns and Koros have defined the upper bound of C_3H_6/C_3H_8 [3]. Before this study, there was no well-defined upper bound for the C_2H_4/C_2H_6 separation. Hereby, in order to compare the obtained CMS membrane

performance with existed polymer membrane materials, published C_2H_4/C_2H_6 permeation results are summarized, and an "approximate" upper bound curve of polymer material for the C_2H_4/C_2H_6 separation is obtained [4-9], as shown in Figure 5.1. The polymers considered in this plot are mostly high-performing 6FDA-dervied glassy polymers in the configuration of self-supported dense films, so this estimated line is probably a reasonable approximation of the actual performance bound using spinnable polymers. Comparing the C_2H_4/C_2H_6 upper bound curve with other widely investigated gas pairs, such as CO_2/CH_4 and C_3H_6/C_3H_8, it is obvious that the separation of C_2H_4 from C_2H_6 using polymeric membranes is truly very challenging.

The Matrimid® precursor dense film permeation results are also plotted in Figure 5.1 with the approximate upper bound curve and clearly fall below it. CMS dense film membranes were produced from vacuum pyrolysis of Matrimid® polymer dense films. The vacuum levels were below 15 mtorr. The pyrolysis temperature included the range from 500 ^oC to 800 ^oC using the temperature protocols A1 and A2 listed in Tables 3.1 and 3.2, respectively. The membranes were tested at 35 ^oC, and the pure gas feed pressure was roughly 50 psi. From the plot, it is obvious that all the dense film CMS separation performance is above the upper bound, which indicates very promising asymmetric CMS membrane application for the C_2H_4/C_2H_6 separation. In most cases, CMS dense films show an increase in both permeability and selectivity compared to the polymer precursor. As pyrolysis temperature increases, C_2H_4 permeability of CMS dense film decreases and meanwhile C_2H_4/C_2H_6 selectivity increases. For the C_2H_4/C_2H_6 pair, the optimum pyrolysis temperature for the Matrimid® precursor lies in the range of 650 ℃-675 ℃ with a C_2H_4 permeability of 13-14 Barrer. This performance is much

higher than the Matrimid® precursor performance in Figure 5.1. The optimum 675 ℃ CMS samples displayed C_2H_4 permeability above 10 Barrer and a C_2H_4/C_2H_6 selectivity of ~12. This performance is also above any other archived literature values we are aware of for non-facilitated transport membranes reported previously.

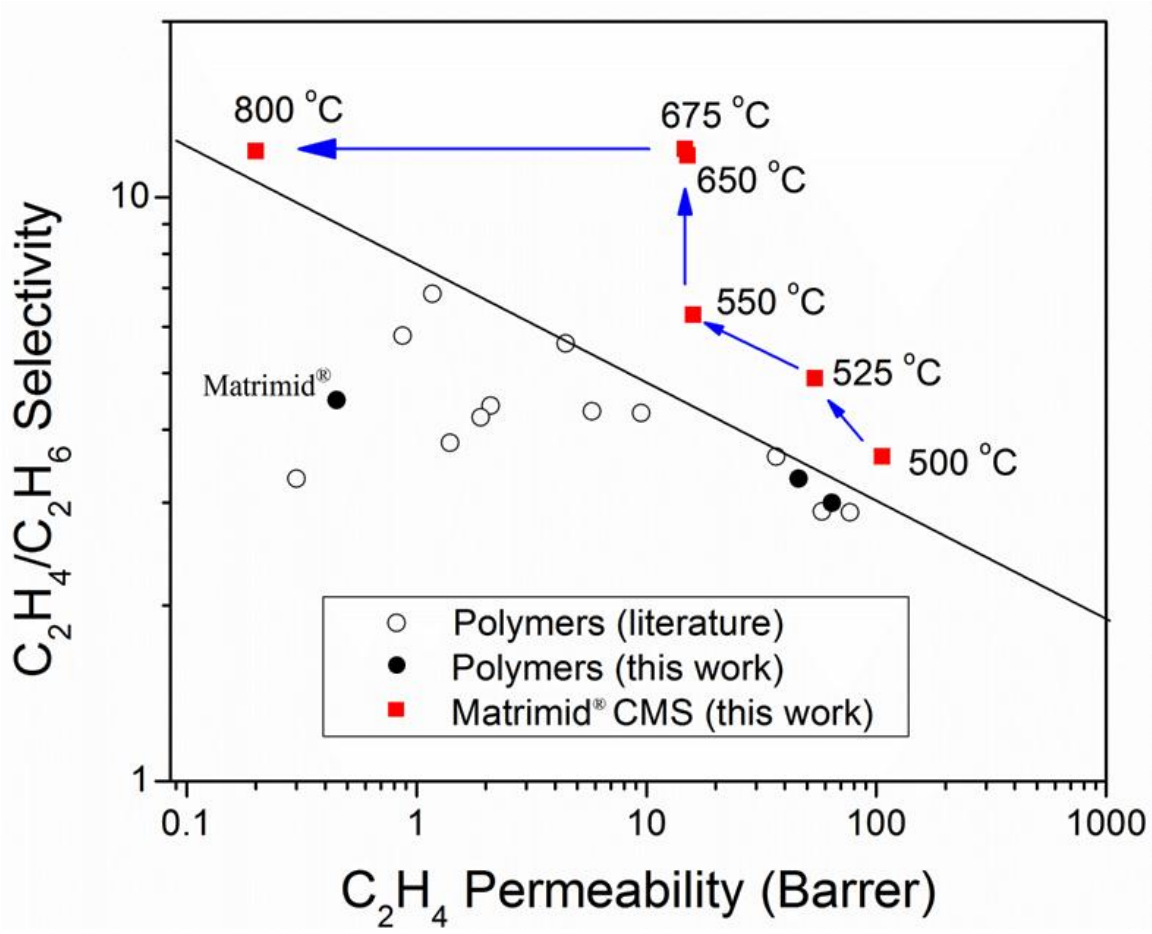

Figure 5.1 Comparison of Matrimid® CMS dense film membrane C_2H_4/C_2H_6 separation performance versus published polymer membrane performance.

5.2 Transport properties of Matrimid® derived CMS hollow fiber membranes

As noted above, the CMS dense film results suggest very promising application of CMS membrane for gas separations, so the extension to hollow fibers was also pursued

by pyrolysis of Matrimid® hollow fibers. This work provides one of the very few direct comparative studies of CMS dense film and hollow fiber permeation properties by using the same precursor polymer and the same pyrolysis setup and protocols.

To avoid complications, in this section, defect-free precursor fibers from a single spinning state were used for pyrolysis. The defect-free property is indicated by an O_2/N_2 selectivity of 6.7 (measured at 35 ℃, 100 psia, pure gas), which is consistent with the value obtained from dense film study of this particular batch of Matrimid®. The pyrolysis temperature protocols and pyrolysis atmosphere were all the same as previously used for dense film pyrolysis. Pure gas permeation tests were used to evaluate the permeation properties at 35 ^{o}C, and pure ethylene and ethane feed pressures were roughly 100 psi. The obtained permeation properties are plotted in Figure 5.2. As shown in Figures 5.1 and 5.2, the qualitative trends for C_2H_4 permeability (C_2H_4 permeance for fiber case) and selectivity change according to the pyrolysis temperature were very close. Especially for the C_2H_4/C_2H_6 selectivity, under most pyrolysis temperatures, CMS dense films and hollow fibers were in good agreement. The C_2H_4 permeance was found to decrease with increasing pyrolysis temperature, and as with dense film, the pyrolysis temperature range of 650~700 ℃ was found to be optimum for C_2H_4/C_2H_6 separation, and a high C_2H_4/C_2H_6 selectivity of ~12. The C_2H_4 permeance of 0.25 GPU obtained for Matrimid® CMS hollow fiber membranes was, however, surprising as is discussed below.

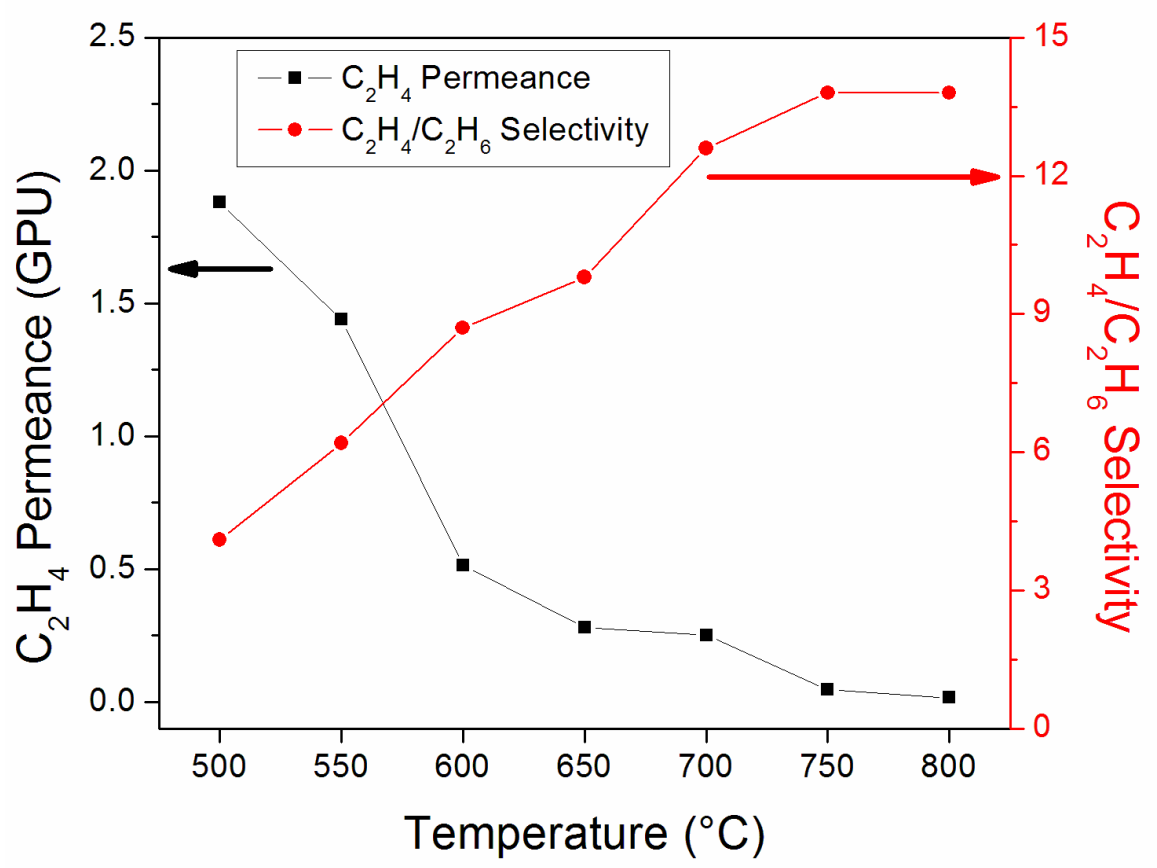

Figure 5.2 Effect of pyrolysis temperature on Matrimid® derived CMS hollow fiber membrane performance for the C_2H_4/C_2H_6 separation.

5.3 Comparison between Matrimid® derived CMS dense film and hollow fiber membranes

The separation layer thickness (l) is not readily known for asymmetric membranes, but it can be estimated as the ratio of intrinsic dense film permeability (P_A) and asymmetric membrane permeance ($(P/l)_A$), viz.,

$$l = \frac{P_A}{(P/l)_A} \tag{5.1}$$

For asymmetric precursor hollow fibers, only the outer dense skin layer is effective for gas separations, if the precursor hollow fiber skin layer is integrally defect-

free. The calculated skin layer thickness for the precursor fiber used previously is about 0.4 μm from N_2 permeation experiments, which is typical for gas separation asymmetric Matrimid® polymer hollow fibers. Assuming that the microporous structure of the effective separation layer in CMS hollow fiber is essentially the same as homogeneous CMS dense film, the effective separation layer thickness can be calculated for the fibers. Very surprisingly, the calculated separation layer is at least 10 μm thick, and in some cases it is close to the full wall thickness, which means the entire fiber wall is effective for separation. These results show that the separation layer of Matrimid® CMS fiber is much thicker than its precursor, suggesting that the Matrimid® CMS fiber loses its high asymmetry during pyrolysis.

To further confirm the observation of permeation properties, SEM images of a Matrimid® polymer fiber and the resultant CMS fiber are compared in Figure 5.3. Figure 5.3 (a) and (c) show the overall morphology of the precursor fiber and the resultant carbon fiber. It is quite obvious that the cross-section of carbon fiber is smooth and featureless as compared to its precursor. The asymmetric structure of polymer fibers is well illustrated by Figure 5.3 (b): the thickness of a dense skin layer is less than 1 μm; the support substructure is very porous and occupies most of the fiber structure. Figure 5.3 (d) shows a typical fiber wall of a CMS fiber. Obviously, the apparent asymmetric structure in precursor fibers is no longer distinguishable from this SEM image. Even near the bore side, which is the most porous part for asymmetric precursor fiber cross-section, the structure looks very dense.

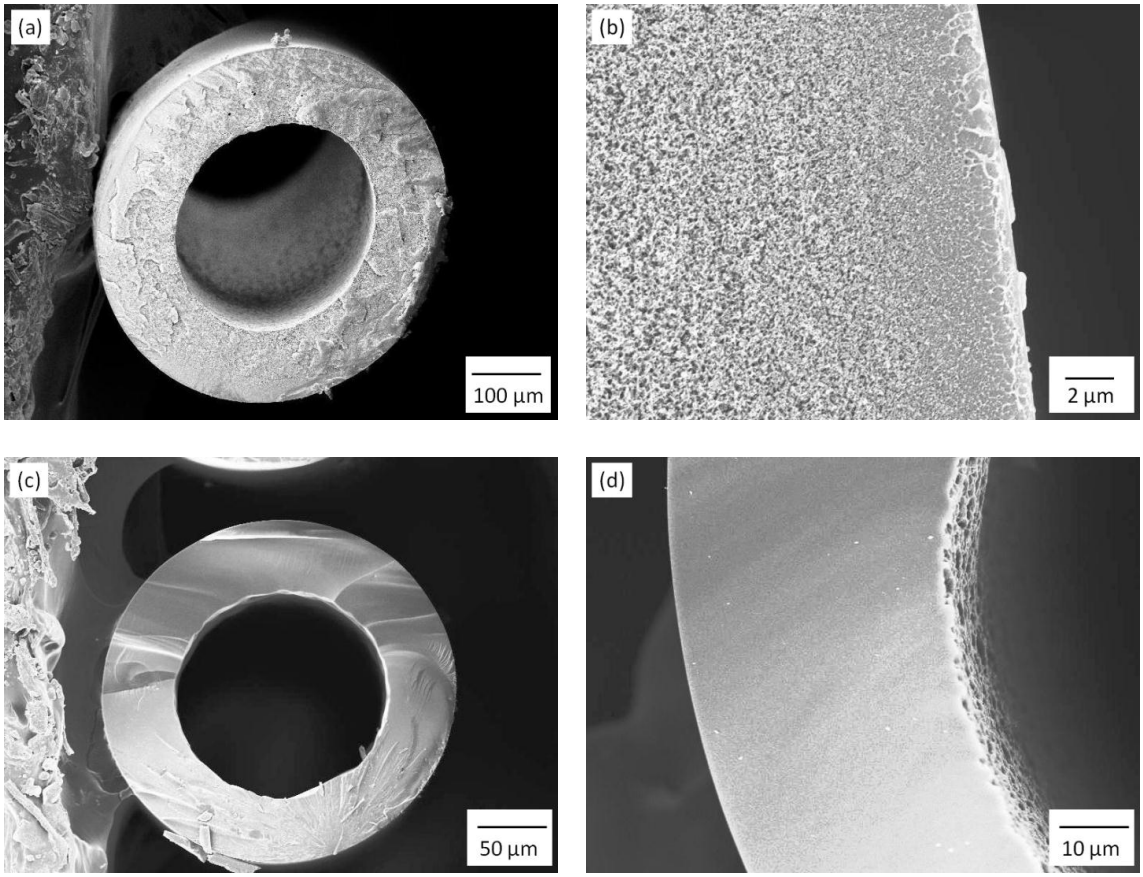

Figure 5.3 SEM images of a Matrimid® precursor fiber and resultant CMS fiber. (a) polymer fiber—cross-section; (b) polymer fiber—skin region; (c) CMS fiber—cross-section; (d) CMS fiber—fiber wall

Based on the macroscopic morphology obtained from SEM images and microscopic gas permeation results, it is clear that the porous substructure of the precursor hollow fiber collapses into a dense separation layer during pyrolysis. Although the permeability of CMS dense films is much higher compared to their precursor, in the fiber case, the permeance is not as high as predicted by the high permeability due to the much thicker effective separation layer.

To probe this phenomenon, we next investigated how substructure collapse occurs. Apparently, temperature plays an important role in the morphological evolution. The

glass transition temperature for Matrimid® is around 305-320 °C. Figure 5.4 shows a Matrimid® fiber that was soaked at 295 °C in argon atmosphere for 10 minutes. The picture obviously shows that the outer half of the fiber wall became very dense and smooth, while the inner half exhibited a clearly different morphology. Moreover, the thermally soaked polymer fiber showed a dramatic decrease in ethylene permeance. Barsema and Wessling showed that Matrimid® dense film heat-treated at 300 °C did not lose significant gas permeability as observed here [10], which indicates that serious densification of the porous fiber support layer happens during the glass transition stage. This temperature, however, is well below the pyrolysis temperature of 500 °C-800 °C needed for CMS formation. Krol and Koops [11] also observed a significant nitrogen permeance decrease of Matrimid® fibers by a factor of 60 after a heat-treatment at 350 °C for only 5 min. Figure 5.5 shows a Matrimid® CMS fiber cross-section with macrovoids, which were created during hollow fiber spinning process. Apparently, these large "pores" remain during the pyrolysis.

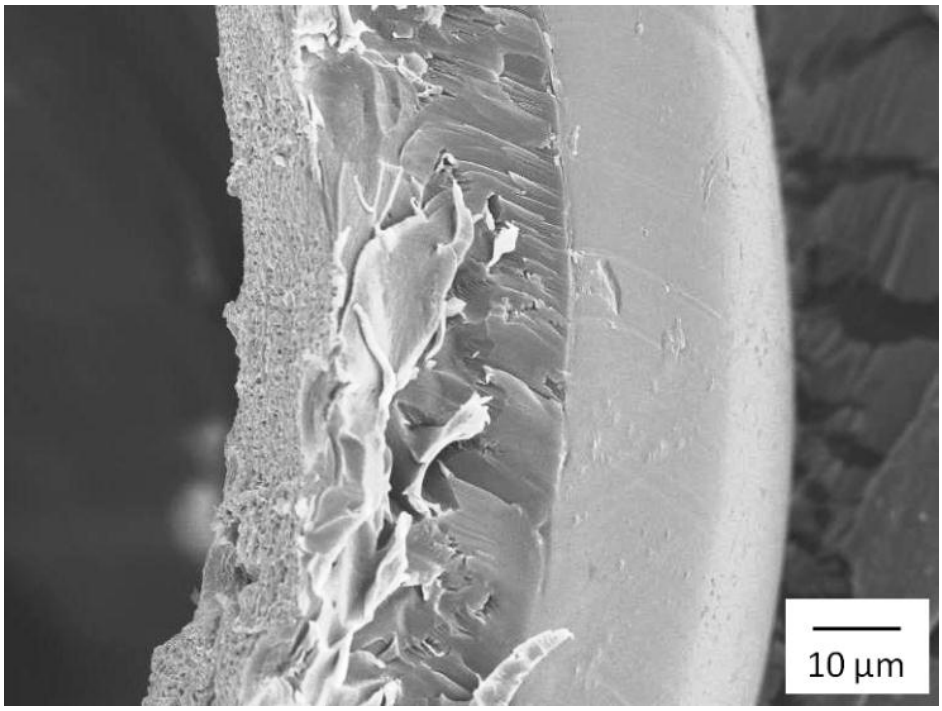

Figure 5.4 SEM image of a Matrimid® fiber heat-treated at 295 ℃ for 10 minutes under argon purge atmosphere

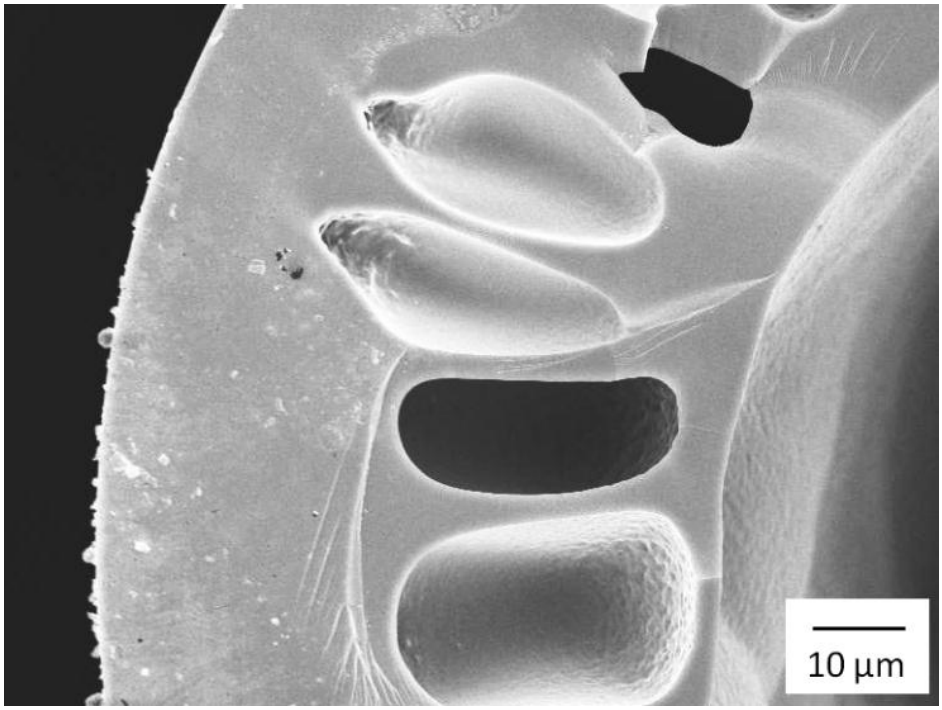

Figure 5.5 SEM image of a Matrimid® CMS fiber cross-section with macrovoids

5.4 Hypotheses regarding substructure collapse

Based on above observations, some hypotheses are proposed to help explain the substructure collapse during glass transition:

(1) The low material rigidity during intense thermal treatments is the fundamental cause, and in the case of Matrimid®, exceeding the glass transition appears to be the trigger of collapse, since at the glass transition, thermal energy is sufficient to overcome steric hindrance restricting rotation of polymer backbone segments. Polymer chains enter a soft viscous state instead of being rigid and tough [12]. Increased chain mobility brings opportunity for polymer chain interactions. Attractive molecular forces make densification happen, which is thermodynamically more stable. From another view, during fiber spinning, the porous substructure of a hollow fiber was "trapped" by water quenching, creating an unstable state. Heat treatment around/above T_g stabilizes the unstable state depending upon the details of the time/temperature exposure.

(2) Pore size and porosity distribution are also important. Small pore sizes provide short distances for polymer chain interactions. Collapse may start from the transition region under the dense skin layer, and move along the porosity gradient to the bore side.

(3) Since heat is transferred from the skin side to the bore side, collapse happens first at the outer layer.

The first hypothesis is supported by the near T_g heat treatment of fibers noted above. The heat-treatment under lower temperatures (i.e. 250 °C) did not cause significant morphological change. Storage modulus can be used to characterize the rigidity of a polymer. Dynamic mechanical analysis (DMA) was used to monitor the storage modulus change of Matrimid® dense film with increasing temperature, and the

result is shown in Figure 5.6. During glass-rubber transition, the storage modulus of the Matrimid® dense film decreased by more than two orders of magnitude, verifying the presence of a highly "soft" nature of Matrimid® above T_g.

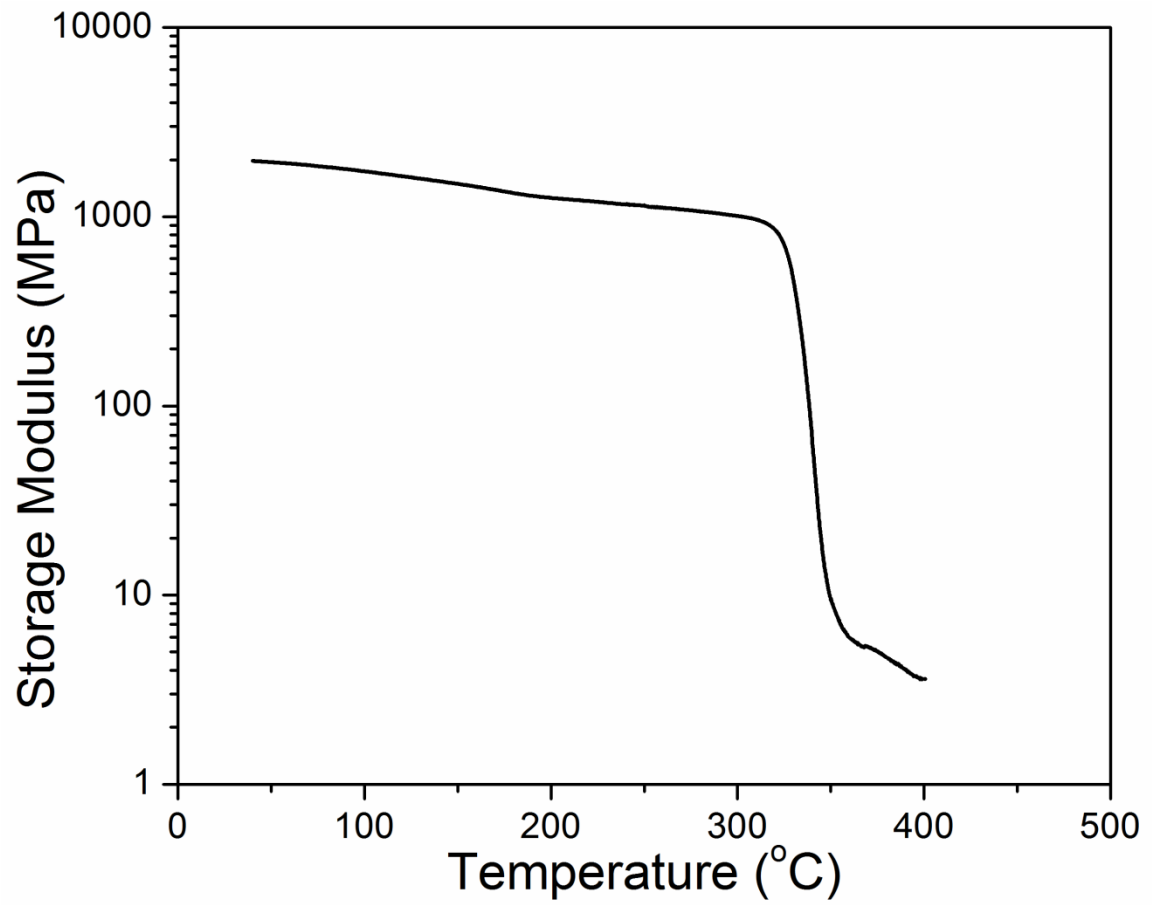

Figure 5.6 Dynamical mechanic analysis (DMA) results of Matrimid® film

Figure 5.5 suggests large pores (macrovoids in the fiber wall, or even the big fiber bore) maintain their original morphology. The dimension of these voids is at the order of 10 μm, and prevents them from collapse. The existence of these big pores suggests that the polymer still maintains some stiffness between T_g and T_d (thermal decomposition temperature), rather than enters a complete flow state. Some asymmetric film work was

then performed to examine hypothesis (2) and (3). Asymmetric film can be used to simulate the asymmetric fiber structure, as shown in Figure 5.7 (b). Meanwhile, the asymmetric film decouples the effect of heat flow and porosity distribution, because both sides of the film can be exposed to heat flow equally. Figure 5.7 (a) shows that the skin side of the film has a much denser structure (and thus may conduct more heat and accelerate the densification), while the other side is highly porous as shown in Figure 5.7 (c). After soaking at 295 °C for 10 minutes (argon atmosphere), the skin side shows a much thicker dense layer (~40 μm) (Figure 5.7 (d)) than the porous side (~10 μm) (Figure 5.7 (f)). These results support the suggestion that porosity affects the densification progress, which helps verify hypothesis (2). Also, the effect of heat flow in hypothesis (3) is supported by Figure 5.7 (f), since the porous part also collapsed, although it is slower than the skin side.

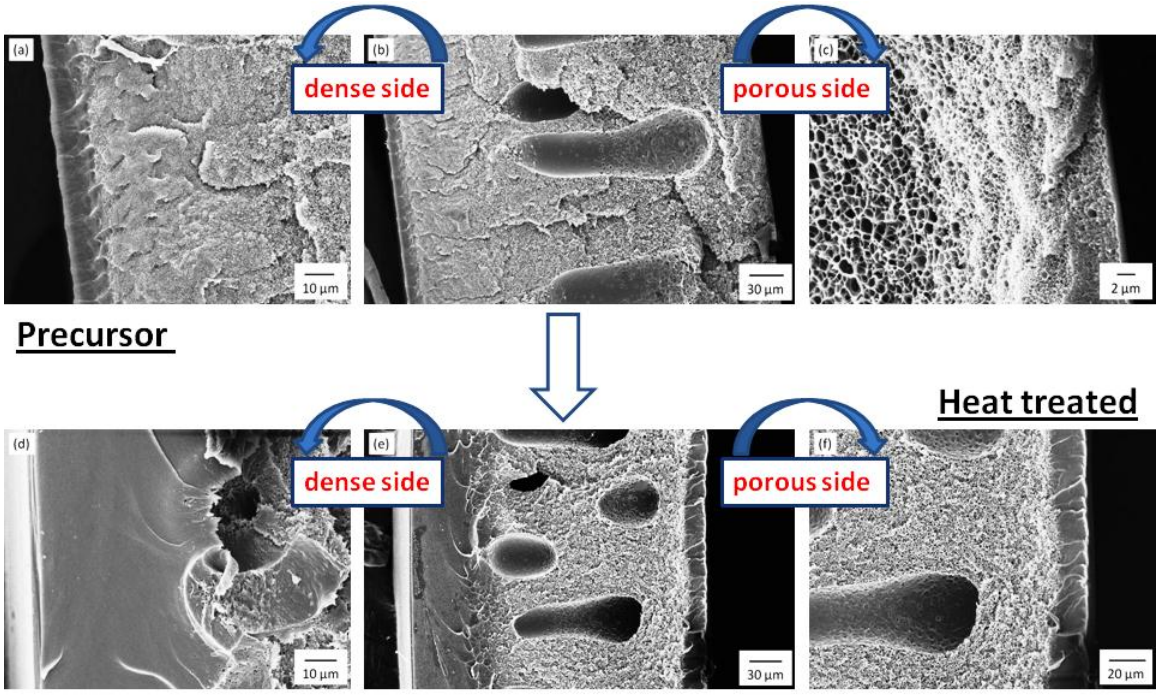

Figure 5.7 SEM images of a Matrimid® asymmetric film precursor and resultant 295 °C/10 minutes heat-treated film. (a) dense side of the precursor film; (b) overall morphology of the precursor film; (c) porous side of the precursor film; (d) dense side of the heat-treated film; (e) overall morphology of the heat-treated film; (f) porous side of the heat-treated film

5.5 Effect of precursor defect-free properties

The defect-free property is very important for polymer membranes. In integral dense skin layers, solution-diffusion mechanism dominates gas permeation. Solution-diffusion mechanism is very slow compared to Knudsen diffusion or viscous flow that occurs through nonselective defects in membranes [13]. Previously, it was believed that "defect-free" CMS hollow fibers must be derived from defect-free precursor fibers [14, 15]. Indeed, considerable effort has been made to prepare precursor fibers with defect-free skin layers, since defects may cause decreased selectivity in CMS fibers. The substantial morphological change between precursor fibers and the resultant CMS fibers

further suggests probably the small defects in the precursor fiber may not impose significant impact on CMS fibers derived from Matrimid®.

Usually, for the "inert interaction" of O_2 and N_2 with polymers, the O_2/N_2 selectivity is widely employed as the most characteristic criterion for integral skin examination of asymmetric membranes. A new 675 °C protocol (protocol B described in Table 3.3, with shorter ramp time and only 10 min thermal soak instead of 2 hrs) was used to pyrolyze precursor fibers with different O_2/N_2 selectivity to probe this issue more carefully. This protocol gives a reasonable high selectivity (~10) for C_2H_4/C_2H_6, and also shows a permeance increase for most gases. For a scale-up purpose, this protocol also saves energy input during pyrolysis. On the other hand, precursor O_2/N_2 selectivity investigated ranges from 6.7 to 0.9, which represents a wide range of precursor skin-integrity from the defect-free fiber (6.7) to the very defective Knudsen diffusion fiber (0.9).

The results of this extensive investigation are shown in Figure 5.8, and verify our hypothesis based on the morphological change. Permeation properties of 7 common gases (C_2H_4, C_2H_6, O_2, N_2, He, CO_2 and CH_4) were tested and the selectivity of 6 gas pairs were plotted. These gases cover a considerable range of gas sizes. As shown in Figure 5.8, the selectivity of most gas pairs is very consistent for precursors with a considerable range in starting selective layer perfection. Surprisingly, there is almost no correlation between the precursor defect-free property and Matrimid® CMS fiber performance. Especially, the "conventional wisdom" that precursor defect-free property is a predictor of resultant CMS fiber performance doesn't exist in these Matrimid® precursors, since defect-free precursors do not show any advantages over defective fibers. For

ethylene/ethane, the plotted selectivity is about 10 (as shown in Figure 5.8 (a)). The highest selectivity observed for some typical samples were close to 12, and the optimized ethylene permeance was above 1 GPU. The CO_2/CH_4 selectivity ranges from 50 to 90 (as shown in Figure 5.8 (c)), which is also well above the corresponding Matrimid® precursor intrinsic selectivity 36. It is interesting that CO_2/CH_4 (as shown in Figure 5.8 (c)) and He/N_2 selectivity (as shown in Figure 5.8 (d)) show much bigger variations than other gas pairs, while the selectivity of C_2H_4/CH_4 (as shown in Figure 5.8 (e)) and also N_2/CH_4 (as shown in Figure 5.8 (f)) are very consistent. This trend may be caused by the fast permeation rate of CO_2 and He, subtle structural changes may cause big variations for CO_2 and He permeation rates. On the other hand, slow gases (C_2H_4, C_2H_6, CH_4 and N_2) are less sensitive [16-19].

In fact, considering the observed porous structure densification noted earlier, it is not so surprising that the defect-free property is a questionable predictor of CMS fiber performance. Even pores of several hundred nm wide in porous support of precursor hollow fibers presumably can be eliminated during the glass-rubbery transition, the small pores (mostly less than 1 nm) existing as defects should be easily cured. Figure 5.9 illustrates the proposed curing mechanism for defective Matrimid® fibers. Small pinhole defects formed in the fiber spinning process can be healed during thermal annealing above T_g (below T_d). In this case, the defect-free fiber and slightly defective fibers experience a similar dense stage between T_g and T_d. Essentially, when carbonization takes place, they are the same. However, precursor fibers with serious defects such as macrovoids cannot be healed due to the need of extremely large segmental and super-segmental motions to heal.

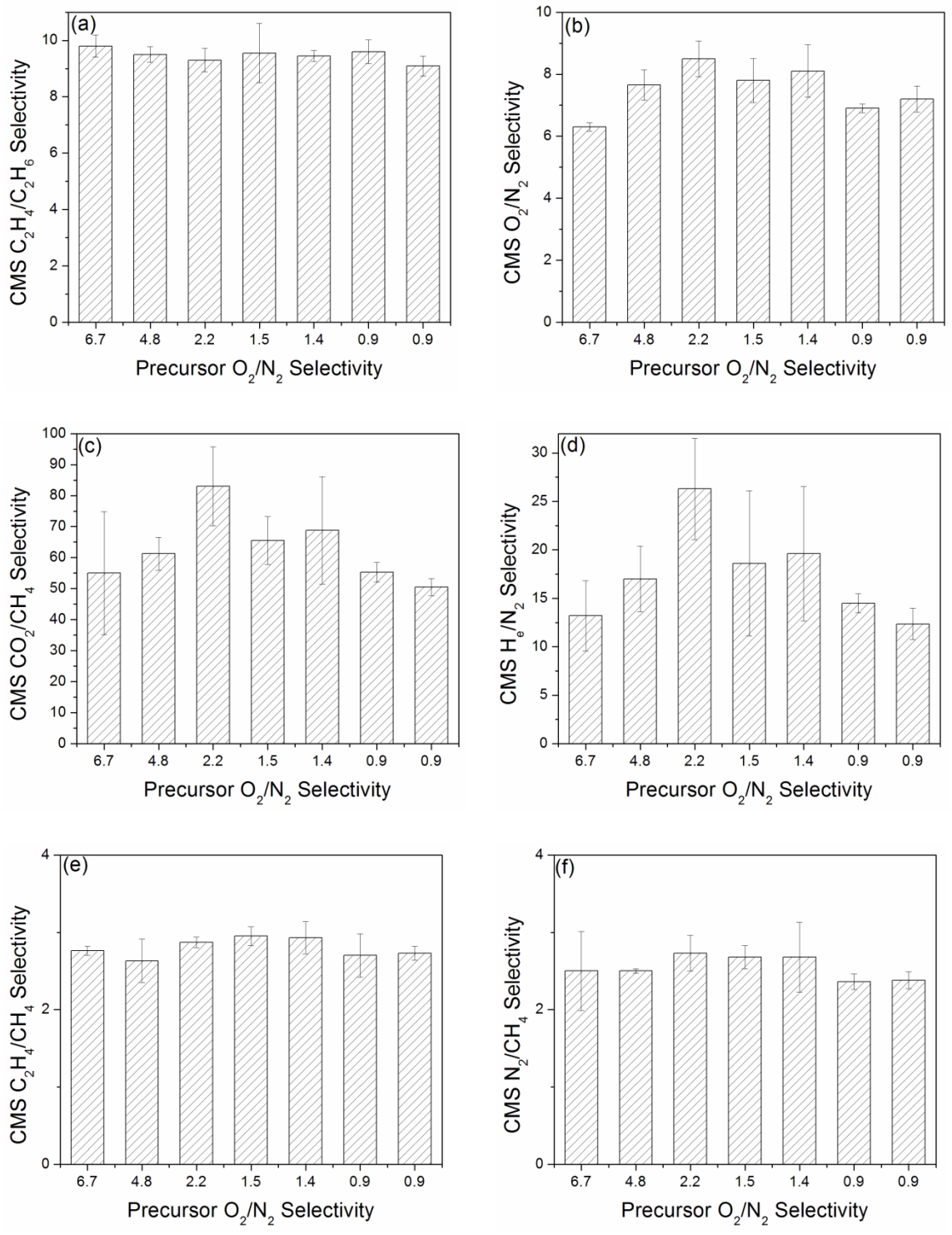

Figure 5.8 Effect of precursor defect-free properties on the Matrimid® CMS fiber performance for various gas pairs (Testing condition: 100 psi pure gas feed and 35 °C)

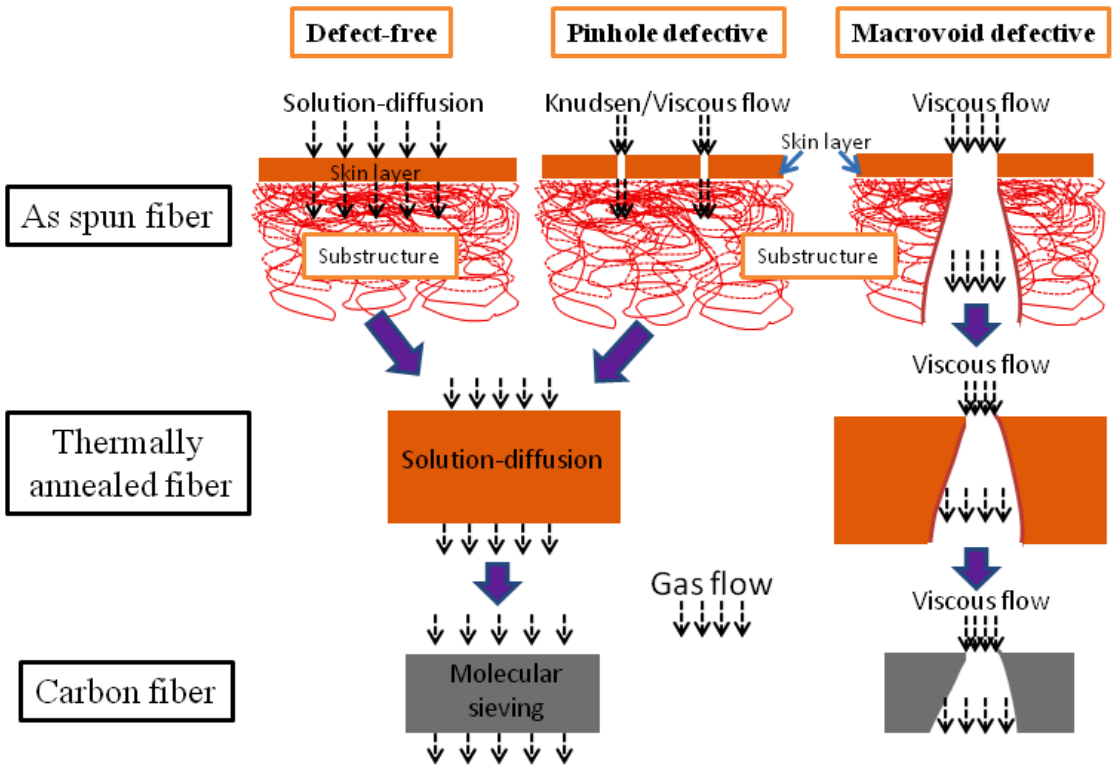

Figure 5.9 Curing mechanism of Matrimid® fibers with pinhole defects.

Thus, we conclude that under certain pyrolysis protocols, the effect of precursor defect-free property on Matrimid® CMS fiber performance seems negligible based on the above results. This conclusion may have significant impact on the development of CMS hollow fiber membranes. Much effort has been made to spin defect-free Matrimid® precursor fiber at the beginning of this research, and it appears unnecessary for the CMS needs. The curing mechanism can also be used to explain previously published results from other researchers. Barsema and Wessling [14] have produced selective gas separation CMS fibers from very porous and non-selective P84 fibers, which were initially designed for ultra-filtration. Jiang and Chung [15] have reported that dual-layer fibers with polysulfone-beta zeolite mixed matrix as sheath and Matrimid® as the core

could be pyrolyzed into carbon-zeolite mixed matrix membranes with high selectivity for O_2/N_2 and CO_2/CH_4 separations. In these cases, precursor fibers also showed Knudsen diffusion selectivity, were very porous and seriously defective. Presumably, the curing effect proposed by our current work also occurred during their pyrolysis: polysulfone collapsed to zeolite surface and created good interfacial adhesions; polysulfone and Matrimid® core layers also became dense layers. Finally, the carbon layer from the Matrimid® core should also be responsible for high selectivity, as suggested by our work. Similar phenomena were also observed by replacing the polymers (polysulfone and Matrimid®) with P84 polyimide [20]. Based on the above discussion, due to the glass-rubbery transition, it seems that the zeolite-polymer adhesion problem, which is crucial for zeolite-polymer mixed matrix membranes, may not cause a big problem for zeolite-carbon mixed matrix membranes for certain polymers used.

The conclusions above, at the present time, however, should be rigorously restricted to Matrimid® CMS fibers until more work shows that the above suggestions are valid. Any other polymer may exhibit different results based on polymer chain mobility. Moreover, one must be cautious not to over-extrapolate the significance of the observations, since the morphological change itself is not sufficient to conclude that the full wall thickness contributes to permeation resistance before permeation results of CMS fibers derived from differently defective precursor fibers are carefully examined. In fact, as will be discussed with the more rigid 6FDA family of precursors, the importance of defect-free precursors appears much more critical as was originally anticipated in Chapter 4.

5.6 Overcoming substructure collapse

CMS membranes offer much higher permeability than its precursor. For example, ethylene permeability of 500 °C/2 hr Matrimid® CMS dense film is 106 Barrers and 675 °C/2 hr CMS is 14.4 Barrers, while the intrinsic permeability of ethylene in Matrimid® precursor is only 0.45 Barrers. This fact means that Matrimid® CMS fibers lose one of their best features in comparison to its asymmetric polymer precursor, the ultra-thin skin layer. The fiber permeance is still reflected by the very high permeability, but it would be much more attractive in the absence of such collapse. This effect is especially important for separations of "big" gases (C_2H_4/C_2H_6, C_3H_6/C_3H_8, etc.), since low gas flux imposes significant increase of footprints of membrane module in applications as well as material costs. The impact on "small" gases can be less serious due to the fast nature of permeation rates (for instance, CO_2 removal or H_2 separation).

This phenomenon of substrate collapse may be a common feature which must be addressed in all cases involving intense heat-treatments, including thermal cross-linking [21, 22] and other thermal rearrangement processes [23]. The complex structural architecture of hollow fibers must be taken into consideration for any extension of dense film work into asymmetric hollow fibers.

Overcoming the substructure problem can be regarded as a major challenge for developing industrially viable CMS hollow fiber membranes for gas separations (and also fibers involving intense heat-treatments). For future research, identifying membrane materials with less collapse extent or even without a collapse problem is an important issue. The real challenge is to obtain a high selectivity meanwhile. The details of seeking novel precursor materials are discussed in Chapter 6. The rest of this section describes the

effort for increasing permeance in Matrimid® CMS fibers.

For Matrimid®, the first attempt is to improve pyrolysis protocols. In the asymmetric film work, it was revealed that the substructure collapse was also a kinetic process. Therefore, it was expected that if the ramp rate was fast enough, porous structure collapse may not happen due to the limited "gap" between glass transition temperature and decomposition temperature. In an extreme case, the furnace was maintained at a temperature above the decomposition temperature, then some precursor fibers were pulled into the high temperature tube furnace under argon purge from room temperature. Unfortunately, the fibers were broken into pieces due to rapid decomposition reactions. Creating asymmetric CMS fiber structure from Matrimid® precursor by simply altering pyrolysis protocols seems to be impossible. Optimization of pyrolysis protocols may give some improvement for the permeability and thus increase the permeance. The temperature protocol B (also referred as 675 ^{o}C/10 min protocol) in Table 3.3 is such an example. 675 ^{o}C pyrolysis temperature gave high selectivity for ethylene/ethane (~10), and the reduced soak time increased the ethylene permeance. Compared to 650 ^{o}C/2 hr protocol, this 675 ^{o}C/10 min protocol improved both permeance and selectivity. This new protocol was later frequently used in Matrimid® fiber pyrolysis. However, somehow the protocol optimization was obviously not sufficient to boost the permeance significantly. Additional approaches regarding the modification of precursor fibers must be pursued.

Engineering approaches can be used to reduce the "apparent" separation layer thickness. This concept does not interfere with the "chemistry" of the starting precursor material. Two approaches have been explored in this research: (1) thin-walled monolithic Matrimid® fiber; (2) dual-layer fiber with a porous core and a dense thin Matrimid®

sheath layer. While the spinning conditions for defect-free fibers are very strict, due to the unnecessary requirement of defect-free precursor fibers, these engineering options somehow became conceptually feasible.

Thin-walled fibers can be spun by adjusting spinning parameters. They were produced by using high bore fluid flow rate, low dope flow rate and high take-up rate. Figure 5.10 shows SEM images of a thin-walled CMS fiber. The fiber wall is about 20 μm. The comparison of permeation results of the thin-walled fiber and a normal fiber (~35 μm wall thickness) is shown in Table 5.1. By reducing the separation layer thickness, permeance of all the gases listed was increased by three times, while selectivity for all the gas pairs was very close. For example, comparing the CO_2/CH_4 separation results with previous work, the CO_2 permeance was increased by three times, meanwhile, the selectivity was slightly higher as well. There are also limitations for the wall thickness due to the current spinning apparatus and consideration of mechanical strength. The practical limit is probably about 10 μm or slightly less.

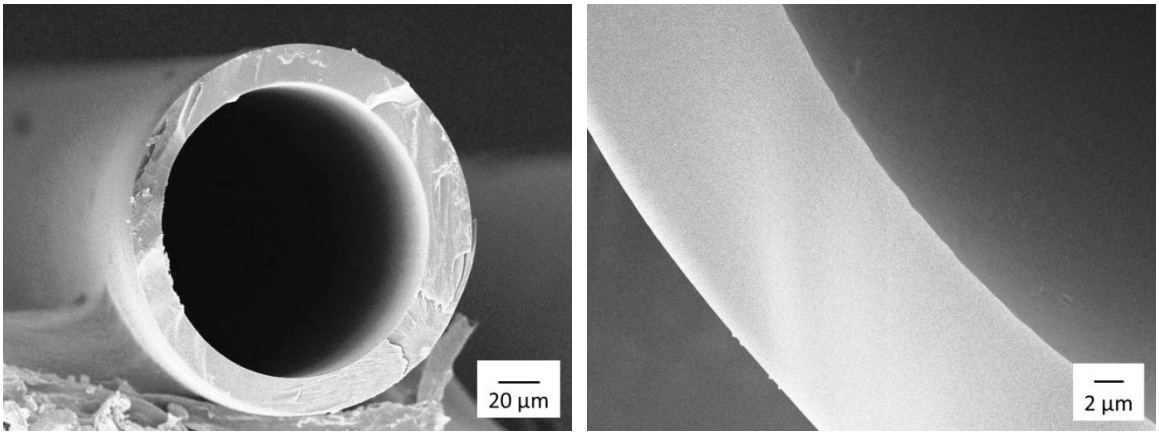

(a) cross-section (b) fiber wall

Figure 5.10 SEM images of a thin-walled Matrimid® CMS fiber

Table 5.1 Permeation results for a thin-walled and a normal CMS fiber

Precursor	$(P/l)_{C2H4}$	$(P/l)_{O2}$	$(P/l)_{CO2}$	$(P/l)_{He}$	$\alpha_{C2H4/C2H6}$	$\alpha_{O2/N2}$	$\alpha_{CO2/CH4}$	$\alpha_{He/N2}$
A: (normal)	0.33	3.1	10.2	11.7	9	9.4	91	35
B: (thin-walled)	1.08	9.5	34	32	9.6	8.9	92	30

100 psi, pure gas feed, 35 ^{o}C. Permeance unit: GPU

Another approach to reduce the separation layer thickness is to create a porous support layer. For example, some porous particles (zeolites with pores accessible for hydrocarbons or some mesoporous materials) can be incorporated in the core layer of dual layer hollow fibers while the sheath layer remains as a pure Matrimid® selective separation layer. Creating a thin and defect-free sheath layer in the presence of porous particles is very challenging, and significantly reduced mechanical strength is expected due to the high loading of porous particles in carbon matrix. Theoretically, for ideal carbon-porous filler mixed matrix, based on the Maxwell model calculation, 50% particles with high permeability must be loaded in order to achieve 4 times increase in the overall permeability for the mixed matrix layer. The industrial scale dual layer fiber spinning is able to achieve ~1 μm thick sheath layer in a polymer-polymer dual layer fiber. The real challenge should be the mechanical strength problem. With the required high loading ratio, the composite fibers can be very brittle. Proof-of-concept experiments have also been performed. 10-20% Zeolite 13X (pore window 8 Å) was used as fillers for the core layer during spinning. As expected, the pyrolyzed fibers were very brittle. The obtained ethylene permeance was higher than the value for the normal fiber listed in Table 5.1, but still less than 1 GPU while the ethylene/ethane selectivity was kept at about 10. The SEM images are shown in Figure 5.11. Again, while the concept remains

viable theoretically, a great deal of effort must be mad in terms of practical considerations.

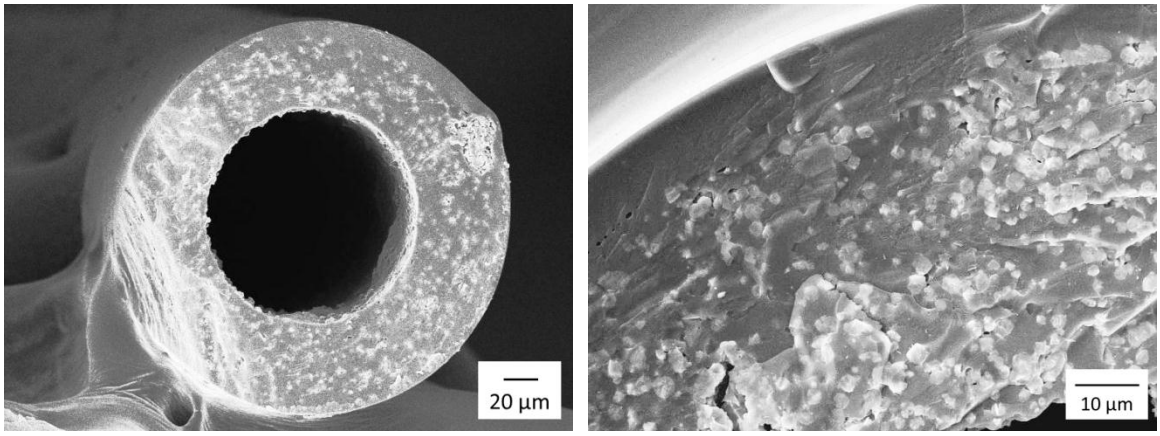

(a) cross-section (10% zeolite loading) (b) fiber wall (20% zeolite loading)

Figure 5.11 SEM images of a carbon-zeolite mixed matrix fiber

After a great deal of effort working on the original Matrimid® polyimide, the previous engineering approaches showed some permeance improvements (< 2 GPU for ethylene permeance while maintaining a high ethylene/ethane selectivity), but still no revolutionary boost in permeance was possible. We conclude, therefore, that without changing the "chemistry" of precursor polymers, it is difficult to substantially increase the permeance of CMS hollow fiber membranes. The further effort is described in Chapter 6.

5.7 Separation performance of CMS membranes under realistic conditions

5.7.1 Mixed gas permeation test under high pressure

Besides the "apparent" separation performance represented by pure gas

permeability and selectivity, there several realistic challenges of membrane applications for ethylene/ethane separations: (1) the difference between mixed gas and pure gas transport behaviors; (2) the high pressure of feed gas mixture; (3) the low temperature of operations. One set of typical conditions of a Dow plant is listed as below: temperature 3.6 ^{o}F, pressure 347.4 psi; the composition is 61.8 wt% ethylene and 38.2 wt% ethane with 29 ppm methane. These conditions may vary at different plants, but can be representative for academic research.

To evaluate the CMS hollow fiber membrane performance under realistic feed conditions, mixed gas permeation tests were performed by using an "improved" module mentioned in Sections 5.5 and 5.6. The feed composition (63.2 mol% ethylene/36.8 mol% ethane) and pressure (350 psia) were identical to the industrial feed conditions. This particular test was at 35 ^{o}C, which was higher to the industrial condition. Pure gas permeation results and mixed gas permeation results were compared in this study. The pressure dependence of permeance and selectivity were considered as well. A series of systematic tests were performed, and the results are shown in Table 5.2. High pressure (350 psia) mixed gas test (test 2 in Table 5.2) showed the same selectivity with 100 psia pure gas test (test 1 in Table 5.2). The decrease in ethylene permeance was checked by a pure gas test under partial pressures of the 350 psia mixed gas test (test 3 in Table 5.2). The result was close to test 2, which means the permeance drop was caused by pressure dependence of permeability (low permeability at high feed pressure due to Langmuir sorption isotherm). No plasticization effect was observed even at such high pressure hydrocarbon mixture feed, which demonstrates the excellent stability of CMS hollow fiber membrane for challenging gas separation applications. These results also reveal that

even pure gas tests are quite reliable for CMS fiber ethylene/ethane separation performance, since the selectivity is quite consistent for all the cases investigated.

Table 5.2 Comparison between mixed gas and pure gas permeation tests

	Test 1	Test 2	Test 3
Test conditions (35 ^{o}C)	100 psia pure gas	350 psia mixed gas	220 psia C_2H_4, 130 psia C_2H_6, pure gas
$(P/l)_{C2H4}$ (GPU)	1.08	0.87	0.89
$\alpha_{C2H4/C2H6}$	11.1	11.1	10.5

5.7.2 Mixed gas permeation test under cryogenic conditions

The testing temperature has a significant impact on gas transport through membranes. The permeability of a penetrant through a membrane follows Arrhenius temperature dependence:

$$P = P_0 \exp(-\frac{E_P}{RT}) \tag{5.2}$$

where P_0 is the pre-exponential factor, E_P is the apparent activation energy of permeation, R is the universal gas constant and T is the absolute temperature.

The activated diffusion increases with temperature according to the Arrhenius relationship (Equation 5.3) and the sorption coefficient decreases with temperature following van't-Hoff equation (Equation 5.4).

$$D = D_0 \exp(-\frac{E_D}{RT}) \tag{5.3}$$

$$S = S_0 \exp(-\frac{H_S}{RT}) \tag{5.4}$$

where D_0 and S_0 are pre-exponential factors for diffusion and sorption respectively, E_D is the apparent activation energy for diffusion and H_S is the apparent heat of sorption.

Typically, the heat of sorption term is negative, while the activation energy of diffusion is positive. The permeability usually increases with increasing temperature since the increase in diffusivity outweighs the decrease in sorption coefficient. In most cases, the selectivity decreases with increasing temperature.

The effect of testing temperature is studied in detail in the parallel dense film work, in order to characterize the fundamentals of gas transport through CMS membranes. In this research, the focus is for more practical purposes. The test hereby aims to evaluate the membrane performance under cryogenic conditions. This test was performed by Mark Brayden and Gregory Barbay in a Dow laboratory. The tests at Georgia Tech were mostly performed in constant volume permeation system; therefore, usually the flux measurement was not a problem. In order to meet the flow requirement for the downstream mass flowmeter, a 20-fiber module was constructed and the test was performed using downstream argon sweep.

The membrane was first fed with ethylene/ethane gas mixture at room temperature, then cooled down to 0 ^{o}F, kept at 0 ^{o}F for 22 hours and finally warmed back to room temperature. The ethylene/ethane selectivity at low temperature was about 16, which was quite high for this challenging gas pair and much higher than the value at room temperature (~11). The flux at low temperature was about half of the value at room temperature. The trend was consistent with the expectation of the effect of testing temperature on membrane transport properties. This test also validated the application of CMS membranes under cryogenic conditions. The long term stability (~22 hours) under

high feed pressure (~300 psig) and very low temperature (~0 ^{o}F) was demonstrated. From these results, it appears that the permeance still requires further improvement while the selectivity can be significantly increased due to the low operation temperature.

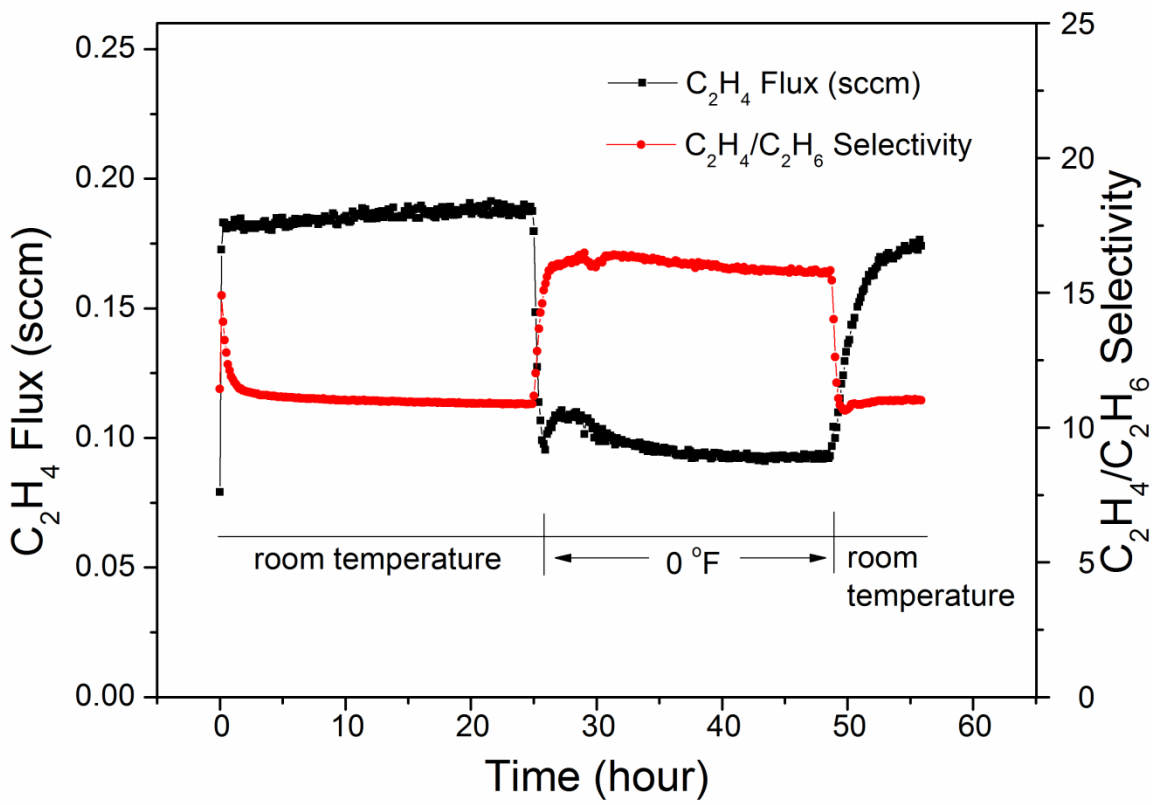

Figure 5.12 Cryogenic testing results of Matrimid® CMS hollow fiber membranes

5.8 Summary and conclusions

Matrimid® derived CMS dense film membranes and hollow fiber membranes have been successfully fabricated for the C_2H_4/C_2H_6 separation. The CMS membranes showed significant improvements over their polymer precursor under a wide range of pyrolysis conditions, and they exceeded the upper bound for spinnable polymers for the C_2H_4/C_2H_6 separation. A high selectivity of 12 for C_2H_4/C_2H_6 separation has been

obtained in both dense flat film and hollow fiber configurations. Our comparative study between dense film and hollow fiber revealed a significant difference of effective separation layer thickness between the precursor fibers and their resultant CMS fibers. SEM results showed that the deviation was essentially due to the collapse of porous substructure of precursor fibers. Polymer chain flexibility (reflected by relatively low T_g of Matrimid®) appears to be the fundamental cause of substructure collapse. Further study showed that the defect-free property of precursor fibers was not a simple predictor of CMS fiber performance. Even some defective precursor fibers (i.e., fibers with Knudsen diffusion selectivity), can be transformed into highly selective CMS fibers by pyrolysis. In order to overcome the substructure collapse issue, several approaches were pursued. The optimized CMS hollow fiber membranes were tested under realistic conditions (mixed gas feed, high feed pressure and cryogenic testing temperature) and excellent stability and performance have been demonstrated.

5.9 References

[1] L.M. Robeson, The upper bound revisited, J. Membr. Sci. 320 (2008) 390-400.

[2] L.M. Robeson, Correlation of separation factor versus permeability for polymeric membranes, J. Membr. Sci. 62 (1991) 165-185.

[3] R.L. Burns, W.J. Koros, Defining the challenges for C_3H_6/C_3H_8 separation using polymeric membranes, J. Membr. Sci. 211 (2003) 299-309.

[4] C. Staudt-Bickel, W.J. Koros, Olefin/paraffin gas separations with 6FDA-based polyimide membranes, J. Membr. Sci. 170 (2000) 205-214.

[5] S.S. Chan, T.-S. Chung, Y. Liu, R. Wang, Gas and hydrocarbon (C2 and C3) transport properties of co-polyimides synthesized from 6FDA and 1,5-NDA (naphthalene)/Durene diamines, J. Membr. Sci. 218 (2003) 235-245.

[6] S.S. Chan, R. Wang, T.-S. Chung, Y. Liu, C2 and C3 hydrocarbon separations in poly(1,5-naphthalene-2,2'-bis(3,4-phthalic) hexafluoropropane) diimide (6FDA-1,5-NDA) dense membranes, J. Membr. Sci. 210 (2002) 55-64.

[7] K. Tanaka, A. Taguchi, J. Hao, H. Kita, K. Okamoto, Permeation and separation properties of polyimide membranes to olefins and paraffins, J. Membr. Sci. 121 (1996) 197-207.

[8] M. Rungta, L. Xu, W.J. Koros, Carbon molecular sieve dense film membranes derived from Matrimid® for ethylene/ethane separation, Carbon 50 (2012) 1488-1502.

[9] L. Xu, M. Rungta, W.J. Koros, Matrimid® derived carbon molecular sieve hollow fiber membranes for ethylene/ethane separation, J. Membr. Sci. 380 (2011) 138-147.

[10] J.N. Barsema, S.D. Klijnstra, J.H. Balster, N.F.A. van der Vegt, G.H. Koops, M. Wessling, Intermediate polymer to carbon gas separation membranes based on Matrimid PI, J. of Membr. Sci. 238 (2004) 93-102.

[11] J.J. Krol, M. Boerrigter, G.H. Koops, Polyimide hollow fiber gas separation membranes: preparation and the suppression of plasticization in propane/propylene environments, J. Membr. Sci. 184 (2001) 275-286.

[12] R.W. Baker, Membrane technology and applications, 2 ed., John Wiley & Sons Ltd, West Sussex, England, 2004.

[13] A.F. Ismail, P.Y. Lai, Effects of phase inversion and rheological factors on formation of defect-free and ultrathin-skinned asymmetric polysulfone membranes for gas separation, Sep. Purif. Technol. 33 (2003) 127-143.

[14] J.N. Barsema, N.F.A. van der Vegt, G.H. Koops, M. Wessling, Carbon molecular sieve membranes prepared from porous fiber precursor, J. Membr. Sci. 205 (2002) 239-246.

[15] L.Y. Jiang, T.S. Chung, R. Rajagopalan, Dual-layer hollow carbon fiber membranes for gas separation consisting of carbon and mixed matrix layers, Carbon 45 (2007) 166-172.

[16] M.R. Kosuri, W.J. Koros, Defect-free asymmetric hollow fiber membranes from Torlon®, a polyamide-imide polymer, for high-pressure CO_2 separations, J. Membr. Sci. 320 (2008) 65-72.

[17] I. Pinnau, W.J. Koros, Relationship between substructure resistance and gas separation properties of defect-free integrally skinned asymmetric membranes, Ind. Eng. Chem. Res. 30 (1991) 1837-1840.

[18] J.M.S. Henis, M.K. Tripodi, Composite hollow fiber membranes for gas separation: the resistance model approach, J. Membr. Sci. 8 (1981) 233-246.

[19] D.T. Clausi, S.A. McKelvey, W.J. Koros, Characterization of substructure resistance in asymmetric gas separation membranes, J. Membr. Sci. 160 (1999) 51-64.

[20] Y. Li, T.S. Chung, Exploratory development of dual-layer carbon-zeolite nanocomposite hollow fiber membranes with high performance for oxygen enrichment and natural gas separation, Micropor. Mesopor. Mat. 113 (2008) 315-324.

[21] I.C. Omole, S.J. Miller, W.J. Koros, Increased molecular weight of a cross-linkable polyimide for spinning plasticization resistant hollow fiber membranes, Macromolecules 41 (2008) 6367-6375.

[22] A.M. Kratochvil, W.J. Koros, Decarboxylation-induced cross-linking of a polyimide for enhanced CO_2 plasticization resistance, Macromolecules 41 (2008) 7920-7927.

[23] H.B. Park, C.H. Jung, Y.M. Lee, A.J. Hill, S.J. Pas, S.T. Mudie, E. Van Wagner, B.D. Freeman, D.J. Cookson, Polymers with cavities tuned for fast selective transport of small molecules and ions, Science 318 (2007) 254-258.

CHAPTER 6

6FDA-POLYIMIDES DERIVED CMS HOLLOW FIBER MEMBRANES

Chapter 5 describes the formation and characterization of Matrimid® derived CMS hollow fiber membranes. The comparative study between CMS dense film and hollow fiber membranes revealed a significant change in the asymmetric hollow fiber morphology. This chapter aims to use alternative precursor polymers to address the substructure collapse problem. 6FDA-DAM and 6FDA/BPDA-DAM were chosen as two promising alternative precursor polymers. Creation of asymmetric CMS fiber morphology and optimization of CMS micro-structure are discussed.

6.1 Strategies for overcoming substructure collapse

As demonstrated in Chapter 5, to overcome substructure collapse, the conceptually feasible engineering approaches require significant effort to address several realistic hurdles. It is desirable to pursue non-collapse or partially collapse precursor materials for CMS membrane formation. By using these materials, the membrane fabrication process will not be complicated and the mechanical strength issue can be avoided.

The major problem caused by substructure collapse is the increased separation layer thickness and the resultant decreased permeance. Therefore, the ability to maintain asymmetric morphology is the first requirement for the new precursor material. Since the glass-rubber transition is the fundamental cause of substructure collapse of Matrimid®,

polymers with high glass-rubber transition temperatures should have better rigidity during intense heat-treatments. The glass-rubber transition temperature (T_g) of Matrimid® is 305 ^oC, well below its decomposition temperature. Previously, as demonstrated in Chapter 5, the storage modulus of Matrimid® decreases by more than two orders of magnitude during glass-rubber transition. Due to the rigid structure and the versatility of monomer choices, 6FDA-polymers potentially provide high T_g that may meet the requirement for asymmetric CMS fiber formation. The T_g of 6FDA-DAM polyimide is 395 ^oC from DSC measurement, and the T_g of 6FDA/BPDA-DAM is 424 ^oC. Dynamic mechanical analysis was performed for these two polyimides used in this study and compared with Matrimid®. The DMA results are shown in Figure 6.1. As demonstrated in Figure 6.1, the storage modulus of Matrimid® drops when the temperature is slightly above 300 ^oC; for 6FDA-DAM, the dramatic reduction occurs around 400 ^oC; for 6FDA/BPDA-DAM, the storage modulus remains quite high even near 450 ^oC. 6FDA-DAM and especially 6FDA/BPDA-DAM have higher rigidity than Matrimid® during intense heat-treatments. Maintaining asymmetric morphology during CMS fiber formation was expected.

In addition, due to the inhibited packing caused by bulky -CF_3 and -CH_3 groups and rigid backbone, as shown in Table 6.1, 6FDA-DAM and 6FDA/BPDA-DAM have much higher precursor permeability compared to Matrimid® [1]. Previous studies revealed that higher precursor permeability resulted in higher CMS permeability [2]. Therefore, with 6FDA-DAM and 6FDA/BPDA-DAM precursor polymers, both asymmetric morphology and CMS permeability were expected to be improved, which should lead to a higher permeance than Matrimid® CMS fibers. Based on the 6FDA-

DAM and 6FDA/BPDA-DAM CMS results, more precursors were then extended in this research, such as cross-linkable precursor and pre-oxidized precursors.

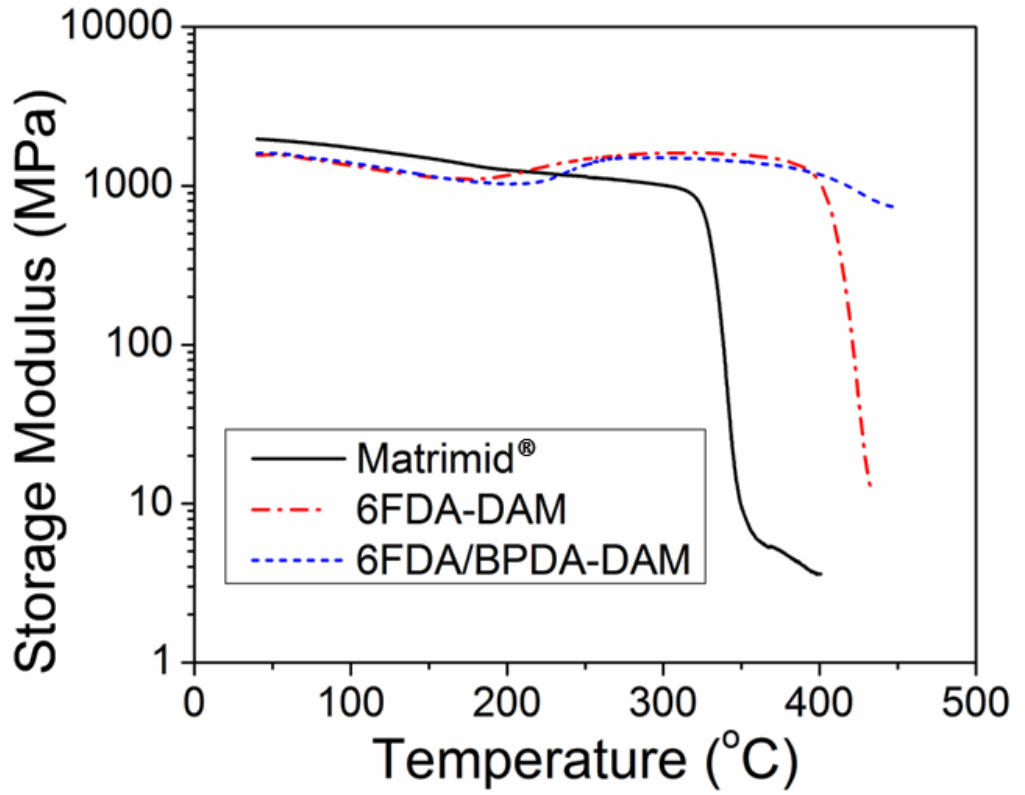

Figure 6.1 Dynamic mechanical analyses of Matrimid®, 6FDA-DAM and 6FDA/BPDA-DAM thin films

Table 6.1 Transport properties of polymer precursors [1]

Polymer	C_2H_4 Permeability (Barrer)	$\alpha_{C2H4/C2H6}$
Matrimid®	0.45	4.5
6FDA-DAM	64	3.0
6FDA/BPDA-DAM	46	3.3

Pure gas measurement at 35 °C, 50 psia

6.2 Morphology of CMS fibers derived from 6FDA-polymers

6.2.1 Morphology of CMS fibers derived from 6FDA-DAM and 6FDA/BPDA-DAM

In Chapter 4, defect-free asymmetric 6FDA-DAM and 6FDA/BPDA-DAM hollow fiber membranes were successfully fabricated. The defect-free 6FDA-DAM and 6FDA/BPDA-DAM precursor fibers were then pyrolyzed into carbon fibers. SEM was used to characterize the morphology of CMS fibers. Figure 6.2 shows the comparison of morphology of carbon fibers derived from Matrimid®, 6FDA-DAM and 6FDA/BPDA-DAM. The Matrimid® CMS fiber shows a completely dense wall in the SEM picture, even on the bore side of the fiber wall, as shown in Figure 6.3 (a); 6FDA-DAM shows some porous feature near the bore side of the fiber compared to Matrimid®, as shown in Figure 6.3 (b); 6FDA/BPDA-DAM shows much better asymmetric structure than Matrimid®. It is clear that a correlation exists between asymmetric CMS fiber morphology and glass-rubber transition temperature. The higher the T_g, the more rigid the polymer is during intense heat-treatments, thus, the more asymmetry the CMS fiber can retain from the precursor polymer fiber during CMS formation. By using 6FDA/BPDA-DAM as a precursor, with a very high T_g (424 ^oC), the asymmetric morphology was successfully achieved in CMS fiber. The thin separation layer thickness was expected to contribute to a high permeance.

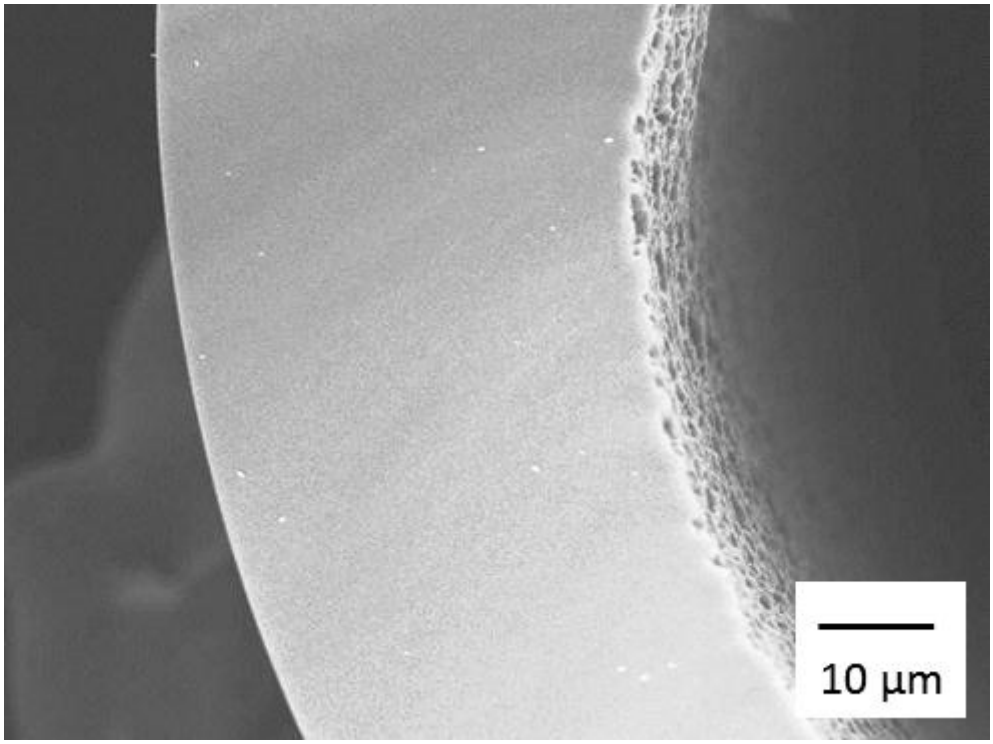

(a) Fiber wall of Matrimid® CMS fiber

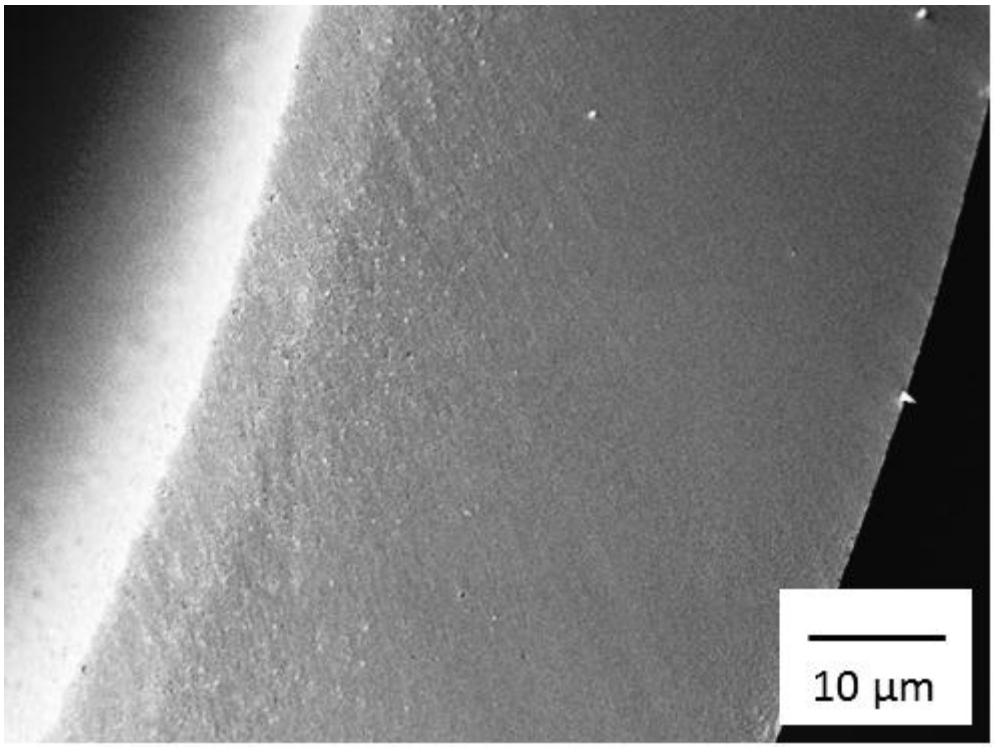

(b) Fiber wall of 6FDA-DAM CMS fiber

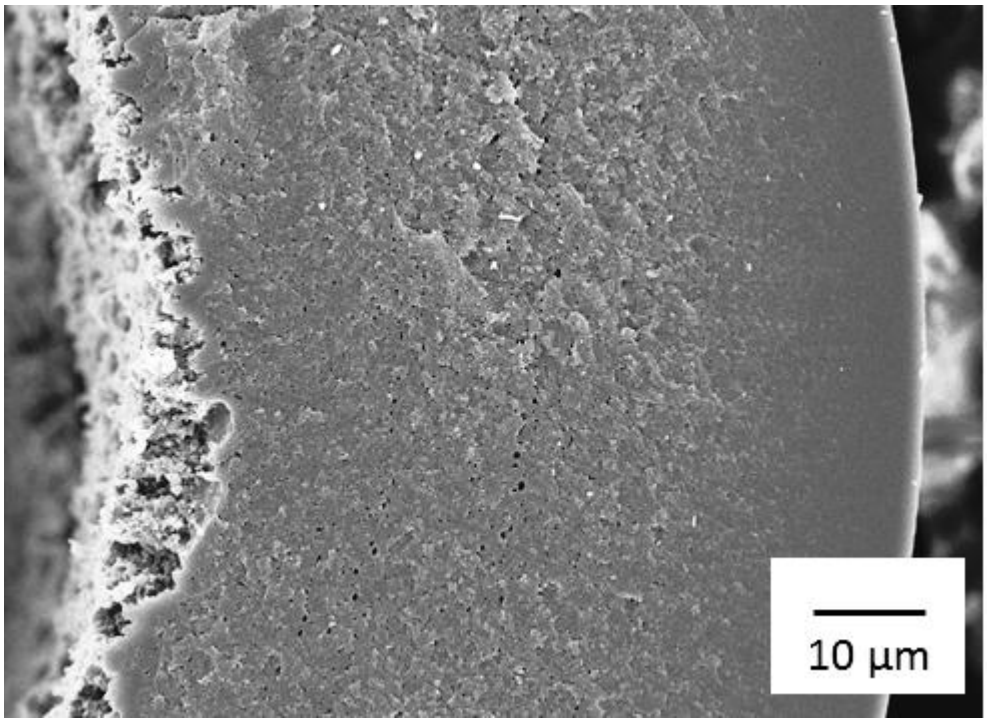

(c) Fiber wall of 6FDA-DAM CMS fiber

Figure 6.2 Wall morphology of CMS hollow fiber membranes produced from 3 precursor polymers: (a) Matrimid®; (b) 6FDA -DAM; (c) 6FDA/BPDA-DAM

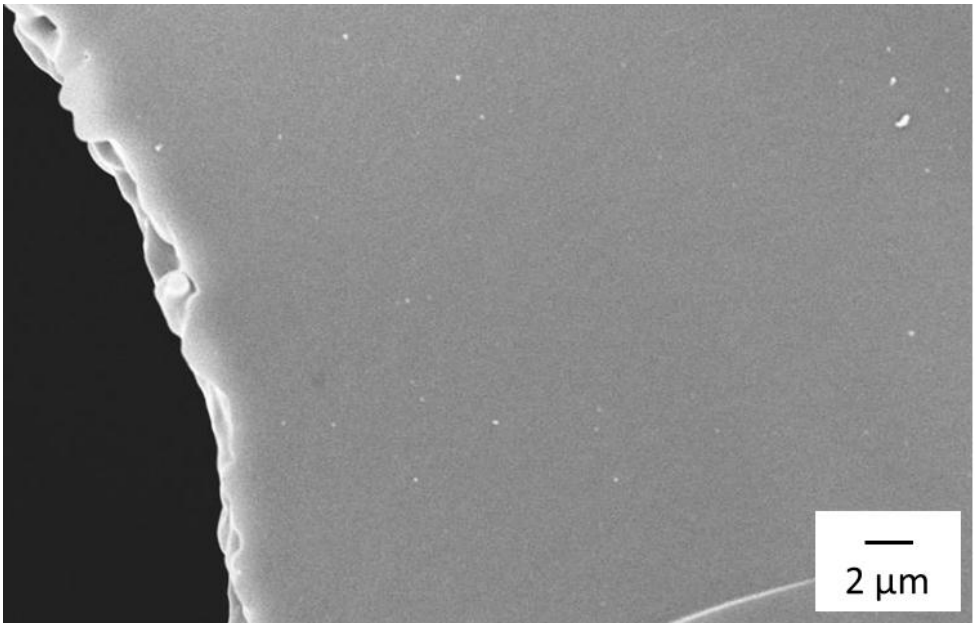

(a) Bore side of Matrimid® CMS fiber

(b) Bore side of 6FDA-DAM CMS fiber

Figure 6.3 Bore side morphology of CMS hollow fiber membranes produced from (a) Matrimid® and (b) 6FDA -DAM

6.2.2 Morphology of CMS fibers derived from cross-linkable precursor polyimide

Based on the established correlation mentioned above, it is obvious that cross-linkable polymers are very promising precursor candidates. With the cross-linked polymer matrix, negligible porous support structure densification is expected for CMS fibers; therefore, the thin skin layer from the asymmetric precursor fiber can be maintained. It is also important to note, with the increased polymer rigidity, the pinhole defects in precursor skin may persist and thus the ability to spin defect-free precursor fibers becomes even more important.

Crosslinking methods have been investigated intensively with the polymeric membranes for natural gas separations, in order to stabilize the membrane structure during aggressive CO_2 feed conditions. 6FDA-DAM/DABA (3:2) is a polyimide that can

be cross-linked by decarboxylation-induced thermal cross-linking [3, 4]. The crosslinking occurs through the decarboxylation of the carboxylic acid group at high temperatures, which creates free radical sites capable of crosslinking at several proposed sites along the polymer backbone. Defect-free asymmetric 6FDA-DAM/DABA (3:2) hollow fiber membranes have been successfully spun and thermally cross-linked by Chen et al [5]. The crosslinking conditions were investigated extensively, including crosslinking temperature, atmosphere, soaking time, etc.

Since the crosslinking occurs in a thermal treatment process and the carbonization temperature required for carbon membrane formation is well above the crosslinking temperature, the crosslinking reaction may happen during the thermal ramp step in a standard pyrolysis process. In this work, the defect-free precursor fibers were pyrolyzed under the standard protocols described in Chapter 3. The morphology of the resultant CMS fibers is shown in Figure 6.4.

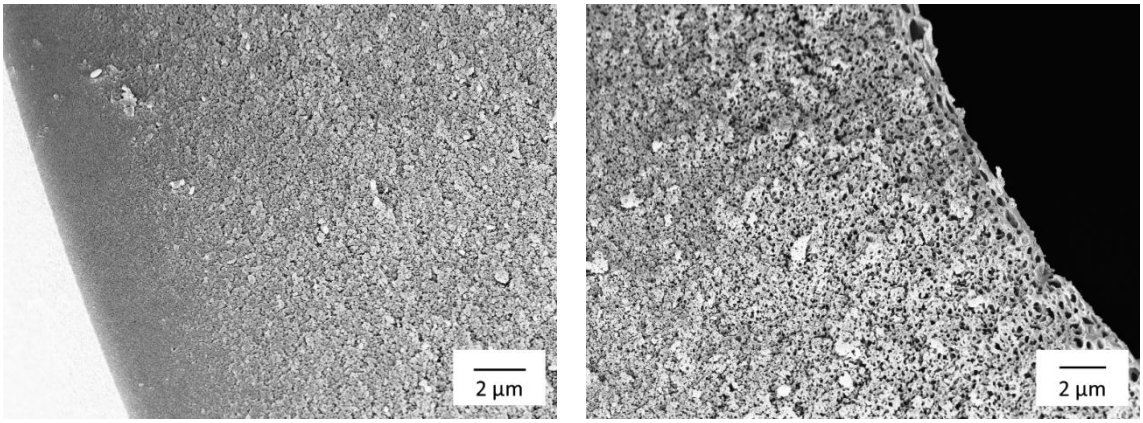

(a) Skin side (b) Bore side

Figure 6.4 SEM images of CMS fibers derived from 6FDA-DAM/DABA (3:2)

As demonstrated in Figure 6.4, CMS fibers derived from cross-linkable 6FDA-DAM/DABA (3:2) precursor polyimide retained their asymmetric morphology. The skin layer thickness estimated from SEM picture was about 2-3 μm. The support structure was very porous. The glass transition temperature of 6FDA-DAM/DABA (3:2) measured from DSC is about 387 ^{o}C. Before pyrolysis, if the crosslinking step is performed well below its T_g and the precursor fiber matrix is cross-linked sufficiently, the skin layer thickness may be further reduced [3]. This experiment demonstrated the advantages of cross-linkable precursor fibers for asymmetric CMS hollow fiber membrane fabrication. By using cross-linkable precursor fibers, the separation layer thickness in carbon fibers can be minimized.

6.2.3 Maintaining asymmetric morphology by pre-oxidation

As discussed in Chapter 2, sometimes, pre-treatment may be used to stabilize the polymer matrix. Oxidative treatment at high temperature is the most commonly used method. The mechanism has not been well understood. It is hypothesized that, in the oxidative atmosphere, O_2 may induce crosslinking reactions for polymers. Unlike the decarboxylation crosslinking which requires the carboxylic acid group, the pre-oxidation method may be applied to polymers without the need of introducing such functional groups.

The oxidative atmosphere can be created by simple atmospheric air exposure or compressed air purge at elevated temperature. The temperature is very critical. First, the temperature should be sufficiently high to induce oxidative reactions; second, the temperature should be below the temperature that substructure collapse occurs. Therefore,

an optimum temperature range exists for the effective pre-oxidation. SEM can be used to evaluate the morphology of the treated fibers, since the substructure collapse in the pretreatment process must be avoided. If the pre-treated fibers are cross-linked, then the polymer should not dissolve even in strong solvents. Therefore, hot NMP can be used to check if the polymer matrix is cross-linked.

In this study, precursor fibers from the three major polyimides were treated in air under 300 ^{o}C, 350 ^{o}C and 400 ^{o}C. SEM was used to check the fiber morphology and hot NMP (110 ^{o}C) was used to evaluate the solubility of the treated polymer. The results are shown in Table 6.2. For Matrimid®, since the glass-rubber transition temperature is slightly above 300 ^{o}C, substructure collapse occurred to each temperature investigated. For 6FDA-DAM, the glass transition temperature is 395 ^{o}C, at 300 ^{o}C, the fiber remained in the asymmetric form but it was also soluble in hot NMP; at 350 ^{o}C and 400 ^{o}C, the porous substructure partially or fully collapsed, respectively; for the very rigid 6FDA/BPDA-DAM (with a T_g of 424 ^{o}C), at 300 ^{o}C, the treated fiber was soluble in the hot solvent; at 350 ^{o}C, the fiber remained in asymmetric form and meanwhile the fiber was insoluble in hot NMP, indicating the formation of a cross-linked structure; at 400 ^{o}C, it appeared that the temperature was too high and induced support structure collapse.

Among all these conditions, 6FDA/BPDA-DAM treated at 350 ^{o}C was the most promising for further investigation, in terms of both asymmetric morphology retaining and effective crosslinking. The mechanism of such effect remains unclear. TGA analysis showed that, below 400 ^{o}C, no significant weight loss occurred for 6FDA/BPDA-DAM in air. Most likely, oxygen may induce some free radical and caused inter-chain or intra-chain crosslinking. After heat-treatment, the fiber turned from white to dark brown. The

SEM picture of such a pre-oxidized fiber is shown in Figure 6.5. As shown in Figure 6.5, the asymmetric morphology was well maintained in the pre-oxidized fiber. These fibers were then pyrolyzed into carbon fibers. As shown in Figure 6.6, the asymmetric morphology was also well maintained in the carbon form.

Table 6.2 Effect of treatment temperature on pre-oxidation

Polymer	300 °C		350 °C		400 °C	
	Solubility	Collapse	Solubility	Collapse	Solubility	Collapse
Matrimid®	N	Y	N	Y	N	Y
6FDA/BPDA-DAM	Y	N	**N**	**N**	N	Y
6FDA-DAM	Y	N	Partial	Y	N	Y

Solubility: whether or not the treated fiber is soluble in hot NMP; Collapse: whether or not the substructure of fibers collapses; Y (Yes), N (No)

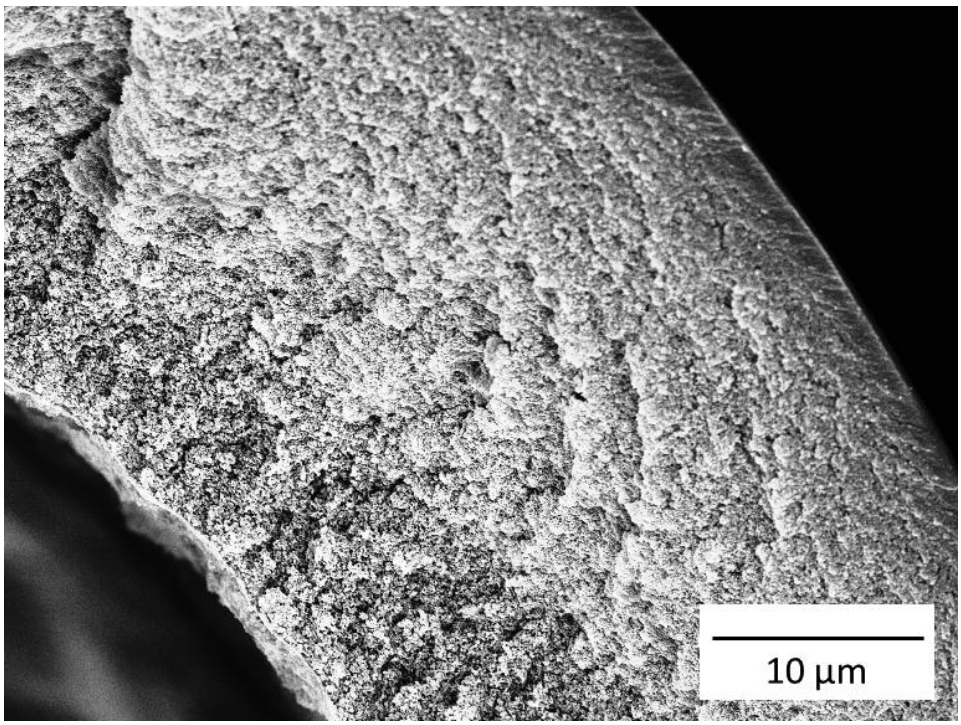

Figure 6.5 SEM image of a pre-oxidized 6FDA/BPDA-DAM fiber

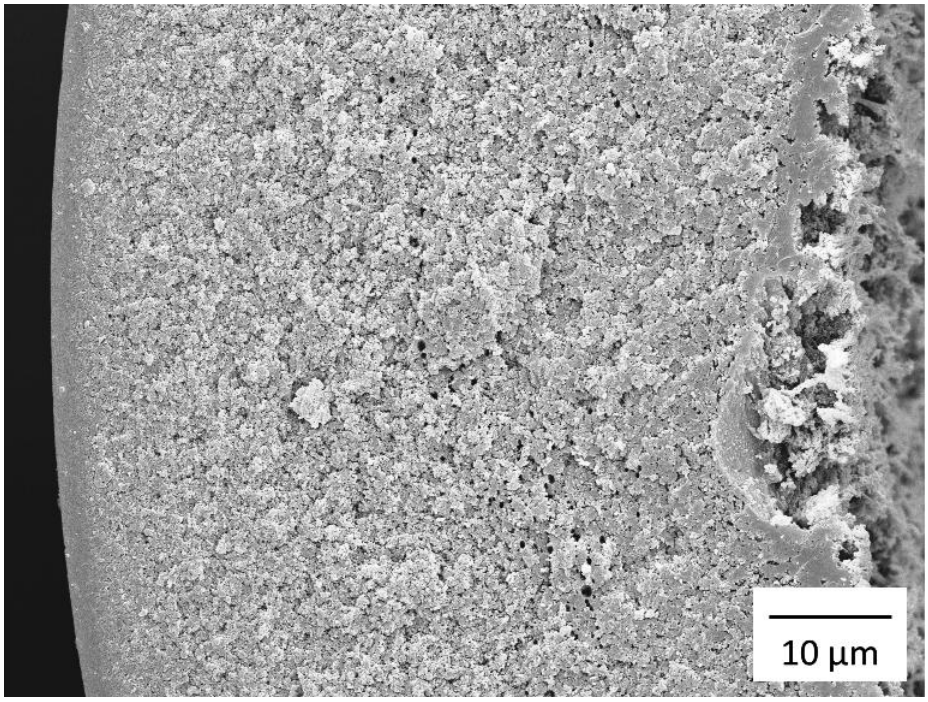

(a) Fiber wall

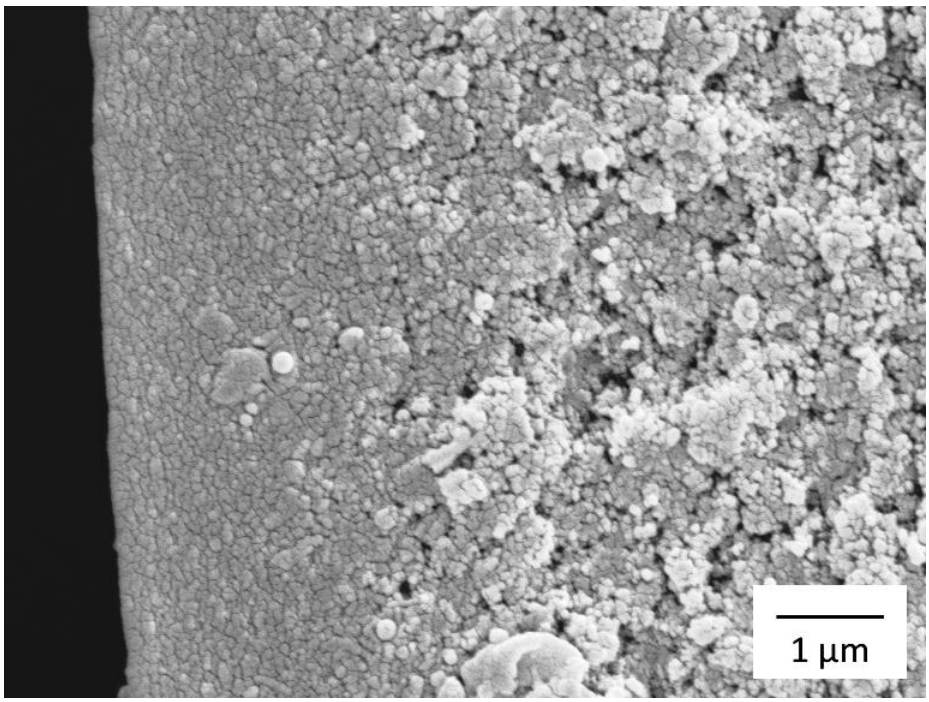

(b) Skin layer

Figure 6.6 SEM images of a CMS fiber produced from a pre-oxidized 6FDA/BPDA-DAM fiber

6.3 Transport properties of CMS hollow fiber membranes derived from 6FDA-polymers

6.3.1 Consideration of precursor material choice

In section 6.2, the morphology of CMS fiber was discussed. Various types of morphology (fully collapsed, partially collapse and highly asymmetric) were observed/created. Asymmetric morphology is desired due to the thin separation layer thickness, and asymmetric CMS hollow fiber membranes are obtainable. However, the ultimate goal for CMS membrane development is to obtain excellent transport properties (high permeance and high selectivity), rather than only the thin separation layer thickness. Asymmetric morphology solely does not necessarily indicate high performance of CMS membranes. Therefore, while creating asymmetric CMS fiber morphology, the intrinsic transport properties should be considered carefully too.

With the highly asymmetric morphology, however, for 6FDA-DAM/DABA (3:2) derived CMS fibers, low ethylene/ethane selectivity (< 2) was observed for multiple pyrolysis protocols (550 ^{o}C, 675 ^{o}C).The permeance was not high as well, which should be caused by the low intrinsic permeability of this material. This material was not pursued in further research for CMS membrane formation. However, the concept of using cross-linkable precursor remains very promising due to the obtainable ultra-thin separation layers. Future effort may be devoted to identify cross-linkable polymers with excellent intrinsic transport properties.

The pre-oxidized 6FDA/BPDA-DAM fiber demonstrated well maintained asymmetric carbon fiber morphology as well. In such CMS fibers, the ethylene permeance was increased by about two times (for both 550 ^{o}C and 675 ^{o}C pyrolysis), as

compared to the untreated fibers. The permeance did not increase as many fold as indicated by the extent of the separation layer thickness reduction. On the other hand, the ethylene/ethane selectivity was decreased by 25% and 43% for 550 ^{o}C and 675 ^{o}C pyrolysis, respectively. Both permeance and selectivity changes indicated that, after pre-oxidation, essentially the precursor material was no longer the original matter. Therefore, the resultant CMS membranes had different intrinsic transport properties. Given the improvement in permeance and decrease in selectivity, research on CMS membranes derived from the pre-oxidized fiber was not pursued rigorously later. However, while the separation for ethylene/ethane seems not quite promising from this material, other gas separations using this material may be attractive. Pre-oxidation can also serve as an alternative crosslinking method for polymer membranes for aggressive gas separations. Also, given the very rigid and non-collapse and insoluble nature, the porous preoxidized fiber can be used as a support layer for membrane coating.

With the above discussion, the precursor materials screened for next step CMS microstructure optimization for olefin/paraffin separations were pristine 6FDA-DAM and 6FDA/BPDA-DAM. Especially, 6FDA/BPDA-DAM demonstrated better asymmetric CMS fiber morphology than 6FDA-DAM, and was selected as the primary focus of this research.

6.3.2 Optimization of 6FDA-DAM and 6FDA/BPDA-DAM CMS hollow fiber membrane transport properties

As discussed in Chapter 2, from previous study, the transport properties of CMS membranes can be tailored by optimizing pyrolysis temperature protocol and pyrolysis

atmosphere. In this research, it was also discovered that the history-dependence may significantly affect CMS membrane transport properties. This phenomenon introduced another variable for controlling CMS membrane performance. The details of the history-dependence phenomenon are discussed in Chapter 7 and not included in this Chapter. In terms of the testing protocol, most CMS hollow fiber membranes were potted into module shortly after pyrolysis, then the membranes were evacuated in permeation systems overnight prior tests. This procedure actually stabilized the membrane rapidly and delivered quite consistent results. The mechanism is discussed in Chapter 7.

6.3.2.1 CMS dense film transport properties

As stated in Section 6.1, one of the reasons for choosing 6FDA-DAM and 6FDA/BPDA-DAM as the precursor materials is their high permeability. Due to the packing disruption caused by $–CH_3$ and $–CF_3$ groups and the rigid backbone, 6FDA-DAM and 6FDA/BPDA-DAM have much higher free volume compared to Matrimid® polyimide. The fractional free volume of 6FDA-DAM, 6FDA/BPDA-DAM and Matrimid® are 0.190, 0.145 and 0.110, respectively [6]. TGA-IR results revealed the evolution of CHF_3 and HF during pyrolysis, therefore, the removal of $–CF_3$ group is expected to create more pore volume in CMS membranes [7, 8]. X-ray photoelectron spectroscopy (XPS) also indicated the complete removal of fluorine element in the resultant carbon membranes.

The dense film work was mostly investigated by my collaborator Meha Rungta [6]. Due to the influence of history-dependence, some of the results showed variations due to the inadequate knowledge of this issue at the beginning of the research.

Nevertheless, there is no doubt that CMS membranes derived from 6FDA-DAM and 6FDA/BPDA-DAM have much higher permeability than Matrimid® under most pyrolysis conditions. For example, under the typical 550 ^{o}C pyrolysis protocol and argon purge conditions, 6FDA/BPDA-DAM derived CMS dense film showed ethylene permeability higher than 100 Barrers, while Matrimid® CMS only delivered about 16 Barrers. The high intrinsic permeability allows the space for finely tuning of the microstructure of CMS membranes. A great deal of effort has been spent to study the pore structure tuning using tools such as pyrolysis temperature and O_2-doping. The dense film study provided insights for the pyrolysis optimization of hollow fiber membranes.

6.3.2.2 Comparison of Matrimid® and 6FDA/BPDA-DAM CMS hollow fiber membrane performance

The major issue for Matrimid® CMS fibers is the relatively low permeance. After pyrolysis, 6FDA/BPDA-DAM CMS fibers demonstrated advantages over Matrimid® CMS fibers. A standard protocol was used to compare Matrimid® and 6FDA/BPDA-DAM CMS fiber performance. All fibers were pyrolyzed under the 550 ^{o}C, 2 hr soak standard protocol and under UHP argon purge. The membranes were tested by using 100 psi pure gas feed and the testing temperature was 35 ^{o}C. For Matrimid®, the thin-walled precursor fibers were used in order to maximize the permeance. The comparison of gas permeation properties are shown in Figure 6.7. Figure 6.7 (a) shows the permeance of multiple gases. It is quite obvious that 6FDA/BPDA-DAM CMS fibers are much more permeable than Matrimid® CMS fibers. For all the gases investigated, the increase in 6FDA/BPDA-DAM CMS fibers was more than 4-5 times. Figure 6.7 (b) shows that the

selectivity for most gas pairs derived under this typical protocol was quite close. The permeance increase should be attributed to both the increase in permeability and reduction in separation layer thickness.

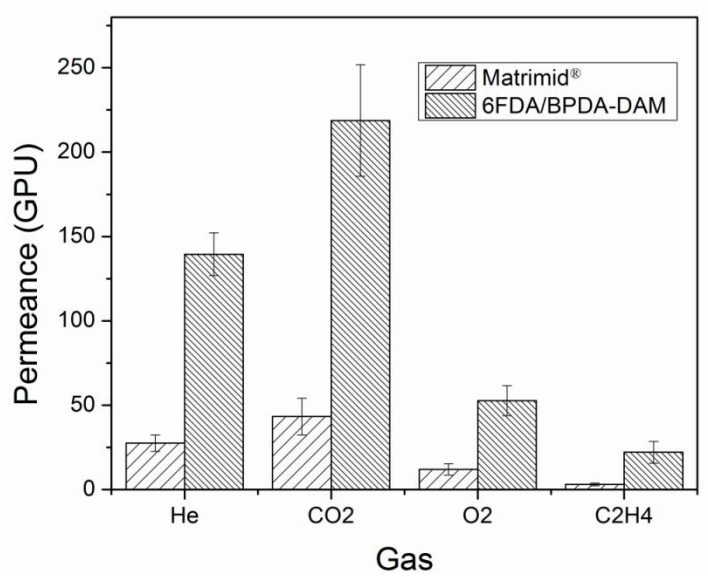

(a) Comparison of gas permeance

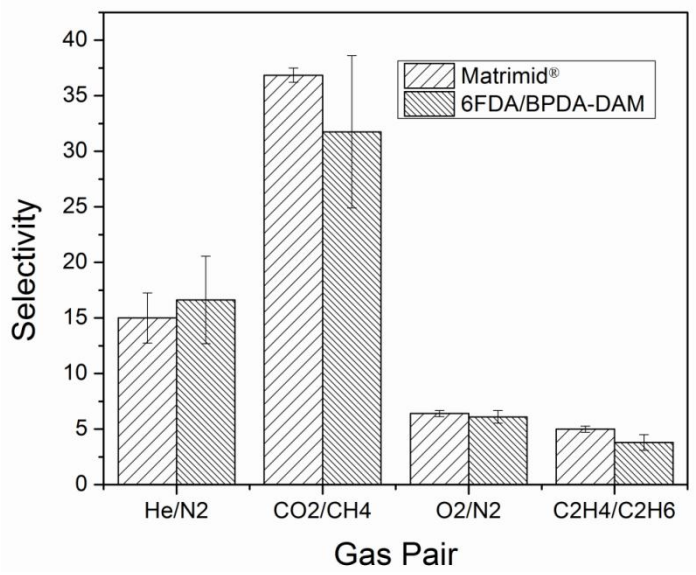

(b) Comparison of selectivity

Figure 6.7 Comparison of Matrimid® and 6FDA/BPDA-DAM CMS hollow fiber membrane performance

6.3.2.3 Effect of pyrolysis temperature

In the study of Matrimid® CMS membrane fabrication, altering pyrolysis temperature was the most effective approach to increase the ethylene/ethane selectivity. 650-675 ^{o}C appears to be the optimum pyrolysis temperature for Matrimid® CMS membranes [1, 9]. Therefore, in this study, the effect of pyrolysis temperature was also investigated. The pyrolysis was performed under UHP argon purge. Three characteristic temperatures were used for pyrolysis: 550 ^{o}C, 675 ^{o}C and 800 ^{o}C. The testing conditions were 100 psi pure gas feed at 35 ^{o}C. The results are shown in Figure 6.8. From the plot, surprisingly, unlike Matrimid® CMS, increasing pyrolysis temperature did not lead to significant increase in ethylene/ethane selectivity while the permeance was decreased. Therefore, the effect of pyrolysis temperature also exhibited precursor dependence.

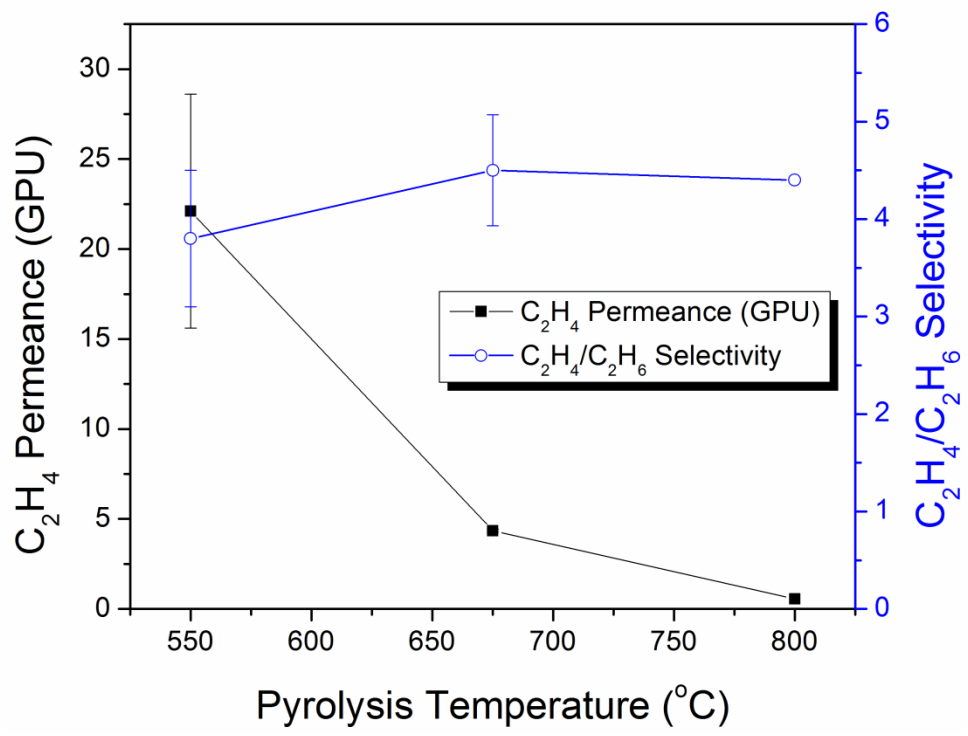

Figure 6.8 Effect of pyrolysis temperature on 6FDA/BPDA-DAM CMS hollow fiber membrane performance

6.3.2.4 Effect of pyrolysis atmosphere

From the study of pyrolysis temperature, it appeared that simply altering pyrolysis temperature was not sufficient to increase the selectivity significantly for 6FDA/BPDA-DAM CMS membranes. The effect of pyrolysis atmosphere was then investigated, including vacuum versus purge conditions, oxygen content in inert purge gas.

Vacuum pyrolysis was traditionally used to prepare CMS membranes. The oxygen exposure under vacuum conditions was difficult to control due to the system sealing and vacuum levels. It was more desirable to use inert gas purge pyrolysis due to its repeatability. The comparison of vacuum and inert gas purge pyrolysis was carried out. The inert gas used was UHP argon. The temperature protocol was the typical 550 ^{o}C, 2 hr soak protocol. The impact on membrane performance was quite obvious, as shown in Figure 6.9. Generally, the permeance was higher and the selectivity was lower in the inert gas purge mode, compared to vacuum pyrolysis. The critical pore size may be smaller in the case of vacuum mode than in the inert gas purge mode. This may be caused by more oxygen exposure in vacuum pyrolysis. The helium permeances under these two modes were quite close due to the small size of helium. Under vacuum condition, the CO_2/CH_4 selectivity was quite high at 64 while the CO_2 permeance was about 79 GPU. From inert gas purge to vacuum, the O_2 permeance decreased from ~53 GPU to ~18 GPU while the selectivity was increased from ~6.1 to ~8.3. For C_2H_4/C_2H_6, in the vacuum mode, C_2H_4 permeance was ~4.1 while the selectivity was 5.4. Vacuum pyrolysis was also performed at 675 ^{o}C, the ethylene permeance decreased to less 1 GPU while the C_2H_4/C_2H_6 selectivity was about 6. Vacuum pyrolysis under high temperature seems to decrease the pore size dramatically.

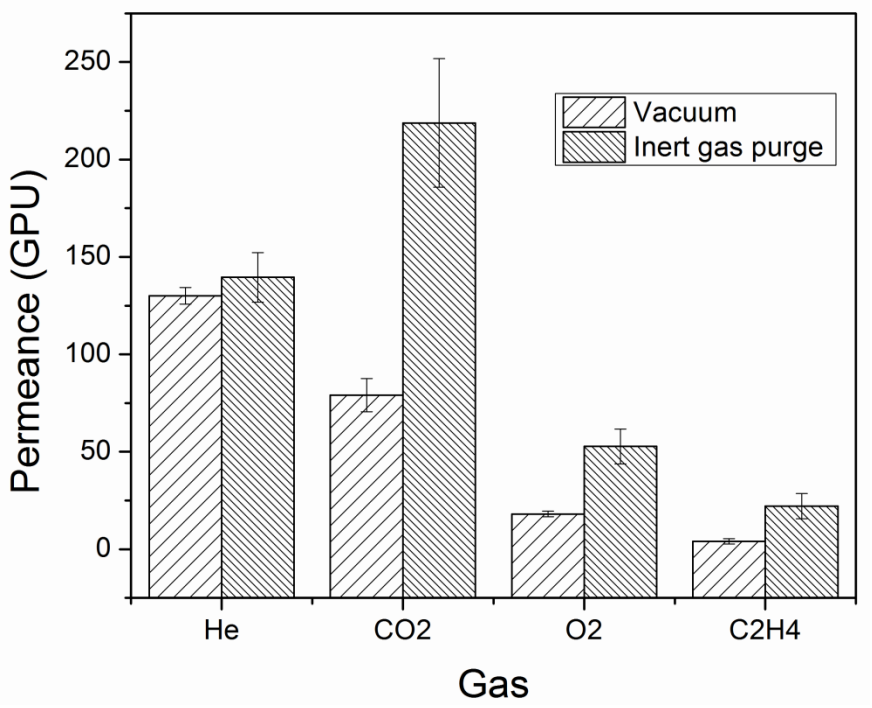

(a) Comparison of permeance

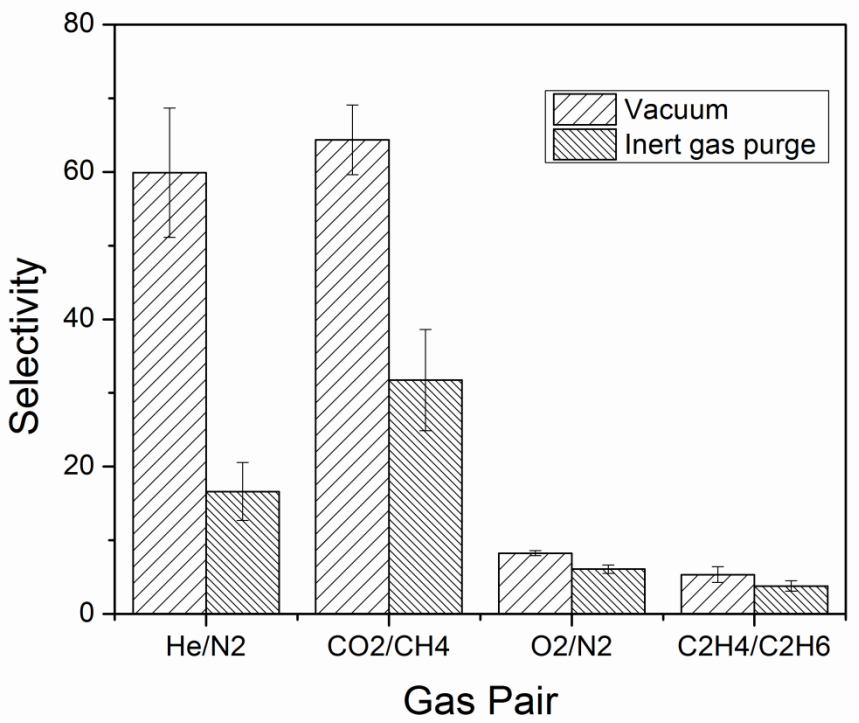

(b) Comparison of selectivity

Figure 6.9 Effect of vacuum and inert gas purge pyrolysis on CMS membrane performance

Oxygen content in the pyrolysis atmosphere can significantly affect CMS membrane performance. O_2-doping has been developed as a tool to tune CMS structure by using this principle. In previous work, dense film 6FDA/BPDA-DAM CMS membrane has been successfully tuned by trace amount of O_2 doping at 550 ^oC for CO_2/CH_4 separation [10]. This work aimed to extend the success to the hollow fiber configuration and also alternative gas pairs. Similar pyrolysis conditions were used to optimize CMS hollow fiber membranes for ethylene/ethane separation. UHP argon, 17 ppm O_2/Ar, 32 ppm O_2/Ar and 53 ppm O_2/Ar were used as the purge gases for pyrolysis. The purge rate was 200 sccm. The impact of oxygen content in purge gas on 6FDA/BPDA-DAM CMS hollow fiber membranes for CO_2/CH_4 separation is illustrated in Figure 6.10. The trend was quite consistent with previous work on dense film study. By increasing the O_2 level in purge gas, the permeance was decreased and the selectivity was increased significantly. At 32-53 ppm O_2 level, the CO_2/CH_4 selectivity was high at about 60 and the CO_2 permeance remained above 90 GPU, which was quite attractive. The deviation for 17 ppm results was quite big in the plot, and this was due to variations in testing protocol. This is further explained in Chapter 7. A similar plot was constructed for C_2H_4/C_2H_6 separation. The trend was quite similar to the case of CO_2/CH_4. O_2 content did impact C_2H_4/C_2H_6 gas pair in a similar way. It is also wise to note that the selectivity of C_2H_4/C_2H_6 was still not quite high after significant amount of O_2 doping, although the trend pointed to the right direction.

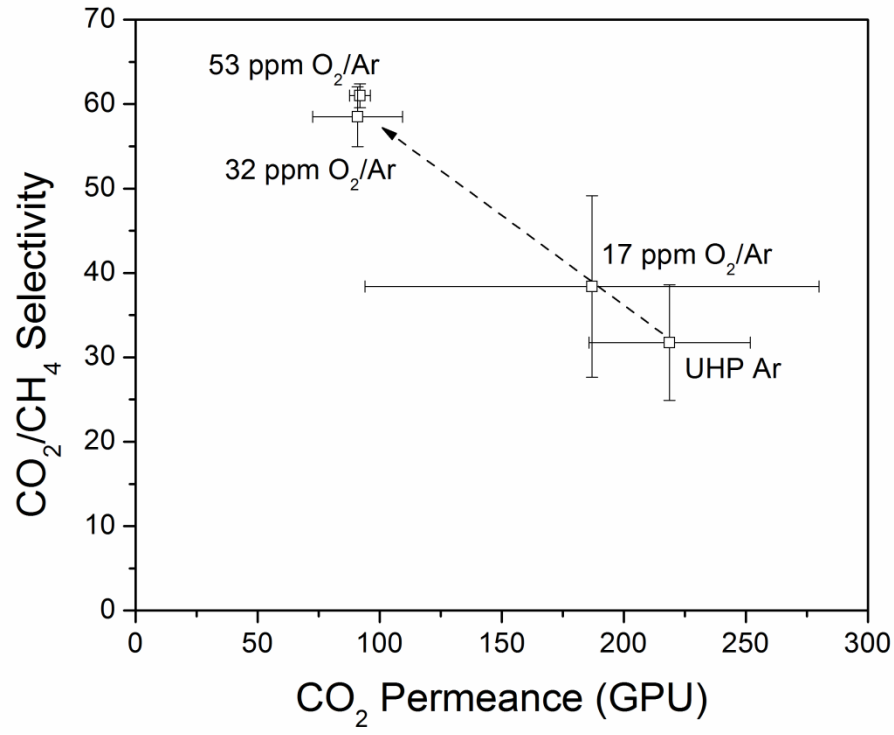

Figure 6.10 Effect of pyrolysis atmosphere on 6FDA/BPDA-DAM CMS hollow fiber membranes for CO_2/CH_4 separation

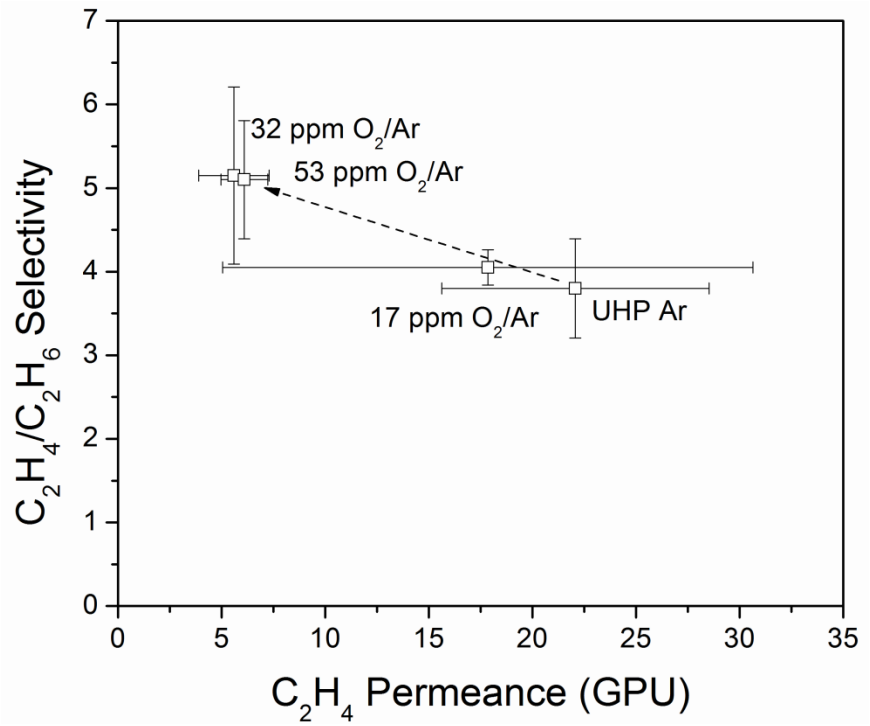

Figure 6.11 Effect of pyrolysis atmosphere on 6FDA/BPDA-DAM CMS hollow fiber membranes for C_2H_4/C_2H_6 separation

Over-doping occurs if the oxygen content is too high in the purge gas. The chemisorbed oxygen may decrease the critical pore size, reduce gas permeability and even decrease selectivity. Hereby, over-doping refers to "slightly higher O_2 amount" in the pyrolysis atmosphere. If the oxygen level is significantly high, the effect may not be limited in doping or chemisorption. For example, 500 ppm O_2/Ar purge gas caused brittle and broken fibers after pyrolysis due to the more extensive decomposition reactions.

The pyrolysis temperature at which the doping is performed can be very important. This determines the intrinsic microstructure for additional tuning provided by oxygen. Therefore, the pyrolysis temperature and O_2 content in the pyrolysis atmosphere must be coordinated in order to optimize the pore structure for specific gas separations. In this work, besides doping at 550 ^oC, various temperatures such as 500 ^oC and 675 ^oC were also investigated; however, the results were not quite impressive for improving the ethylene/ethane separation performance. The parallel dense film work provides more insights for the coupling of pyrolysis temperature and O_2 doping [6].

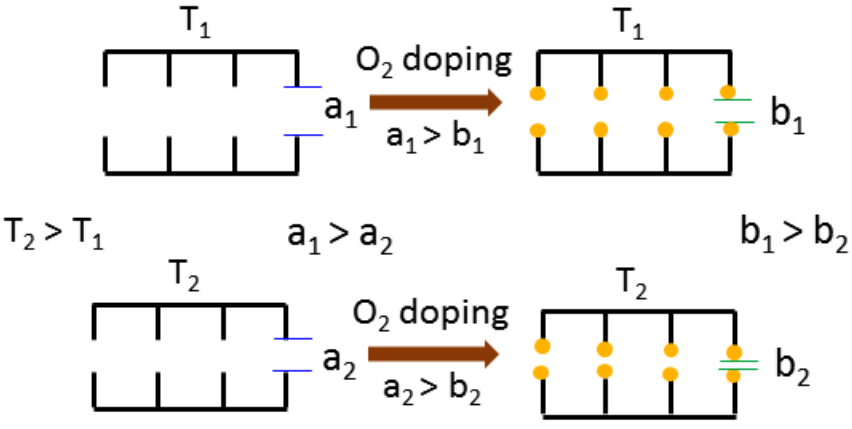

Figure 6.12 Schematic of the effect of O_2 doping at different temperatures

6.4 CMS hollow fiber membranes for propylene/propane separation

The primary focus of this research is the development of CMS membranes for ethylene/ethane separations. In fact, the parallel C3 hydrocarbon separation is more amenable to membrane separation due to slightly greater difference between propylene and propane vs. ethylene and ethane. Recent development revealed that CMS membranes and ZIF-8 membranes are able to deliver separation performance exceeding the polymer upper bound. Considering advantages of scalability consistent with the existing fiber spinning platform, hybrid polymer-ZIF-8 and pure CMS fibers appear to be the best options [11]. This section discusses the propylene/propane separation by CMS hollow fiber membranes.

Previously, CMS membranes for propylene/propane separation have been investigated by several researchers. Steel and Koros studied Matrimid® and 6FDA/BPDA-DAM dense film CMS membranes for propylene/propane separation and obtained very promising results [2, 12]. Hayashi et al. prepared carbonized BPDA-pp'ODA polyimide membranes on a porous alumina tube and demonstrated high selectivity for propylene/propane separation [13]. Yoshino et al. formed carbonized asymmetric carbon hollow fiber membranes from 6FDA/BPDA-DDBT polyimide [14]. Okamoto et al. prepared carbonized membranes from BPDA-DDBT/DABA asymmetric hollow fiber membranes [15]. The above two types of asymmetric carbon hollow fiber membranes showed interesting separation performance for propylene/propane separation.

The research here aims to apply the CMS hollow fiber membranes formed previously for propylene/propane separation. Another motivation is to translate Steel's exciting dense film results into the hollow fiber form.

CMS hollow fiber membranes were prepared from defect-free Matrimid® and 6FDA/BPDA-DAM asymmetric hollow fiber precursors. 550 ^{o}C typical protocol and UHP argon purge (200 sccm) were used. Ethylene and ethane permeations were tested under 100 psi pure gas feed at 35 ^{o}C; propylene and propane permeation were tested under 50 psi pure gas feed at 35 ^{o}C as well. The results are shown in Figure 6.13. It is quite obvious that C_3H_6/C_3H_8 separation is much easier than C_2H_4/C_2H_6 separation from the plot. For the same membrane, the C_3H_6/C_3H_8 selectivity (above 20) is about 5 times higher than the C_2H_4/C_2H_6 selectivity (about 4). Again, the permeance of Matrimid® CMS hollow fiber membranes is limited by the increased separation layer thickness due to substructure collapse, and in this particular case, the propylene permeance was less than 1 GPU. 6FDA/BPDA-DAM CMS hollow fiber membranes are advantageous over Matrimid® CMS fiber in terms of permeance. In this particular example, 6FDA/BPDA-DAM CMS fiber showed 17.5 GPU propylene permeance, which was more than 20 times higher than Matrimid® fibers. Therefore, 6FDA/BPDA-DAM CMS hollow fiber membranes are very promising for propylene/propane separation. Similar performance of 6FDA/BPDA-DAM CMS fiber membranes for propylene/propane separation was also obtained by 500 ^{o}C pyrolysis.

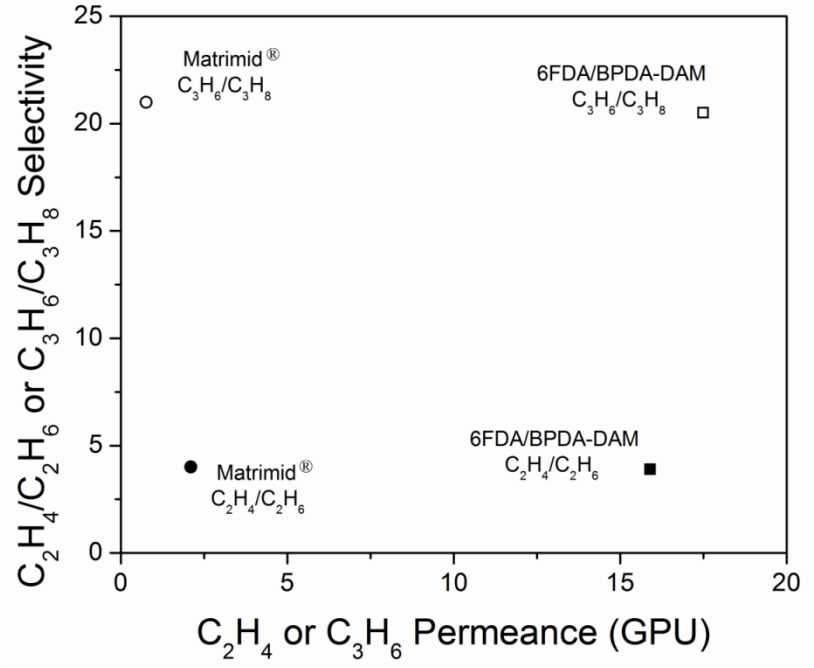

Figure 6.13 Comparison of CMS hollow fiber membranes for ethylene/ethane and propylene/propane separations

Asymmetric 6FDA-DAM polymer fibers were also pryolzyed into carbon membranes and investigated for propylene/propane separation. The separation performance was quite similar to 6FDA/BPDA-DAM CMS fibers. In one example, the pure gas permeation test gave 10.9 GPU propylene permeance and 18.5 propylene/propane selectivity. Therefore, 6FDA-DAM is also a promising precursor material for CMS hollow fiber membrane preparation for propylene/propane separation.

The examples showed above only count the basic cases (550 ^{o}C and 200 sccm UHP argon purge pyrolysis). Factors including pyrolysis temperature and pyrolysis atmosphere still provide opportunities for optimization. The factor that has not been considered in the previous examples is the history-dependence. Previously, the competition effect of propylene and propane in CMS membranes was also showed to be a

major factor for mixed gas permeation [16]. All of these parameters not only make the systematic investigation quite challenging, but also provide opportunities for performance tuning. Even for the basic cases mentioned above, the performance was quite attractive. Later investigations including mixed gas permeation tests showed that selectivity of ~30 and propylene permeance of 10 GPU with 6FDA/BPDA-DAM and 6FDA-DAM derived CMS hollow fiber membranes could be achieved. This performance is not reachable by any polymer materials reported so far. Hypothetical examples can be used to demonstrate. The pure gas propylene/propane polymer upper bound defined by Burns and Koros and the mixed gas propylene/propane polymer upper bound summarized by Chen and Koros are shown in Figure 6.14 [17, 18]. As shown in the figure, the mixed gas propylene/propane separation performance for polymer materials was much lower than the pure gas performance. On the pure gas upper bound, if the propylene/propane selectivity reaches 30, then correspondingly the upper limit for propylene permeability is less than 0.3 Barrer. Even assuming a 100 nm skin layer, the deliverable propylene permeance is less than 3 GPU. On the mixed gas upper bound, the corresponding propylene permeability for propylene/propane selectivity of 30 is less than 0.03 Barrer, so the deliverable propylene permeance with a 100 nm skin layer is less than 0.3 GPU. Therefore, there is no doubt that the CMS hollow fiber membranes we have outperform any spinnable polymer materials. Another comparison is with very promising 6FDA-DAM/ZIF-8 mixed matrix membranes. At 48.0 wt% ZIF-8 loading, the pure gas selectivity is about 31; however, the mixed gas selectivity drops below 20 [18]. CMS hollow fiber membranes clearly demonstrated the advantages in realistic testing conditions.

With the relative simplicity of the binary separation and deliverable CMS membrane performance, the propylene/propane separation appears to be the best option for the first implementation of practical CMS membrane applications. Of course, significant effort must be invested for further material optimization, realistic testing and process integration.

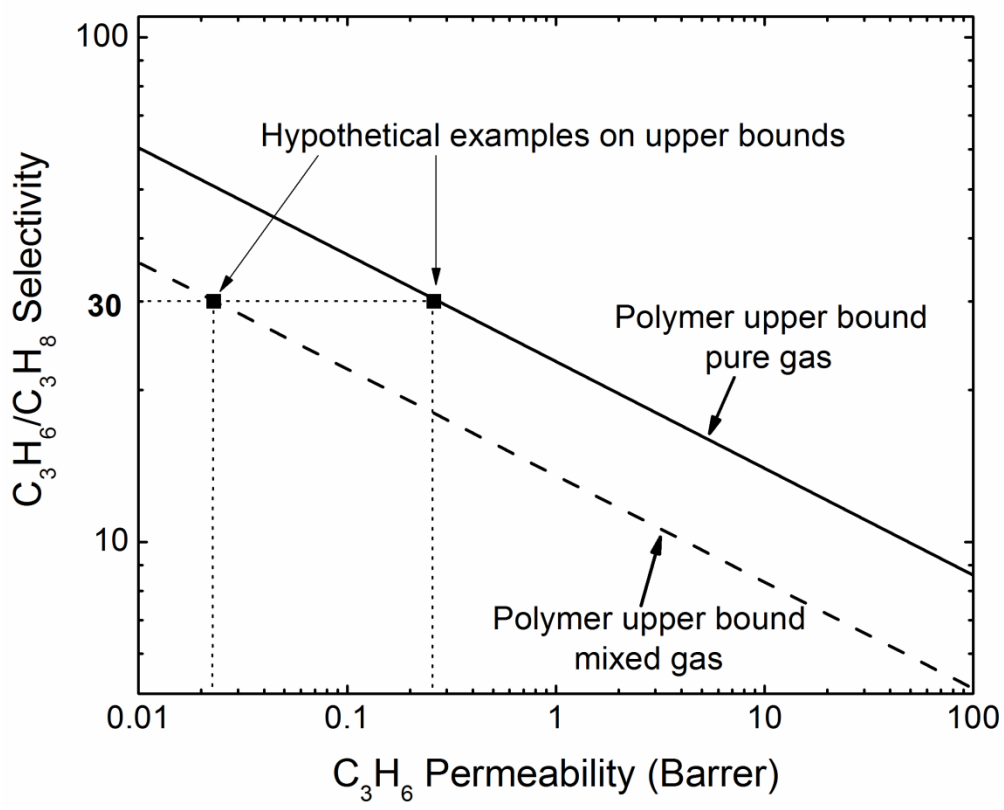

Figure 6.14 Pure gas and mixed gas polymer upper bound for propylene/propane separation [17, 18]

6.5 Effect of defect-free properties

In Chapter 5, the precursor defect-free properties were found not necessarily correlated to the Matrimid® CMS hollow fiber membrane performance [9]. The pinhole

defects can be cured during the intense thermal annealing stage of the polymer fiber. This feature was offered by the low Matrimid® polymer chain rigidity at high temperature. For polymers with high rigidity, the polymer chain mobility may not be sufficient to heal the pinhole defects. As shown in Figure 6.1, unlike the two orders of magnitude decrease below 350 ^{o}C for Matrimid®, the storage modulus of 6FDA/BPDA-DAM remains at a very high level even at 450 ^{o}C. Therefore, experimentally examining the effect of precursor defect-free properties is quite important for guiding the preparation of precursor hollow fibers. Again, observation of the morphology change may not be sufficient due to the scale of pinhole defects. Permeation tests must be performed for CMS membranes prepared from defect-free and defective precursor fibers.

Some slightly defective 6FDA/BPDA-DAM precursor fibers were pyrolyzed using a 675 ^{o}C protocol under UHP argon purge. The precursor fibers had O_2/N_2 selectivity of 3.0 ± 0.2 and N_2 permeance of 99.2 ± 25.0 GPU. Mixed gas permeation tests (100 psi feed, 35 ^{o}C) were used to evaluate the membrane performance. Results of two pyrolysis experiments are shown in Figure 6.15. It is obvious that the transport properties were scattered, and no clear trend could be found from the results. It is interesting that some of the fibers had low permeance and low selectivity.

Some defect-free precursor fibers were pyrolyzed with the defective precursors in the same pyrolysis experiment. The defect-free precursor fiber had O_2/N_2 selectivity of 4.7 ± 0.1 and N_2 permeance of 9.4 ± 0.2 GPU. The comparative results are shown in Figure 6.16. Obviously, CMS fibers prepared from the defect-free precursor fibers have better consistency. The comparison was quite reliable since the membranes were pyrolyzed in the same experiment. Another experiment with another defect-free precursor fiber state

also demonstrated more consistency of defect-free fibers over defective precursor fibers.

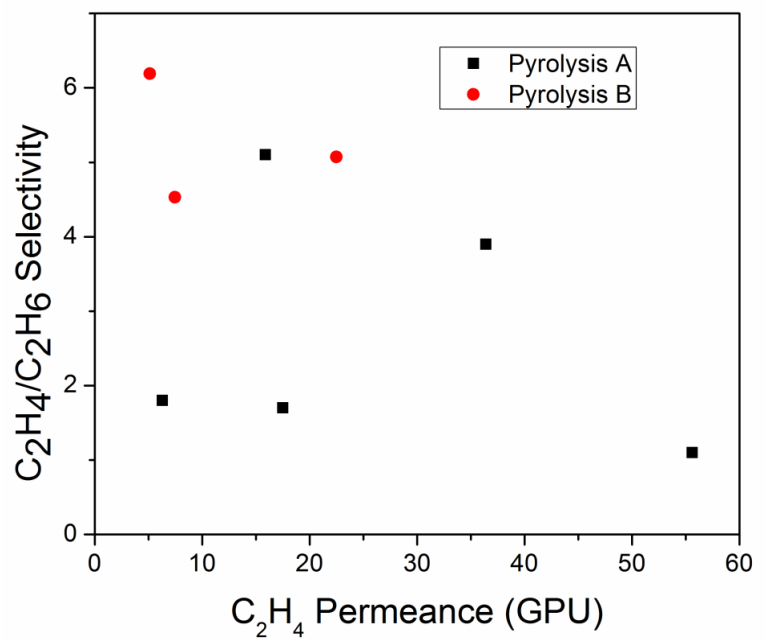

Figure 6.15 CMS hollow fiber membrane performance from defective 6FDA/BPDA-DAM precursor fibers

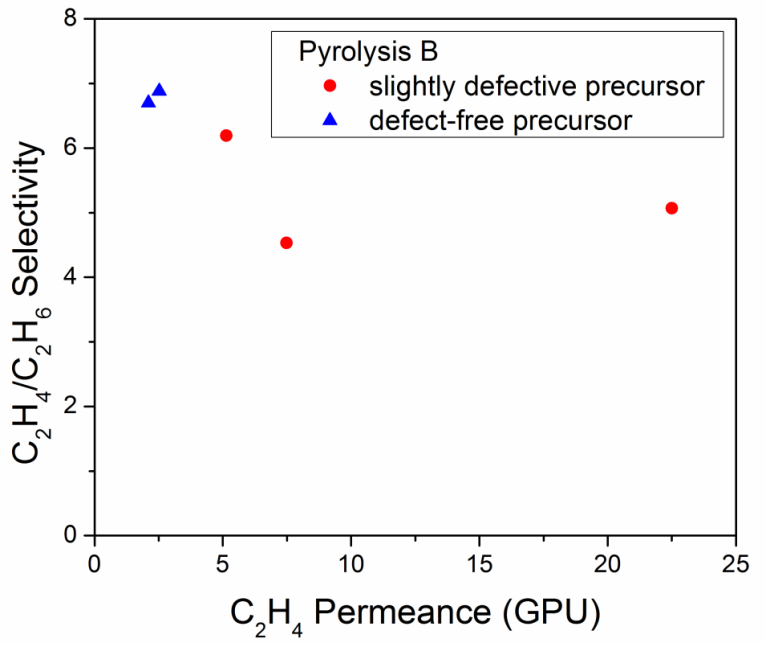

Figure 6.16 Comparison of CMS hollow fiber membrane performances from defective and defect-free precursor fibers

The results above reveal that it is better to start with defect-free precursor for 6FDA/BPDA-DAM CMS hollow fiber membrane preparation. Defective fibers may lead to inconsistent results. Since defects in the skin layer vary with spinning conditions, some small defects may also be healed and the curing effect can be similar to Matrimid® CMS membrane preparation. More studies are required to draw a rigorous conclusion on this topic.

The precursor defect-free properties can be extremely important if cross-linkable precursor polymers are used. Previously, it was demonstrated that the asymmetric morphology of such precursor fibers can be maintained. With the very rigid cross-linked polymer matrix, the defects on the skin layer are expected to impact on carbon fibers. Figure 6.16 can be used to illustrate the mechanism. Therefore, defect-free skin layer must be obtained for this class of precursor polymers.

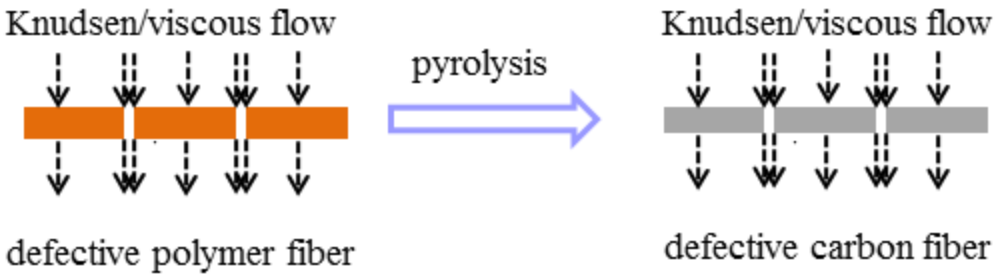

Figure 6.17 Effect of defect-free properties on CMS fiber performance for cross-linkable precursors

6.6 Summary and conclusions

Since the application of Matrimid® derived CMS hollow fiber membranes was limited by the permeance loss induced by substructure collapse, alternative precursor

polymers 6FDA-DAM and 6FDA/BPDA-DAM were chosen in order to overcome the substructure collapse. 6FDA-DAM and 6FDA/BPDA-DAM have higher glass-rubber transition temperatures, as compared to Matrimid®. The increased rigidity during intense heat-treatments finally resulted in improved asymmetric morphology of 6FDA-DAM and 6FDA/BPDA-DAM CMS hollow fiber. Further exploration revealed that asymmetric CMS hollow fiber morphology could be maintained by cross-linkable precursor fibers. On the other hand, 6FDA-DAM and 6FDA/BPDA-DAM polyimides have much higher precursor permeability, and this feature also impacted on the CMS membrane permeability. 6FDA/BPDA-DAM CMS hollow fiber membranes showed significant improvement in permeance for multiple gas separation applications. A great deal of effort was made to tailor the microstructure of CMS membranes by optimizing pyrolysis temperature and pyrolysis atmosphere. 6FDA-DAM and 6FDA/BPDA-DAM derived CMS hollow fiber membranes were found to be ideal for debottlenecking C3 splitters. In addition, unlike Matrimid®, for 6FDA/BPDA-DAM CMS hollow fiber membrane preparation, defect-free precursor fibers led to better consistency, the ability for spinning defect-free precursor fibers becomes even more important.

6.7 References

[1] M. Rungta, L. Xu, W.J. Koros, Carbon molecular sieve dense film membranes derived from Matrimid® for ethylene/ethane separation, Carbon 50 (2012) 1488-1502.

[2] K.M. Steel, W.J. Koros, An investigation of the effects of pyrolysis parameters on gas separation properties of carbon materials, Carbon 43 (2005) 1843-1856.

[3] W. Qiu, C.-C. Chen, L. Xu, L. Cui, D.R. Paul, W.J. Koros, Sub-T_g cross-linking of a polyimide membrane for enhanced CO_2 plasticization resistance for natural gas separation, Macromolecules 44 (2011) 6046-6056.

[4] A.M. Kratochvil, W.J. Koros, Decarboxylation-induced cross-linking of a polyimide for enhanced CO_2 plasticization resistance, Macromolecules 41 (2008) 7920-7927.

[5] C.-C. Chen, W. Qiu, S.J. Miller, W.J. Koros, Plasticization-resistant hollow fiber membranes for CO_2/CH_4 separation based on a thermally crosslinkable polyimide, J. Membr. Sci. 382 (2011) 212-221.

[6] M. Rungta, Carbon molecular sieve dense film membranes for ethylene/ethane separations, in: Chemical Engineering, Georgia Institute of Technology, 2012.

[7] M. Kiyono, Carbon molecular sieve membranes for natural gas separations, in: Chemical Engineering, Georgia Institute of Technology, 2010.

[8] P.J. Williams, Analysis of factors influenceing the performance of CMS membranes for gas separation, in: Chemical Engineering, Georgia Insitute of Technology, 2006.

[9] L. Xu, M. Rungta, W.J. Koros, Matrimid® derived carbon molecular sieve hollow fiber membranes for ethylene/ethane separation, J. Membr. Sci. 380 (2011) 138-147.

[10] M. Kiyono, P.J. Williams, W.J. Koros, Effect of pyrolysis atmosphere on separation performance of carbon molecular sieve membranes, J. Membr. Sci. 359 (2010) 2-10.

[11] W.J. Koros, R.P. Lively, Water and beyond: Expanding the spectrum of large-scale energy efficient separation processes, AIChE J. 58 (2012) 2624-2633.

[12] K.M. Steel, W.J. Koros, Investigation of porosity of carbon materials and related effects on gas separation properties, Carbon 41 (2003) 253-266.

[13] J. Hayashi, H. Mizuta, M. Yamamoto, K. Kusakabe, S. Morooka, S.H. Suh, Separation of ethane/ethylene and propane/propylene systems with a carbonized BPDA-pp'ODA polyimide membrane, Ind. Eng. Chem. Res. 35 (1996) 4176-4181.

[14] M. Yoshino, S. Nakamura, H. Kita, K.-i. Okamoto, N. Tanihara, Y. Kusuki, Olefin/paraffin separation performance of carbonized membranes derived from an asymmetric hollow fiber membrane of 6FDA/BPDA–DDBT copolyimide, J. Membr. Sci. 215 (2003) 169-183.

[15] K.-i. Okamoto, S. Kawamura, M. Yoshino, H. Kita, Y. Hirayama, N. Tanihara, Y. Kusuki, Olefin/paraffin separation through carbonized membranes derived from an asymmetric polyimide hollow fiber membrane, Ind. Eng. Chem. Fundam. 38 (1999) 4424-4432.

[16] K.M. Steel, Carbon membranes for challenging gas separations, in: Chemical Engineering, The University of Texas at Austin, 2000.

[17] R.L. Burns, W.J. Koros, Defining the challenges for C_3H_6/C_3H_8 separation using polymeric membranes, J. Membr. Sci. 211 (2003) 299-309.

[18] C. Zhang, Y. Dai, J.R. Johnson, O. Karvan, W.J. Koros, High performance ZIF-8/6FDA-DAM mixed matrix membrane for propylene/propane separations, J. Membr. Sci. 389 (2012) 34-42.

CHAPTER 7

AGING OF CMS MEMBRANES

In Chapter 6, 6FDA-DAM and 6FDA/BPDA-DAM were used as alternative precursor polyimides for CMS membranes fabrication. During the membrane characterization, the history dependence of transport properties (also referred as "aging") was observed. This chapter first reviews aging in glassy polymers and CMS membranes. Then, the discovery and underlying mechanism of physical aging in CMS membranes are described in detail. Finally, the impacts of aging on various key performance properties are discussed.

7.1 Review of physical aging in glassy polymers

Generally, aging in polymeric membranes refers to *physical aging* in glassy polymers. Glassy polymers are inherently non-equilibrium materials that undergo physical aging toward an equilibrium state. Figure 7.1 illustrates the non-equilibrium nature of glassy polymers in terms of volume versus temperature relationship [1, 2]. Above the glass transition temperature (T_g), the polymer exists in an equilibrium state; however, as the polymer is cooled from a rubbery state and passes through the glass transition temperature, long-range polymer chain movements become drastically hindered, and the polymer "vitrifies" to form segmental-scale microvoids. These microvoids are also known as "excess free volume" or "unrelaxed volume". Below the glass transition temperature, the polymer densifies over time and approaches thermodynamic equilibrium due to the removal of the excess free volume. This process is

known as physical aging and can result in significant time-dependent membrane transport properties [3-9]. Generally, permeability decreases and selectivity increases over time as a result of physical aging.

The state of a glassy polymer and its corresponding aging behavior depend not only on the immediate environment but also on its previous history (i.e., thermal history, vapor exposure) [5]. Physical aging accelerates with increasing temperature and decreasing membrane thickness [4, 6]. Thin films have been shown to age much faster than thick films of the same materials. Due to the thin separation layer in asymmetric hollow fiber membranes, physical aging is an important topic for polymeric membrane research.

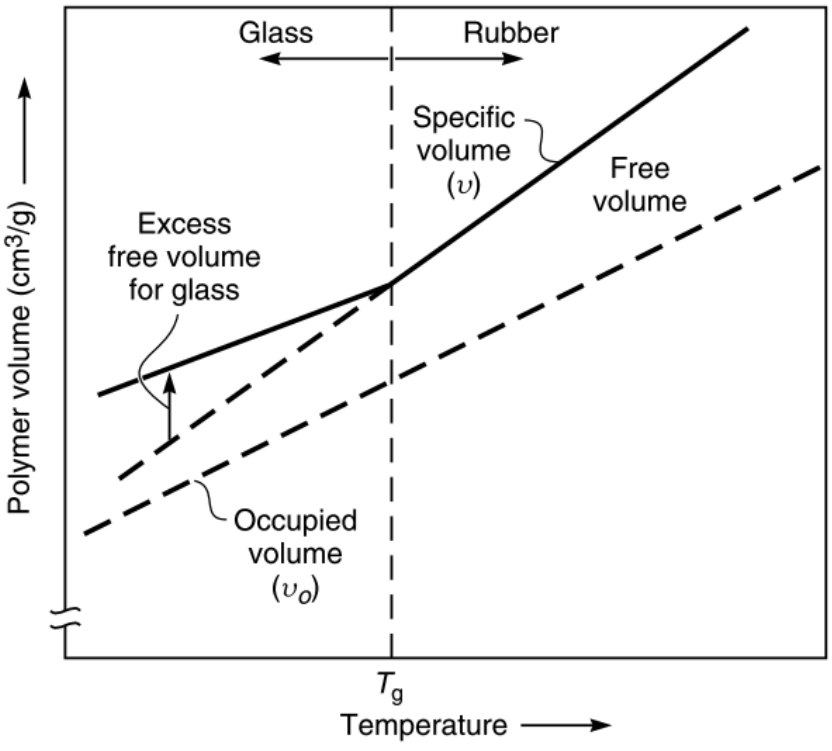

Figure 7.1 Schematic of the physical aging process of a glassy polymer [2]

7.2 Review of aging in CMS membranes

The development of CMS membranes with high separation performance, specifically, high permeability and high selectivity, is the focus of most CMS work. Little work has been done on the stability of CMS membranes. This is partially due to the rigid nature of CMS membranes and their enhanced chemical and thermal resistance compared to polymeric materials.

Chemical aging of carbon membranes under different environments were investigated. Unlike physical aging found in polymeric membranes, the major stability issues of CMS membranes revealed previously were the oxygen chemisorption and other adsorption [10-14]. Water adsorption was found by several researchers to decrease membrane performance [12, 13]. Jones and Koros also exposed CMS membranes to organic contaminants (hexane, vacuum pump oil, phenol and toluene, etc.), and found the membranes experienced significant permeance loss [14]; however, most of the loss was reversible upon exposure to propylene, indicating a chemical aging rather than a physical aging. Menedez and Fuertes investigated the aging of carbonized phenolic resin films on porous alumina tubes in different environments (air, nitrogen and propylene) [11]. With the comparison between oxygen exposed and oxygen free conditions, they concluded that the exposure to oxygen was the major cause for aging of carbon membranes. Further effort was made by Lagorsse and Mendes et al. for the impact of air and humidity exposure on cellulose derived CMS membranes [4]. They found that water strongly adsorbed on CMS membranes at medium to high humidity. Again, chemisorption of oxygen was found to the cause of membrane aging in dry conditions.

The aging phenomena revealed previously can be illustrated using cartoons in

Figure 7.2. Oxygen chemisorption is similar to the previously described oxygen doping concept [15], but more extreme. Oxygen selectively chemisorbs on the "tips" of ultramicropores. When disordered carbon materials are exposed to air at room temperature, chemisorption of oxygen takes place slowly [11, 16]. This process is slower than the oxygen doping at high pyrolysis temperatures. The carbon surfaces are generally hydrophobic, thereby adsorb organics (hexane, toluene, etc.) [12]. There are also some oxygen-containing surface groups on carbon surfaces, and these oxygen-containing surface groups can presumably act as primary sites to attract additional water molecules through hydrogen bonding and eventually formation of water clusters [12].

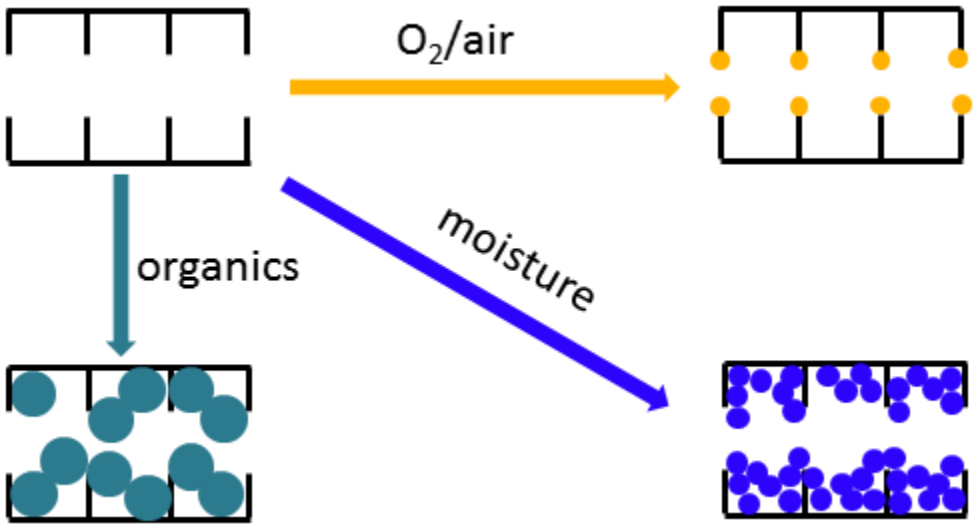

Figure 7.2 Cartoon representation of mechanisms of aging in CMS membranes caused by adsorptions

To address the stability issue noted above, several approaches were proposed. For the vulnerability to water vapor, drying the membrane at elevated temperatures was one solution; Jones and Koros also formed carbon composite membranes with water resistant

Teflon coating to address the problem [12]. For membranes after organic exposure, pure propylene at unit or near-unit activity was found to be an ideal cleaning agent to remove most organics [14]. For the aging caused by oxygen chemisorption, heat-treatments in a reduced atmosphere at high temperatures were used to remove oxygen surface groups [10].

7.3 Discovery of physical aging in CMS membranes

Prior to the current research, there was no report on *physical aging* of CMS membranes. In this research, the change of transport properties of CMS membranes over time was observed. This phenomenon was not obvious in the early Matrimid® CMS study, but became important and impacted several cases when the work progressed to 6FDA CMS study.

One example is demonstrated in Figure 7.3, for which the CMS hollow fiber membrane was prepared from a 6FDA-DAM precursor fiber using a 675 ^{o}C/2 hr protocol under UHP argon purge. The CMS fiber was tested using 100 psi pure gas ethylene and ethane at 35 ^{o}C. Unlike previous investigations, vacuum storage was used. In vacuum storage, the membrane module was stored in a constant volume permeation system, and both upstream and downstream were under active vacuum conditions. Besides vacuum, the module was capped in atmospheric air during the rest of time. As shown in Figure 7.3, the ethylene permeance decreased over time, and the ethylene/ethane selectivity increased over time. The transport properties changed quickly at the first days after production, and tended to approach a steady state quickly. Previous researchers proposed that aging in carbon membranes were attributed to oxygen chemisorption or water or

organic adsorptions. Therefore, the permeance loss in atmospheric storage might be attributed to oxygen chemisorption; however, this is not consistent with the essentially identical response of the vacuum-stored membrane. In the vacuum conditions, all these adsorption processes should be absent and the membrane should preserve its original state. This led to the hypothesis that true physical aging probably also exists in CMS membranes.

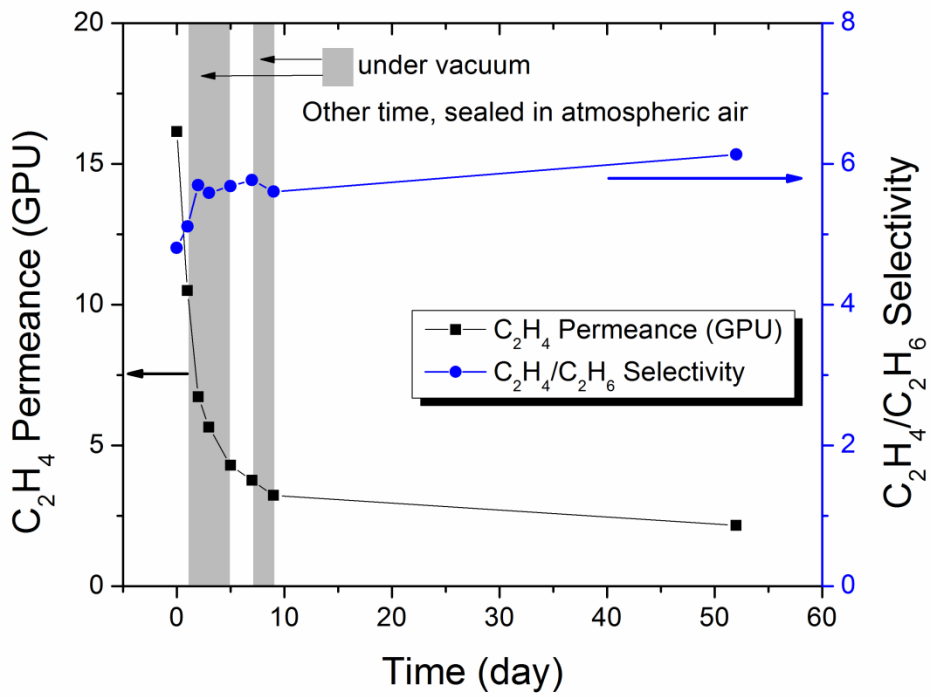

Figure 7.3 Aging of a 6FDA-DAM derived CMS hollow fiber

With the above hypothesis, causes for aging of CMS membranes were expanded to the following possibilities: water vapor adsorption, organic adsorption, oxygen chemisorption and physical aging. In the active vacuum conditions, water vapor and oxygen were absent in the membrane module and could be excluded for the rapid permeance reduction. It was still possible that vacuum pump oil vapor may back diffuse

to the membrane, although it was unlike to happen due to the installation of aluminum foreline trap. As demonstrated previously, some organic contaminants could be removed by propylene regeneration. Propylene with unit activity or near unity activity (about 148 psi at 20 ^{o}C) was used to clean the membrane. The propylene stream was fed on the bore side and permeated through the membrane to the shell side. The cleaning usually lasted several hours, typically more than 12 hrs. Regeneration was performed for the module showed in Figure 7.3 after aging for 52 days. The results are shown in Figure 7.4. The ethylene permeance was slightly increased from 2.2 GPU to 2.5 GPU, but still well below its original value of 16.1 GPU. The selectivity was slightly reduced. This suggests that removable organic contaminants was not the major cause for the permeance loss, otherwise, the regeneration should have been more effective.

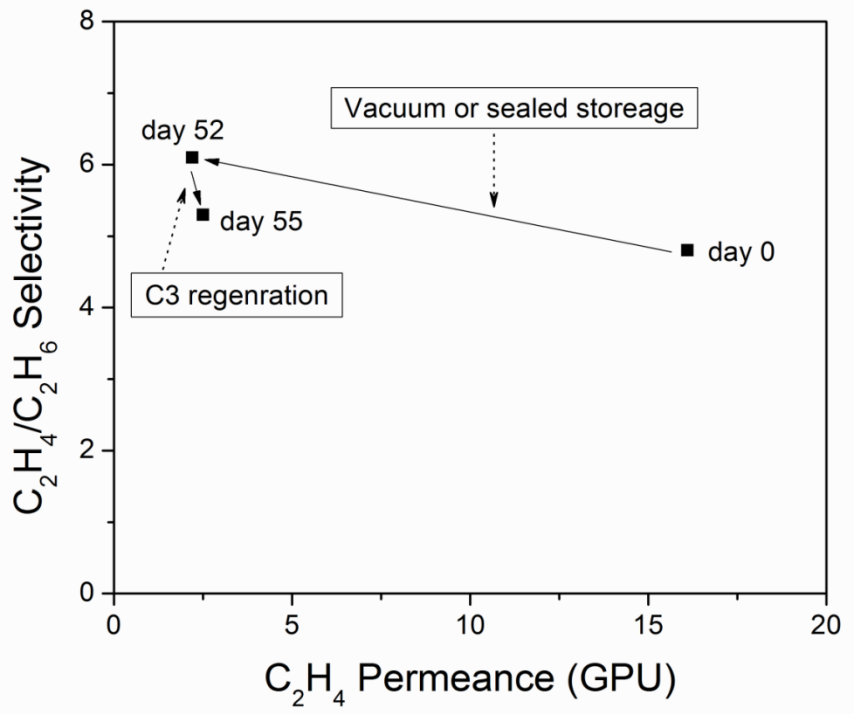

Figure 7.4 Regeneration of an aged 6FDA-DAM CMS hollow fiber membrane by propylene cleaning

Propylene regeneration was also performed on other membrane modules with various aging histories. In all cases, the permeances could be recovered to only a small extent, but well below their initial values. Of course, the argument at this point can be: (1) aging was not caused by organic adsorption; or (2) the organics from vacuum pump oil caused aging but the regeneration method was not effective. Further tests must be carried out with vacuum free conditions to exclude the pump oil effect.

CMS membrane modules were then investigated under dry gas storage conditions. The comparison was made between air and argon. The first objective was to exclude any exposure to organics or water vapor. The second objective was to investigate the effect of oxygen exposure. Fresh 6FDA/BPDA-DAM CMS hollow fiber membranes from a 675 ^{o}C/2 hr protocol were stored under active 30 psig feed conditions under UHP argon and compressed air. Oxygen and moisture contents in the gas were less than 1 ppm according to Airgas. The membranes were retested after 5 days and 145 days storage. The results are shown in Figure 7.5. Figure 7.5 (a) shows for both cases ethylene permeance decreased over time, and the decrease in air storage was somewhat higher than in argon storage. Figure 7.5 (b) shows that for both cases, ethylene/ethane selectivity increased over time, and the increase in air storage was higher than in argon storage. Although aging was more obvious in the case of air storage, one fact cannot be ignored was the substantial aging in argon. Somehow, since the trend in air storage conditions was more obvious than in argon storage, oxygen chemisorption still remained as one of the partial causes. With the inert noble gas argon, the membrane still underwent aging; therefore, other adsorptions could be excluded at this point. Like glassy polymers, it appears clear that significant physical aging also occurs in *some* CMS materials.

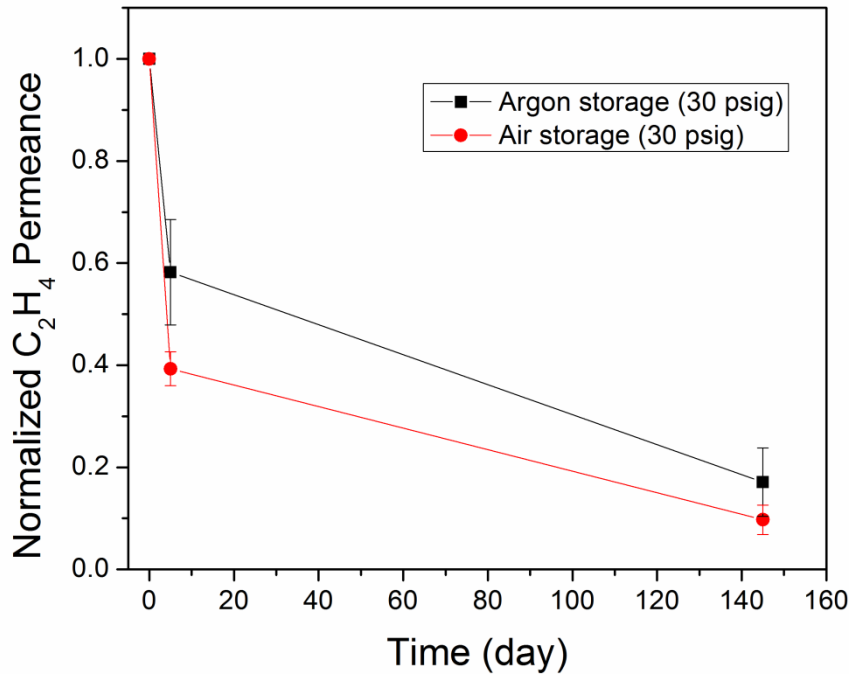

(a) Permeance

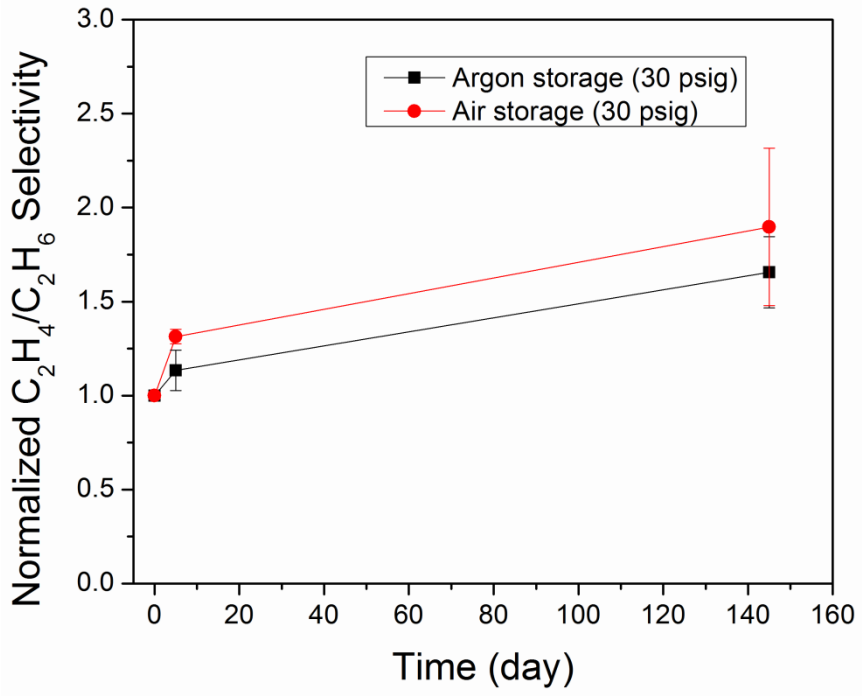

(b) Selectivity

Figure 7.5 Comparison of aging of CMS membranes in argon and air storage conditions

7.4 Structural considerations of physical aging in CMS membranes

The above discovery was made mainly by exclusion of other possible aging mechanisms. It was also critical to justify the physical aging from a structural perspective.

On the elemental level, for 6FDA-DAM and 6FDA/BPDA-DAM, precursor polymers consists of carbon (C), hydrogen (H), oxygen (O), nitrogen (N) and fluorine (F) elements. After pyrolysis (500-800 ^{o}C, mostly 550 ^{o}C or 675 ^{o}C), fluorine was completely removed, and this was confirmed by XPS measurement of the precursor and the resultant carbon fiber. The XPS spectra are shown in Figure 7.6. XPS also provide information of some quantitative elemental compositions except for hydrogen and helium. This 6FDA-DAM CMS membrane prepared by a 675 ^{o}C protocol contained 85.8 ±1.6 % atomic carbon, 11.1 ±3.0 % atomic oxygen, and 3.1 ±1.8% atomic nitrogen. Compared to literature values, the carbon content above was at the low end [17-19]. Since XPS is highly surface sensitive (the typical detection depth is ~5 nm), works by other researchers have shown that the surface carbon content could be increased by using long argon ablation to remove surface-sorbed oxygen to probe the "true" value within the bulk of the material [17, 20].

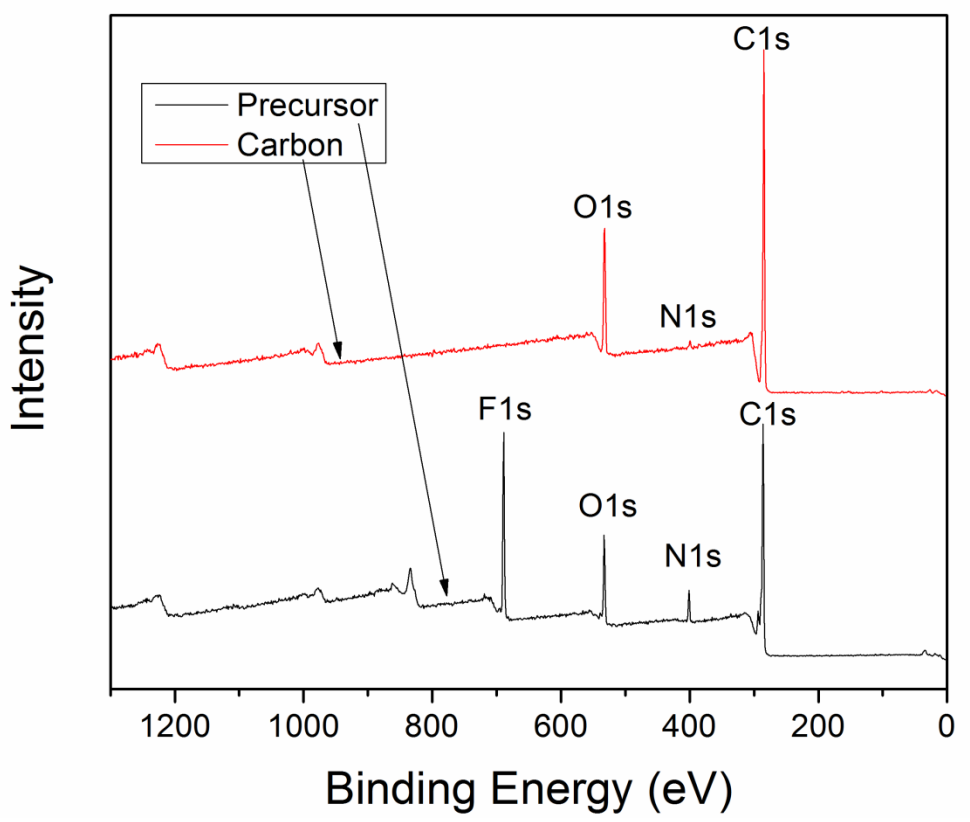

Figure 7.6 Comparison of 6FDA-DAM precursor and CMS (675 ^{o}C) XPS spectra

The second structural level (porous structure) is important for CMS membrane transport properties. Previously, it was noted that the pores in CMS materials are formed by packing imperfections of small graphene-like sheets. On the long range, CMS materials are amorphous. Raman spectroscopy is useful to characterize disorder in sp^2 carbon materials [21-23]. The Raman spectrum of crystalline graphite is marked by the presence of two strong peaks at 1580 cm^{-1} and 2700 cm^{-1}, named the G and G' bands, respectively. Samples with small crystallite size show an additional dispersive peak centered at approximately 1350 cm^{-1}. This peak has been named the D band (D for defect or disorder). The D band is not present in single crystals of graphite. The intensity of the D band and the ratio between the intensities of the disorder-induced D band and the

graphite G band provides a parameter that can be used to quantify disorder. Raman spectra of Matrimid®, 6FDA-DAM and 6FDA/BPDA-DAM CMS membranes pyrolyzed at 550 ^{o}C are shown in Figure 7.7. As clearly illustrated by the spectra, the structure of CMS membranes fall into the amorphous carbon form described previously. Both G and D bands are present. Another critical feature revealed from this plot is that the spectra of the CMS membranes derived from three different polyimides are very close, indicating a similar degree of disorder.

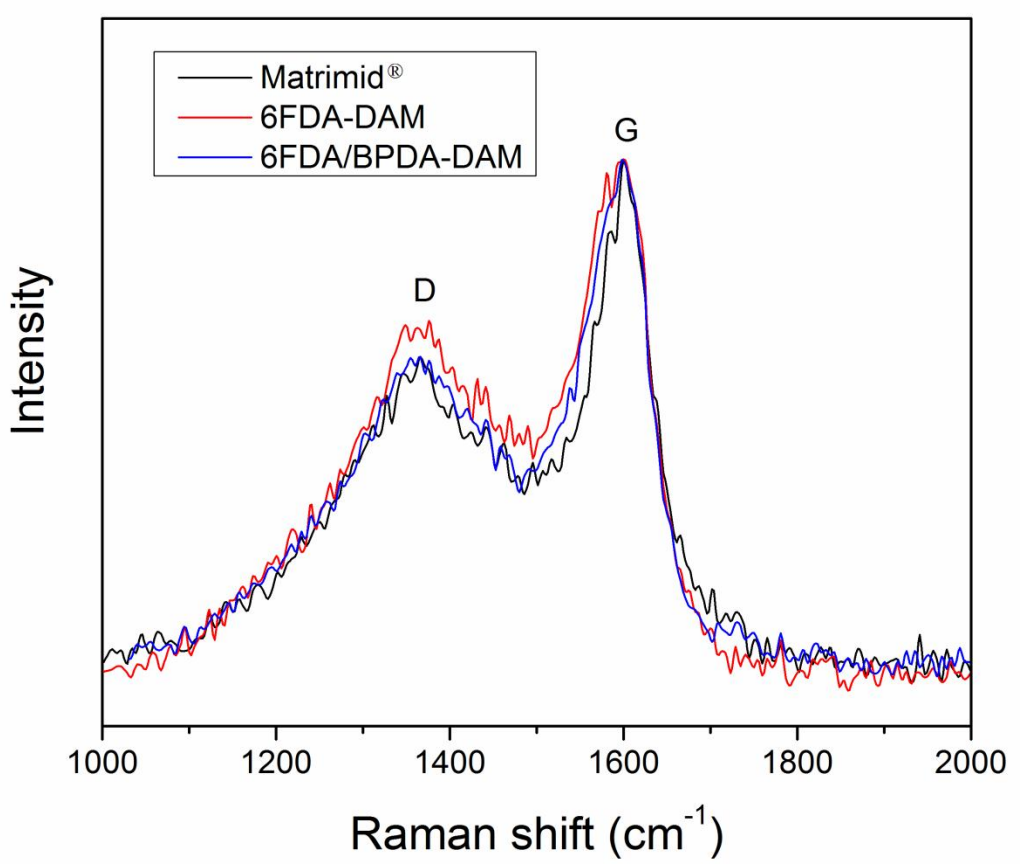

Figure 7.7 Comparison of Raman spectra of Matrimid®, 6FDA-DAM and 6FDA/BPDA-DAM CMS membranes pyrolyzed at 550 ^{o}C

Based on the above structural verifications, it is reasonable to infer the physical

aging of CMS membranes. The pores are believed to be created by packing imperfections or disorder of grapheme-like sheets that are not in a thermodynamically stable state [24]. These pores are believed to tend to rearrange and achieve denser packing. This mechanism is, therefore, believed to be analogous to physical aging in glassy polymers. The pore volume in CMS materials is believed to be like the "excess free volume" in glassy polymers. The schematics in Figure 7.8 illustrate the envisioned physical aging in glassy polymers and CMS materials. The phenomena were also observed in the parallel dense film work. Permeation showed the permeability loss and slight selectivity enhancement over time. Sorption experiments demonstrated that, at the very early stage, the sorption isotherm of ethylene and ethane in 6FDA-DAM CMS showed poor fits to Langmuir model, but fit better into dual mode better. This means CMS materials at the very beginning behave similar to glassy polymers. The aged membrane tended to fit well into Langmuir mode, which was expected for a typical molecular sieving material.

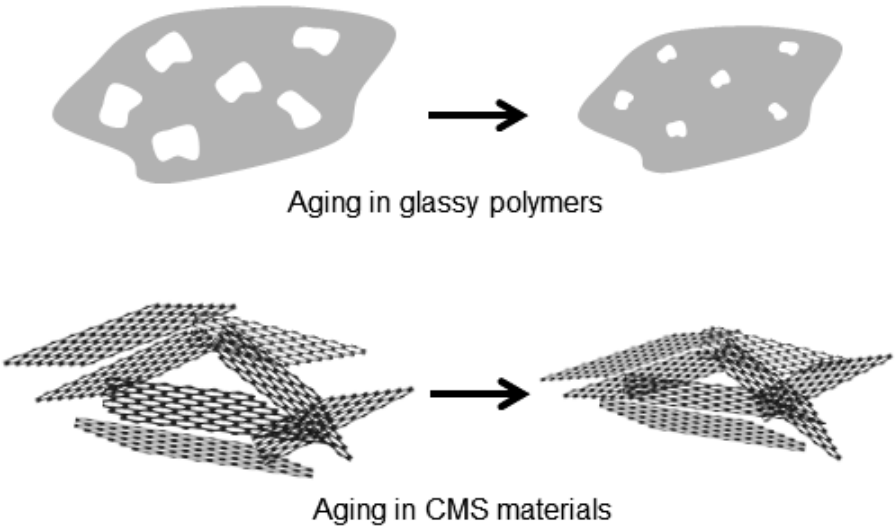

Figure 7.8 Cartoon representation of physical aging in glassy polymers and CMS materials

7.5 Effect of precursor polymers and processing conditions

The aging kinetics of CMS membranes based on different precursors was also investigated. Like glassy polymers, the starting materials and the processing conditions were expected to have significant impacts on aging of CMS membranes. Glassy polymers with more open structures age faster than the less open ones.

The aging kinetics of CMS membranes prepared from Matrimid®, 6FDA-DAM and 6FDA/BPDA-DAM were investigated for samples prepared by using the 550 ^{o}C/2 hr protocol and under UHP argon purge. Vacuum and atmospheric conditions were pursued for the storage of CMS membranes. In the vacuum case, the membrane module was installed in constant volume permeation systems, and both upstream and downstream were pulled vacuum except the testing time. In the atmospheric storage, the membrane modules were sealed using Swagelok fittings and atmospheric air was trapped in the modules.

The results are shown in Figures 7.9, 7.10 and 7.11, respectively. The normalized permeance and selectivity change are shown in Figure 7.12 for easy comparison. 6FDA-DAM CMS started with the highest permeance, Matrimid® CMS had the lowest permenace, and 6FDA/BPDA-DAM CMS was in between. Also, the aging of 6FDA-DAM CMS was the fastest, Matrimid® CMS was the most stable, and 6FDA/BPDA-DAM CMS was in the middle. Comparing vacuum and atmospheric storage, in all cases, membranes stored in vacuum conditions aged more than the ones in atmospheric conditions. Among these three polymers, it seems still 6FDA/BPDA-DAM derived CMS had a reasonably stable performance after aging. The ethylene permeance was stable in about one week and remained higher than 10 GPU.

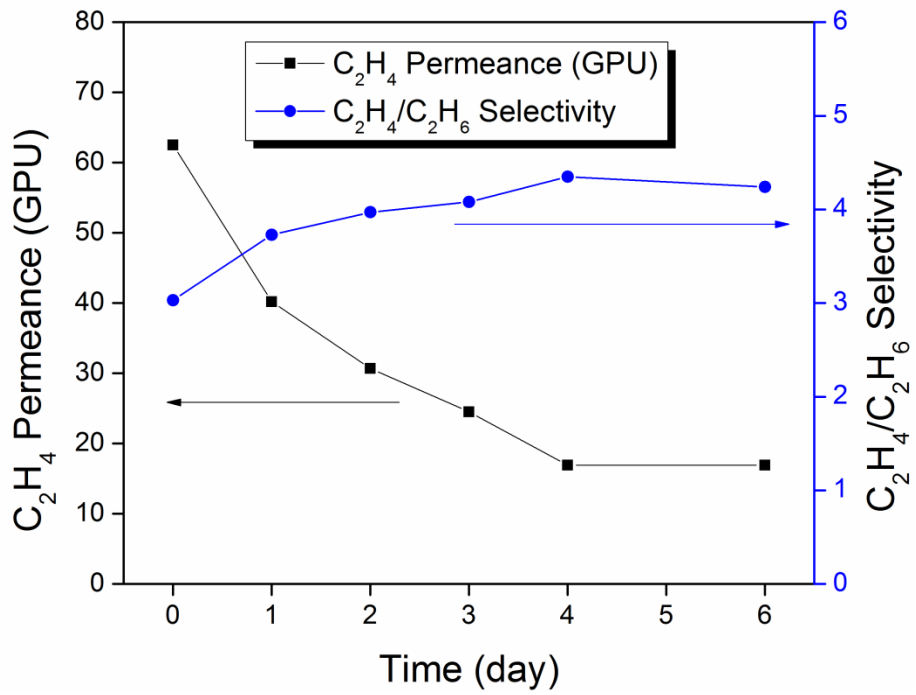

(a) Atmospheric storage

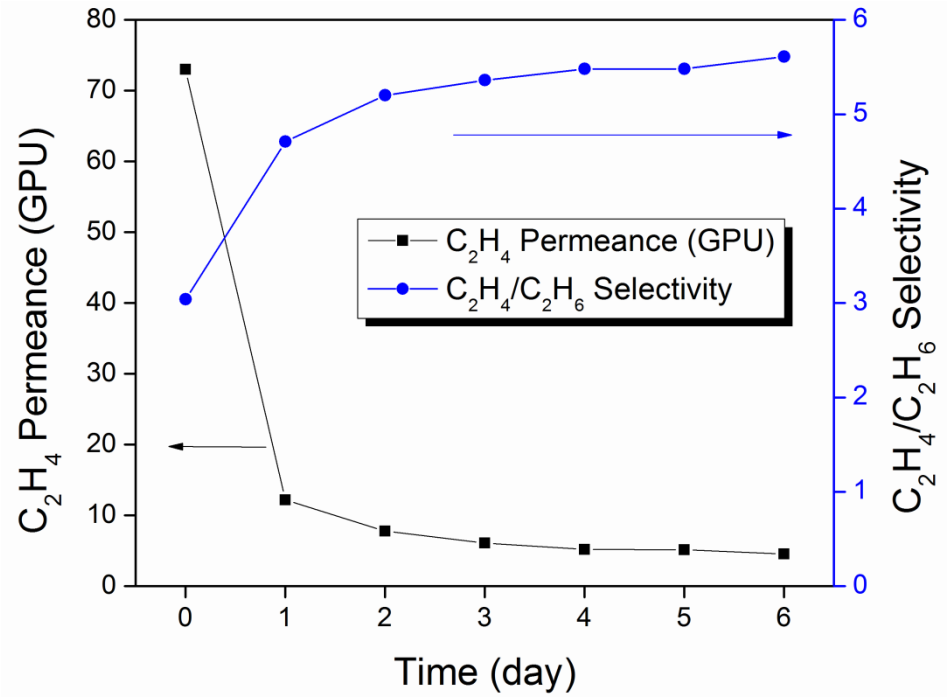

(b) Vacuum storage

Figure 7.9 Aging kinetics of 6FDA/BPDA-DAM CMS hollow fiber membranes

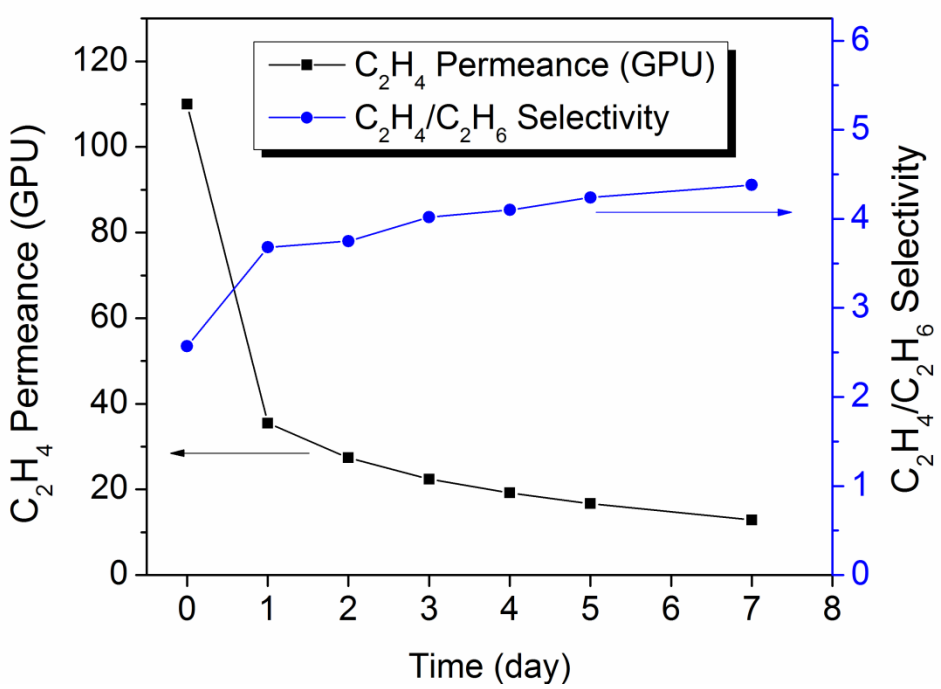

(a) Atmospheric storage

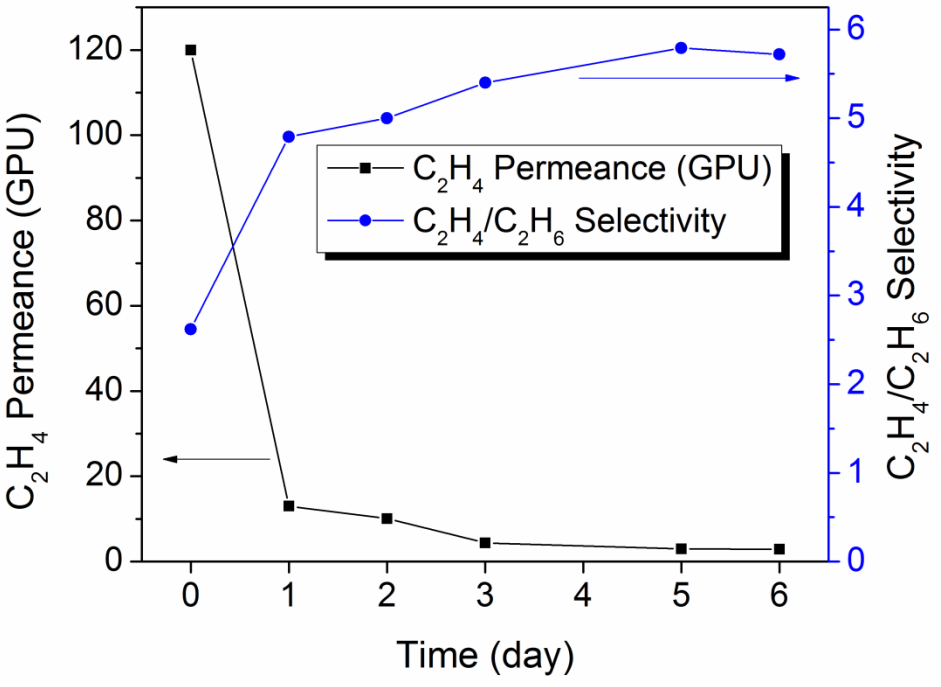

(b) Vacuum storage

Figure 7.10 Aging kinetics of 6FDA -DAM CMS hollow fiber membranes

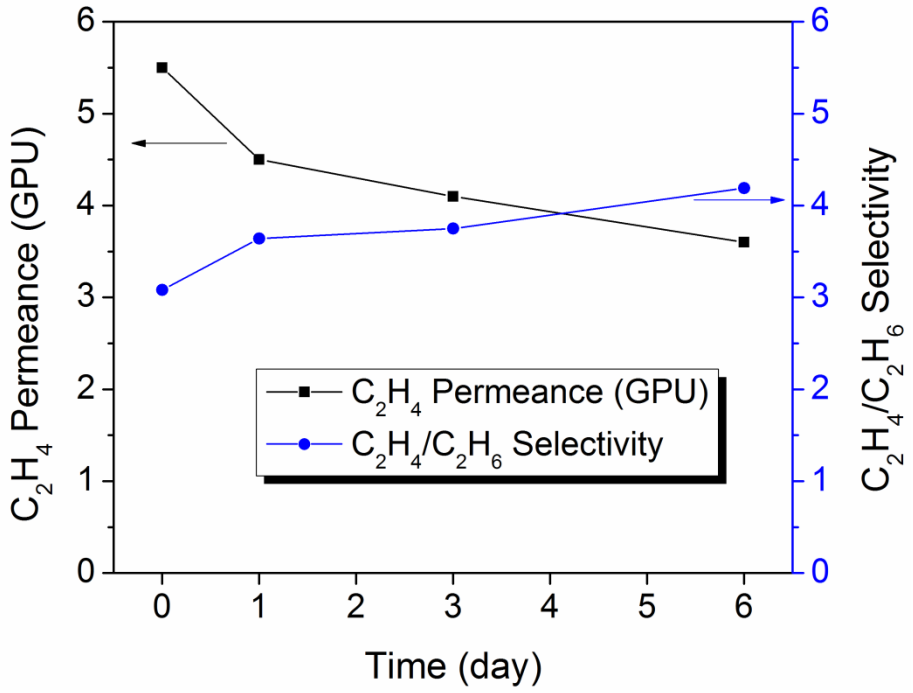

(a) Atmospheric storage

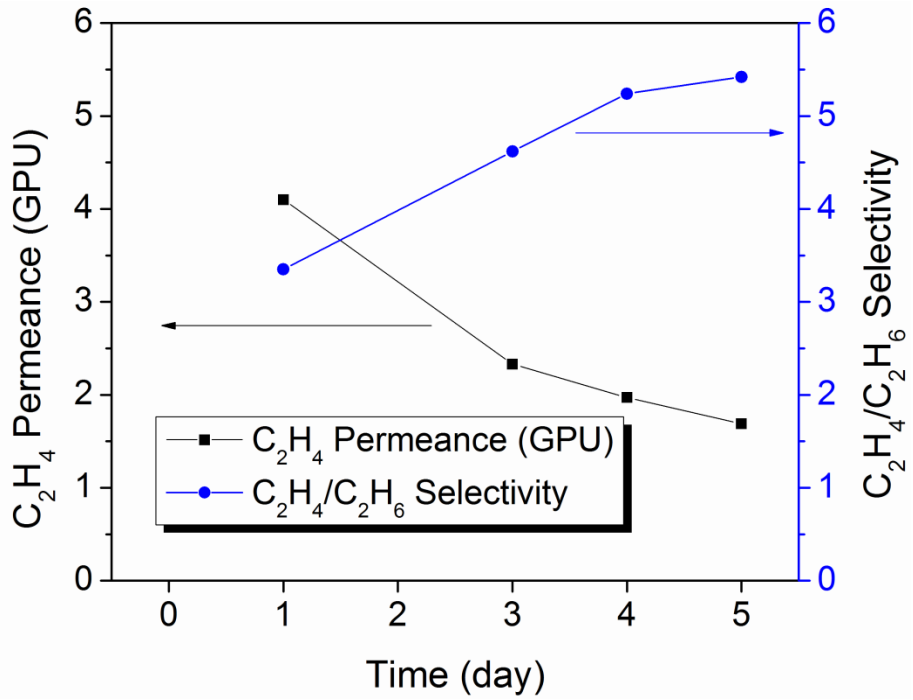

(b) Vacuum storage

Figure 7.11 Aging kinetics of Matrimid® CMS hollow fiber membranes

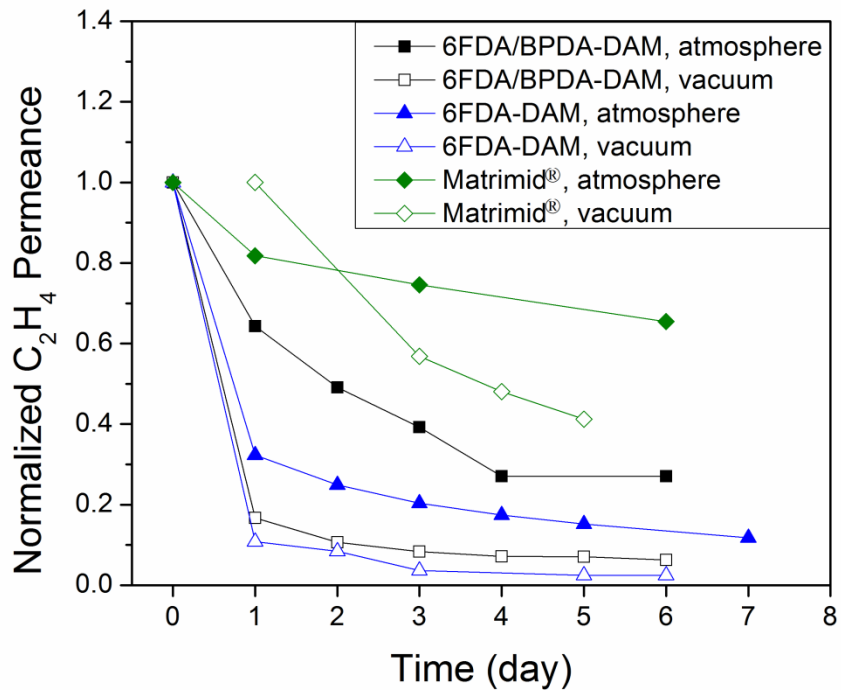

(a) Permeance

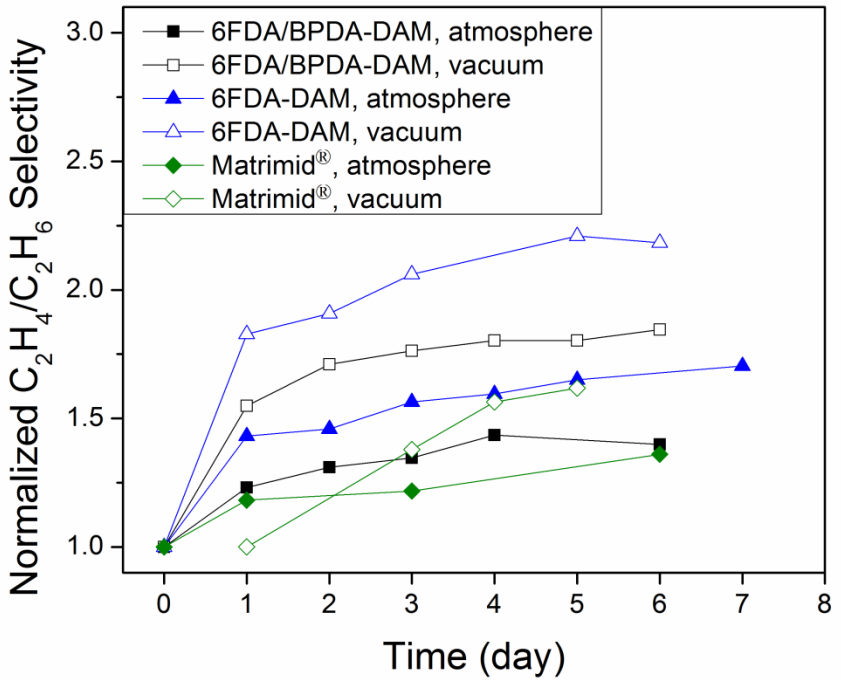

(b) Selectivity

Figure 7.12 Normalized aging kinetics of CMS hollow fiber membranes

Inspired by the aging study of 6FDA-DAM CMS membranes, another fact observed in pyrolysis may be explained. Illustrated by Figure 7.10, after stored in vacuum for 6 days, 6FDA-DAM CMS membrane ethylene permeance dropped dramatically to about 3 GPU. In several independent pyrolysis of 6FDA-DAM at 550 ^{o}C, vacuum pyrolysis yielded very low permeance less than 1 GPU (in some cases even lower than 0.1 GPU), while the inert gas purge pyrolysis gave permeance higher than 10 GPU. 6FDA/BPDA-DAM and Matrimid® pyrolysis did not show such phenomena. Previously, the only difference inferred for vacuum and inert gas purge pyrolysis was the oxygen content. The above results may lead to another explanation for the phenomena described above. In 6FDA-DAM vacuum pyrolysis, probably accelerated ultramicroporous structure collapse occurs at high temperature, thereby resulting in extremely low permeance of 6FDAM-DAM CMS hollow fiber membranes.

7.6 Impact of aging on transport properties of penetrant gases

Responses of penetrant gases vary to membrane aging. After CMS membrane aging, permeances of all penetrant gases decrease. Meanwhile, selectivities of a fast gas to a slow gas increase. The extent of permeance loss depends on gas molecule sizes. Small gases are less affected by aging and the influence on large gases is more dramatic. Figure 7.13 illustrates an example of such trends. The CMS membrane was aged for about 228 days after the initial test, and the permeances of 7 penetrant gases were measured. The measured permeance values were calculated and compared to the fresh samples. It is obvious that small gases such as helium (only ~18.6% decrease in permeance) were less affected and large gases such as ethane (about ~75.4% decrease in

permenace) was affected more. With increasing gas molecule sizes, in most cases, the influence becomes more obvious. Changes of pore size distribution during aging process at this point are still not clear. Learning from this, separations of fast gas pairs are less affected, such as natural gas application of CO_2/CH_4 separation; separations of big gas pairs are much more sensitive, such as olefin/paraffin separation, especially C_3H_6/C_3H_8 separation.

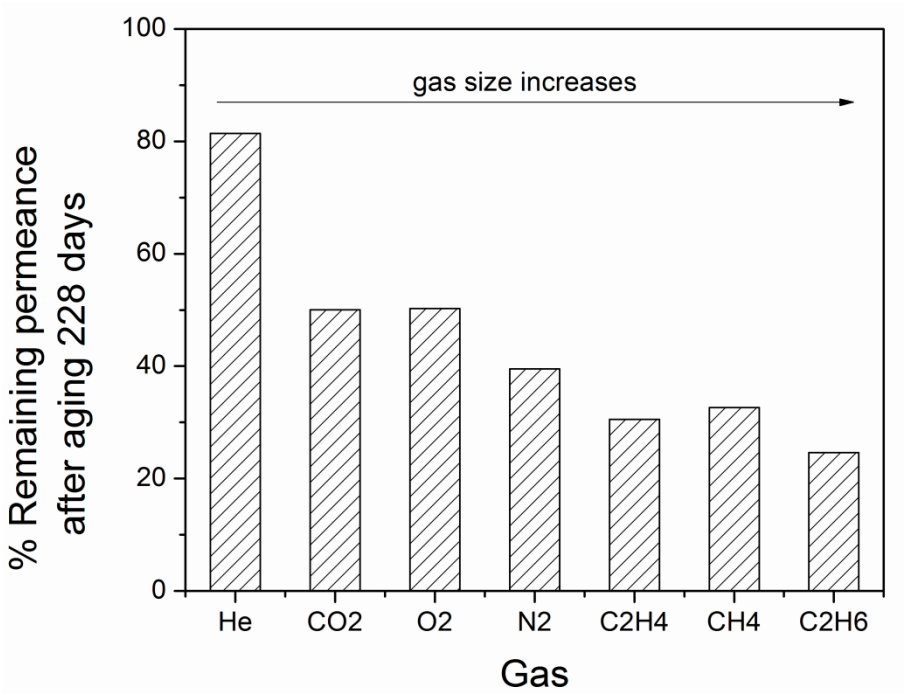

Figure 7.13 Impact of aging on transport properties of penetrant gases with different sizes

7.7 Permeance-selectivity tradeoff induced by CMS membrane aging

As noted previously, as a result of aging, permeability decreases and selectivity increases. Therefore, there is a tradeoff between permeability and selectivity for samples with various aging histories. Since aging only affects the microporous structures of

membranes and does not change the thickness of separation layers, in the asymmetric membrane form, permeance can represent the permeability without complications. Figure 7.14 shows mixed gas transport properties of multiple 6FDA/BPDA-DAM CMS membranes pyrolyzed by the 675 ^{o}C/2hr, UHP argon purge protocol with different aging histories. As clearly illustrated by the plot, there is a tradeoff trend between permeance and selectivity. Based on this trend, the history dependence may be employed as another tool for tailoring CMS membrane performance. Different processing conditions (vacuum, inert gas, air and hydrocarbon storage conditions) offer opportunities.

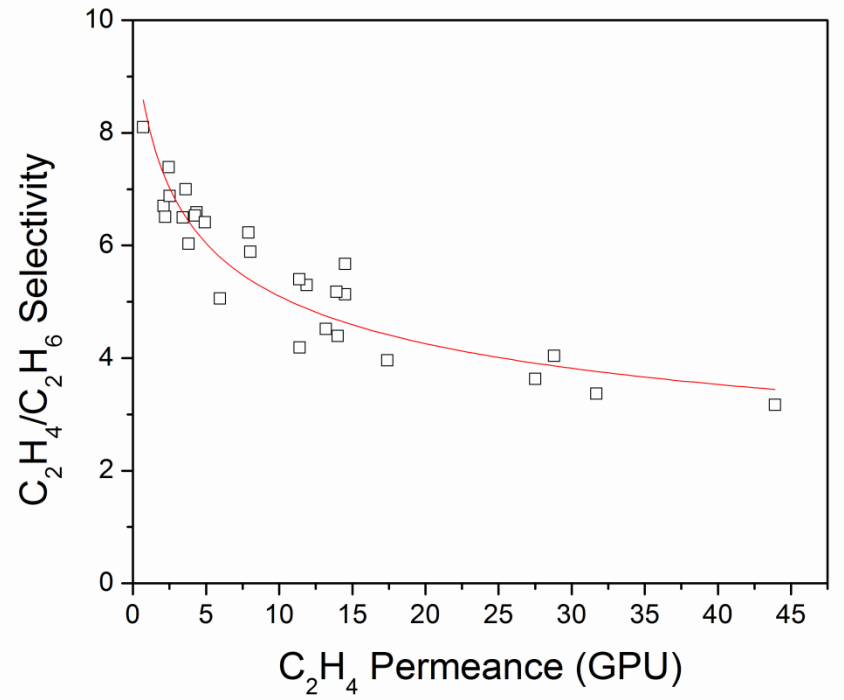

Figure 7.14 Permeance-selectivity tradeoff of CMS membranes with different aging histories

7.8 Considerations of testing protocols

As demonstrated by the previous section, transport properties of CMS membranes

have strong history dependence. The post-pyrolysis processing conditions affect the membrane performance significantly. Without knowing the history dependence, CMS membranes were assumed to be rigid and stable over time. Before realizing this property, most CMS membrane tests were performed in constant volume systems. Most membranes were evacuated under active vacuum in order to remove sorbed gas molecules in CMS membranes. In fact, this evacuation has another role as the rapid stabilization. This explains the divergence of some measured values caused by changing testing protocols. For example, at the very beginning, 10-20 GPU ethylene permeance for 6FDA/BPDA-DAM CMS produced by 550 ^{o}C/argon purge pyrolysis was reported by tests with the long term evacuation protocol, while the intrinsic values right after pyrolysis and before dramatic aging should be much higher.

For CMS hollow fiber testing, the protocol may be adjusted relatively easily based on various purposes due to the relatively fast permeation rates. For example, in order to stabilize the membrane efficiently, vacuum can be applied to the membranes. Otherwise, limited vacuum time can be applied to obtain intrinsic transport properties. However, for CMS dense membrane testing, the situation is more complicated. In most dense film cases, to ensure the complete removal of sorbed gases in the membrane, a long term evacuation is a must before starting gas permeation tests. Therefore, unavoidably, the membranes age quickly during this period. Maintaining a consistent testing protocol or stabilizing membranes effectively before testing is important for achieving consistent permeation results. Of course, alternatively, without adequate evacuation prior to tests, steady state permeation rates in constant volume permeation systems may still be obtained by monitoring the pressure increase rates in the downstream, but it is

challenging to judge without knowing the time lag. This can also be extrapolated to the comparison of mixed gas tests and pure gas tests. Prior to each pure gas test, the membrane has to experience sufficient evacuation, meanwhile, the membrane ages. Therefore, for an unstable membrane, separate pure gas permeation tests are actually performed on different "membranes" due to structural changes. It is complicated to compare pure gas permeation results and mixed gas permeation results, since not only competition effect is playing. In any case, mixed gas permeations tests are much more reliable, and do not overestimate or underestimate the transport properties due to the artifact of history dependence.

7.9 Realistic stability of CMS membranes

As shown by the aging kinetics, the significantly unstable state only exists within very short period of time after membrane fabrication. Some metastable states may provide interesting transport properties, and trapping the membrane structure in such states could be an interesting topic for future investigations. The primary interest here is the properties of stabilized membranes.

After 5 to 12 months aging, 4 samples of 6FDA/BPDA-DAM CMS membranes (550 ^{o}C/2 hr, UHP argon pyrolysis) showed very consistent ethylene permeance about 8-9 GPU after quick mixed gas permeation tests at 35 ^{o}C. This permeance is still very attractive compared to Matrimid® CMS membranes.

The long term membrane stability under realistic feed conditions is another important topic. Most of lab scale characterization studies were performed with downstream vacuum permeation conditions, which were efficient for materials

characterization but too idealistic for industrial applications. Therefore, in this test, the downstream pressure was kept at 1 atm, and the ethylene/ethane mixed gas feed pressure was kept at ~115 psi, thereby giving driving force of about 100 psi. The active testing was run for ~150 hours, and the results are shown in Figure 7.15. In the first 35 hours, the ethylene permeance increased from 8.8 GPU to 12.9 GPU, and the ethylene/ethane selectivity decreases from 4.3 to about 3.9. After this period of time, the performance was quite stable for the next 115 hours. The standard deviation of permeance was only 0.09 GPU, and the standard deviation of selectivity was only 0.02. For the initial equilibrium step, two factors may be used to explain. One reason can be the relatively slow sorption equilibrium of ethylene and ethane in the membrane. The other explanation can be the "flexible" CMS structure. As shown by the aging study, the skeleton of CMS membranes shows some flexibility, of course, it is still much more rigid than polymers. Probably the intense hydrocarbon feed may also open the pore structure a little and lead to some increase in the permeance and a subtle decrease in selectivity. Nevertheless, after achieving equilibrium, the membrane is very stable in the aggressive hydrocarbons feed conditions.

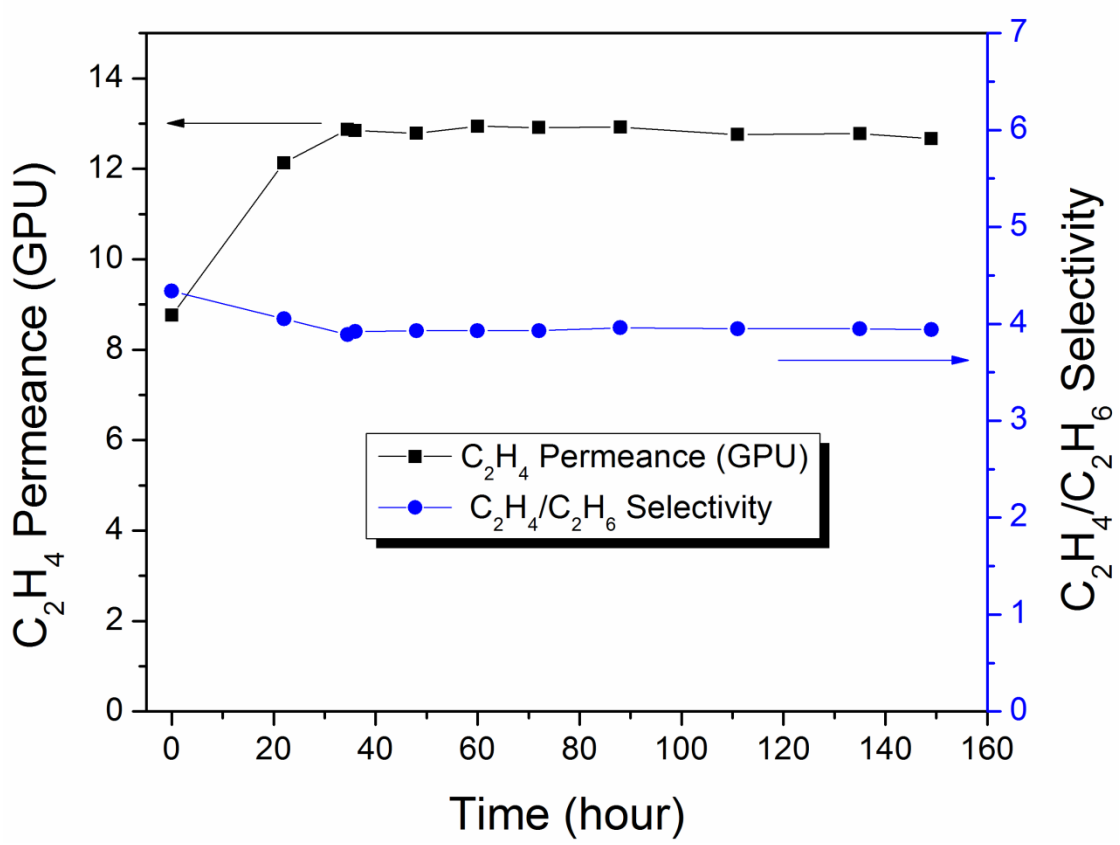

Figure 7.15 Long term stability test of a stabilized 6FDA/BPDA-DAM CMS hollow fiber membrane

7.10 Summary and conclusions

This chapter described unexpected physical aging in CMS membranes. Physical aging was studied extensively in polymeric membranes and aging in CMS membranes revealed previously were mostly related to adsorption: chemisorption of oxygen, physical adsorption of water and organics in the pore structures. Experimentally, in this study, all of the above adsorption induced aging was excluded by aging study in vacuum storage, inert gas atmosphere storage and propylene cleaning. Physical aging appeared to be the cause for rapid changes of transport properties at the early stage after the membrane fabrication. The pores are believed to be formed by packing imperfection of graphene-

like sheets, and age analogously to the "unrelaxed free volume" in glassy polymers. Over time, these pores tend to collapse in order to achieve thermodynamically more stable states. Aging kinetics of Matrimid®, 6FDA-DAM and 6FDA/BPDA-DAM CMS membranes were investigated. The dense Matrimid® CMS showed relative slow aging, the open 6FDA-DAM CMS showed rapid aging, and 6FDA/BPDA-DAM CMS was in between. For storage conditions, vacuum storage showed faster aging than atmospheric storage. The impact of structural aging on the transport properties for slow gases was more obvious than for fast gases. Aging in CMS membranes also induced a permeance-selectivity tradeoff. The history dependence led to more careful considerations about the testing protocols for both hollow fiber and dense film membranes. The history dependence can actually be employed as another tool to tailor the CMS membrane transport properties. A long term permeation test demonstrated the excellent stability of stabilized CMS membranes under realistic conditions.

7.11 References

[1] Y. Huang, D.R. Paul, Effect of film thickness on the gas-permeation characteristics of glassy polymer membranes, Ind. Eng. Chem. Res. 46 (2007) 2342-2347.

[2] R.W. Baker, Membrane technology and applications, 2 ed., John Wiley & Sons Ltd, West Sussex, England, 2004.

[3] L.L. Cui, W.L. Qiu, D.R. Paul, W.J. Koros, Physical aging of 6FDA-based polyimide membranes monitored by gas permeability, Polymer 52 (2011) 3374-3380.

[4] L.L. Cui, W.L. Qiu, D.R. Paul, W.J. Koros, Responses of 6FDA-based polyimide thin membranes to CO_2 exposure and physical aging as monitored by gas permeability, Polymer 52 (2011) 5528-5537.

[5] B.W. Rowe, B.D. Freeman, D.R. Paul, Influence of previous history on physical aging in thin glassy polymer films as gas separation membranes, Polymer 51 (2010) 3784-3792.

[6] J.H. Kim, W.J. Koros, D.R. Paul, Effects of CO_2 exposure and physical aging on the gas permeability of thin 6FDA-based polyimide membranes - Part 2. with crosslinking, J. Membr. Sci. 282 (2006) 32-43.

[7] Y. Huang, D.R. Paul, Effect of temperature on physical aging of thin glassy polymer films, Macromolecules 38 (2005) 10148-10154.

[8] Y. Huang, D.R. Paul, Physical aging of thin glassy polymer films monitored by gas permeability, Polymer 45 (2004) 8377-8393.

[9] P.H. Pfromm, W.J. Koros, Accelerated physical ageing of thin glassy polymer films: evidence from gas transport measurements, Polymer 36 (1995) 2379-2387.

[10] S. Lagorsse, F.D. Magalhaes, A. Mendes, Aging study of carbon molecular sieve membranes, J. Membr. Sci. 310 (2008) 494-502.

[11] I. Menendez, A.B. Fuertes, Aging of carbon membranes under different environments, Carbon 39 (2001) 733-740.

[12] C.W. Jones, W.J. Koros, Carbon composite membranes - a solution to adverse humudity effects, Ind. Eng. Chem. Res. 34 (1995) 164-167.

[13] C.W. Jones, W.J. Koros, Characterization of ultrmicroporous carbon membranes with humidified feeds, Ind. Eng. Chem. Res. 34 (1995) 158-163.

[14] C.W. Jones, W.J. Koros, Carbon molecular-sieve gas separation membranes-II. Regeneration following organic exposure, Carbon 32 (1994) 1427-1432.

[15] M. Kiyono, P.J. Williams, W.J. Koros, Effect of pyrolysis atmosphere on separation performance of carbon molecular sieve membranes, J. Membr. Sci. 359 (2010) 2-10.

[16] H.P. Boehm, Free radicals and graphite, Carbon 50 (2012) 3154-3157.

[17] C.W. Jones, W.J. Koros, Carbon molecular sieve gas separation membranes-I. Preparation and characterization based on polyimide precursors, Carbon 32 (1994) 1419-1425.

[18] D.Q. Vu, W.J. Koros, S.J. Miller, High pressure CO_2/CH_4 separation using carbon molecular sieve hollow fiber membranes, Ind. Eng. Chem. Res. 41 (2002) 367-380.

[19] H. Suda, K. Haraya, Gas permeation through micropores of carbon molecular sieve membranes derived from Kapton polyimide, J. Phys. Chem. B 101 (1997) 3988-3994.

[20] A. Singh, Membrane materials with enhanced selectivity: an entropic interpretation, in: Chemical Engineering, The University of Texas at Austin, 1997.

[21] F. Tuinstra, J.L. Koenig, Raman spectrum of graphite, J. Chem.Phys. 53 (1970) 1126-1130.

[22] M.S. Dresselhaus, A. Jorio, A.G. Souza Filho, R. Saito, Defect characterization in graphene and carbon nanotubes using Raman spectroscopy, Philos. Transact. A Math. Phys. Eng. Sci. 368 (2010) 5355-5377.

[23] S. Reich, C. Thomsen, Raman spectroscopy of graphite, Philos. Transact. A Math. Phys. Eng. Sci. 362 (2004) 2271-2288.

[24] A. Oberlin, Carbonization and graphitization, Carbon 22 (1984) 521-541.

CHAPTER 8

CMS MEMBRANE FOR HYBRID MEMBRANE-DISTILLATION PROCESSES

The initial motivation of this work was to develop robust high performing CMS membranes for ethylene/ethane separation, and the focus was mainly on membrane material development. In Chapter 6, the application was extended to propylene/propane separation due to the excellent performance of CMS membranes derived from 6FDA polymers. This chapter describes a newly discovered olefins-selective feature of CMS membranes and the enabled hybrid membrane-distillation processes [1, 2].

8.1 Debottlenecking concept

Currently, replacing distillation columns with membrane modules is still not feasible due to the inadequate selectivity of membranes and the purity requirement of olefin products. Nevertheless, a hybrid membrane distillation system may still offer significant energy savings, and is practically viable as a retrofitting concept.

The previous concept for hybrid membrane-distillation was mainly for debottlenecking the energy intensive distillation. In our previous studies of olefin/paraffin separations, binary systems (ethylene/ethane, propylene/propane) were investigated extensively. Debottlenecking C2 and C3 splitters is also the focus of most researchers [3-6], as demonstrated in Figure 8.1. Separations by membranes have been mainly focused on separating ethylene from ethane and separating propylene from propane. While C2 and C3 splitters are the last two columns in the cracked gas processing process, the

demand for improving energy efficiency for other distillation units also remains, such as with deethanizer and demethanizer. As shown in Figure 1.1 in Chapter 1, membranes may potentially fit into various positions of the large purification units in ethylene plants. However, very few studies have been targeted for other applications, since even the relatively simple binary separations have been very challenging for current membranes.

Including membranes for deethanizer applications, the debottlenecking hybrid membrane-distillation concept is represented in Figure 8.1. For each distillation column (C2 splitter, C3 splitter and deethanizer), a parallel membrane unit is incorporated for debottlenecking. The membrane modules reduce the loading for distillation units, and mainly serve as alternative technology for retrofitting the current distillation platform.

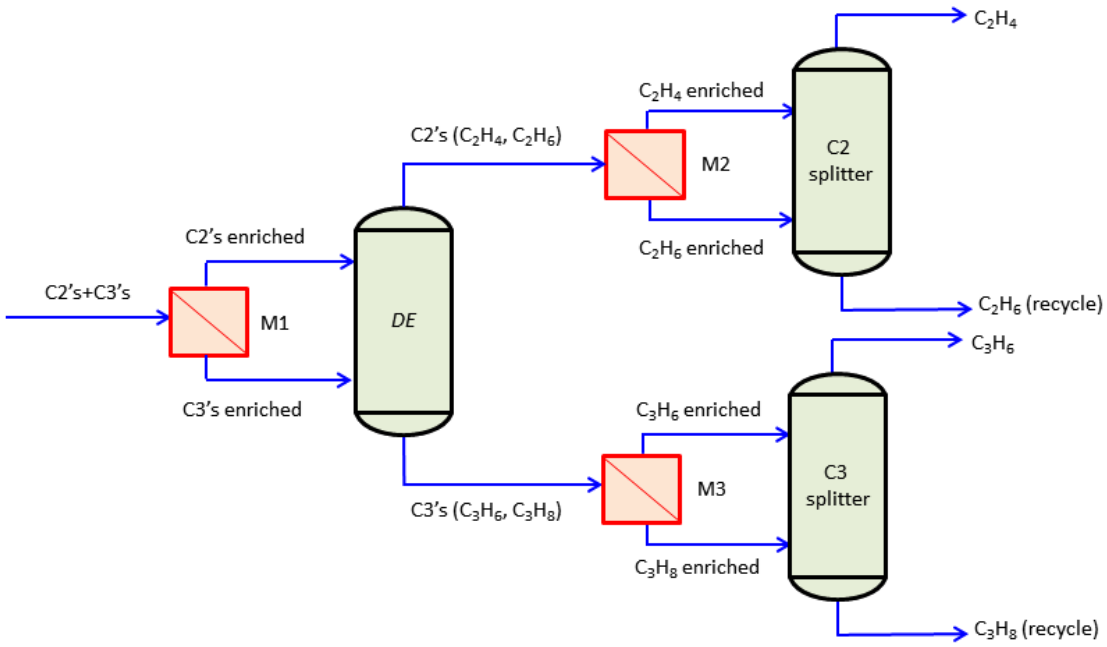

Figure 8.1 Schematic of the debottlenecking hybrid membrane-distillation concept for olefin/paraffin separations

8.2 Membranes for C2's and C3's separation

In order to debottleneck the deethanizer, the separation task for membranes involves separating C2's (ethylene and ethane) from C3's (propylene and propane). First, polymer materials were looked for bulk C2's and C3's separation. Transport properties of Matrimid® and 6FDA/BPDA-DAM polyimides are listed in Table 8.1. From the transport properties, it is obvious that ethane/propane selectivity is very close to unity for both polyimides, which means polymer materials are not able to separate C2's from C3's. This property is probably due to the higher solubility of propylene over ethane in polymers, which is determined by the critical temperature (365.1 K for propylene versus 305.4 for ethane) and compressibility. Even assuming polymer materials may deliver some selectivity of C2's over C3's, the stability of polymer membranes are still worrisome for the aggressive hydrocarbons stream. Serious plasticization is expected under the hydrocarbon feed conditions. As described in Chapter 4, plasticization occurred in defect-free polymer hollow fiber membranes under less than 100 psi feed pressure of ethylene and ethane, and the case of propylene and propane is expected to be worse.

Table 8.1 Olefin/paraffin transport properties in polymer membrane materials [7-10]

Polymer	Permeability (Barrer)				Selectivity			
	C_2H_4	C_2H_6	C_3H_6	C_3H_8	$\frac{C_2H_4}{C_2H_6}$	$\frac{C_3H_6}{C_3H_8}$	$\frac{C_2H_6}{C_3H_6}$	$\frac{C_2H_4}{C_3H_6}$
Matrimid®	0.45	0.1	0.1	0.01	4.5	10	1.0	4.5
6FDA/BPDA-DAM	46	13.9	11.8	0.9	3.3	13	1.2	3.3

35 ^{o}C testing temperature, pure gas tests, <100 psi testing pressure

Next, CMS hollow fiber membranes were investigated for bulk C2's and C3's

separation (as in the deethanizer). The membranes were produced by 550 ^{o}C/2 hr, UHP argon purge pyrolysis. One typical set of permeation properties is listed in Table 8.2. Interestingly, the propylene permeance of CMS hollow fiber membranes is higher than ethane, for both Matrimid® and 6FDA/BPDA-DAM CMS membranes in this particular case. Therefore, CMS membranes produced from this specific condition are not able to separate bulk C2's from C3's, either.

Table 8.2 Olefin/paraffin transport properties in carbon molecular sieve hollow fiber membranes

Precursor	Permeance (GPU)				Selectivity			
	C_2H_4	C_2H_6	C_3H_6	C_3H_8	$\frac{C_2H_4}{C_2H_6}$	$\frac{C_3H_6}{C_3H_8}$	$\frac{C_3H_6}{C_2H_6}$	$\frac{C_2H_4}{C_3H_6}$
Matrimid®	2.1	0.53	0.76	0.04	4.0	21.0	1.43	2.76
6FDA/BPDA-DAM	15.9	4.0	17.5	0.85	3.9	20.5	4.38	0.91

35 ^{o}C testing temperature, pure gas tests, 100 psi C_2H_4 and C_2H_6, 50 psi C_3H_6 and C_3H_8

8.3 Olefins-selective membranes for olefin/paraffin separation

It appears that both polymer and carbon membranes can hardly separate C2's from C3's; however, one very favorable feature was realized from Table 8.2. CMS membranes are able to separate bulk olefins from paraffins. Since Matrimid® CMS membrane performance is limited by the relatively low permeance, the main focus switches to 6FDA/BPDA-DAM based carbon membranes for further investigation. Ethylene and propylene pass the carbon membrane at a similar permeance, which is about 4 times higher than ethane and more than 20 times higher than propane. This actually means that the CMS membrane is an *olefins-selective device*, and is able to enrich olefins

(ethylene and propylene) in a single membrane separation operation. This can be further explored for advanced process designs for hybrid membrane-distillation systems.

Since the transport properties in Table 8.2 were from pure gas measurement, to validate the realistic separation performance, a multi-component mixed gas permeation test was performed. Another membrane module with one year aging history was used for the mixed gas test. The test was performed in a Dow laboratory by Mark Brayden and Gregory Barbay. The feed gas mixture was from the bottom of a demethanizer (feed for deethanizer), a gas mixture that predominantly contained two and three carbon atoms hydrocarbons (C2's and C3's). The testing was at 25 ^{o}C with a feed pressure of 60 psig and 30 psig argon as permeate sweep. The feed composition and permeate composition are listed in Table 8.3, and transport properties of the membrane are listed in Table 8.4. It is clear that olefins (ethylene and propylene) were enriched to more than 91 mol%, while 7.2 mol% ethane and only 0.7 mol% propane were retained in the permeate stream. The above evaluation demonstrated the high performance of olefins-selective membranes for mixed carbon number olefin/paraffin separations under realistic conditions.

Table 8.3 Feed and permeate compositions of a mixed gas permeation test using the deethanizer feed as feed mixture

Gas	Feed (mol%)	Permeate (mol%)
C_2H_4	54.4	75.3
C_3H_6	14.8	16
C_2H_6	17.1	7.2
C_3H_8	13.5	0.7
Other hydrocarbons	0.2	0.8

Table 8.4 Transport properties of a CMS membrane in a mixed gas permeation test using the deethanizer feed as feed mixture

Permeance (GPU)				Selectivity			
C_2H_4	C_2H_6	C_3H_6	C_3H_8	C_2H_4/C_2H_6	C_3H_6/C_3H_8	C_2H_4/C_3H_6	C_3H_6/C_2H_6
8.6	2.6	6.7	0.308	3.3	22	1.3	2.6

A new hybrid membrane-distillation concept is proposed based on the olefins-selective membranes. Two new process configurations are shown in Figures 8.2 and 8.3. They share the same olefins-selective membrane unit at the beginning. Based on the current membrane performance, olefins (ethylene and propylene) are enriched in the permeate stream and propane is retained in the retentate stream. Ethane probably distributes in both permeate and retentate stream due to its intermediate flux. Propane and ethane in the retentate can be sent back to a cracker for recycle. The biggest advantage of this concept is that the two useful products (ethylene and propylene) are enriched together in the membrane separation process. Based on current membrane capabilities, ethane is still present in the permeate stream, so a single distillation column afterwards is not able to obtain purified ethylene and propylene. For the ternary permeate stream (ethylene, propylene and minor ethane), several routes are proposed to separate the three components.

One of many processes using this concept is demonstrated in Figure 8.2. After the olefins-selective membrane, a distillation column is used to separate C2's and propylene. This is an easy-to-implement version of the deethanizer. The main separation is splitting ethylene and propylene, and the minor amount of ethane goes to the top of the column with ethylene. As a retrofitting concept, the current deethanizer works well with much lighter duties since propane and part of ethane are removed by the membrane unit. The

capacity can be increased significantly. After propylene is removed by the first distillation column, the second distillation column can be used to separate ethylene and ethane. Since ethylene is the major component in the feed stream and only a small amount of ethane exists, the second distillation column is similar to the one in Figure 8.1. New columns can be shorter, or alternatively, perhaps the capacity could be increased in the current column, as reflux ratio is reduced. Compared with previously proposed retrofitting hybrid concept, significant savings can be achieved in the new process. This is "beyond debottlenecking", and the new process can actually change the separation order of hydrocarbons, and reduce the number of distillation columns for future installations. For the time being, however, debottlenecking seems possible by reconfiguring the column flows for maximum productivity.

Figure 8.3 demonstrates an even more ambitious separation process. After the olefins-selective membrane unit, another subsequent membrane unit is further used to remove ethane and enrich the valuable ethylene and propylene. Of course, the olefins-selective membrane has to be improved, or a series of membranes can be used. Afterwards, ethylene and propylene is separated by a distillation column. The separation of ethylene and propylene by distillation is relatively easy due to the large difference in boiling points. Potentially, this process also saves significant energy in a practical way, since this could actually free up two columns (and their heat duties) to allow further capacity increases. Moreover, the remaining distillation columns would do the easy ethylene/propylene split, reducing its heat duty and eliminating the need for cryogenics. Of course, with the complexity of heat integration in existing olefins production units, the specific energy improvements available would need be studied on a case by case basis.

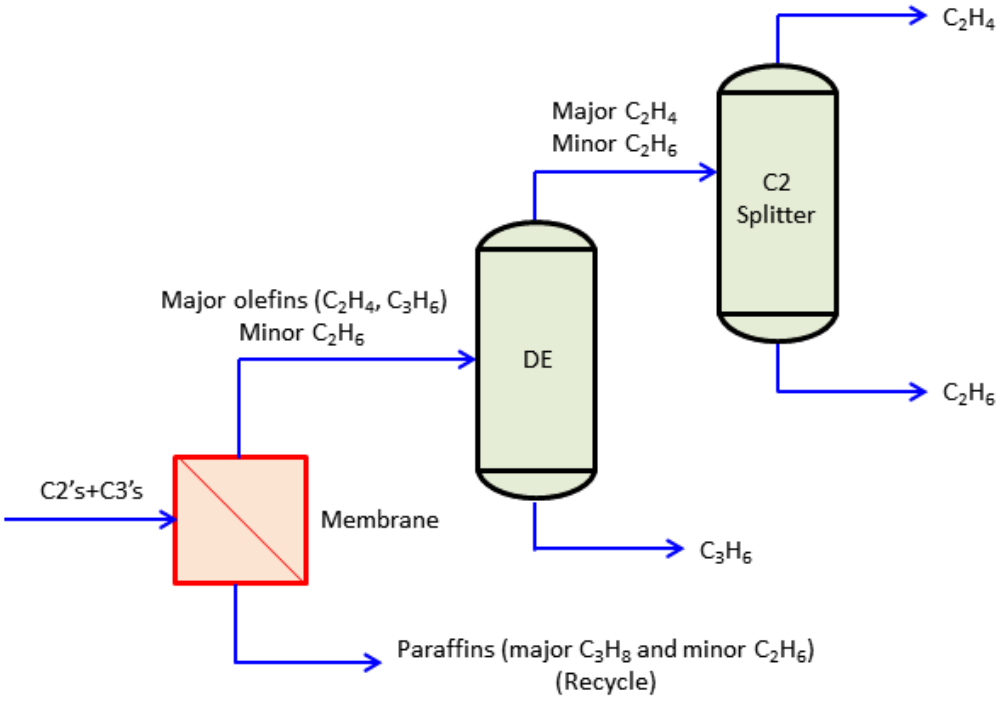

Figure 8.2 Schematic of a new hybrid process consisting of one olefins-selective membrane unit and two distillation columns

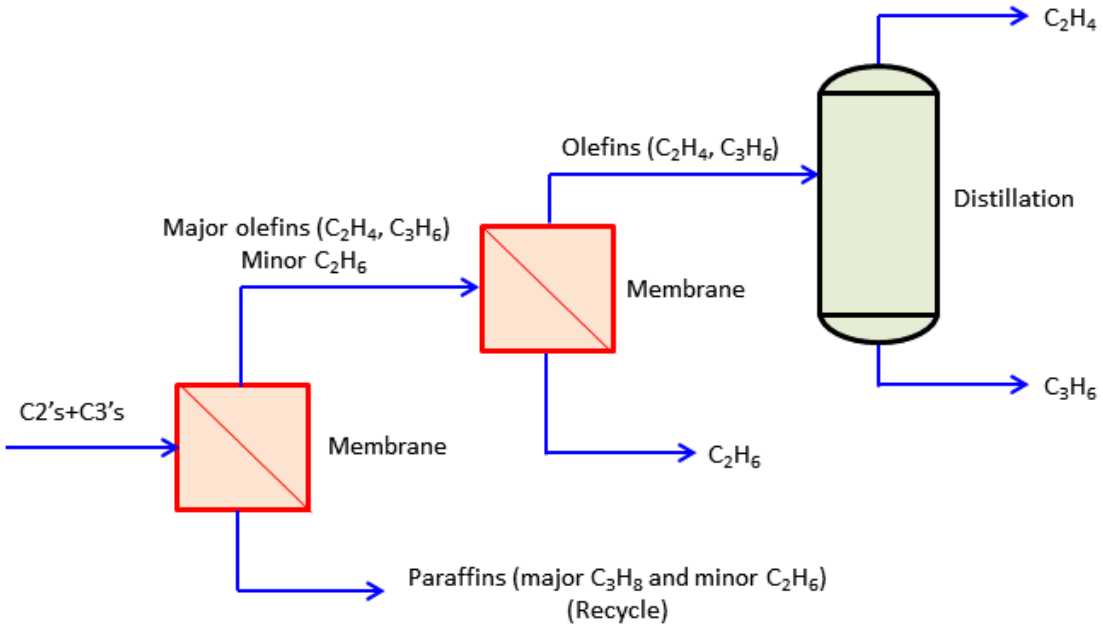

Figure 8.3 Schematic of a new hybrid process consisting of a series of olefins-selective membrane units and one distillation column

8.4 Ideal membranes for hydrocarbons processing

The CMS membrane is demonstrated to be outstanding for the deethanizer application, which also impacts the downstream C2 splitter and C3 splitter operations. The olefins-selective feature of CMS membranes is unique, as compared to other membrane materials. Transport properties of polymer materials are shown in Table 8.1. Even with microporous materials (zeolites, metal organic frameworks (MOFs)) with defined pore sizes, the olefins-selective membrane has not been reported previously. One recent publication shows the transport properties of ethylene, ethane, propylene and propane in a ZIF-8 membrane [11]. The permeance of gases follows the order: $(P/l)_{C2H4}>(P/l)_{C2H6}> (P/l)_{C3H6}> (P/l)_{C3H8.}$ This membrane can actually separate C2's from C3's. However, the ZIF-8 membrane is *not able to separate olefins from paraffins*. It is clear that CMS membranes have advantages in olefin/paraffin separations. One particular feature is that CMS membranes have an idealized "slit-like" pore structure. While olefins have a planar or partially planar molecular configuration, the "slit-like" pores will enable relatively easy passage of olefins over the bulky paraffins. On the other hand, zeolites or zeolites-like materials have 2-dimensional pore windows, which restrict the configuration advantages of olefins. From this perspective, CMS membranes with a "slit-like" pore structure are truly ideal for olefin/paraffin separations.

Based on the above discussion, with CMS membranes, more ambitious applications can be explored for the cracked hydrocarbon processing. For example, the membrane unit can be moved up further in the process and applied for the demethanizer application. Demethanizer separates methane and hydrogen from C2's and C3's hydrocarbons. In this case, methane and hydrogen are present in the feed gas mixture.

The feed gas for the test was from the actual feed for a demthanizer in a Dow plant. The feed and permeate compositions are listed in Table 8.5, and transport properties of the membrane are listed in Table 8.6. As shown in Table 8.5, similar to the deethanizer application, in the permeate stream, paraffins only count for 7.0 mol%, and the rest are hydrogen, ethylene and ethane. This experiment demonstrates that the membrane is also very effective in the demethanizer application. Therefore, the olefin/paraffin separation can be moved up to the demethanizer. The separation of bulk hydrogen from ethylene and propylene will be an easy separation due to the significant size difference. It is interesting that, in Table 8.6, methane permeance is even lower than ethane, and of course, is lower than olefins (ethylene and propylene), which is very favorable. This is again enabled by the slit-like pores of CMS and the bulky shape of methane molecules. The lower critical temperature compared to other hydrocarbons also contributes to the low permenace of methane, especially when comparing methane and ethane.

Table 8.5 Feed and permeate compositions of a mixed gas permeation test using the demethanizer feed as feed mixture

Gas	Feed (mol%)	Permeate (mol%)
H_2	26.9	66.4
CH_4	24.1	4.8
C_2H_4	28.4	22.3
C_3H_6	6	4.2
C_2H_6	7.8	1.9
C_3H_8	6.7	0.3
Other hydrocarbons	0.1	0.1

Table 8.6 Transport properties of a CMS membrane in a mixed gas permeation test using the demethanizer feed as feed mixture

Permeance (GPU)					
H_2	CH_4	C_2H_4	C_2H_6	C_3H_6	C_3H_8
24.68	2.00	7.86	2.45	7.02	0.49

To further extend the applications, acetylene, methylacetylene (MA) and propadiene (PD) were included in the feed mixture, which are present in the gas mixture produced from a cracking process. Tables 8.7 and 8.8 show the results for a 9-component permeation test. The mixture was from the feed for a front end acetylene hydrogenation reactor.

Table 8.7 Feed and permeate compositions for a 9-component permeation test

Gas	Feed (mol%)	Permeate (mol%)
H_2	24.1	60.6
CH_4	24.1	6.8
C_2H_4	30.2	24
C_3H_6	7.3	4.6
C_2H_6	8.0	2.0
C_3H_8	6.3	0.35
C_2H_2	0.32	0.93
C_3H_4 (Propadiene)	0.05	0.26
C_3H_4 (Methylacetylene)	0.11	0.48

Table 8.8 Permeance of gases in a 9-component permeation test

Acetylenes			Hydrogen	Olefins		Paraffins		
PD	MA	C_2H_2	H_2	C_2H_4	C_3H_6	CH_4	C_2H_6	C_3H_8
53.76	47.05	31.76	27.20	8.62	6.87	3.05	2.65	0.59

Permeance unit: GPU

From Table 8.7, almost 90 mol% of the permeate was hydrogen, ethylene and propylene, and the acetylenes were increased from 0.48 mol% to 1.67 mol%. Less than 10 mol% of paraffins remained in the permeate stream. As also demonstrated by Table 8.8, the CMS membranes are able to deliver excellent separation performance for the complex hydrocarbon mixture. More specifically, the membranes are able to classify hydrogen, linear/partially linear acetylenes, planar/partially planar olefin molecules and bulky paraffin molecules. This consequence is based on the size, shape and critical temperature of the gas molecules, as well as the interactions with the "slit-like" pore structures of CMS membranes. The space filling models and critical temperatures of hydrocarbon molecules are shown in Figure 8.4, and they can be used to explain the transport properties of hydrocarbon molecules in CMS membranes.

A previous study has revealed that ethylene has a significant entropic advantage over ethane in CMS membranes [7]. The similar effect should also work for the comparison of ethylene and methane permeation. Other cases can also be explained. For example, higher propylene permeance over methane may be attributed to the higher sorption coefficient of propylene in CMS membranes, since the size and shape feature should favor methane diffusion but sorption favors propylene due to the higher critical temperature of propylene. Although molecular sieving is the dominant separation

mechanism in CMS membranes, in many cases, sorption can play an important role. For example, CO_2 (kinetic diameter 3.3 Å, critical temperature 304.2 K) can be faster than He (kinetic diameter 2.6 Å, critical temperature 5.2 K) due to the stronger sorption of CO_2 over He. In the hydrocarbons separation, as indicated in Table 8.8, for this particular membrane, due to the sorption effect caused by low hydrogen critical temperature (T_c=33 K) and relatively high critical temperatures of acetylenes (shown in Figure 8.4), the hydrogen permeance was lower than MA, PD and C_2H_2.

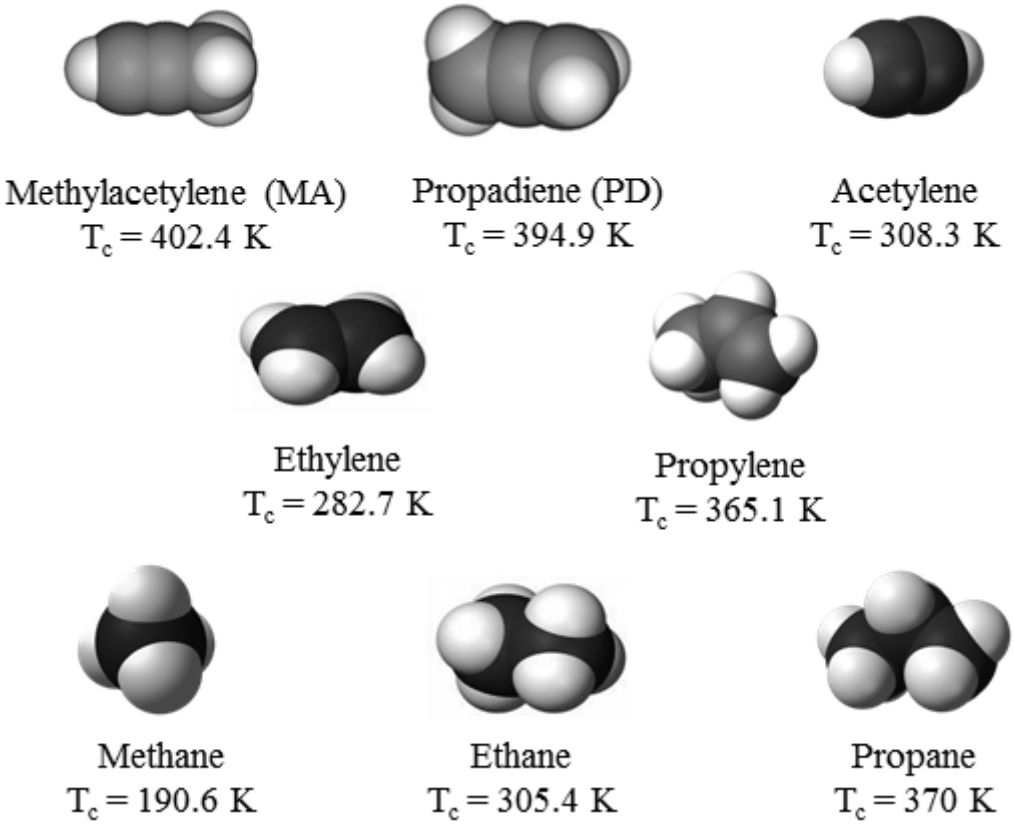

Figure 8.4 Space filling models and critical temperatures of C1, C2 and C3 hydrocarbons

8.5 Design of hydrocarbon processing with the incorporation of CMS membranes

As described in the previous section, the separation performance offered by CMS membranes is quite ideal for hydrocarbon processing. This opens numerous applications for CMS membranes in the hydrocarbons processes. The original debottlenecking concept for C2 and C3 splitters remains very attractive. More ambitiously, rather than previously proposed retrofitting concepts, reconfiguring the entire separation process of ethylene plants is also possible. Membranes will save significant capital costs, operational energy and reduce the footprint. Of course, process integration and materials development accordingly must be performed rigorously in order to realize the process.

With the unique CMS membranes, Mark Brayden at Dow designed a new ideal hydrocarbon separation process with the incorporation of CMS membranes, as shown in Figure 8.5 [2]. The entire process consists of three CMS hollow fiber membrane units M1, M2 and M3, an acetylene hydrogenation reactor (Rxr) and two distillation units ("Demethanizer Dist" and "Olefins Splitter Dist"). The associated feed streams, product or output streams from each of the units, and the reactor are also illustrated.

The process flow scheme differs from a conventional process flow scheme that begins with the same STRWAM 1 and uses at least four distillation units (nominally one for demethanizing or "Demethanizer Dist", one for deethanizing or "Deethanizer Dist", one for ethylene purification or "C2 Splitter" and one for propylene purification or "C3 Splitter"). The C3 splitter unit may comprise two or more distillation columns due to the number of stages needed to effect separation of propane and propylene due to their very similar volatilities or boiling points. The Figure 8.5 schematic illustration shows just two distillation columns, one for demethanizing, the same or nearly the same as in the

conventional process flow scheme, and one effecting an olefin split in place of both the C2 splitter and C3 splitter of the conventional process flow scheme.

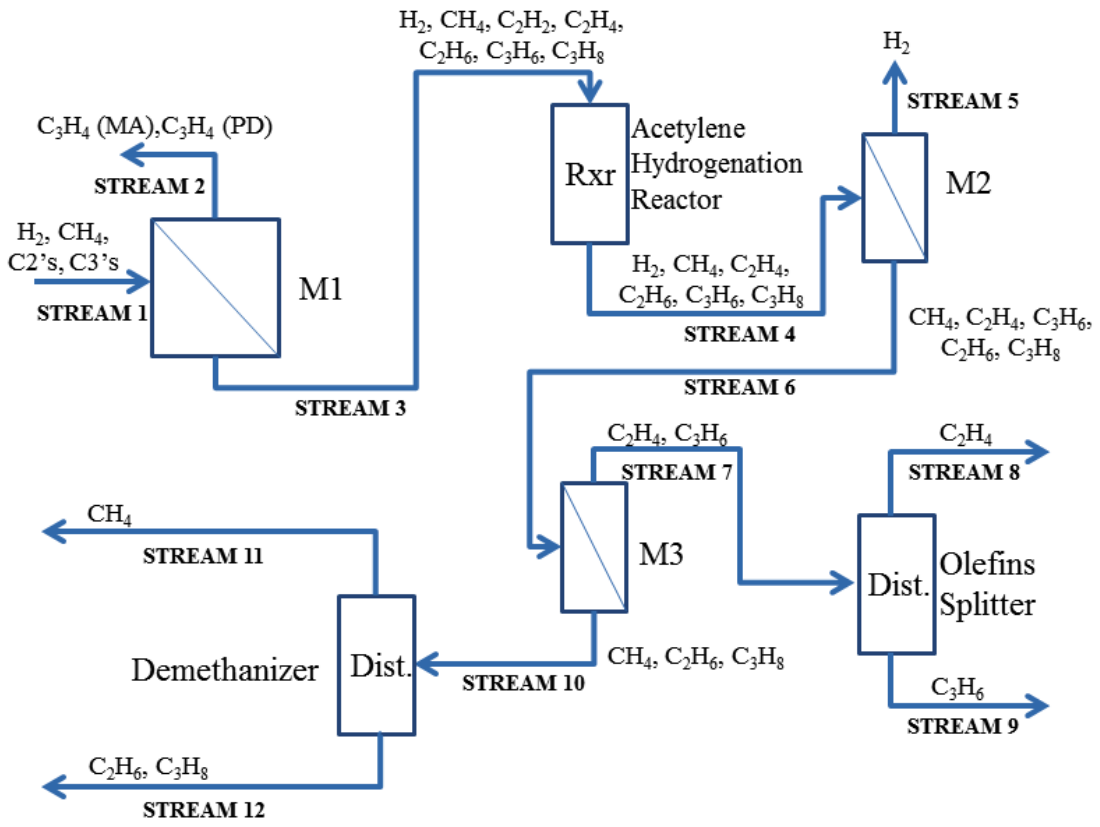

Figure 8.5 Process flow scheme incorporating CMS membranes for hydrocarbon processing

In Figure 8.5, STREAM 1 contains hydrogen (H_2), methane (CH_4), ethane, ethylene and acetylene (C_2's), and propane, propylene, methylacetylene, and propadiene (C_3's). STREAM 1 typifies the lighter of two "cracked gas" fractions from an ethylene production unit (as shown in Figure 1.1), which fraction is sometimes referred to as an overhead stream from a depropanizer unit. Plants built during the period from approximately 1990 to date for cracking primarily liquid feedstocks ("naphtha cracker

plants") or a mixture of feeds ("flexicracker plants") typically have a depropanizer as their first purification column.

Enabled by the fast permeation of MA and PD in CMS membranes noted in Table 8.8, CMS membranes can be used to separate MA and PD from STREAM 1. Therefore, for membrane unit M1, the permeate, designated as "STREAM 2", contains MA and PD, and the retentate, designated as "STREAM 3", contains H_2, CH_4, C_2H_4, C_2H_6, C_2H_2, C_3H_6, and C_3H_8. MA and PD in STREAM 2 can be used for specialty fuels or can be further hydrogenated into propene and propane.

STREAM 3 serves as a feed stream to an "acetylene hydrogenation reactor" in order to remove acetylene, deemed a product impurity in a final ethylene product. Output from the reactor (Rxr), designated as "STREAM 4", typically contains less than 1 ppm C_2H_2 in STREAM 4 based upon weight.

STREAM 4 serves as a feed stream to membrane unit M2. M2 effects separation of H_2 as permeate or STREAM 5 from remaining components of STREAM 4 as retentate to yield STREAM 6 that has very little, preferably no H_2. The hydrogen separation membrane can be further optimized based on the current CMS work, which is promising due to the big size difference between hydrogen and other hydrocarbon molecules.

STREAM 6 serves as a feed stream to membrane unit M3, which is the previously described olefins-selective membrane. The membrane effect an olefin/paraffin separation with olefins (C_2H_4 and C_3H_6) being present in the permeate or STREAM 7 and paraffins (CH_4, C_2H_6 and C_3H_8) being present as M3 retentate or STREAM 10.

Feed STREAM 7 is sent to an olefins splitter distillation unit to effect separation of olefins into STREAM 8 (C_2H_4) and STREAM 9 (C_3H_6). Feed STREAM 10 is sent to

a demethanizer distillation unit to effect separation of STREAM 10 into STREAM 11 (CH_4) and STREAM 12 (C_2H_6 and C_3H_8). Recycled CH_4 in STREAM 11 may be used as fuel, while the combined ethane and propane stream may be sent to an ethylene furnace as a recycle feedstock to produce additional cracked gas.

8.6 Summary and conclusions

This chapter expands previous membrane applications for binary ethylene/ethane and propylene/propane separations, which are mainly for debottlenecking C2 and C3 splitters. The debottlenecking concept was also expected to effectively retrofit deethanizer and demethanizer. In the case of deethanizer, both polymeric membranes and CMS membranes are not able to deliver the desired separation of C2's (ethylene and ethane) from C3's (propylene and propane). However, during this investigation, CMS membranes were found to be olefins-selective, and this is a very favorable case in hydrocarbons processing. Olefins-selective membranes are able to separate olefins (ethylene and propylene) from paraffins (methane, ethane and propane). This unique property enables the reconfiguration of separations performed by demethanizer, deethanizer and the C2, C3 splitters. Further investigations revealed that CMS membranes also delivered desirable properties for cracked gas stream containing hydrogen (H_2), methane (CH_4), ethane, ethylene and acetylene (C_2's), and propane, propylene, methylacetylene, and propadiene (C_3's). CMS membranes are able to effectively fraction the complex gas stream in a very preferable way. The consequence is enabled by the "slit-like" pores in CMS and the off-setting contributions of penetrant size, shape and condensability. Rather than retrofitting distillation columns with parallel

membrane units, advanced integrated processes of membranes and distillation were proposed. Significant energy savings and reduced footprint can be achieved by reconfiguring the separations in the hydrocarbons processes.

8.7 References

[1] L. Xu, M. Rungta, M.K. Brayden, M.V. Martinez, B.A. Stears, G.A. Barbay, W.J. Koros, Olefins-selective asymmetric carbon molecular sieve hollow fiber membranes for hybrid membrane-distillation processes for olefin/paraffin separations, J. Membr. Sci. 10.1016/j.memsci.2012.08.028.

[2] W.J. Koros, L. Xu, M.K. Brayden, M.V. Martinez, B.A. Stears, A hollow fiber carbon molecular sieve membrane and preparation and use thereof, in: U.S. Patent (Ed.) United States Patent Application, US, 2012.

[3] M. Benali, B. Aydin, Ethane/ethylene and propane/propylene separation in hybrid membrane distillation systems: Optimization and economic analysis, Sep. Purif. Technol. 73 (2010) 377-390.

[4] E. Ayotte-Sauve, M. Sorin, F. Rheault, Energy requirement of a distillation/membrane parallel hybrid: a thermodynamic approach, Ind. Eng. Chem. Res. 49 (2010) 2295-2305.

[5] J.A. Caballero, I.E. Grossmann, M. Keyvani, E.S. Lenz, Design of hybrid distillation-vapor membrane separation systems, Ind. Eng. Chem. Res. 48 (2009) 9151-9162.

[6] A. Motelica, O.S.L. Bruinsma, R. Kreiter, M. den Exter, J.F. Vente, Membrane retrofit option for paraffin/olefin separation—a technoeconomic evaluation, Ind. Eng. Chem. Res. 10.1021/ie300587u (2012).

[7] M. Rungta, L. Xu, W.J. Koros, Carbon molecular sieve dense film membranes derived from Matrimid® for ethylene/ethane separation, Carbon 50 (2012) 1488-1502.

[8] O. Esekhile, W. Qiu, W.J. Koros, Permeation of butane isomers through 6FDA-DAM dense films, J. Polym. Sci., Part B: Polym. Phys. 49 (2011) 1605-1620.

[9] K.M. Steel, W.J. Koros, An investigation of the effects of pyrolysis parameters on gas separation properties of carbon materials, Carbon 43 (2005) 1843-1856.

[10] M. Das, W.J. Koros, Performance of 6FDA–6FpDA polyimide for propylene/propane separations, J. Membr. Sci. 365 (2010) 399-408.

[11] Y. pan, Z. Lai, Sharp separation of C2/C3 hydrocarbon mixtures by zeolitic imidazolate framework-8 (ZIF-8) membranes synthesized in aqueous solutions, Chem. Commun 47 (2011) 10275-10277.

CHAPTER 9

CONCLUSIONS AND RECOMMENDATIONS

9.1 Conclusions

The goal of this research was to develop high performance carbon molecular sieve hollow fiber membranes for olefin/paraffin separations. To achieve this goal, membrane material fabrication, evaluation and process integration have been studied extensively and satisfactory results have been obtained.

Three polyimides, Matrimid®, 6FDA-DAM and 6FDA/BPDA-DAM, were chosen as precursor polymers for CMS membrane formation. Defect-free asymmetric polymer hollow fiber membranes were successfully spun from a dry-jet/wet-quench spinning process. Dope formulation and spinning parameters were optimized to achieve desirable asymmetric hollow fiber properties.

Matrimid® was employed as a model precursor for exploring CMS hollow fiber formation. CMS membranes prepared from Matrimid® delivered separation performance well above the polymer upper bound for C_2H_4/C_2H_6 separation. A high selectivity of 12 for C_2H_4/C_2H_6 separation was obtained in both dense flat film and hollow fiber configurations. A substructure collapse phenomenon was revealed in the comparative study between CMS dense film and hollow fiber membranes. The significant decrease of polymer rigidity during glass-rubber transition was found to be the fundamental cause for substructure collapse. Substructure collapse resulted in a significant permeance loss of Matrimid® CMS hollow fiber membranes, due to the increased separation layer thickness. Another consequence of the porous structure collapse was the curing of pinhole defects in

the skin layer of precursor fibers. In order to overcome the substructure collapse issue, several approaches were pursued. The optimized CMS hollow fiber membranes were tested under realistic conditions (mixed gas feed, high feed pressure and cryogenic testing temperature) and excellent stability and performance have been demonstrated.

6FDA-DAM and 6FDA/BPDA-DAM were chosen as alternative precursor polymers due to their high glass-rubber transition temperatures and high intrinsic permeability. The increased glass-rubber transition temperatures resulted in high rigidity during intense heat-treatments and finally led to improved asymmetric morphology of 6FDA-DAM and 6FDA/BPDA-DAM CMS hollow fibers. The rigidity-asymmetry correlation was also extended to cross-linkable polymers with very rigid polymer matrix. The high precursor permeability also led to the high CMS membrane permeability. 6FDA/BPDA-DAM CMS hollow fiber membranes showed significant improvement in permeance for multiple gas separation applications. A great deal of effort was made to tailor the microstructure of CMS membranes by optimizing pyrolysis temperature protocols and pyrolysis atmosphere. 6FDA-DAM and 6FDA/BPDA-DAM derived CMS hollow fiber membranes were found to be ideal for debottlenecking C3 splitters. In addition, unlike Matrimid®, for 6FDA/BPDA-DAM CMS hollow fiber membrane preparation, defect-free precursor fibers led to better consistency, and the ability for spinning defect-free precursor fibers becomes even more important.

Unexpected physical aging was discovered in CMS membranes. In this work, chemical aging including oxygen chemisorption and other adsorption was excluded for the rapid aging of CMS membranes by vacuum storage, inert gas storage and propylene cleaning. The pores are believed to be formed by packing imperfection of graphene-like

sheets, and age analogously to the "unrelaxed free volume" in glassy polymers. Over time, these pores tend to collapse in order to achieve thermodynamically more stable states. Aging kinetics of Matrimid®, 6FDA-DAM and 6FDA/BPDA-DAM CMS hollow fiber membranes were obtained. The impacts of aging on various key performance properties were investigated. The history dependence can actually be employed as another tool to tailor the CMS membrane transport properties. A long term permeation test demonstrated the excellent stability of stabilized CMS membranes under realistic conditions.

CMS membranes were found to deliver excellent performance in mixed carbon number hydrocarbons processing. In the investigation of membranes for C2's and C3's olefin/paraffin separation, CMS membranes were found to be olefins-selective, which means that CMS membranes are able to separate olefins (ethylene and propylene) from paraffins (methane, ethane and propane). Further investigations revealed that CMS membranes are able to effectively fractionate the complex cracked gas stream in a very preferable way. The consequence is enabled by the "slit-like" pores in CMS and the off-setting contributions of penetrant size, shape and condensability. Rather than retrofitting distillation columns with parallel membrane units, advanced integrated processes of membranes and distillation were proposed. Significant energy savings and reduced footprint can be achieved by reconfiguring the separations in the hydrocarbons processes.

9.2 Recommendations

In this research, significant progresses have been made in many aspects of CMS membranes for olefin/paraffin separations. This final section contains recommendations

for future work for this project.

9.2.1 Performance evaluation under realistic conditions

In many cases, the lab scale permeation tests for CMS membranes have been idealized. Although several "proof of concept" tests under realistic conditions have been performed and very promising results were demonstrated, it is wise to perform more systematic studies of CMS membranes under practical testing conditions. Several operational parameters must be considered carefully, including feed gas pressure, permeate gas pressure, feed gas composition, stage cut and testing temperature. This study has demonstrated the stability of CMS hollow fiber membranes under high pressure. In most lab scale tests, the permeate gas pressure is usually kept under vacuum or relatively low pressure, while the desirable permeate pressure is much higher under realistic testing conditions. Appropriate stage cut is important for achieving effective separation while obtaining a high recovery. The testing temperature has a significant impact on membrane transport properties, as shown in preliminary tests. Especially, transport properties of olefin/paraffin in CMS membranes under cryogenic conditions are very interesting and important for practical implementation of the membranes.

9.2.2 Controlling macroscopic asymmetric morphology of CMS hollow fiber membranes

The impact of separation layer thickness on asymmetric hollow fiber membrane permeance is obvious and significant. This work has demonstrated the formation of various CMS hollow fiber morphologies. Even for the 6FDA/BPDA-DAM CMS hollow fiber membranes formed in this work, the separation layers were still on the scale of 10

μm, although significant improvement has been achieved compared to fully collapsed Matrimid® CMS membranes. Cross-linkable polymers have been shown to maintain the highly asymmetric morphology from their precursor fibers. Future effort may be made to explore additional cross-linkable precursors, in order to create thin CMS separation layer with high performance intrinsic transport properties. Alternative methods that can be used to stabilize the polymer matrix are of great interest. The so-called "V-grafting" developed by Nitesh Bhuwania in Koros Research Group is effective in creating asymmetric CMS hollow fiber morphology from several precursor polymers, and deserves future pursuit.

9.2.3 Understanding and optimizing the micro-structure of CMS membranes

Characterization of CMS porous micro-structure has been very challenging. Gas permeation and sorption have been used as the primary techniques. To physically understand the pore structure of CMS materials is important for understanding phenomena such as physical aging described in this work. Analytical techniques such as Raman spectroscopy, X-ray diffraction (XRD) and positron annihilation lifetime spectroscopy (PALS) may provide insights for the CMS structure.

Physical aging in CMS membranes is a newly discovered phenomenon. Characterization of physical aging from a structural perspective is of great interest. The history dependence has now been employed as another tool for structural tuning besides the previous pyrolysis temperature protocol and O_2-doping. A combination of the above methods is expected to better control CMS membrane micro-structure for specific applications. Besides the performance tuning, attention must be paid for the stability of CMS membranes, in both intrinsic transport property characterization and practical

operations.

The precursor-CMS structure relationship remains as an important but not well-understood topic. Polymer rigidity has been added as an important property for precursor screening. The impact of precursor structure on CMS membrane transport properties and aging behavior remains quite vague. Future researches in this topic are quite challenging but are of high pay-off value. In situ monitoring of the pyrolysis process (evolved gases and structural change of samples) would be useful.

9.2.4 Optimizing CMS membranes for specific applications

Besides conventional ethylene/ethane and propylene/propane separations, many applications have been proposed for hydrocarbons processing during this research. Most concepts have been proved by using a common membrane. However, for each application, the dominant factor(s) and correspondingly the requirement of pyrolysis conditions and operation conditions can be significantly different.

Table 9.1 summarizes the potential applications of CMS membranes in cracked gas processing, including the previously proposed debottlenecking binary separations of ethylene/ethane (Case 1) and propylene/propane (Case 2) as well as fully integrated mixed carbon number hydrocarbons separations (Cases 3, 4 & 8). Cases 3, 4 and 8 correspond to M1, M2 and M3 in Mark Brayden's innovative design [1], as shown in Figure 8.5 in Chapter 8. Cases 5, 6 and 7 are essential elements to enable the olefins-selective membranes of Case 8. The dominant factor(s) for each separation and the guidelines for future optimization in both pyrolysis and operation are also provided in Table 9.1. In case 1, both size and shape difference of ethylene and ethane enable the

separation; the low temperature operation is a requirement of the application and also enhances the selectivity. In case 2, due to the relatively large size of both propylene and propane, high pyrolysis temperature may result in a decrease of pore size and significant decrease of propylene permeability as well as propylene/propane selectivity; therefore, low temperature pyrolysis is preferred. In Case 3, higher MA (methylacetylene) & PD (propadiene) permeance over H_2 is enabled by the critical temperature and sorption effect; therefore, low temperature pyrolysis helps lower the size advantage of H_2, and low operational temperature maximizes the sorption advantage of MA & PD. In case 4, to maximize the size advantage of H_2, high temperature pyrolysis can be used to decrease the pore size of CMS membranes and high operation temperature can be used to lower the sorption advantage of olefin/paraffin molecules; therefore, from both diffusion and sorption, the selectivity of H_2 over other hydrocarbons can be increased. The olefins-selective membranes are more complicated, as shown in the essential Cases 5, 6 and 7. The olefins-selective feature is enabled by the "slit-like" pores in CMS and the off-setting contributions of penetrant size, shape and condensability. Both membrane structure and the properties of relevant gas components must be considered in a balanced way. In most cases in Table 9.1, low operation temperature is preferred from the perspective of selectivity enhancement for effective separations; however, when the flux of membranes becomes more important, high operation temperature can be used. Further optimization is required for each application.

Table 9.1 CMS membranes for potential cracked gas applications

Case	Gas Pair	Dominant factor(s)			Optimization	
		Size	Shape	T_c	Pyrolysis	Operation
1	C_2H_4/C_2H_6	√	√	-	-	low T
2	C_3H_6/C_3H_8	√	√	-	low T	low T
3	(MA & PD)/H_2	-	-	√	low T	low T
4	H_2/(CH_4, C_2H_4, C_3H_6, C_2H_6, C_3H_8)	√	√	-	high T	high T
5	C_2H_4/CH_4	-	√	√	-	low T
6	C_3H_6/CH_4	-	-	√	-	low T
7	C_3H_6/C_2H_6	-	√	√	-	low T
8	(C_2H_4, C_3H_6)/(CH_4, C_2H_6, C_3H_8)	√	√	√	-	low T

9.2.5 Scale-up of CMS hollow fiber membrane fabrication

The extension of lab scale CMS hollow fiber membrane fabrication to a commercial scale production is really the crucial step for realizing this exciting technology. In this work, modules with more than 20 carbon fibers have been made. Batch pyrolysis in Koros Research Group has been scaled up to more than 200 fiber capacity in a large furnace. To further increase the capacity or maybe an ultimately more streamlined operation should be performed. In addition, the impact of scale-up on pyrolysis, module construction and permeation behaviors should be studied in detail.

9.3 References

[1] W.J. Koros, L. Xu, M.K. Brayden, M.V. Martinez, B.A. Stears, A hollow fiber carbon molecular sieve membrane and preparation and use thereof, in: U.S. Patent (Ed.) United States Patent Application, US, 2012.